CARRIER TEMPERATURE AND GAIN DYNAMICS

IN SEMICONDUCTOR LASER MEDIA

By

TIGRAN SARKISYAN

Master of Science

Moscow Engineering Physics Institute

Moscow, Russia

1991

Submitted to the Faculty of the
Graduate College of the
Oklahoma State University
in partial fulfillment of
the requirements for
the Degree of
DOCTOR OF PHILOSOPHY
May, 2000

CARRIER TEMPERATURE AND GAIN DYNAMICS

IN SEMICONDUCTOR LASER MEDIA

Thesis Approved:

Donna Kay Bandy

Thesis Adviser

James P. Wicksted

Albert T. Rosenberger

Dean of the Graduate College

Dedicated to My Parents

ACKNOWLEDGMENTS

I wish to express my gratitude to my thesis adviser Professor Donna K. Bandy for her guidance and encouragement since I became a member of her research group. Her continuous support was crucial for completion of my studies, adjustment to Oklahoma and Western Hemisphere in general. I am greatly indebted to Dr. Bandy for her help in every aspect of my life during the years of my study at Oklahoma State University.

I would also like to thank Professor Anatoly Oraevsky who was my mentor during my studies in Moscow Engineering-Physics Institute and later in the Lebedev Physics Institute of Russian Academy of Sciences. Significant part of my research at OSU was completed with his active involvement.

I would like to thank my advisory committee members Drs. Jerzy Krasinski, Al Rosenberger, and James Wicksted for agreeing to be on my thesis committee despite their very busy schedule and for helpful suggestions. Special thanks are due to Dr. Al Rosenberger for collaboration and many fruitful discussions. His critical remarks helped me in cleaning up many obscurities that existed in the theory.

I am grateful to Dr. Paul Westhaus for his constant help with numerous problems that I have faced as a graduate student. Also I wish to express my gratitude to the Center for Laser and Photonics Research and Dr. Jin-Joo Song for financial support during the summer of 1999.

I would like to express my appreciation to Drs. P. Tong, S. Nandi, T. Wilson and S. McKeever with whom I worked as a teaching assistant and hopefully developed some teaching skills.

I am grateful to the members of Quantum Optics Group for providing a quiet environment in the lab – an ideal condition for a theoretical research. Special thanks goes to Todd Edmondson for keeping our computers alive while he was our system manager.

It would be impossible to acknowledge in detail the enormous amount of help that I have received from my colleagues and friends. I enjoyed the company and support of my friends and colleagues Sergiy Bidnyk, Alex Brener, Sasha Gorokhova, George Kamburoglou, Brian Little, Michael Humphrey, Jeromy Rezac and many others whose names are not printed here but not forgotten. On-line communications with my friends in Armenia, Russia, Canada and USA kept me in good spirit over last five years.

Finally, I would like to thank my wife Hasmik Stepanyan and my family for the support they provided me all these years.

TABLE OF CONTENTS

LIST OF TABLES viii

LIST OF FIGURES ix

1. INTRODUCTION 1
   - 1.1. Gain Nonlinearities in Semiconductors 2
   - 1.2. Semiconductor Laser Dynamics with and without the Gain Function 6
   - 1.3. Modified Rate Equations for Semiconductor Laser Dynamics 9
   - 1.4. Phenomenology of Carrier Heating Effects 11
   - 1.5. Preview of Thesis 16

2. MODEL DESCRIPTION 18
   - 2.1. Model Equations 18
   - 2.2. Free Carrier Absorption 24
   - 2.3. Two-Photon Absorption 26
   - 2.4. Gain Function 28
   - 2.5. Carrier Energy Density Equation 35
   - 2.6. Relations Among Dynamic Variables 39
   - 2.7. The Logic Behind the Pumping Term 42
   - 2.8. Limitations and Advantages of the Model 45

3. CARRIER TEMPERATURE DYNAMICS IN STEADY STATE LASER OPERATION 47
   - 3.1. Steady State Gain and Carrier Temperature 47
   - 3.2. Steady-State Behavior 48
   - 3.3. Carrier Temperature Behavior Below the Threshold 59
   - 3.4. Laser Response to External Pulses 64

4. TEMPERATURE DYNAMICS OF A RECOMBINING FREE-CARRIER ENSEMBLE 68
   - 4.1. Temperature Relaxation Rate 69
   - 4.2. Energy Dependent Recombination Rate 70
   - 4.3. Boltzmann Ensemble (Nondegenerate Semiconductor) 71
   - 4.4. Fermi Ensemble (Degenerate Semiconductor) 73

5. CARRIER HEATING INFLUENCE ON GAIN 79
5.1. Medium Parameters 80
5.2. Gain Dynamics 83
5.3. Analysis of Carrier Heating Influence on Gain 88
5.4. Gain Behavior Far From Transparency Region 91
5.5. Gain Behavior in a Transparent Medium 96

6. GAIN AND CARRIER TEMPERATURE DYNAMICS 99
6.1. Dynamic Behavior in an Amplifying Medium 100
6.2. Dynamic Behavior in An Absorbing Medium 103
6.3. Carrier Temperature Behavior 111
6.4. Influence of Two-Photon and Free-Carrier Absorption 115
Amplifying Sample 116
Absorbing Sample 124
Summary of Temperature Behavior With and Without FCA and TPA.. 132

7. SUMMARY AND CONCLUSIONS 138

8. BIBLIOGRAPHY 142

Appendix A. Relationship between Electromagnetic Field and Photon Density 151

Appendix B. Derivation of Photon Density Equation from the Field Equation 155

Appendix C. Spontaneous Recombination Rate 158

Appendix D. Calculation of Integrals with the Exact Fermi Function 162

Appendix E. Expressions for Carrier Density and Carrier Energy Density 166

Appendix F. Calculation of Integrals with an Approximate Fermi Function 169

Appendix G. Calculation of Integrals for Pumping Terms with a Barrier 176

Appendix H. Dimensionless Model Equations 188

LIST OF TABLES

Table 2.1. Electron Energy Relaxation Times 37

Table 3.1. Parameter Values for $In_{0.75}Ga_{0.25}As_{0.55}P_{0.45}$ Diode Laser 49

Table 3.2. Steady State Values For Photon Density and Carrier Temperature Deviation from the Lattice Temperature 56

Table 3.3. Influence of Carrier Heating Processes on Steady State Values 57

Table 3.4. Slopes for Linearly Decreasing Part of Temperature Graphs 62

Table 5.1. Parameter Values for GaAs Medium 80

Table 6.1. Curve Fitting Parameters 114

LIST OF FIGURES

Figure 1.1. Gain function deformations due to (a) spectral hole burning, and (b) carrier heating. The blue curves correspond to undeformed gain function. The red curves correspond to deformed gain functions. The green dashed line in (a) represents the level of losses. The green curve in (b) demonstrates the carrier heating effect with fixed chemical potentials of carriers 14

Figure 1.2. Electron distribution function affected by (a) spectral hole burning, and (b) carrier heating. The blue curves correspond to unperturbed distribution function. The red curves correspond to perturbed distribution functions. 15

Figure 2.1. The gain coefficient as a function of photon energy for fixed carrier temperature and chemical potential calculated from Eq. (2.37). The expression (2.43) is used for G(ω). The blue and red curves correspond to different temperatures ($T_{red} > T_{blue}$). The blue and green curves correspond to different chemical potentials ($\mu_{blue} < \mu_{green}$). The material parameters used for these calculations correspond to GaAs. 34

Figure 2.2. Exact and approximate Fermi functions at 70K (solid lines) and 300K (dashed lines). The exact Fermi functions (blue lines) are plotted according to Eq.(D.2) (p. 163); the approximate Fermi functions (red lines) are plotted according to (Eq.(2.49)). 41

Figure 3.1. Laser transition to cw behavior for pumping at 1% above the threshold rate: (a) photon density, (b) carrier density, and (c) carrier temperature 52

Figure 3.2. Laser transition to cw behavior for pumping at 10% above the threshold rate: (a) photon density, (b) carrier density, and (c) carrier temperature. 53

Figure 3.3. Laser transition to cw behavior for pumping at 10 times the threshold rate: (a) photon density, (b) carrier density, and (c) carrier temperature. 54

Figure 3.4. Laser transition to cw behavior for pumping at 25 times the threshold rate: (a) photon density, (b) carrier density, and (c) carrier temperature. 55

Figure 3.5. Laser transition to cw behavior for pumping at twice the threshold rate (red curves, with temperature dynamics; blue curves, without temperature dynamics; green curves, with temperature dynamics but FCA excluded: (a) photon density, (b) carrier density, and (c) carrier temperature. 58

Figure 3.6. Carrier temperature deviation from the lattice temperature in the time interval between initiation of pumping and laser emission for pumping rates that are (a) 1%, (b) 10% above and (c) twice the threshold value 60

Figure 3.7. Laser response (red curves, with temperature dynamics; blue curves, without temperature dynamics) to an external 0.1 pJ Gaussian pulse peaked at $t = 0$: (a) 10 ps pulse width, (b) 25 ps pulse width, (c) 50 ps pulse width.................. 66

Figure 3.8. Carrier temperature behavior in cw laser response to an external 0.1 pJ Gaussian pulse peaked at $t = 0$ with 10 ps (red curve), 25 ps (green curve), and 50 ps pulse width (blue curve). 67

Figure 5.1. Subpicosecond gain dynamics; gain suppression due to carrier heating and recovery in the case of: (a) amplification; (b) transparency; (c) absorption......... 84

Figure 5.2. Carrier temperature behavior in the case of amplification (red), transparency (green), and absorption (blue). 85

Figure 5.3. Gain (a) and carrier temperature (b) behavior in the case of a medium with initially zero gain.. 87

Figure 5.4. Gain (a) and carrier temperature (b) behavior in the case of an absorbing medium far from transparency ($\boldsymbol{J} = 0.5\boldsymbol{J}_0$). 92

Figure 5.5. Gain (a) and carrier temperature (b) behavior in the case of an absorbing medium far from transparency ($\boldsymbol{J} = 0.75\boldsymbol{J}_0$). 94

Figure 5.6. Gain (a, b) and carrier temperature (c) behavior in the case of an amplifying medium far from transparency ($\boldsymbol{J} = 1.5\boldsymbol{J}_0$ (red) and $\boldsymbol{J} = 1.25\boldsymbol{J}_0$ (blue)). 95

Figure 5.7. Gain (a) and carrier density (b) behavior in a medium that is transparent for the 1.0-ps pulse with 0.1 pJ energy (green curves). Blue curves correspond to a 1.0-ps pulse with 0.2 pJ energy and red curves correspond to a 1.0-ps pulse with 0.05 pJ energy.. 97

Figure 5.8. Gain (a) and carrier density (b) behavior in a medium that is transparent for the 1.0-ps pulse with 0.1 pJ energy (green curves). Blue curves correspond to a 0.25-ps and red curves correspond to a 1.0-ps pulse, both with 0.1 pJ energy......... 98

Figure 6.1. Gain (a) and carrier temperature (b) behavior in a strongly amplifying medium pumped at a rate of $1.75\boldsymbol{J}_0$. The external pulse has 1.0 ps (FWHM) duration with energy: 0.1 pJ (blue curves), 1.0 pJ (green curves), and 2.0 pJ (red curves). 101

Figure 6.2. Gain (a) and carrier temperature (b) behavior in a medium pumped at a rate of $1.75\boldsymbol{J}_0$. The external pulse has 1.0 ps (FWHM) duration with energy: 3.0 pJ (blue curves), 5.0 pJ (green curves), and 25.0 pJ (red curves). 102

Figure 6.3. Carrier density behavior for various pulse energies**.**................................... 103

Figure 6.4. Gain (a) and carrier temperature (b) behavior in a strongly absorbing medium pumped at a rate of $0.25\boldsymbol{J}_0$. The external pulse has 1.0 ps (FWHM) duration with energy: 0.1 pJ (blue curves), 1.0 pJ (green curves), and 2.0 pJ (red curves). 105

Figure 6.5. Gain (a) and carrier temperature (b) behavior in a strongly absorbing medium pumped at a rate of $0.25\boldsymbol{J}_0$. The external pulse has 1.0 ps (FWHM) duration with energy: 3.0 pJ (blue curves), 5.0 pJ (green curves), and 25.0 pJ (red curves). 106

Figure 6.6. Carrier density behavior for various pulse energies. 107

Figure 6.7. Gain (a) and carrier temperature (b) behavior in an absorbing medium pumped at a rate of $0.75\boldsymbol{J}_0$. The external pulse has 1.0 ps (FWHM) duration with energy: 3.0 pJ (blue curves), 5.0 pJ (green curves), and 25.0 pJ (red curves)........... 109

Figure 6.8. Gain (a) and carrier temperature (b) behavior in an absorbing medium pumped at a rate of $0.5\boldsymbol{J}_0$. The external pulse has 1.0 ps (FWHM) duration with energy: 3.0 pJ (blue curves), 5.0 pJ (green curves), and 25.0 pJ (red curves)........... 110

Figure 6.9. The maximum carrier-lattice temperature difference as a function of external pulse energy in a strongly amplifying (pumped at a rate of $\boldsymbol{J} = 1.75\boldsymbol{J}_0$), transparent ($\boldsymbol{J} = \boldsymbol{J}_0$) and strongly absorbing ($\boldsymbol{J} = 0.25\boldsymbol{J}_0$) medium. 112

Figure 6.10. Gain (a) and carrier temperature (b) behavior in a strongly amplifying medium pumped at a rate of $1.75\boldsymbol{J}_0$. The external pulse has 1.0 ps (FWHM) duration and 0.1 pJ energy. The curves correspond to calculations with FCA and TPA (blue), without FCA (green), without TPA (red), and without FCA and TPA (pink). The blue curve is overlapped with the red, and the green curve overlapped with the pink curve. 118

Figure 6.11. Gain (a) and carrier temperature (b) behavior in a strongly amplifying medium pumped at a rate of $1.75\boldsymbol{J}_0$. The external pulse has 1.0 ps (FWHM) duration and 1.0 pJ energy. The curves correspond to calculations with FCA and TPA (blue), without FCA (green), without TPA (red), and without FCA and TPA (pink). The blue curve is almost overlapped with the red, and the green curve overlapped with the pink curve. 119

Figure 6.12. Gain (a) and carrier temperature (b) behavior in a strongly amplifying medium pumped at a rate of $1.75\boldsymbol{J}_0$. The external pulse has 1.0 ps (FWHM) duration and 2.0 pJ energy. The curves correspond to calculations with FCA and TPA (blue), without FCA (green), without TPA (red), and without FCA and TPA (pink). 120

Figure 6.13. Gain (a) and carrier temperature (b) behavior in a strongly amplifying medium pumped at a rate of $1.75\boldsymbol{J}_0$. The external pulse has 1.0 ps (FWHM) duration and 3.0 pJ energy. The curves correspond to calculations with FCA and TPA (blue), without FCA (green), without TPA (red), and without FCA and TPA (pink). 121

Figure 6.14. Gain (a) and carrier temperature (b) behavior in a strongly amplifying medium pumped at a rate of $1.75\boldsymbol{J}_0$. The external pulse has 1.0 ps (FWHM) duration and 5.0 pJ energy. The curves correspond to calculations with FCA and TPA (blue), without FCA (green), without TPA (red), and without FCA and TPA (pink). 122

Figure 6.15. Gain (a) and carrier temperature (b) behavior in a strongly amplifying medium pumped at a rate of $1.75\boldsymbol{J}_0$. The external pulse has 1.0 ps (FWHM) duration and 25.0 pJ energy. The curves correspond to calculations with FCA and TPA (blue), without FCA (green), without TPA (red), and without FCA and TPA (pink).. 123

Figure 6.16. Gain (a) and carrier temperature (b) behavior in a strongly absorbing medium pumped at a rate of $0.25\boldsymbol{J}_0$. The external pulse has 1.0 ps (FWHM) duration and 0.1 pJ energy. The curves correspond to calculations with FCA and TPA (blue), without FCA (green), without TPA (red), and without FCA and TPA (pink). All curves are overlapped. 126

Figure 6.17. Gain (a) and carrier temperature (b) behavior in a strongly absorbing medium pumped at a rate of $0.25\boldsymbol{J}_0$. The external pulse has 1.0 ps (FWHM) duration and 1.0 pJ energy. The curves correspond to calculations with FCA and TPA (blue), without FCA (green), without TPA (red), and without FCA and TPA (pink). The gain curves are overlapped. In temperature graph the blue curve is almost overlapped with red, and the green curve overlapped with pink curve. 127

Figure 6.18. Gain (a) and carrier temperature (b) behavior in a strongly absorbing medium pumped at a rate of $0.25\boldsymbol{J}_0$. The external pulse has 1.0 ps (FWHM) duration and 2.0 pJ energy. The curves correspond to calculations with FCA and TPA (blue), without FCA (green), without TPA (red), and without FCA and TPA (pink). The blue curves are almost overlapped with the red, and the green curves are overlapped with pink curve. 128

Figure 6.19. Gain (a) and carrier temperature (b) behavior in a strongly absorbing medium pumped at a rate of $0.25\boldsymbol{J}_0$. The external pulse has 1.0 ps (FWHM) duration and 3.0 pJ energy. The curves correspond to calculations with FCA and TPA (blue), without FCA (green), without TPA (red), and without FCA and TPA (pink). 129

Figure 6.20. Gain (a) and carrier temperature (b) behavior in a strongly absorbing medium pumped at a rate of $0.25\boldsymbol{J}_0$. The external pulse has 1.0 ps (FWHM) duration and 5.0 pJ energy. The curves correspond to calculations with FCA and TPA (blue), without FCA (green), without TPA (red), and without FCA and TPA (pink). 130

Figure 6.21. Gain (a) and carrier temperature (b) behavior in a strongly absorbing medium pumped at a rate of $0.25\boldsymbol{J}_0$. The external pulse has 1.0 ps (FWHM) duration and 25.0 pJ energy. The curves correspond to calculations with FCA and TPA (blue), without FCA (green), without TPA (red), and without FCA and TPA (pink) 131

Figure 6.22. The maximum carrier- lattice temperature difference as a function of external pulse energy in (a) a strongly amplifying (pumped at a rate of $\boldsymbol{J} = 1.75\boldsymbol{J}_0$) medium and (b) a transparent ($\boldsymbol{J} = \boldsymbol{J}_0$) medium. 133

Figure 6.23. The first (a) and second (b) peaks of the carrier- lattice temperature difference as a function of external pulse energy in a strongly absorbing ($\boldsymbol{J} = 0.25\boldsymbol{J}_0$) medium. 134

1. INTRODUCTION

Since the first diode lasers were theoretically considered [1–3] and later experimentally realized [4–8], the temperature dependence of the laser characteristics, especially the gain coefficient, has been identified as one of the important issues in semiconductor laser physics. Generally the optical gain is considered as a function of temperature in reference to the lattice temperature, while the temperature of the electron and hole ensembles are assumed to be equal to the lattice temperature. Possible temperature differences between the carrier ensembles and the lattice vanish on a short time scale ($\sim 10^{-13} - 10^{-12}$ sec) because of phonon emission. Thus, assumption of equal carrier and lattice temperatures is justified unless fast processes in the semiconductor laser medium are considered.

Over the last three decades the development of lasers that produce ultrashort (picosecond and shorter) pulses has lead to new methods of measurements that allow the investigation of ultrafast phenomena in semiconductor media [9, 10]. Besides academic interest, there are several technological problems that require understanding of ultrafast processes in semiconductor optoelectronic devices. These problems originate from the increased demand for high-speed devices with very short response times. The theoretical models that are used to describe the steady-state or slow transient behavior of optoelectronic devices are inadequate on these short time scales and new, improved theories are necessary. In particular, it is important to understand the functional behavior

of the gain with respect to the carrier temperature in semiconductor diode lasers and amplifiers when they interact with ultrashort pulses.

1.1. Gain Nonlinearities in Semiconductors

The results of experiments where the ultrafast response of semiconductor laser amplifiers are investigated indicate that gain nonlinearities in the form of a substantial gain suppression are present on picosecond and femtosecond time scales [11–16]. These experiments emphasize the limitations of theoretical models that describe the dynamics of light-matter interaction in semiconductor optoelectronic devices using the rate equations with a linear gain [17–21].

The term linear gain means that the gain coefficient is approximated as a linear function of the carrier density. To avoid confusion in terminology the gain coefficient and gain function are considered here as distinct terms. The gain or gain (absorption) coefficient is generally defined and measured using the premise of Lambert's law $\boldsymbol{I}(z) = \boldsymbol{I}(z_0)\exp(\boldsymbol{g}z)$:

$$\boldsymbol{g} = \frac{1}{\boldsymbol{I}}\frac{d\boldsymbol{I}}{dz}, \tag{1.1}$$

where $\boldsymbol{I}$ is the intensity of field, and z is the coordinate along the direction of propagation.

The term gain function is used to refer to any function that represents a certain relationship between the gain (absorption) coefficient and other parameters, such as carrier density, temperature, etc. The particular form of the gain function depends upon the relevant structural details of the medium and the model chosen for its calculation, i.e. the gain function represents the gain coefficient in the frame of a particular theoretical

model. For example, in semiconductor laser theories where the matter-field interaction is described using first-order perturbation theory only single-photon band-to-band transitions are included in the gain function calculation. However, there are many processes that contribute to the increase (decrease) of photon numbers in the semiconductor medium that are not explicitly included in the gain function calculation. The influence of these processes is either neglected or taken into account indirectly. Therefore, the gain coefficient defined by Eq. (1.1) and used for experimental measurements is distinguished from the gain function, a term more closely connected to the theoretical or empirical model.

The term gain nonlinearity is usually used to describe the deviation of the gain coefficient from its linear functional dependence on carrier density:

$$g = \gamma(N_c - N_{c0}), \tag{1.2}$$

where γ is the differential gain coefficient and N_{c0} is the carrier density at transparency Here the transparency condition is identified with the condition of zero gain function. Equation (1.2) is purely an empirical expression; it is not the result of any particular theoretical analysis. Nevertheless, the linear form of the gain is widely accepted because it adequately represents the gain coefficient in many practical cases. If any deviation from the linear gain is observed, there is a tendency to account for nonlinearities by simply modifying the right hand side of Eq. (1.2). This procedure usually requires one or more fitting parameters. A typical modified gain function has the form:

$$g = \frac{\gamma\left(N_c - N_{c0}\right)}{\left(1 + sN_p\right)^{\delta}}, \tag{1.3}$$

where N_p is the photon density, and s and δ are fitting parameters (s is also known as the gain suppression coefficient). Depending on the particular system under consideration, the value of parameter δ that best fits the experiment usually ranges between 0.5 and 1.0. The value of s is also obtained by an experimental fitting and is considered to be influenced by many factors such as spectral hole burning (SHB) and carrier heating (CH). For a low intensity field the gain function (Eq. (1.3)) can be approximated by a simpler form:

$$g = \gamma(N_c - N_{c0})(1 - sN_p). \tag{1.4}$$

Although usage of these nonlinear forms of the gain coefficient provides an agreement between theoretical models and experimental results, the physical picture behind these fitting parameters remains vague, especially when it is generally accepted that there are many factors that lead to nonlinear gain behavior.

The nonlinear forms of the gain coefficient (Eqs. (1.3) and (1.4)) are convenient in modeling because they are expressed in terms of easily measured quantities and also because they are able to describe gain nonlinearities (such as gain suppression on a short time scale). However, in these expressions there is no parameter that directly reflects the influence of a specific nonlinear phenomenon. If we are interested in, for example, CH effects then expressions (1.3) or (1.4) do not show explicit dependence in on carrier temperature, carrier energy density, or any other parameter that may describe carrier heating. In fact, there is no way to tell whether an observed gain suppression is the result of carrier heating, spectral hole burning, or other phenomena, unless the gain coefficient is explicitly expressed through parameters that account for these processes.

In order to describe the carrier heating effect in diode laser (amplifier) dynamics, Oraevsky et al. [22, 23] introduced a nonlinear gain function that includes the carrier temperature:

$$g = \gamma\left(N_c - N_{c0} - N_c \beta\, \Delta T / T_l\right), \tag{1.5}$$

where ΔT is the deviation of carrier temperature from that of the lattice, and β is a fitting parameter. This form of the gain function describes gain suppression due to carrier heating; however, it still contains a fitting parameter that needs to be inferred from a quantitative fit to experimental results. Thus, the empirical expressions for the gain function are not adequate for the description of the temperature dependence of the gain and a more accurate theoretical approach is required.

The gain function that is based on a simple free-carrier model or a more sophisticated model for semiconductor medium is much different from expression (1.2) or its nonlinear modifications. The free-carrier quasi-equilibrium theory in a two-band approximation leads to the following expression for the gain function [24]:

$$g = C(\omega, T_l)|\mathbf{M}|^2 \rho_r \left[f(\mu_e, T_e) + f(m_h, T_h) - 1\right] = g(\omega, T_l, T_e, T_h, \mu_e, \mu_h), \tag{1.6}$$

where C is a function that depends on the material parameters and the transition frequency, $\mathbf{M}$ is the transition matrix element, ρ_r is the reduced density of states, f is the Fermi distribution function, and $\mu_{e(h)}$ and $T_{e(h)}$ are the electron (hole) chemical potential and temperature, respectively. This gain function is not convenient for analysis of the laser dynamics. Except for the frequency and perhaps the lattice temperature the other parameters that explicitly influence the gain function are not easily measured. This probably explains why the empirical form of the gain function has general acceptance.

1.2. Semiconductor Laser Dynamics with and without the Gain Function

The gain coefficient (and its functional form) is perhaps the most important characteristic parameter of a semiconductor laser medium. Usually the laser media are described by the material polarization, population inversion, and their relationship with the electromagnetic field. In the case of semiconductor laser media the polarization decays in a time scale ($\sim 10^{-14}$ -10^{-13} sec) which is much shorter than the decay times for the population inversion (carrier lifetime ~ 10^{-9} sec) and the field (photon lifetime ~ 10^{-12} sec) [18]. For very fast relaxation times adiabatic elimination of material polarization becomes possible and one can use the gain function in the semiconductor laser dynamics. If the dependence of the gain on the electromagnetic field and carrier density is found it significantly simplifies investigations by lowering the number of independent variables. Often an empirically obtained linear gain function (1.2) or its modified nonlinear version with one or more fitting parameters (similar to Eq. (1.3)) satisfactorily describe dynamic behavior of the systems under consideration. The accuracy of the simplified dynamic models depends on the functional form of the gain function.

The gain function can also be obtained using theoretical models that are based on our understanding of the structure of semiconductor laser media. In this case no fitting parameters are used, however the theoretical models are based on certain assumptions and, therefore, produce gain functions that represent the gain coefficient with limited accuracy. For example, the gain function (1.6) is derived assuming quasi-equilibrium Fermi-Dirac distribution of carriers. It is obvious that it cannot be used when the carrier ensemble is disturbed in such a way that it is no longer in quasi-equilibrium. In particular, this is the case when spectral hole burning is observed, i.e. there is a dip in the

carrier distribution function. As a result, the carrier temperature becomes a physically meaningless value because the temperature as a thermodynamic parameter is defined only for the systems at equilibrium [25, 26]. The Fermi distribution function with a dip at some energy (spectral hole) is not associated with any particular value of temperature; it is no longer a Fermi-Dirac distribution function. In this case expression (1.6) is not an adequate representation of the gain coefficient.

A non-equilibrium carrier system eventually relaxes and becomes a Fermi ensemble, and only then does the system have a definite temperature which can be determined to be different or not from the lattice temperature. The time scale of relaxation is determined by carrier-carrier scattering and is roughly given by [27, p. 175]

$$\tau_{c-c} \approx 10^5 \boldsymbol{N}_c^{-1}, \tag{1.7}$$

where $\boldsymbol{N}_c$ has units of cm^{-3}. In lasers and amplifiers the carrier density is on the order of 10^{18} cm^{-3} or more, which makes τ_{c-c} about 10^{-13} sec. Experimental results idicate even shorter relaxation times; for example, the experiments with a GaAs sample excited by a femtosecond pulses leads to $\tau_{c-c} \approx 3\times10^{-14}$ sec at $\boldsymbol{N}_c = 10^{17}$ cm^{-3} and $\tau_{c-c} \approx 13\times10^{-15}$ sec at $\boldsymbol{N}_c = 10^{18}$ cm^{-3} [12, 28]. On this time scale the elimination of the polarization is no longer justified; hence, the gain function is no longer an appropriate parameter in the dynamical picture.

For time scales shorter than 10^{-13} sec. the material polarization must be included into the dynamical picture and a microscopic theory is used to describe the semiconductor lasers. In microscopic theories the gain is calculated using its relationship with material polarization ($\boldsymbol{P}$) and the electromagnetic field ($\boldsymbol{E}$) [19]:

$$\boldsymbol{g} \sim \mathrm{Im}\left(\boldsymbol{P}/\boldsymbol{E}\right), \tag{1.8}$$

but the gain function itself is not a dynamic variable in those theories. Currently, there is no well-developed theory that, with proper adjustment, can be used for all types of semiconductor laser media. This situation is partially explained by the diversity of the semiconductor laser media and the complexity of semiconductor materials themselves.

Microscopic theories for semiconductor media as a part of solid state physics have been developed during the last fifty years [29–32]. The current state of these theories can be found in a number of textbooks and review papers [33–35]. Most theoretical models for semiconductor lasers utilize certain analogies between the two-level system and the two-band model of semiconductors by considering semiconductor media as complex ensembles of two-level systems with specific selection rules and line broadening mechanisms. These models are usually described using a density-matrix theory [36].

Interaction of the electromagnetic field with semiconductors can also be described using kinetic theory, which is based on the Boltzmann equation for the carrier distribution function. For example, the theory developed by Galitskii and Elesin [37–39] describes gain suppression, spectral hole burning, and other effects in semiconductor lasers. Both kinetic and density-matrix-based theories lead to rate equations when appropriate approximations are made.

During the past two decades a significant effort has been made to develop a microscopic theory for dynamics in semiconductor laser media that is conceptually similar to Maxwell-Bloch equations for two-level systems [40]. The theory based on Maxwell-Bloch equations for semiconductors is a very effective tool in the description of nonlinear phenomena and spatio-temporal dynamics in semiconductor laser media [19, 41–46]. Progress in this direction is tangible; however, this theory (and most microscopic

theories) require a significant numerical effort and computer CPU time. In most cases a large number of equations must be solved in order to deduce the gain spectrum. Even with modern computers some problems cannot be solved in a reasonable time period. Although microscopic theories can provide accurate descriptions of phenomena in semiconductor laser media, they are rarely used in device modeling and semiconductor laser dynamics. In general, the lack of simplicity, and in many cases lack of clarity in microscopic theories make them unattractive for qualitative analysis and quick estimations, which are usually important for experimentalists. This task is usually left to the rate equations.

1.3. Modified Rate Equations for Semiconductor Laser Dynamics

Rate equations are widely used in semiconductor laser dynamics and device modeling because of their conceptual simplicity and physical clarity. They can be derived phenomenologically [20, 47, 48], from the wave equation [18], or from quantum-mechanical considerations [39, 49] and consist of two differential equations for photon density and for carrier density:

$$\frac{dN_p}{dt} = -\frac{1}{\tau_p} N_p + \Gamma g N_p + \Gamma \beta_{sp} \frac{N_c}{\tau_s}, \tag{1.9a}$$

$$\frac{dN_c}{dt} = J - \frac{N_c}{\tau_s} - g N_p, \tag{1.9b}$$

where τ_p is the photon lifetime, τ_s is the spontaneous lifetime of carriers, Γ is the confinement factor, β_{sp} is the spontaneous emission factor, and J is the effective pumping rate.

This system of equations is a basic form of the rate equations for a semiconductor laser. Depending on the particular problem under consideration, the system of equations (1.9) can be modified to include additional terms or equations. For example, the model based on modified rate equations that describe the dynamic behavior of a semiconductor laser with delayed optical feedback is known as the Lang-Kobayashi model [50]. Modified rate equations can also be used to describe external cavity semiconductor lasers [51], semiconductor microcavity lasers [52, 53], and a variety of other laser structures [54–56].

The rate equations are easily modified to include the gain nonlinearities. No other modification of the rate equations except for the gain function is necessary when a nonlinear gain function of the form (1.3) or (1.4) is used because the gain function is expressed in terms of dynamical variables that are already included into the dynamics. However, when the gain function is expressed in terms of parameters other than photon and carrier densities, then the rate equations need to be modified. For example, when the gain function is used with explicit (carrier) temperature dependence such as Eq. (1.5), then the system of the rate equations (1.9) becomes incomplete. To obtain a closed set of equations, we must modify Eqs. (1.9) to include an equation for the carrier temperature. Conceptual simplicity of the rate equations makes it easy to incorporate a new dynamical variable if necessary. The modified rate equations obtained in such a way are powerful tools for semiconductor laser dynamics. They have the clarity of the rate equations and extend their applicability. Furthermore, on short time scales, the modified rate equations are complementary to microscopic theories. Although less accurate in details compared to the microscopic theories, they offer clear physical interpretations.

1.4. Phenomenology of Carrier Heating Effects

The observation of gain suppression in semiconductor amplifiers on a subpicosecond time scale [11–15] has stimulated an active theoretical effort to describe and interpret these results. SHB and CH are pointed out as one of the main reasons for gain suppression in these systems. In some cases all the observed gain nonlinearities were explained by dynamic carrier heating [13], which triggered special attention to the carrier heating influence on gain dynamics. Although different aspects of the influence of CH on the behavior of diode lasers have also been considered [57–59], the Kesler-Ippen experiment underlines the significance of CH effects on the subpicosecond time scale.

Carrier heating (or dynamic carrier heating) can roughly be described in the following way: excitation of the semiconductor disturbs the ensemble of carriers, which initially have a quasi-Fermi distribution with a temperature (T_c) corresponding to the lattice temperature (T_l). As a result of this excitation the carrier ensemble redistributes to form a quasi-Fermi distribution with a temperature different from the lattice temperature ($T_c \neq T_l$). This is a consequence of the smaller heat capacity of the electron ensemble compared to the heat capacity of the lattice. The electron ensemble is heated almost instantaneously because of the small heat capacity and some time is required for relaxation. During this time the electrons and the lattice have distinct temperatures.

The term, carrier heating, can be misleading when carriers do not form a quasi-equilibrium ensemble because a non-equilibrium ensemble does not have a definite temperature and an actual increase in temperature cannot be calculated or measured. In this case the term means that the system has higher occupation probabilities for carriers in the high-energy states of the band compared to the Fermi distribution. For example, an

external pulse with a carrier frequency larger than that of the bandgap can excite electrons to energy levels deep within the conduction band so that the electron distribution function is no longer given by the Fermi function. In this case the electron system is heated because hot particles (high energy electrons) are added to the electron ensemble or cold particles are removed fr0m it by stimulated emission. The same logic suggests that removing hot particles from the system cools the ensemble; however, this is not always the case (see Chapter 4).

Carrier heating is a result of a variety of processes (see below for details) that involve carrier injection and/or excitation of a semiconductor medium by an electromagnetic field, and the subsequent cascade of recombination processes that take place on different time scales. A description of the individual heating mechanisms is detailed in subsequent chapters.

A most profound result of CH is a gain nonlinearity that is exhibited in the form of gain suppression and recovery on the time scale of the order of a picosecond. Gain suppression due to CH is similar to gain suppression due to SHB – a major suppression factor on a sub-picosecond time scale. However, there are significant differences between CH and SHB. CH influences the medium at all frequencies, i.e. it affects amplifying, absorbing and even the transparent medium, while SHB affects the gain coefficient at certain frequencies and an amplifying medium only. This is the most important difference between CH and SHB, which is simply a dip in the gain spectrum caused by stimulated emission.

Figures 1.1 and 1.2 (pp. 14-15) schematically demonstrate the deformation of the gain spectrum and electron distribution functions in a bulk semiconductor laser medium

due to SHB and CH. In the case of SHB the gain function is affected only when it is above the level of the losses, i.e. only certain frequencies are affected. When CH is considered the gain shifts downward affecting all frequencies.

We emphasize the schematic nature of Figs. 1.1 and 1.2 because in reality, depending on the time scale, SHB and CH may be present simultaneously. For time scales shorter than 0.1 ps SHB is dominant, while CH may last up to several picoseconds or more. Also it is worth mentioning that in the case of CH the transparency photon energy $\hbar\omega_0$, which is determined from the limiting case of the gain condition [1, 2]

$$\hbar\omega \leq \mu_e - \mu_h, \qquad (1.10)$$

is shifted because the chemical potentials of electrons (μ_e) and holes (μ_h) are temperature dependent. The green curve in Fig. 1.1b (p. 14) shows the gain function with fixed chemical potentials.

The theoretical description of CH is complicated because various radiative and non-radiative processes directly or indirectly affect the carrier ensemble. Both microscopic and rate equation approaches are applied to investigate different aspects of the carrier heating effects. Microscopic theories, briefly described in Section 1.2, in principle account for all possible effects in the medium including SHB and CH effects. However, in most cases the modified rate equations appear to be more convenient and widely used in the literature [22, 23, 60–66]. The latter approach requires the inclusion of the carrier temperature (or energy density) in the gain dynamics.

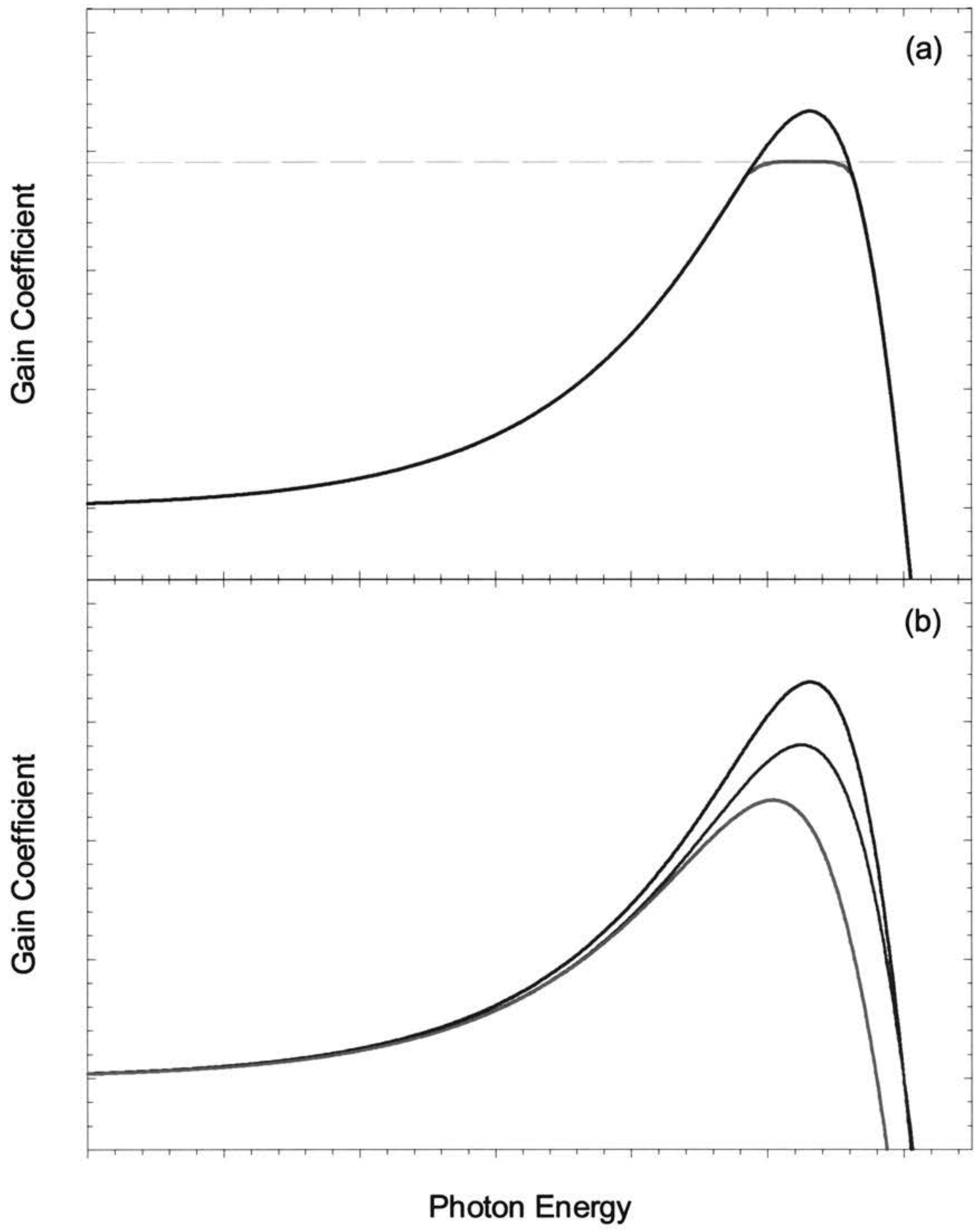

Figure 1.1. Gain function deformations due to (a) spectral hole burning, and (b) carrier heating. The blue curves correspond to undeformed gain function. The red curves correspond to deformed gain functions. The green dashed line in (a) represents the level of losses. The green curve in (b) demonstrates the carrier heating effect with fixed chemical potentials of carriers.

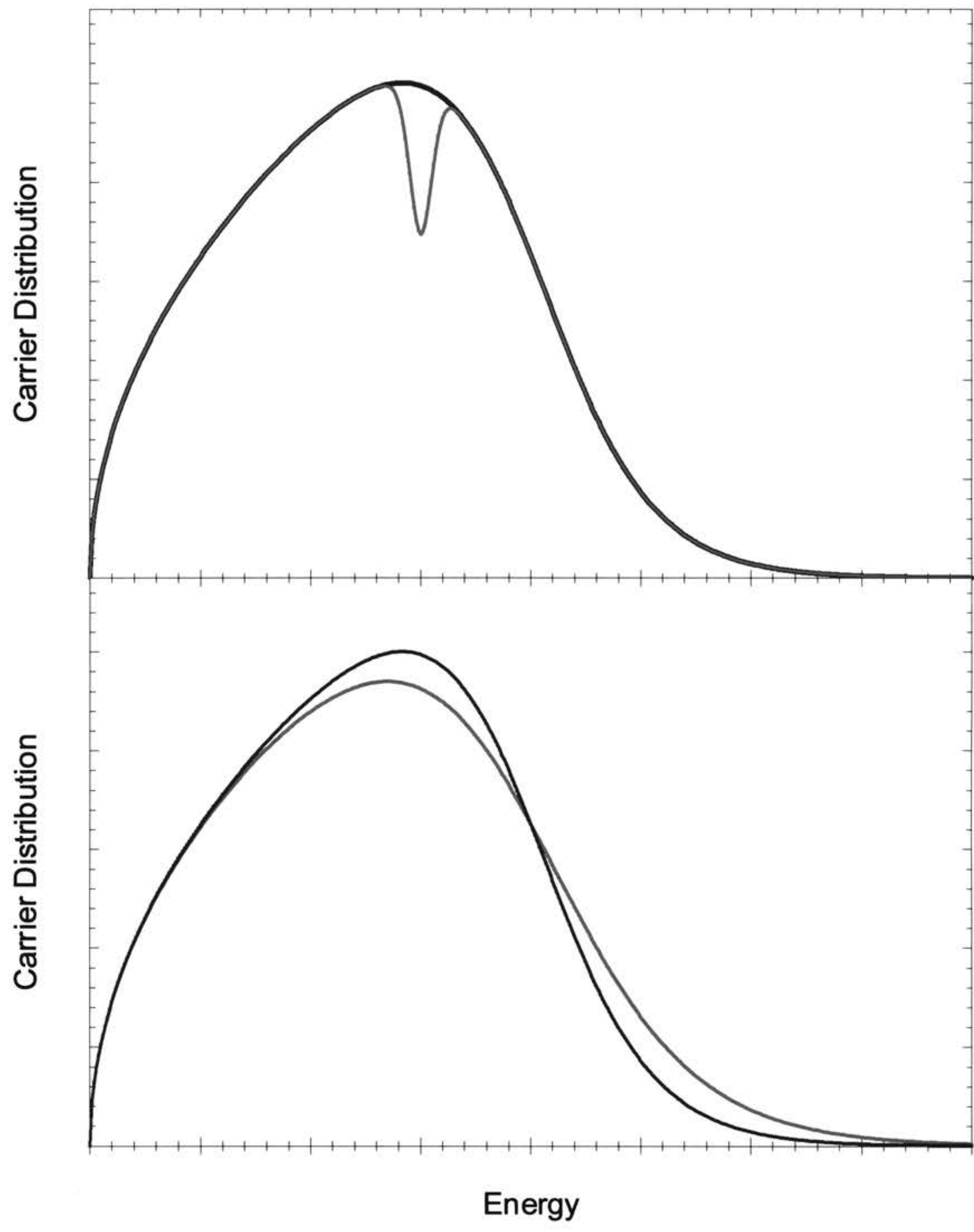

Figure 1.2. Electron distribution function affected by (a) spectral hole burning, and (b) carrier heating. The blue curves correspond to unperturbed distribution function. The red curves correspond to perturbed distribution functions.

The gain (absorption) nonlinearity due to CH can be theoretically described in the same way as all nonlinearities, i.e. by introduction of the nonlinear gain function into the rate equations. For example, the gain function Eq. (1.5) describes gain suppression due to CH, which itself is described by the corresponding carrier temperature increase that is a result of an increased number of photons produced in a medium and/or brought on by an external signal.

1.5. Preview of Thesis

Although the carrier heating influence on gain dynamics has attracted much attention, the dynamic behavior of the carrier temperature is usually not of interest. In most cases the carrier temperature appears only in an ad hoc explanation of the nonlinear behavior of the gain. However, the efficiency of CH by an external signal depends on the gain; furthermore, changes in the gain influence the carrier temperature. This feedback leads to interesting dynamic behavior of both the gain and the carrier temperature. Therefore, the gain dynamics should be considered along with the carrier temperature dynamics.

This thesis reports the investigation of the dynamic behavior of the gain function and the carrier temperature in semiconductor laser media. As a basis for this research we use modified rate equations. The details and the logic behind the model are discussed in Chapter 2. Temperature dynamics of a cw diode laser and the laser response to external picosecond pulses are discussed in Chapter 3. The temperature dynamics of the spontaneously recombining carrier ensemble with a discussion of differences between Fermi and Boltzmann statistics is considered in Chapter 4. Chapter 5 is devoted to gain

and temperature dynamics in semiconductor laser medium close to transparency. The laser medium far from transparency is considered in Chapter 6, where the gain and temperature dynamics is considered for different external-pulse energies. Chapter 7 summarizes the results. The thesis is supplemented with Appendices, which address issues related to certain physical aspects relevant to the model and the derivation of analytical expressions. The results of the investigation are published in the literature [67–70] and have been reported at annual meetings of Optical Society of America [71, 72].

2. MODEL DESCRIPTION

In this chapter we present a model for the theoretical investigation of gain and carrier temperature dynamics in semiconductor laser media. We consider the relationship between the gain coefficient and the carrier temperature through a temperature-dependent gain function. Regardless of the structure of the laser medium (bulk or lower dimensional structures) the theoretical models show that the gain is an explicit function of the carrier temperature. Therefore, the system of rate equations (1.9) must be extended to accommodate the new dynamic variable: the carrier temperature.

The next section describes the model equations, definitions of dynamical variables, the significance of each term, and the physics behind them. The free-carrier and two-photon absorption terms, the gain function, and the carrier energy density equation are described separately in subsequent sections.

2.1. Model Equations

The model equations are:

$$\frac{dN_p}{dt} = -\frac{1}{\tau_p} N_p + \Gamma v_{gr} g N_p + \Gamma \beta_{sp} \frac{N_c}{\tau_s} - v_{gr} s_{FCA} N_c N_p - v_{gr} s_{TPA} N_p^2 + kN_{px}, \qquad (2.1\text{ a})$$

$$\frac{dN_c}{dt} = J - \frac{N_c}{\tau_e} - v_{gr} g N_p + v_{gr} s_{TPA} N_p^2, \qquad (2.1\text{ b})$$

$$\frac{dU}{dt} = Q - \frac{U}{\tau_s} - \frac{U - U_l}{\tau_l} - \hbar\omega v_{gr} g N_p + \hbar\omega v_{gr} s_{FCA} N_c N_p + 2\hbar\omega v_{gr} s_{TPA} N_p^2, \qquad (2.1\text{ c})$$

where N_p is the photon density, N_{px} is the external pulse photon density, N_c is the carrier density, U is the carrier energy density, U_l is the carrier energy density at the lattice temperature, τ_p is the photon lifetime, Γ is the confinement factor, v_{gr} is the group velocity, β_{sp} is the spontaneous emission factor, τ_s is the spontaneous lifetime of carriers, τ_e is the carrier recombination time, τ_l is the energy density relaxation time, s_{FCA} is the free-carrier absorption (FCA) cross-section, s_{TPA} is the two-photon absorption (TPA) cross-section, k is the coupling coefficient, $\hbar\omega$ is the photon energy, g is the gain function (in cm^{-1}), J is the effective carrier injection rate, and Q represents the pumping in energy density equation.

The photon density is related to the electric component of the electromagnetic field, E, through the following expression [18, 20]

$$N_p = nn_{gr}\frac{|E|^2}{8\pi\hbar\omega}, \tag{2.2}$$

where n is the refractive index, n_{gr} is the group velocity index. It is derived in Appendix A (p. 151). In certain cases it is preferable to use the field equation instead of photon density equation. The photon density equation with external signal can be derived from the field equation (see Appendix B, p. 155).

The photon lifetime in the cavity is given by

$$\tau_p^{-1} = \mathbf{v}_{gr}\alpha_c, \tag{2.3}$$

where α_c denotes the cavity losses, which consists of facet losses,

$$\alpha_m = \frac{1}{2L}\ln\left(\frac{1}{R_1 R_2}\right), \tag{2.4}$$

where $\boldsymbol{L}$ is the cavity length, $\boldsymbol{R}_1$ and $\boldsymbol{R}_2$ are facet reflectivities, and internal losses α_i. Usually the internal losses include FCA, scattering and diffraction losses, however because FCA is an important heating factor we include it as a separate term. For a typical semiconductor laser $\alpha_i \approx 40$ cm^{-1} [18], including 10-15 cm^{-1} that is attributed to the FCA [17, 73]. In this theory the internal losses are considered as scattering and diffraction losses only unless specified otherwise.

The second term in Eq. (2.1a) represents the gain or single-photon interband absorption. The gain function, $\boldsymbol{g}$, is discussed in detail in Section 2.4 below. The third term represents the photon density change due to spontaneous recombination of carriers. We identify this term along with the spontaneous recombination rate in the carrier density equation. The spontaneous recombination of carriers plays an interesting role in the temperature dynamics of the carrier ensemble when there is no external signal. This topic is discussed further in Chapter 4. The FCA and TPA terms are discussed in Sections 2.2 and 2.3.

The last term in Eq. (2.1a) describes an external signal. The external signal is included in the model because carrier heating is observed in the interaction of the medium with short optical pulses. The expression for the coupling coefficient is obtained from the following consideration. In steady state and in the absence of gain (or absorption) or other less important effects (i.e. there is no production and loss of photons in the medium), the photon density in the medium must be equal to (1-$\boldsymbol{R}$) times the photon density of the external signal. Thus,

$$\boldsymbol{k} = \frac{1-\boldsymbol{R}}{\tau_p}. \tag{2.5}$$

where $\boldsymbol{R}$ is the power reflection coefficient of the laser facet through which the external signal enters the laser medium. This expression is appropriate for a medium with a low reflectivity facet. In the case of a high reflectivity facet the expression for the coupling coefficient is derived using the coupling coefficient of the field (see Appendix B, p. 155).

The external optical signal is considered as a Gaussian pulse in the following form

$$\boldsymbol{N}_{px}(\boldsymbol{t}) = \frac{\boldsymbol{N}_{px0}}{\sqrt{\pi}\Delta\tau} \exp\left[-\left(\frac{\boldsymbol{t} - \boldsymbol{t}_a}{\Delta\tau} \right)^2 \right]. \tag{2.6}$$

From this expression we obtain the peak photon density of the pulse

$$\boldsymbol{N}_{px}^{\max} = \boldsymbol{N}_{px}(\boldsymbol{t}_a) = \frac{\boldsymbol{N}_{px0}}{\sqrt{\pi}\Delta\tau}. \tag{2.7}$$

The time parameter $\boldsymbol{t}_a$ corresponds to the pulse peak arrival time. The pulse photon density is equal to its half-maximum value $\boldsymbol{N}_{px}^{\max}/2$ when

$$\exp\left[-\left(\frac{\boldsymbol{t} - \boldsymbol{t}_a}{\Delta\tau} \right)^2 \right] = \frac{1}{2}, \tag{2.8}$$

or when $\boldsymbol{t}_{\pm} = \boldsymbol{t}_a \pm \Delta\tau\sqrt{\ln 2}$ and therefore the Full-Width Half-Maximum (FWHM) pulse duration is

$$\Delta\tau\big|_{FWHM} = \boldsymbol{t}_{+} - \boldsymbol{t}_{-} = 2\sqrt{\ln 2}\,\Delta\tau. \tag{2.9}$$

The external pulse energy is defined as

$$\mathcal{E} = \int \boldsymbol{N}_{px}(\boldsymbol{t})\hbar\omega \boldsymbol{dV}, \tag{2.10}$$

where $\boldsymbol{dV} = \boldsymbol{S} \cdot \boldsymbol{cdt}$, $\boldsymbol{S}$ is the external beam cross-section, $\boldsymbol{c}$ is the speed of light in free space, so that

$$\mathcal{E} = \int_{-\infty}^{+\infty} \boldsymbol{N}_{px}(\boldsymbol{t})\hbar\omega \cdot \boldsymbol{Scdt} = \boldsymbol{N}_{px0}\hbar\omega \cdot \boldsymbol{Sc}. \tag{2.11}$$

To consider the transverse profile of the photon density in the external optical beam one must integrate over the transverse plane taking into account N_{px0}, which is not a constant but a function of the transverse coordinates. In this case the external pulse energy is given by

$$\mathcal{E} = \hbar\omega \cdot c \iint N_{px0}(x, y) dxdy \, . \tag{2.12}$$

However, we do not consider this case because the active medium transverse profile is much smaller than the external beam profile and we can take N_{px0} as a constant value. In our calculations we deal with not the total energy of the external pulse, $\mathcal{E}$, but the energy of the portion of the pulse that overlaps the cross section of the active region of the sample, i.e.

$$\mathcal{E}_x = \frac{\tilde{S}}{S} \mathcal{E} \, , \tag{2.13}$$

where $\tilde{S}$ is the cross section of the medium facet.

The carrier density is defined by the integral expression:

$$N_c(\mu, T) = \int \rho(\varepsilon) f(\varepsilon, \mu, T) d\varepsilon \, , \tag{2.14}$$

where $f(\varepsilon, \mu, T)$ is the Fermi-Dirac distribution function, $\rho(\varepsilon)$ is the density of states in the corresponding band, ε is the energy of an individual electron, and μ is the chemical potential. For definiteness, since N_c is the same for electrons and holes (local electroneutrality condition), we consider the words "electron" and "carrier" to be synonymous and we take the zero of energy to be at the top of the valence band.

The effective carrier injection rate is given by

$$J = \eta_{inj} i / q_e V \, , \tag{2.15}$$

where η_{inj} is the efficiency of the carrier injection, i is the bias current, q_e is the

elementary charge, and V is the active volume. The effective injection rate can also be considered as the loss rate of the carriers from the adjacent region to the active region

$$J = N_J / \tau_s , \tag{2.16}$$

where N_J is the carrier density in the adjacent region. This form of the effective pumping rate is useful when the optical pumping is used.

The recombination term in Eq. (2.1b) represents the carrier leakage rate from the active region and the spontaneous carrier recombination rates. The later we split into radiative and non-radiative parts. Several processes contribute to the spontaneous non-radiative recombination of carriers; such as the recombination involving traps and Auger recombination [74]. The rate of recombination involving traps is proportional to the carrier density over a wide range of N_c. The Auger recombination rate is proportional to N_c^3, and for $N_c \leq 10^{19}$ cm^{-3} is significantly less than the spontaneous radiative and trap-involving recombination rates.

In general, the carrier recombination time, τ_e, can be written as

$$\frac{1}{\tau_e} = A + BN_c + CN_c^2 , \tag{2.17}$$

where A is a coefficient that describes the carrier leakage and recombination via traps, B is bimolecular recombination coefficient [20], and C is the Auger recombination coefficient. The spontaneous recombination rate BN_c^2, which is commonly used in the literature, corresponds to the non-degenerate carrier ensemble. In some cases linear dependence on N_c is used [75]. In Appendix C (p. 158) we show that the spontaneous radiative recombination is proportional to N_c^2 for non-degenerate and to N_c for degenerate carrier ensemble. In the semiconductor laser the carrier ensemble is

degenerate, therefore we use the spontaneous recombination term which is proportional to the carrier density. An approximate expression that works for both degenerate and non-degenerate semiconductors is considered in Appendix C (p. 158), where the spontaneous radiative recombination is discussed in detail and an expression for spontaneous recombination rate is derived for both degenerate and non-degenerate carrier ensembles. If we ignore nonradiative recombination processes and Auger recombination (which is justified for moderate carrier densities $N_c \leq 10^{19}$-10^{20} cm^{-1}) then τ_e is equal to the spontaneous lifetime of carriers τ_s.

2.2. Free Carrier Absorption

Free-carrier absorption is an intraband indirect transition of carriers (the energy change is accompanied by momentum change). From energy and momentum conservation laws it follows that free carriers cannot absorb photons without assistance of phonons or impurities [76, 77].

Formally, we define the FCA coefficient in the same way as the interband (gain) absorption coefficient and it is related to the time rate of change of the photon density as follows:

$$\alpha_{FCA} = -\frac{1}{I}\frac{dI}{dz}. \qquad (2.18)$$

In the classical description the free-carrier absorption in semiconductors is treated in the same manner as in the theory of metals, i.e. on the basis of the Drude model. The only difference is that in semiconductors the free carrier concentration is several orders of magnitude less than in metals.

The free-carrier absorption coefficient calculated classically is given by [76– 79]

$$\alpha_{FCA}(\omega) = \frac{4\pi N_c e^2}{m_{eff} c n} \frac{\tau_m}{1+(\omega\tau_m)^2}, \tag{2.19}$$

where e is the elementary charge, m_{eff} is the effective mass, and τ_m is the momentum relaxation time. In the low-frequency limit ($\omega\tau_m << 1$)

$$\alpha_{FCA}(\omega) = \frac{4\pi N_c e^2}{m_{eff} c n} \tau_m = \frac{4\pi\sigma}{cn}, \tag{2.20}$$

where σ is the low-frequency conductivity. Since we are interested in near-infrared and optical frequencies, i.e. the high frequency limit where $\omega\tau_m >> 1$,

$$\alpha_{FCA}(\omega) = \frac{4\pi N_c e^2}{m_{eff} c n \omega^2} \frac{1}{\tau_m}. \tag{2.21}$$

In general, the FCA coefficient has a more complicated frequency dependence than Eq.(2.21) suggests, because τ_m depends on the character of the involved scattering processes [27, 79]. Experimental results suggest that $\alpha_{FCA} \sim \omega^{-p}$, where the parameter p varies between 1.5 and 3 [77, 80]. Note that because α_{FCA} is inversely proportional to the effective mass, the holes are less affected by FCA than electrons.

In our model we use the FCA cross-section as a parameter instead of α_{FCA}. Comparing the time rate of change of the photon density that is due to FCA (see Eq. (A.17) in Appendix A, p. 154).

$$\frac{dN_p}{dt} = -v_{gr} \alpha_{FCA} N_p. \tag{2.22}$$

With the FCA term in (2.1a) we obtain

$$s_{FCA} = \frac{\alpha_{FCA}}{N_c}. \tag{2.23}$$

Using s_{FCA} as a parameter is more appropriate for the problems we are considering because in this case the carrier density dependence in the dynamic equations is explicit. Indeed, the frequency dependence of s_{FCA} is implied.

The free-carrier absorption is usually considered as a minor factor in semiconductor laser dynamics and is often ignored. However, FCA is one of the major heating factors and must be always present in carrier energy density equation, even if one can neglect the FCA term in the photon density equation. Finally, there is no FCA term in (2.1b) because it does not affect the carrier density.

2.3. Two-Photon Absorption

Most experiments where the gain suppression that is attributed to carrier heating is observed use the pump-probe technique [9]. Existence of two overlapping pulses in the medium increases the probability of TPA, however, the effect in most experiments is usually negligible, and consequently most carrier heating theories do not include TPA as a serious heating factor either. Mark and Mørk used TPA to explain a negative component opposing SHB in the absorption region, near the transparency point [16]. In our theory we are interested in the heating effect of TPA, which could be significant when high-energy external pulses are interacting with the medium.

The TPA coefficient is defined phenomenologically as follows

$$\alpha_{TPA} = -\frac{1}{I^2}\frac{dI}{dz}. \tag{2.24}$$

The quantum mechanical consideration that uses the second-order perturbation theory leads to the following expression [81–83]

$$\alpha_{TPA} = K \frac{\sqrt{E_p}}{n^2 \varepsilon_g^3} \left(2\hbar\omega/\varepsilon_g - 1 \right)^{3/2} \left(\hbar\omega/\varepsilon_g \right)^{-5}. \tag{2.25}$$

Here

$$K = \frac{2^9 \pi}{5\sqrt{m_0}} \frac{e^4}{c^2}, \tag{2.26}$$

and

$$E_p = 2\frac{|p_{cv}|^2}{m_0}, \tag{2.27}$$

where m_0 is the free electron mass (not the effective mass) and p_{cv} is the interband momentum matrix element. K is a material-independent constant equal to 1940 in units such that α_{TPA} is measured in cm/GW. E_p is a nearly material-independent constant and for most direct gap semiconductors is equal to 21 eV [83]. Comparison of the theoretical expression with experimental results for α_{TPA} indicates that Eq. (2.25) underestimates TPA coefficient several times. To overcome this discrepancy the parameter K is adjusted so that α_{TPA} fits the experimental results [83].

As was pointed out in the previous section, in our theory it is preferable to work with absorption cross-sections rather than coefficients. The TPA cross-section can be obtained in the following way. First, we find the time rate of change for photon density at a given position using (2.24) and (A.15) (see Appendix A, p. 153) so that

$$\frac{dN_p}{dt} = -v_{gr}\alpha_{TPA}\left(\hbar\omega v_{gr}\right)N_p^2. \tag{2.28}$$

Now comparing the right hand side of Eq. (2.28) with the TPA term in Eq. (2.1a) we obtain

$$s_{TPA} = \alpha_{TPA} v_{gr} , \tag{2.29}$$

We note that because of the band-gap energy dependence on carrier density the value of α_{TPA} will change with the carrier density, however it does not change significantly when the change in carrier density is within two orders of magnitude. We have the TPA term in all dynamic equations because TPA affects all dynamical variables.

2.4. Gain Function

In this section we consider a simple model for the medium, which allows us to obtain an analytical expression for the gain function in order to describe the carrier temperature dynamics in a semiconductor laser media. Because a simple analytical expression for the gain function is not available we need an approximate analytical expression. We are interested in such an approximation because any approximation of the gain function that contains the carrier temperatures should intrinsically account for gain nonlinearity due to carrier heating.

In Eq. (1.6) the electron and hole temperatures appear in the gain function through the corresponding distribution functions:

$$f(\varepsilon_e, \mu_e, T_e) - \frac{1}{2} + f(\varepsilon_h, \mu_h, T_h) - \frac{1}{2} = \frac{1}{2}\left\{ \tanh\left[\frac{\mu_e - \varepsilon_e}{2k_B T_e}\right] + \tanh\left[\frac{\mu_h - \varepsilon_h}{2k_B T_h}\right]\right\}, \tag{2.30}$$

where ε_e and ε_h are electron and hole energies respectively, and k_B is the Boltzmann constant. By choosing the top of the valence band to be the zero level of energy one can write:

$$\varepsilon_e = \varepsilon_g + \left(\hbar\omega - \varepsilon_g\right)\overline{m}/m_e \,, \tag{2.31a}$$

$$-\varepsilon_h = \left(\hbar\omega - \varepsilon_g\right)\overline{m}/m_h \,, \tag{2.31b}$$

where $\overline{m} = m_e m_h / \left(m_e + m_h\right)$, $m_{e(h)}$ is the electron (hole) effective mass, and ε_g is the bandgap energy. From Eqs. (2.31) we obtain:

$$\varepsilon_e = \varepsilon_g - \frac{m_h}{m_e}\varepsilon_h . \tag{2.32}$$

At zero temperature the highest energy that the carriers can have is equal to their chemical potential:

$$\mu_e = \varepsilon_g - \frac{m_h}{m_e}\mu_h . \tag{2.33}$$

For non-zero temperatures relation (2.33) is not exact but remains a good approximation even at room temperature. Using the above relations we can write the right hand side of Eq. (2.30) as

$$\frac{1}{2}\left\{\tanh\left[\frac{\mu_e - \varepsilon_e}{2k_B T_e}\right] + \tanh\left[\left(\frac{m_e}{m_h}\frac{T_e}{T_h}\right)\frac{\mu_e - \varepsilon_e}{2k_B T_e}\right]\right\}. \tag{2.34}$$

Here we note that the argument of the second hyperbolic tangent is much smaller than that of the first because

$$\frac{T_e}{T_h}\frac{m_e}{m_h} << 1 , \tag{2.35}$$

which is guaranteed by the small electron-hole effective mass ratio and provided that the hole temperature is close to the electron temperature. The later condition is usually satisfied because the electron-hole scattering process ensures energy exchange between both carrier ensembles, especially for high carrier densities [84]. Thus, Eq. (2.30) along

with expression (2.34) and provided that condition (2.35) is satisfied indicates that the gain function has a much weaker dependence on hole temperature variations than on electron temperature variations. As a result we neglect the second term in Eq. (2.30):

$$f(\varepsilon_e, \mu_e, T_e) + f(\varepsilon_h, \mu_h, T_h) - 1 \cong \frac{1}{2} \tanh\left[\frac{\mu_e - \varepsilon_e}{2k_B T_e}\right]. \tag{2.36}$$

Therefore, it is sufficient to consider only the electron dynamics.

Using the previous argument, the gain function (1.6) can be written as

$$g = G(\omega) \tanh\left(\frac{\mu_e - \varepsilon_e}{2k_B T_e}\right), \tag{2.37}$$

where ε_e is given by Eq. (2.30a). For simplicity of formulas from now on we will drop the sub-index e. The frequency-dependent function $G(\omega)$ in (2.37) has the form [24]:

$$G(\omega) = \frac{2q_e^2 |M|^2}{ncm_0^2 \omega} \left(\frac{2\overline{m}}{\hbar^2}\right)^{3/2} \sqrt{\hbar\omega - \varepsilon_g}\ , \tag{2.38}$$

However expression (2.37) combined with Eq. (2.38) does not fit experimental data for the gain function very well. That is, the square-root dependence on photon energy does not fit experimental data. Gain spectra in semiconductors show tail states below the band edge that modify the density of states [17, 18]. The origin of the exponential tail below the conduction band is explained by the fluctuation of the periodic potential of the lattice, which is caused by dopants [74, 85–87]. Even in pure semiconductors a tail below the conduction band is observed experimentally and is known as Urbach's tail [32, 33, 88–90]. The tail states in a pure material, in particular, can be explained as a result of exciton-phonon interactions that lead to broadening of excition absorption spectrum. As a result the exciton absorption spectrum merges with the fundamental absorption edge of the conduction band. The resulting absorption

spectrum has an exponential tail below the conduction band. This justifies the exponential form of the density of states for electrons in the model for a laser medium with an undoped active region.

In order to have a more realistic form of the gain function that is close to the experimental gain spectra in our calculations we use Rivlin's model [47, 48], which approximates the electron density of states near the band edge as an exponential. Rivlin's model is based on homostructure lasers and describes a diode laser made of a p-n junction where the p-type dopants form narrow acceptor levels at the top of the valence band. Therefore, the density of states for holes is approximated by a δ-function. The density of states for electrons is approximated by the exponential function

$$\rho(\varepsilon) = \rho_t \exp\left(\frac{\varepsilon}{\varepsilon_t}\right), \tag{2.39}$$

with

$$\rho_t \equiv \frac{\xi}{\varepsilon_t} \exp\left(-\frac{\varepsilon_g}{\varepsilon_t}\right), \tag{2.40}$$

where ξ is the density of the dopants and ε_t is an empirical band tail parameter. This density of states function merges with the square-root function that is obtained from the free-carrier model for a semiconductor material

$$\rho_e(\varepsilon) = \left(\frac{2\boldsymbol{m}_e}{\hbar^2}\right)^{3/2} \sqrt{\varepsilon - \varepsilon_g}\,. \tag{2.41}$$

This model allows to obtain an analytical form for the gain function that works very well not only for homostructure lasers but also for heterostructure lasers.

Currently produced semiconductor lasers, which are made of a bulk material, are

heterostructure lasers with an active region that is made of undoped material. For this type of laser we can argue that a model similar to Rivlin's model for a semiconductor laser medium is also applicable. The δ-function-like density of states for holes can be justified in the following way. The majority of the optical transitions are taking place between the heavy-hole valence band and the conduction band [17, 19]. Because of the large effective mass ratio of the holes and electrons the interband transitions take place between a very narrow strip on top of the valence band, which can be approximated by the δ-function, and a wide region around the bottom of the conduction band, which can be approximated by exponential function. Also, this large effective mass ratio means that the reduced density of states is almost equal to the electron density of states [20]

$$\rho_r^{-1} = \rho_e^{-1} + \rho_h^{-1} \approx \rho_e^{-1} \tag{2.42}$$

Thus, in Rivlin's model the gain function has the form of Eq. (2.37) with the coefficient

$$\boldsymbol{G}(\omega) = \frac{\boldsymbol{n}_g \hbar \pi^2 \boldsymbol{c}^2}{\tau_s \omega^2 \boldsymbol{n}^3} \frac{\xi}{\varepsilon_t} \exp\left(-\frac{\varepsilon_g - \hbar\omega}{\varepsilon_t}\right), \tag{2.43}$$

for transitions from the band edge including tail states. For transitions from higher energy states of the conduction band Eq.(2.38) is used as long as the band can be considered as parabolic. For moderate injection rates most of the stimulated transitions occur near the band edge where Eq. (2.33) is applied.

In heterostructure lasers, where the active region is not necessarily doped, the parameter ξ can also be considered an empirical parameter that can be deduced from experimental absorption curves. The material parameters (refractive index, bandgap, etc.) depend on the lattice temperature and photon frequency. Although expression (2.43) is

derived for homostructure lasers [17, 19], it represents the temperature and frequency dependence of the gain function for heterostructure lasers very well. Figure 2.1 (p. 34) demonstrates the behavior of the gain (Eqs. (2.37) and (2.43)) as a function of the photon energy for a fixed temperature and chemical potential. For current theory the most important property of the gain function is its temperature dependence, which is represented by Eq. (2.37) very well. This temperature dependence is the same for even the low-dimensional laser media. Of course, $G(\omega)$ is different for lower dimensional structures because it is directly proportional to the reduced density of states.

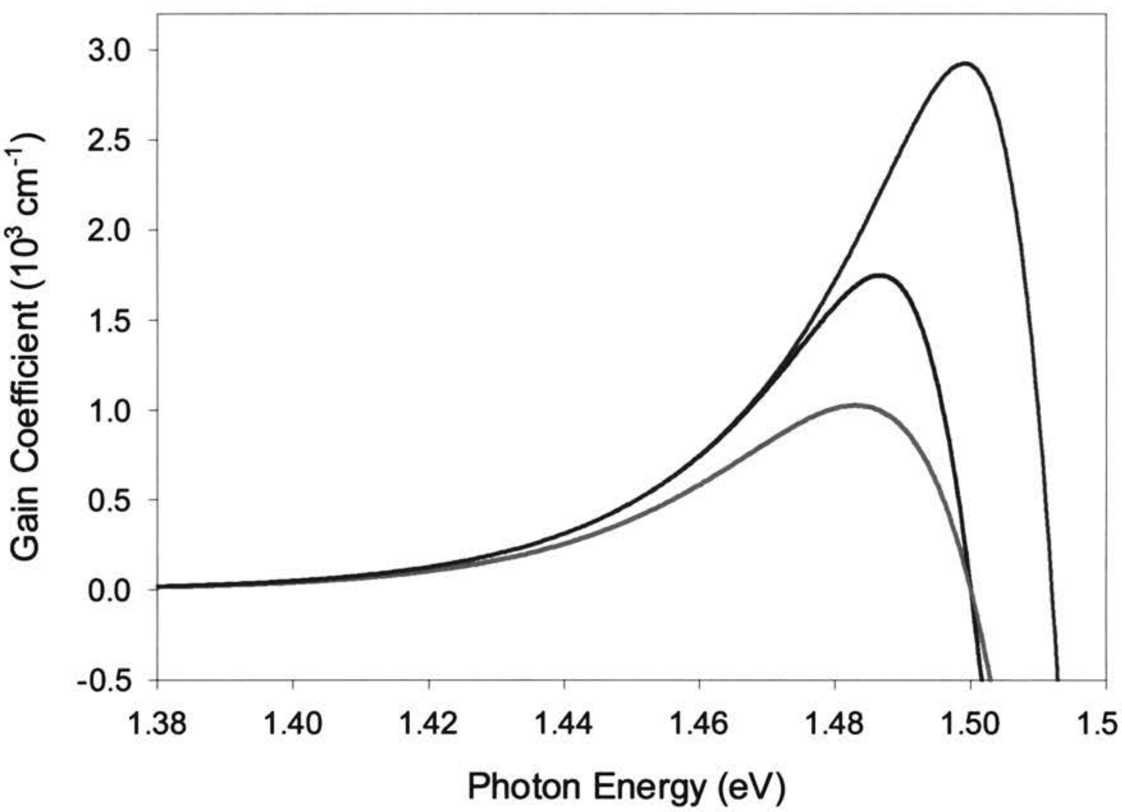

Figure 2.1. The gain coefficient as a function of photon energy for fixed carrier temperature and chemical potential calculated from Eq. (2.37). The expression (2.43) is used for G(ω). The blue and red curves correspond to different temperatures ($T_{red} > T_{blue}$). The blue and green curves correspond to different chemical potentials ($\mu_{blue} < \mu_{green}$). The material parameters used for these calculations correspond to GaAs.

2.5. Carrier Energy Density Equation

The carrier energy density equation is a major extension of the rate equations that makes it possible to describe the carrier heating effects. We begin with the definition of carrier energy density

$$U(\mu,T) = \int \varepsilon\rho(\varepsilon) f(\varepsilon,\mu,T)d\varepsilon \tag{2.44}$$

The similarity of this integral with Eq. (2.14) suggests that the carrier energy density equation can be derived along with the carrier density equation using semiclassical density-matrix equations (see, for example, Refs [91] and [92] for details). The resulting equation is similar to Eq. (2.1c), however, it does not include FCA and TPA. We include them phenomenologically. The FCA term is present in the photon density equation as an additional loss factor and in the energy density equation as a heating factor. There is no FCA term in the carrier density equation because FCA is an intraband process and does not change the carrier density. However, there is a TPA term in all equations. We ignore intraband (i.e. free-carrier) TPA absorption as a process with much smaller probability compared with interband TPA.

In general, all terms in the carrier energy density equation reflect the influence of processes that are included in either the photon density or the energy density equations. As a result the equation for carrier energy density can be constructed from ordinary rate equations. Below we describe each term in Eq. (2.1c) and its origin.

We start with the pumping term Q. In general, it is an independent external factor. However in some cases it is possible to express this term explicitly via the carrier and lattice temperatures, the injection current and other relevant parameters. This requires information about the relationship among the dynamical parameters, which is

discussed in the next section. We address the issue of the pumping term of Eq. (2.1c) separately in Section 2.7 (p. 42).

The second term in Eq. (2.1c) represents carrier energy loss due to spontaneous recombination and is analogous to the spontaneous radiative recombination term in the carrier density equation. The influence of spontaneous recombination on carrier temperature is a topic of special discussion and is considered in Chapter 4. The third term accounts for the energy density relaxation due to interaction with the lattice and is assumed to be exponential with a characteristic time τ_l determined by carrier-lattice interactions. The parameter $\boldsymbol{U}_l$ is the carrier energy density at the temperature of the lattice $\boldsymbol{U}_l = \boldsymbol{U}_c(\mu, \boldsymbol{T}_l)$.

The time parameter τ_l is related to the electron energy relaxation time in the band. The highly excited carriers transfer energy to the lattice by phonon emission (intravalley electron-phonon scattering). For both acoustic and optical phonons the longitudinal modes dominate the transverse modes [78]. The scattering between electrons and acoustic phonons is quasi-elastic and leads to mainly electron momentum relaxation. This is a result of energy and momentum conservation that restricts the scattering by acoustic phonons to long-wavelength modes [27, 77]. The same restriction applies to the optical phonons but their energy is higher and as a result the energy relaxation is mainly due to longitudinal optical (LO) phonon emission. The energy of LO phonons is about 30 meV and highly excited electrons emit many phonons during the relaxation. As a result, the energy relaxation time depends on the electron energy.

Table 2.1 below contains several values for energy relaxation time τ_{LO} due to LO phonons with a corresponding number of emitted LO phonons ν:

$$\nu = \frac{\varepsilon - \varepsilon_g}{\hbar\Omega_{LO}}, \tag{2.45}$$

where $\hbar\Omega_{LO}$ is the LO phonon energy. The numerical values in Table 2.1 are inferred from Fig. 5.3 in Ref. [77] (p.203).

Table 2.1. Electron Energy Relaxation Times

ν	5	10	15	20
τ_{LO} (sec)	3×10^{-13}	5×10^{-13}	6×10^{-13}	7×10^{-13}

The carrier energy density relaxation time τ_l is related to the carrier energy relaxation time through the integral

$$\frac{1}{\tau_l} = \frac{\int \frac{1}{\tau_{LO}(\varepsilon)} \varepsilon\rho(\varepsilon) f(\varepsilon,\mu,T) d\varepsilon}{\int \varepsilon\rho(\varepsilon) f(\varepsilon,\mu,T) d\varepsilon}. \tag{2.46}$$

In our theory we consider τ_l as a constant and use $\tau_l = 0.5$ ps in numerical simulations.

The last three terms in Eq. (2.1c) represent the major heating (or cooling) factors, namely, single-photon interband transitions, free-carrier absorption (FCA), and two-photon absorption (TPA). The energy density variation due to these processes is intuitively understandable and the signs of each term in Eq. (2.1c) represent either an increasing or decreasing effect. However, the energy density increase (decrease) does not imply that the carrier temperature also increases (decreases). For example, consider the energy change due to interband transitions[1]. Carrier absorption leads to an increase in

[1] Throughout this thesis the term *interband transitions* refers to *the single-photon interband transitions*)

carrier energy density and the corresponding term ($-\hbar\omega v_{gr} g N_p$) is positive because $g < 0$ for the absorbing medium. For an amplifying medium ($g > 0$) a decrease in carrier energy density occurs, however the carrier temperature increases because only cold carriers satisfy the gain condition (Eq. (1.10)) and their stimulated recombination leaves the carrier ensemble with hot carriers. Thus, photon emission leads to carrier heating. Does this mean that the single photon absorption leads to carrier cooling? Absorption leads to the increase in carrier density and therefore the energy per particle should decrease, however we cannot answer this question unambiguously. The dynamic variables have a mutual influence so the effect of each process must be considered along with other processes.

In order to be specific, we correlate carrier heating (cooling) with the carrier temperature increase (decrease). The example in the previous paragraph demonstrates that the carrier temperature and energy density do not adequately represent each other. In order to have a closed set of equations in the system Eqs. (2.1) we must either replace Eq. (2.1c) by the carrier temperature equation or supplement these equations with a relationship between dynamic variables.

The form of the gain function Eq. (2.37) suggests that we need relationships between the carrier density and the chemical potential, and between the carrier temperature and carrier energy density. In fact, we have five dynamic variables: N_p, N_c, U, μ, and T; any pair of functions taken from the different sets {N_c, μ} and {U, T} along with N_p may be chosen as a set of dynamical variables for Eqs. (2.1).

The carrier temperature equation is derived from a mathematical manipulation of

the carrier density and carrier energy density equations. Using the differential relationship between functions it can be written formally as:

$$\frac{dT}{dt}=\left(\frac{\partial U}{\partial T}\frac{\partial N_c}{\partial \mu}-\frac{\partial U}{\partial \mu}\frac{\partial N_c}{\partial T}\right)^{-1}\left(\frac{\partial N_c}{\partial \mu}\frac{dU}{dt}-\frac{\partial U}{\partial \mu}\frac{dN_c}{dt}\right). \tag{2.47}$$

The carrier temperature equation obtained in this way still requires the knowledge of the functional relationship between the dynamic variables and does not simplify the problem. Note, that the carrier temperature equation has a rather simple form when the electron ensemble is assumed to obey the Boltzmann statistics [22, 23]. This assumption is valid for low carrier densities. The problems we are interested in deal with a carrier ensemble that obeys Fermi statistics. If analytical expressions of the functions $N_c = N_c(\mu,T)$ and $U_c = U_c(\mu,T)$ are known then it is more convenient to work with the carrier density equation which is mathematically simpler and intuitively clearer.

2.6. Relations Among Dynamic Variables

The system of equations (2.1) needs to be supplemented by expressions that describe the relationships among the dynamic variables. The mathematical difficulty here is associated with the integrals that contain the Fermi function. In general, these integrals do not have analytical solutions. Nevertheless, certain assumptions allow for the derivation of satisfactory approximate expressions. Below we discuss two methods for calculation of the analytical expressions for $N_c(\mu,T)$ and $U_c(\mu,T)$.

In Appendix D (p. 162) we derive an expression that approximates integrals of the following form

$$I = \int_0^\infty \rho(\varepsilon) f(\varepsilon) d\varepsilon, \tag{2.48}$$

where $\rho(\varepsilon)$ is an arbitrary differentiable function and $f(\varepsilon)$ is the Fermi-Dirac distribution function. This method of calculation uses the Taylor expansion of $\rho(\varepsilon)$. By applying the approximate expression obtained in Appendix D (p. 162) we can calculate the integrals (2.14) and (2.44) for both the parabolic band edge and the exponential band tail models. Details of these calculations can be found in Appendix E (p. 166).

The second method of calculation uses the following approximation for the Fermi-Dirac function:

$$f(\varepsilon,\mu,T) = \begin{cases} 1 - 0.5\exp[(\varepsilon-\mu)/k_B T], & \varepsilon \le \mu \\ 0.5\exp[(\mu-\varepsilon)/k_B T], & \varepsilon > \mu \end{cases}. \tag{2.49}$$

This approximation is more accurate for low temperatures and exact at zero temperature. Figure 2.2 (p. 41) demonstrates the degree of accuracy of the chosen approximation. The expressions for $N_c(\mu,T)$ and $U_c(\mu,T)$ based on this approximation are derived in Appendix F (p. 169).

The degree of accuracy for the expressions that use both methods mentioned above is about the same. Mathematically, the first method manipulates the density of states while the second method manipulates the distribution function. In both cases the resulting expressions are more accurate for low temperatures. The expressions that are obtained and based on approximation (2.49) are particularly simple. An advantage of using Eq. (2.49) is the possibility of calculating the integrals with a finite upper limit, which becomes necessary when the pumping terms are calculated (see Section 2.7, p. 42).

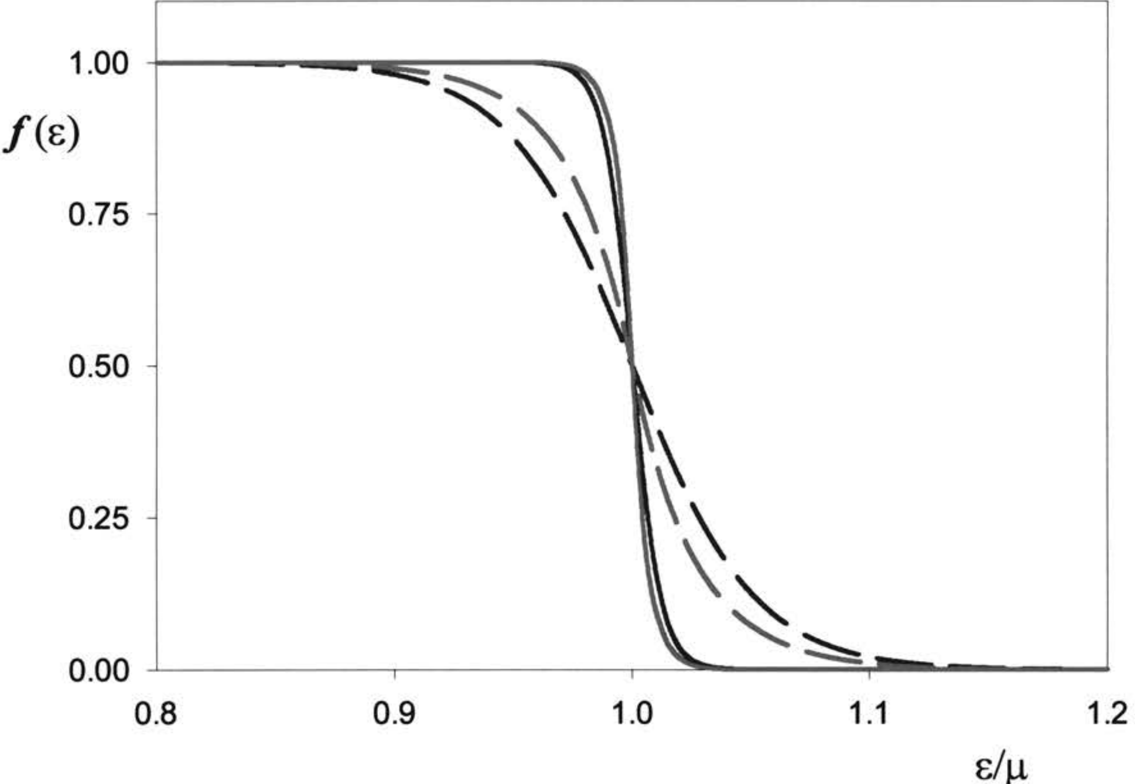

Figure 2.2. Exact and approximate Fermi functions at 70K (solid lines) and 300K (dashed lines). The exact Fermi functions (blue lines) are plotted according to Eq.(D.2) (p. 162); the approximate Fermi functions (red lines) are plotted according to (Eq.(2.49)).

The model for the medium that we choose for our theory (see Section 2.4) uses the conduction band with an exponential band tail. The expressions for this case are:

$$\boldsymbol{N}_c = \frac{\rho_t \varepsilon_t}{1-\theta^2}\exp\left(\frac{\mu}{\varepsilon_t}\right), \tag{2.50}$$

$$\boldsymbol{U} = \boldsymbol{N}_c\left\{\mu - \varepsilon_t \frac{1-3\theta^2}{1-\theta^2}\right\}, \tag{2.51}$$

where we introduce the dimensionless temperature $\theta = \boldsymbol{k}_B \boldsymbol{T}_e / \varepsilon_t$. From these expressions one can calculate the chemical potential, carrier temperature and hence the gain coefficient at any given moment, thus making it possible to follow the behavior of all the dynamic variables.

2.7. The logic behind the pumping term

Having analytical expressions for $N_c(\mu,T)$ and $U_c(\mu,T)$ clarifies the meaning of the pumping term Q in Eq. (2.1c). The pumping term in this equation has the meaning of an effective energy flow into the active region due to the carrier injection. In general, Q is an independent parameter of the problem. However, it can be expressed explicitly via other dynamical variables; in particular, one can express Q in terms of the effective pumping rate J. This can be done using the fact that Q is related to the pumping term in carrier density equation J in the same way as U is related to N_c.

We consider the carrier injection as an effective carrier density decay away from the adjacent regions into the active region:

$$J = \frac{N_J}{\tau_s}, \tag{2.52}$$

where

$$N_J = \int_0^\infty \rho(\varepsilon) f(\varepsilon,\mu_J,T_l) d\varepsilon . \tag{2.53}$$

The chemical potential μ_J must be larger than the chemical potential inside the active region in order to ensure the current flow through the diode (semiconductor laser is a forward biased diode). We assume that the carrier temperature in Eq. (2.53) is equal to that of the lattice because the injected carriers before reaching the active region interact with the lattice long enough to reach a common temperature.

Using the results of Appendix F, namely Eq. (F.20) (p. 173) we obtain

$$J = \frac{1}{\tau_s} \frac{\rho_0 \varepsilon_d}{1-\theta_l^2} \exp\left(\frac{\mu_J}{\varepsilon_d}\right). \tag{2.54}$$

Similarly for the pumping term in Eq.(2.1c) we can write

$$\boldsymbol{Q} = \frac{1}{\tau_s}\int_0^{\infty} \varepsilon\rho(\varepsilon)\boldsymbol{f}(\varepsilon,\mu_J,\boldsymbol{T}_l)d\varepsilon \; . \tag{2.55}$$

This integral is calculated in the same way as $\boldsymbol{U}$ in Appendix F (p. 169) and the result is

$$\boldsymbol{Q} = \frac{\boldsymbol{N}_J}{\tau_s}\left\{\mu_J - \varepsilon_t \frac{1-3\theta_l^2}{1-\theta_l^2}\right\} = \boldsymbol{J}\left\{\mu_J - \varepsilon_t \frac{1-3\theta_l^2}{1-\theta_l^2}\right\}. \tag{2.56}$$

Using Eq. (2.54) we obtain an expression for μ_J:

$$\mu_J = \varepsilon_t \ln\left[\boldsymbol{J}\tau_s \frac{\left(1-\theta_l^2\right)}{\rho_t\varepsilon_t}\right], \tag{2.57}$$

and thus obtain an expression for $\boldsymbol{Q}$ in terms of known parameters and the effective injection rate:

$$\boldsymbol{Q} = \boldsymbol{J}\varepsilon_t\left\{\ln\left[\boldsymbol{J}\tau_s \frac{\left(1-\theta_l^2\right)}{\rho_t\varepsilon_t}\right] - \frac{1-3\theta_l^2}{1-\theta_l^2}\right\}. \tag{2.58}$$

Expression (2.58) is obtained assuming that there are no barriers to separate the active region from adjacent regions. Now suppose that before entering the active region the carriers must overcome an energy barrier of height ε_b. In this case the injection rate with a barrier $\boldsymbol{J}_b$ can be written as

$$\boldsymbol{J}_b = \frac{1}{\tau_s}\int_{\varepsilon_b}^{\infty} \rho(\varepsilon)\boldsymbol{f}(\varepsilon,\mu_J,\boldsymbol{T}_l)d\varepsilon = \boldsymbol{J} - \frac{1}{\tau_s}\int_0^{\varepsilon_b} \rho(\varepsilon)\boldsymbol{f}(\varepsilon,\mu_J,\boldsymbol{T}_l)d\varepsilon \equiv \boldsymbol{J} - \tilde{\boldsymbol{J}} \; . \tag{2.59}$$

Similarly,

$$\boldsymbol{Q}_b = \frac{1}{\tau_s}\int_{\varepsilon_b}^{\infty} \varepsilon\rho(\varepsilon)\boldsymbol{f}(\varepsilon,\mu_J,\boldsymbol{T}_l)d\varepsilon = \boldsymbol{Q} - \frac{1}{\tau_s}\int_0^{\varepsilon_b} \varepsilon\rho(\varepsilon)\boldsymbol{f}(\varepsilon,\mu_J,\boldsymbol{T}_l)d\varepsilon \equiv \boldsymbol{Q} - \tilde{\boldsymbol{Q}} \; . \tag{2.60}$$

Thus, the barrier lowers the pumping rate; however, we note that mainly cold (low

energy) carriers are blocked by the barrier, and therefore mainly hot carriers are injected into the active region. As a result the carrier temperature in the active region should increase. This is another heating mechanism: injection heating [66] .

The integrals in Eqs. (2.59) and (2.60) can be handled using the approximate Fermi function (2.49) and by applying the same technique as in Appendix F (p. 169). The details of the calculation can be found in Appendix G (p. 176) and the resulting expressions for the barriers that are higher than μ_J are obtained from Eqs. (G.25) and (G.28) (pp. 183 and 185):

$$\boldsymbol{J}_b \approx \boldsymbol{J}\theta_l \frac{(1+\theta_l)}{2} \exp\left[-\frac{(\varepsilon_b-\mu_J)}{\varepsilon_t}\left(\frac{1-\theta_l}{\theta_l}\right)\right], \tag{2.61}$$

$$\boldsymbol{Q}_b = \boldsymbol{J}\varepsilon_t \frac{\theta_l^2}{2}\frac{1+\theta_l}{1-\theta_l}\left(1+\frac{\varepsilon_b}{\varepsilon_t}\frac{1-\theta_l}{\theta_l}\right)\exp\left[-\left(\frac{\varepsilon_b-\mu_J}{\varepsilon_t}\right)\frac{1-\theta_l}{\theta_l}\right], \tag{2.62}$$

For low barriers $\varepsilon_b < \mu_J$ and using Eqs. (G.26) and (G.30) of Appendix G (pp. 184, 187) we have

$$\boldsymbol{J}_b \approx \boldsymbol{J}\left\{1-(1-\theta_l^2)\left\{\exp\left(\frac{\varepsilon_b-\mu_J}{\varepsilon_t}\right)-\frac{\theta_l}{2(1+\theta_l)}\exp\left[\left(\frac{\varepsilon_b-\mu_J}{\varepsilon_t}\right)\left(\frac{1+\theta_l}{\theta_l}\right)\right]\right\}\right\}, \tag{2.63}$$

$$\boldsymbol{Q}_b = \boldsymbol{J}\varepsilon_t\left(\mu_J - \frac{1-3\theta_l^2}{1-\theta_l^2}\right)\left\{1-(1-\theta_l^2)\exp\left(\frac{\varepsilon_b-\mu_J}{\varepsilon_t}\right)\tilde{\boldsymbol{R}}\right\}. \tag{2.64}$$

where $\tilde{\boldsymbol{R}}$ denotes the expression in the figure brackets in Eq. (G.29) (p. 186). We note, however, that when the barrier is lower than the Fermi energy it is usually neglected. The influence of the barrier is affected by the pumping rate. The above expressions for the pumping terms do not include tunneling effects. Our main interest is in laser devices where the pumping rate is high enough to overcome barriers, which is accomplished by increasing bias voltage across the p-n junction.

2.8. Limitations and Advantages of the Model

In this section we summarize the usefulness and limitations of our model which is created to describe carrier temperature and gain dynamics in semiconductor laser media. Our model is based on ordinary rate equations for a semiconductor laser extended to include carrier energy density. Thus, the model shares all the useful characteristics of the rate equations and at the same time their limitations. The advantage of the rate equations compared to microscopic theories is their clarity and simplicity. Despite limited accuracy the rate equations remain a versatile tool in the investigation of the dynamical behavior of semiconductor laser devices. An important advantage of the model is its simple structure that allows easy comparison of different heating effects. This can be done by artificially increasing, decreasing, or even shutting down a particular heating mechanism.

The model does not include SHB, but it can be incorporated into the theory rather easily, if necessary. if we modify the gain function (2.37) by the nonlinear factor $\left(1+sN_p\right)^{-\delta}$ as in Eq. (1.3), where s is the gain suppression coefficient due to spectral-hole burning. This demonstrates the flexibility of the model that easily modifies to accommodate more rigorous requirements of a particular problem where particular effects are important.

The main goal of this model is description of the mutual influence of the gain and carrier temperature; the inclusion of other effects makes the nature of interaction less clear. On a time scale longer than 0.1-0.2 ps the influence of SHB is negligible compared with the carrier heating effect. For shorter time scales SHB becomes important and the model becomes inadequate. For longer time scales, in principle, there is no limitation, however, the carrier heating effects are only important on the picosecond time scale.

The gain function used in this theory includes only the electron temperature. The hole temperature is not considered because of condition (2.35), i.e. the electron temperature is not several times higher than the hole temperature. With very high-energy pulses this condition may no longer be satisfied and the rate equations themselves may no longer be adequate for even qualitative theoretical description.

The analytical expressions that we have derived are accurate for low temperatures, $T_e < \varepsilon_t / k_B$. This limitation is highlighted mathematically by terms proportional to $(1-\theta)$ in the denominators of certain expressions. For a band tail parameter ε_t ~20 meV they are accurate for temperatures up to ~230 K. For higher temperatures the integral expressions (2.14) and (2.44) should be used instead of the corresponding analytical approximations. The integrals with Fermi functions allow approximate analytical solutions only in the low temperature limit. This imposes another limitation on the external pulse energy because high-energy pulses can heat the electrons to very high temperatures. Here we note that in the high temperature limit the electron system can be described by the Boltzmann distribution function and a different model needs to be applied for this case.

Our analysis of gain and temperature dynamics is based on the solution of Eqs. (2.1) using Eqs. (2.37) and (2.43); the carrier temperature and chemical potential are found using Eqs. (2.50) and (2.51). For the numerical procedures Eqs. (2.1) are converted to dimensionless form (see Appendix H, p. 188) and solved using the the 4th order Runge-Kutta method [93]. The parameters for calculations are chosen in such a way that during the calculations the values of all dynamic variables remain within the limits of applicability of the model to ensure validity of the analytical expressions.

3. CARRIER TEMPERATURE DYNAMICS IN STEADY STATE LASER OPERATION

The nonlinearity of the gain that is caused by carrier heating is observed in experiments with short (picosecond and femtosecond) pulses suggesting that sudden changes in photon density play a significant role in the dynamics of semiconductor lasers. Thus it is of interest to investigate the relationship between the carrier temperature and photon density in the medium. A diode laser in a cw operation regime is a convenient system to study this relationship because the gain and the photon density are constant. The photon density can also be controlled by carrier injection rate, thus making it possible to examine the relationship between the carrier temperature and photon density.

3.1. Steady State Gain and Carrier Temperature

The steady-state laser operation is maintained by a constant injection rate that is high enough to compensate for the energy losses. Therefore, the gain coefficient in a cw laser is constant and given by

$$g_0 = \frac{1}{\Gamma}\left(\alpha_i + \frac{1}{2L}\ln\left(\frac{1}{R_1 R_2}\right)\right). \tag{3.1}$$

This expression is obtained from the steady-state solution of Eq. (2.1a), ignoring TPA and including FCA in the internal losses. Sub index 0 is used for the steady-state values in this chapter.

The steady-state value for the carrier temperature can be obtained from Eq. (2.37)

$$T_0 = \frac{(\mu_0 - \varepsilon_e)}{k_B}\left[\ln\left(\frac{G+g_0}{G-g_0}\right)\right]^{-1}, \tag{3.2}$$

where ε_e is given by Eq. (2.31a) and is approximately equal to the photon energy $\hbar\omega$. The steady-state value of the chemical potential is obtained from Eq. (2.1b) using Eq. (2.50), and is given by

$$\mu_0 = \varepsilon_t \ln\left[\left(J + v_{gr} g_0 N_{p0}\right)\tau_s \frac{\left(1-\theta_0^2\right)}{\rho_t \varepsilon_t}\right], \tag{3.3}$$

where $\theta_0 = k_B T_0 / \varepsilon_t$.

The transcendent form of Eq. (3.2) does not lead to a clear analytical expression for relationship between the carrier temperature and photon density. Therefore we use numerical calculations to study the behavior of the carrier temperature in the cw diode laser.

3.2. Steady-State Behavior

We choose an InGaAsP diode laser that is operating on a single mode for numerical calculations. The parameter values used in these calculations are presented in Table 3.1 (p. 49). The material characteristics are calculated for an $In_{1-x}Ga_xAs_yP_{1-y}$ quaternary alloy with y = 0.55 and x = 0.25 using the following expressions found in Ref. [18]:

$$\varepsilon_g = 1.35 - 0.72y + 0.12y^2, \tag{3.4}$$

and

$$n = \left\{(1-y)\left[8.4x + 9.6(1-x)\right] + y\left[13.1x + 12.2(1-x)\right]\right\}^{1/2}. \tag{3.5}$$

Table 3.1. Parameter Values for $In_{0.75}Ga_{0.25}As_{0.55}P_{0.45}$ Diode Laser

Parameter	Symbol	Value
Cavity length	L	200 μm
Active region width	L_w	2 μm
Active layer thickness	L_t	0.2 μm
Facet reflectivity	R	0.32
Confinement factor	Γ	0.3
Spontaneous emission factor	β_{sp}	10^{-5}
Refractive index	n	3.319
Group velocity index	n_{gr}	4
Band gap energy	ε_g	0.99 eV
Band tailing parameter	ε_t	20 meV
Dopant concentration	ξ	10^{18} cm^{-3}
Energy density relaxation time	τ_l	5×10^{-13} sec
Spontaneous recombination time	τ_s	2×10^{-9} sec
Free carrier absorption cross-section	s_{FCA}	5×10^{-18} cm^2
Photon energy	$\hbar\omega$	0.989 eV
Internal losses (without FCA loss)	α_i	30 cm^{-1}
Two-photon absorption coefficient	α_{TPA}	35 cm/GW
Lattice temperature	T_l	70 K

The photon lifetime in the cavity is calculated using expression (2.3). The laser facets are assumed identical $\boldsymbol{R}_1 = \boldsymbol{R}_2 \equiv \boldsymbol{R}$ and we assume that there is no barrier between the active and adjacent regions. This means that the temperature of the pumped carriers is equal to the lattice temperature; i.e., there is no injection heating. The lattice temperature is maintained constant (e.g., by a cryogenic bath) at 70 K. The other parameter values in Table 3.1 (p. 49) are either calculated using the corresponding expressions from Chapter 2 or taken from the literature, mainly from Ref. [18]. The threshold current density is obtained from numerical calculations.

The initial conditions for Eqs. (2.1) are taken arbitrarily because for ordinary differential equations the final solution is independent of its initial conditions. We choose the lattice temperature as the initial condition for the carrier temperature in each numerical experiment. The initial value of carrier density is 1.08×10^{18} cm^{-3}, a value slightly below the carrier density at threshold. This particular value is chosen to avoid the collection of an unnecessarily large amount of numerical data when the laser is below threshold. From the initial values of $\boldsymbol{T}$ and $\boldsymbol{N}_c$ we calculate the initial conditions for the chemical potential and carrier energy density. The equations are solved using the 4th order Runge-Kutta method [93].

The laser threshold for the chosen parameter values is reached with an effective injection current ($\eta_{inj}\boldsymbol{I}$) approximately equal to 7.1 mA. This value is chosen as a reference injection current. Calculations are done for injection rates 1%, 10%, twice, 10 times, and 25 times above the threshold. Our focus of interest is in the carrier temperature behavior (the gain coefficient is constant) and its relationship to the photon density.

Figures 3.1-3.4 (pp. 52 - 55) show the evolution of three dynamical variables N_p, $\boldsymbol{N_c}$, and $\boldsymbol{T}$ during a typical semiconductor laser turn-on transition through the relaxation oscillations to cw behavior. We do not include the external signal in these calculations ($\boldsymbol{N_{px}} = 0$). The results for the photon density and carrier density steady-state behavior are similar to those of a laser without including the carrier temperature dynamics (i.e. assuming instantaneous temperature relaxation). This indicates that the carrier temperature has a little impact on steady-state laser output power. Nevertheless, the carrier temperature behavior is of interest because it provides information about the relationship between carrier ensemble and photon density in the medium.

In the cw regime of laser operation, the carrier temperature is affected, in general, by processes such as stimulated emission, free carrier absorption, two-photon absorption, spontaneous recombination, carrier-lattice interactions, and carrier injection. Other minor effects are disregarded in this analysis (e.g., nonradiative recombination). Overall, these processes keep the carrier temperature above the lattice temperature, even before the laser starts to produce photons. There is an apparent difference in carrier temperature behavior before and after the threshold is reached. The carrier temperature behavior before threshold is considered in Section 3.3.

The qualitative behavior of the carrier temperature mimics the behavior of the photon density when the laser is in a cw regime. As one can see in Figs. 3.1-3.4 (pp. 52 - 55), the temperature difference between the carriers and the lattice in the cw limit becomes noticeable at high pumping rates.

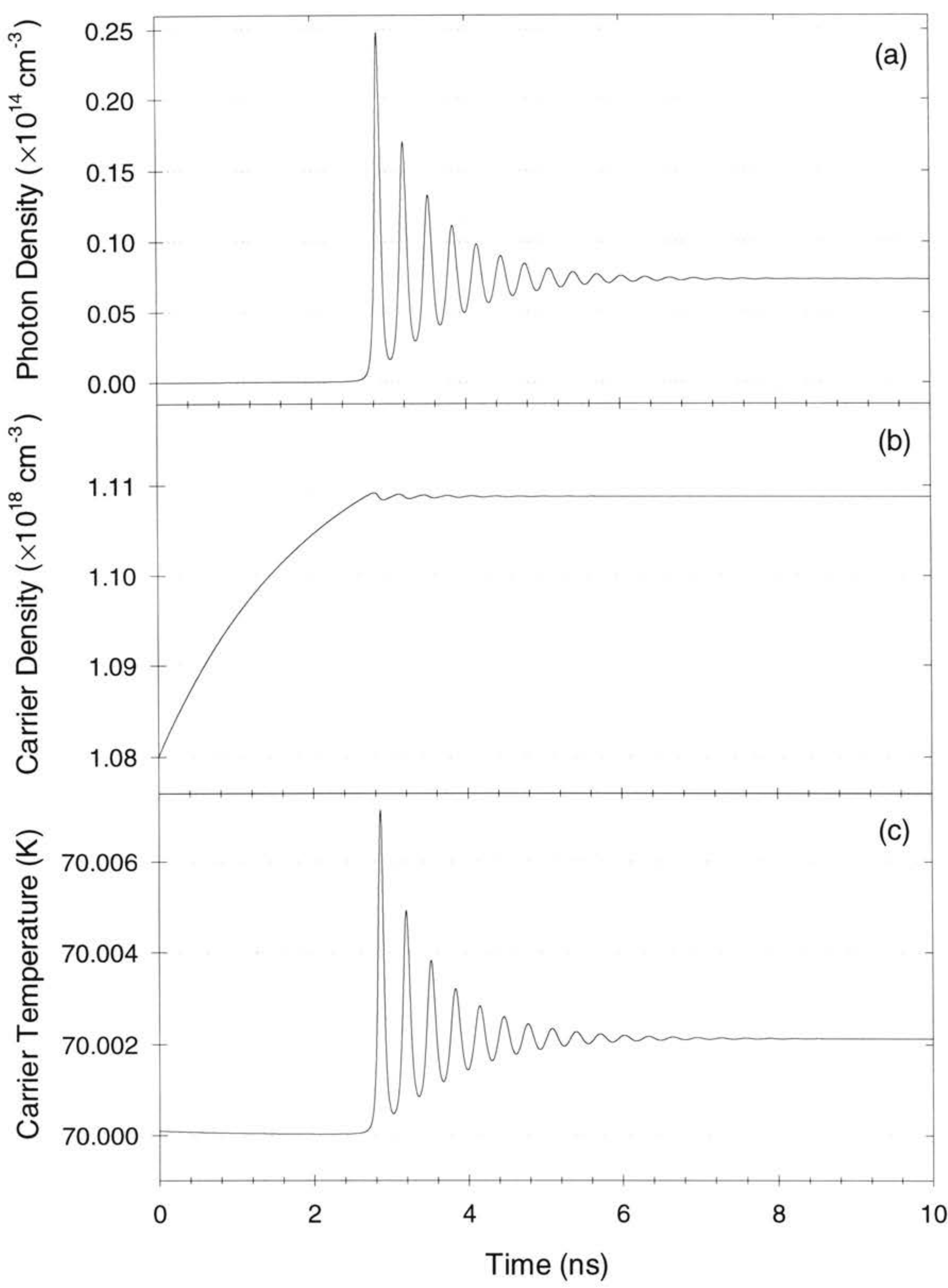

Figure 3.1. Laser transition to cw behavior for pumping at 1% above the threshold rate: (a) photon density, (b) carrier density, and (c) carrier temperature.

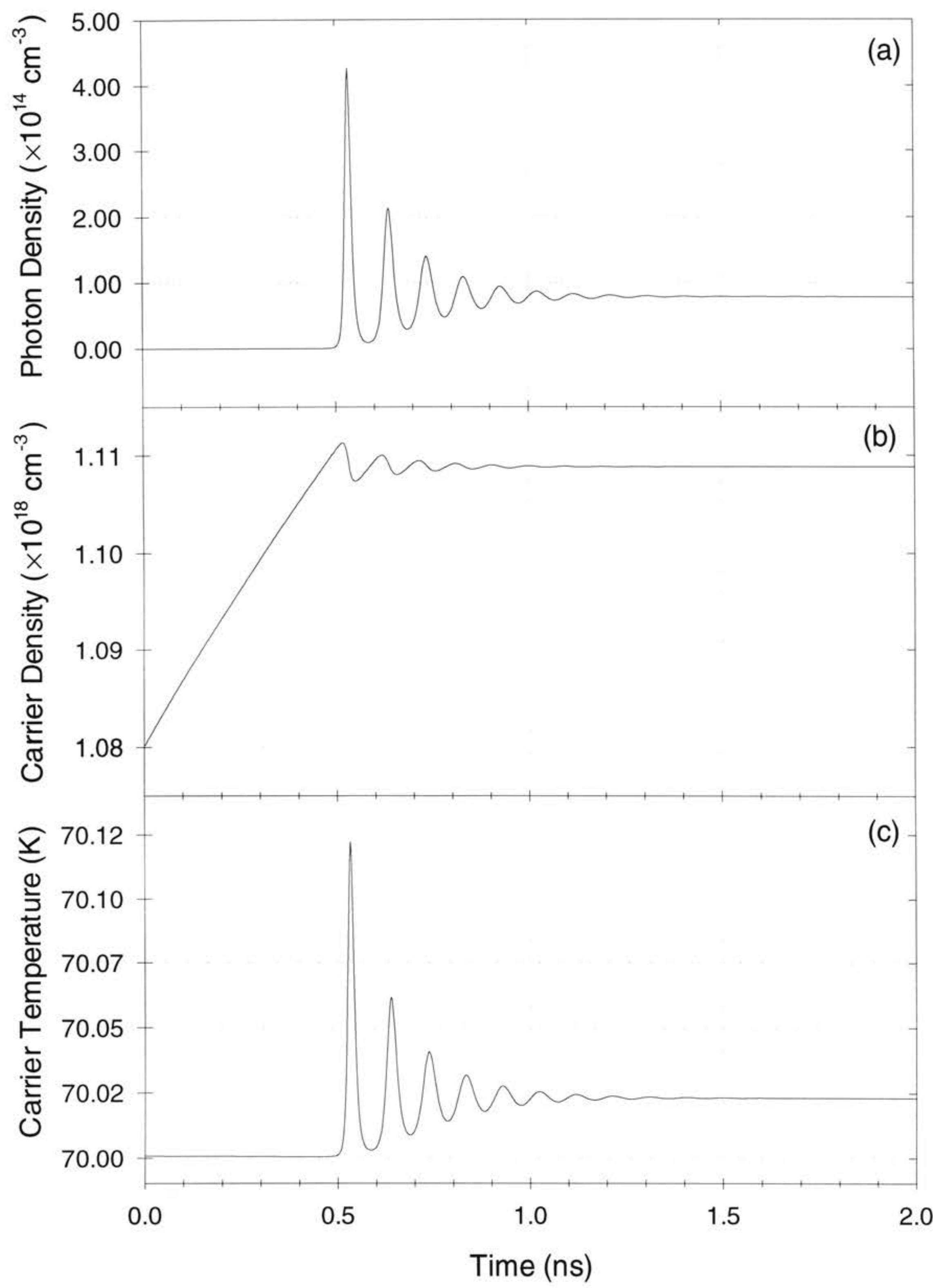

Figure 3.2. Laser transition to cw behavior for pumping at 10% above the threshold rate: (a) photon density, (b) carrier density, and (c) carrier temperature.

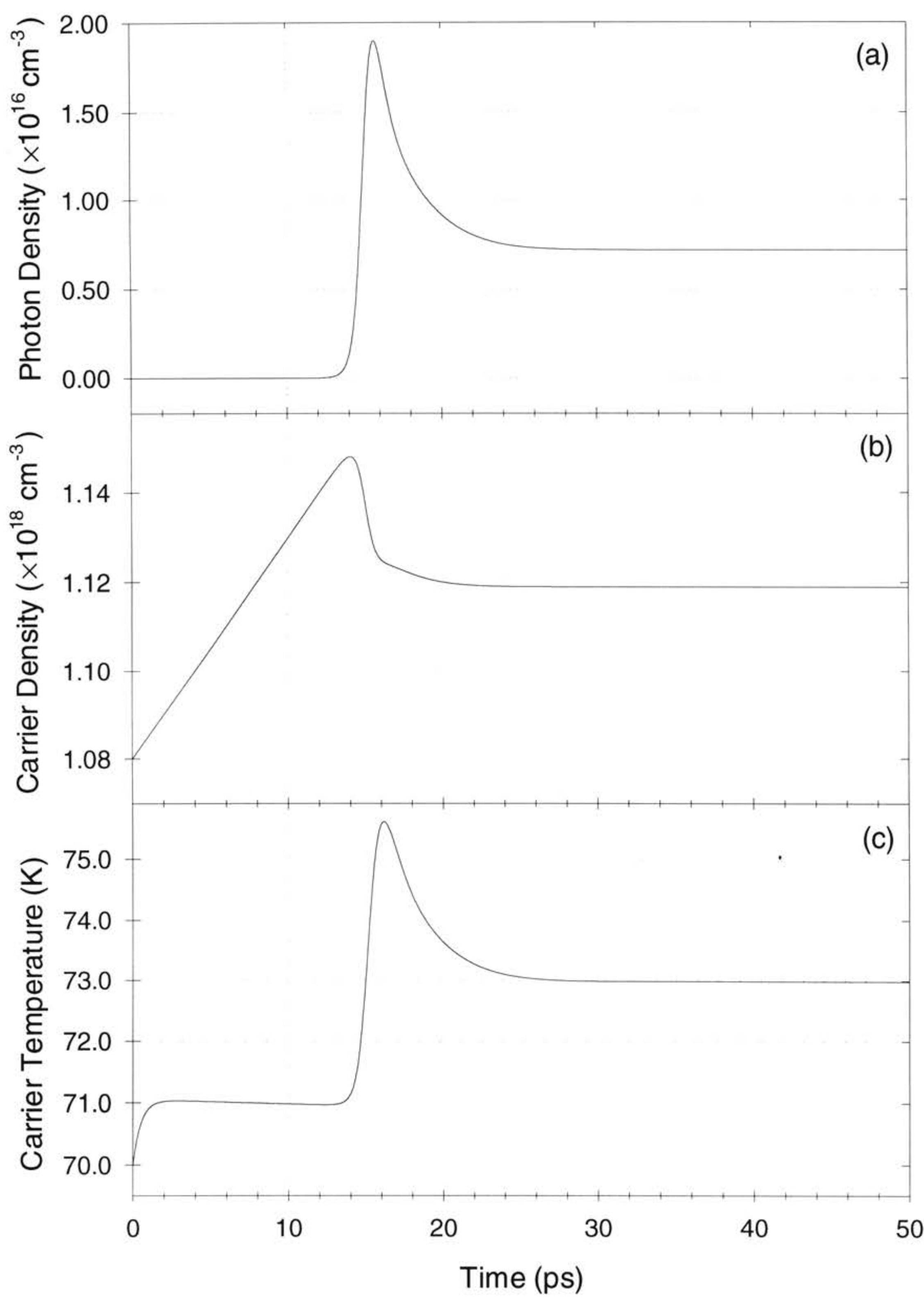

Figure 3.3. Laser transition to cw behavior for pumping at 10 times the threshold rate: (a) photon density, (b) carrier density, and (c) carrier temperature.

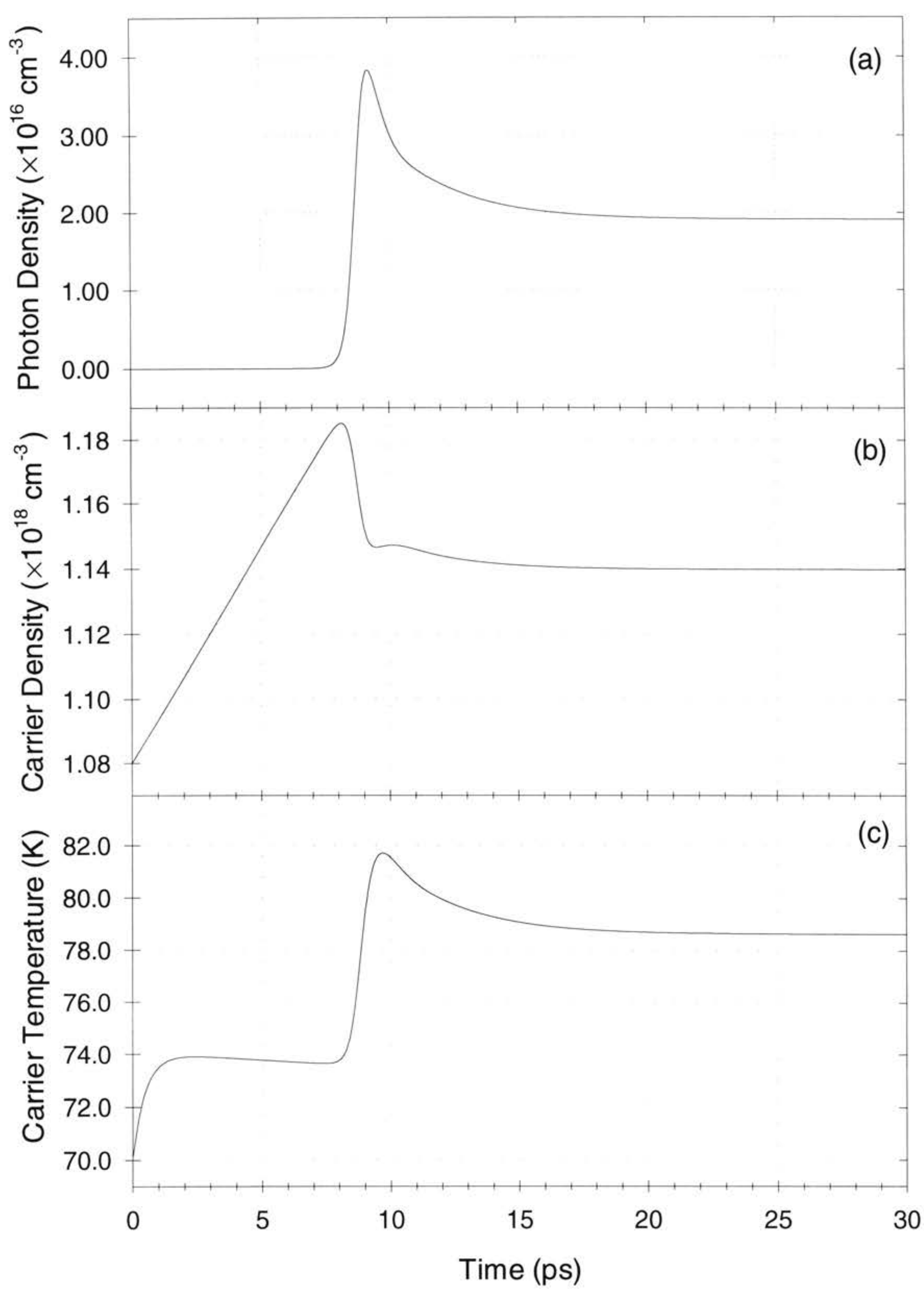

Figure 3.4. Laser transition to cw behavior for pumping at 25 times the threshold rate: (a) photon density, (b) carrier density, and (c) carrier temperature.

However, we find that this temperature difference has negligible influence on the output power of the laser. In fact, when we compare the photon densities that are calculated in the model without the temperature dynamics we obtain only a quarter percent difference even when the pumping current is 25 times threshold. Numerical values are presented in Table 3.2 for the carrier and lattice temperature differences ($T_0 - T_l$), the photon densities that are calculated with and without carrier temperature dynamics, and the percent difference between them when different pumping rates are used.

Table 3.2. Steady State Values For Photon Density and Carrier Temperature Deviation from the Lattice Temperature

Pumping Rate (J)	$T_0 - T_l$	N_{p0} ($T_0 \neq T_l$)	N_{p0} ($T_0 = T_l$)	% diff.
$1.01 J_{th}$	0.0021 K	0.73544×10^{13} cm^{-3}	0.73540×10^{13} cm^{-3}	0.005 %
$1.10 J_{th}$	0.0232 K	0.79196×10^{14} cm^{-3}	0.79252×10^{14} cm^{-3}	0.041 %
$2.00 J_{th}$	0.2579 K	0.79759×10^{15} cm^{-3}	0.79818×10^{15} cm^{-3}	0.074 %
$10.0 J_{th}$	2.9842 K	0.71780×10^{16} cm^{-3}	0.71892×10^{16} cm^{-3}	0.156 %
$25.0 J_{th}$	8.6356 K	1.91232×10^{16} cm^{-3}	1.91724×1016 cm-3	0.257 %

In Fig. 3.5 (p. 58) we compare the laser behavior with and without the carrier temperature dynamics for a pumping rate twice the threshold value. Apparently, when the carrier temperature dynamics is taken into account, the transient oscillations damp faster. Thus, the carrier temperature has little effect on the laser performance as a light source but it does affect the laser response to external perturbations such as the injection modulation or external pulses. The modulation response of the laser with carrier

temperature dynamics is considered in Refs. [64, 94]. We will consider the cw laser response to external pulses in Section 3.4.

Calculations show that except for FCA all other carrier heating effects have negligible influence on the carrier temperature and photon density. In Table 3.3 we present data for $\Delta T \equiv T_0 - T_l$ and N_{p0} that is calculated for J=2J_{th} and where FCA, TPA, and the spontaneous (radiative) recombination are separately excluded from the equations. This is done by setting the corresponding coefficient (s_{FCA}, β_{sp}, or α_{TPA}) to zero. In addition, in Fig. 3.5 (p. 58) we present the laser dynamics for J=2J_{th} with FCA excluded from the model equations. These results once again show that the carrier heating processes have little impact on cw laser operation. Thus, when a cw laser is considered without an external signal one can neglect the carrier heating effects (usually in semiconductor laser rate equations FCA is accounted for by including it in the internal losses).

Table 3.3. Influence of Carrier Heating Processes on Steady State Values For Photon Density and Carrier Temperature Deviation from the Lattice Temperature for J=2J_{th}

Process	ΔT	N_{p0} (Process excluded)	N_{p0} (Process included)	% diff.
Spontaneous Emission	2.4×10^{-5} K	7.9758 ($\times10^{14}$ cm^{-3})	7.9759 ($\times10^{14}$ cm^{-3})	0.001%
Two-Photon Absorption	1.3×10^{-5} K	7.9776($\times10^{14}$ cm^{-3})	7.9759($\times10^{14}$ cm^{-3})	0.021%
Free-Carrier Absorption	0.21457 K	8.4941($\times10^{14}$ cm^{-3})	7.9759($\times10^{14}$ cm^{-3})	6.293%

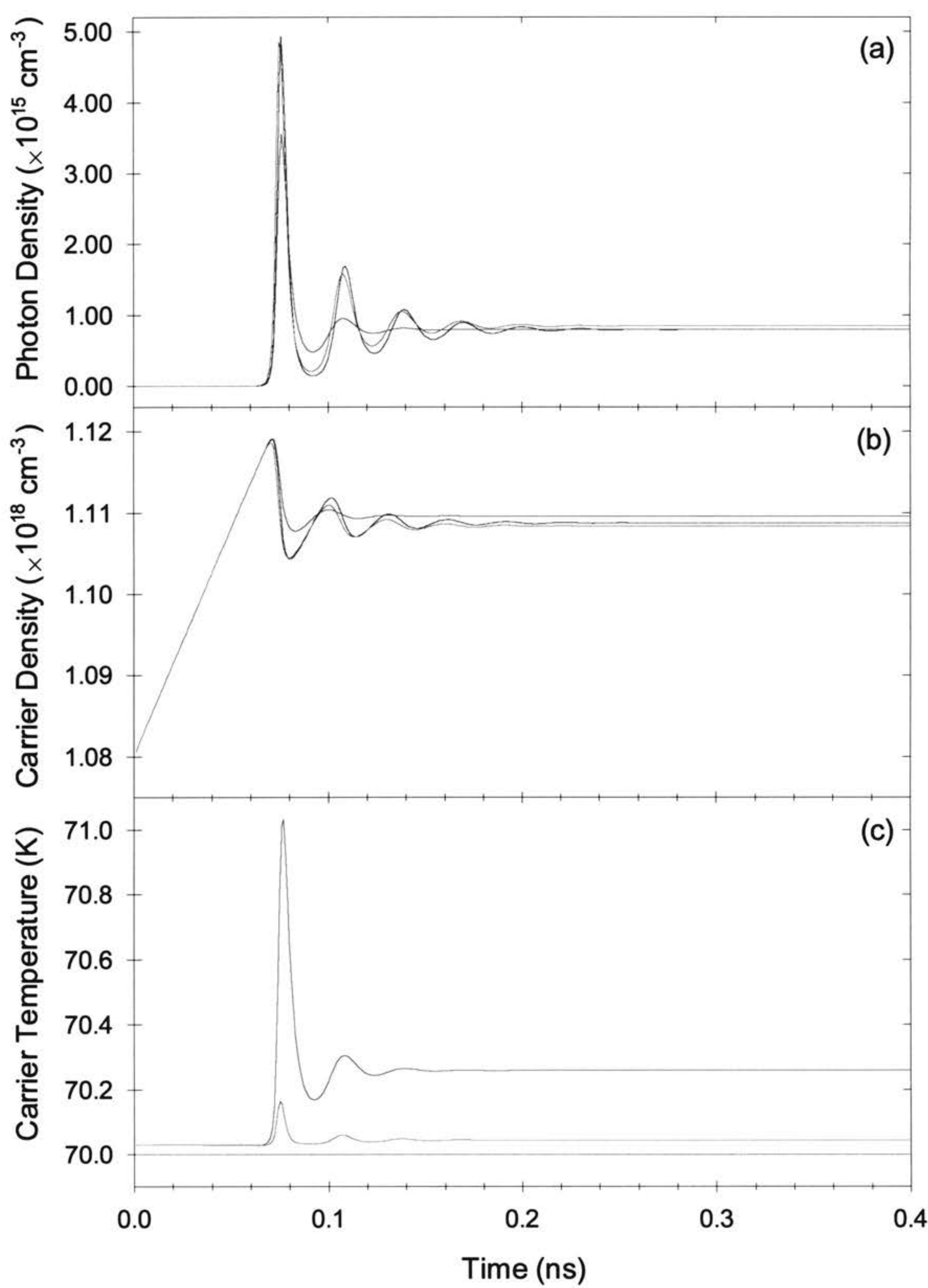

Figure 3.5. Laser transition to cw behavior for pumping at twice the threshold rate (red curves, with temperature dynamics; blue curves, without temperature dynamics; green curves, with temperature dynamics but FCA excluded: (a) photon density, (b) carrier density, and (c) carrier temperature.

3.3. Carrier Temperature Behavior Below the Threshold

The carrier temperature behavior in the time interval between the initiation of the pumping and the laser emission (below threshold interval) is determined mainly by spontaneous recombination, carrier-lattice interactions and pumping rate. For low pumping rates the behavior of the carrier temperature is almost constant; however, in all cases the carrier temperature behavior is qualitatively the same in the interval below threshold and is best represented by Fig. 3.4c (p. 55; note the time scale differences in graphs). For comparison, in Fig. 3.6 (p. 60) we present the enhanced-scale graphs for carrier and lattice temperature difference $\boldsymbol{T}-\boldsymbol{T}_l$ for pumping rates that are 1%, 10% and twice above the threshold value. The qualitative behavior is almost identical for all pumping rates. Initially the temperature increases to a value that is higher than that of the lattice. The time scale of this behavior is about a picosecond, close to the carrier energy relaxation time (0.5 ps). Then a longer period of gradual decrease follows until the laser reaches the threshold. The time interval required to reach the threshold is shorter for high pumping rates (see Figs. 3.1-3.5, pp. 52 - 55, 58).

The behavior described above needs interpretation. First we consider initial fast increase of the carrier temperature. Note that we start our numerical calculations with a fixed value of the carrier density, which we assume was already pumped into the system. Thus, mathematically, the carrier and carrier energy densities experience a sudden jump. From the other side, by setting the initial carrier temperature equal to the lattice temperature we ignored the fact that the pumping which is accompanied by FCA, TPA and spontaneous recombination processes affects the carrier temperature and, therefore, the temperature of carrier ensemble is in fact different from the lattice temperature.

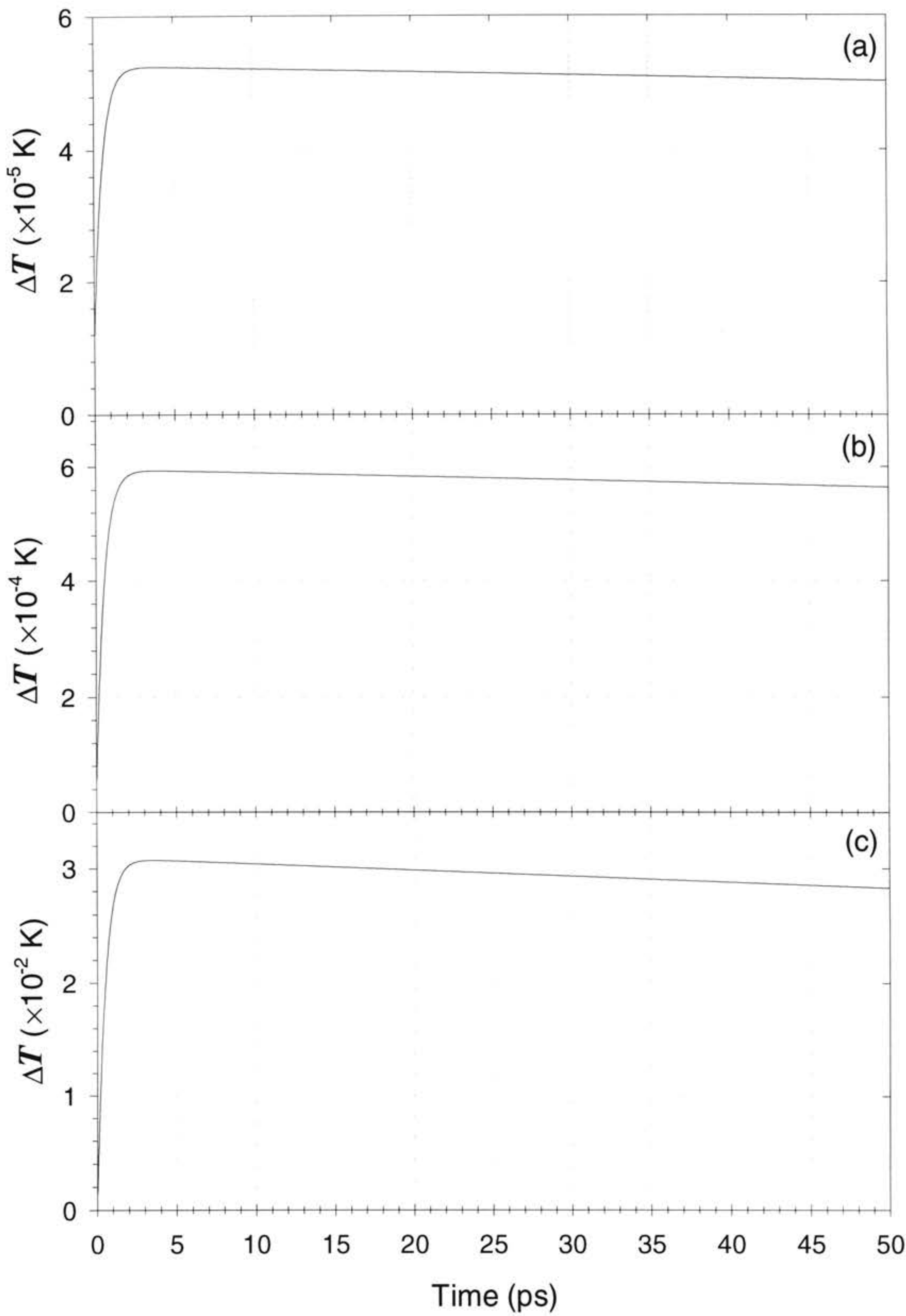

Figure 3.6. Carrier temperature deviation from the lattice temperature in the time interval between initiation of pumping and laser emission for pumping rates that are (a) 1%, (b) 10% above and (c) twice the threshold value

Therefore, when we start numerical calculations the initial carrier temperature (arbitrarily chosen to be equal to the lattice temperature) immediately relaxes to its true value. Of course, the model equations do not allow immediate relaxation; the fastest relaxation time is the energy density relaxation time. Thus, the initial increase in the carrier temperature is a result of the arbitrary choice of the initial conditions. Note that one cannot start from zero values for carrier density because then it is meaningless to use a statistical model for carriers in the conduction band.

The observed behavior remains qualitatively the same for calculations that were carried out with different initial conditions. However, it should be pointed out that even in experiments when the carrier injection is applied (bias voltage is turned on) the carrier ensemble is disturbed and a certain time is required to relax. The carrier temperature after relaxation is not necessarily the same but is determined by the corresponding relationships with all other ensemble characteristics that might be changed by the carrier injection. Thus, it is plausible that the carrier temperature initially may experience fast changes when pumping is turned on and, therefore, the behavior described above is not entirely a mathematical artifact (numerical turn-on effect).

Now we discuss the slow decrease in carrier temperature that follows its initial fast behavior. This part of the graph can be approximated by a linear function; however, the slopes are larger for high pumping rates. The numerical values for the slopes that are calculated for different pumping rates are presented below in Table 3.4. In all cases the slopes are negligibly small but noticeably different from each other. The latter fact indicates that the overall temperature decrease is related to the rate of carrier density increase.

Table 3.4. Slopes for Linearly Decreasing Part of Temperature Graphs

Pumping Rate (J)	$1.01J_{th}$	$1.10J_{th}$	$2.00J_{th}$	$10.0J_{th}$	$25.0J_{th}$
Slope	-4.90×10^{-8}	-6.26×10^{-7}	-5.43×10^{-3}	-6.49×10^{-3}	-5.19×10^{-2}

Increasing the number of carriers leads to less energy per particle and hence a lower temperature of carrier ensemble. The carrier density is increasing linearly (see Figs. 3.1c-3.5c, pp. 52 - 55, 58), however the relationship between carrier temperature and inverse carrier density is not linear. The functional relationship between T and N_c can be obtained by rearranging Eq. (2.51):

$$T = \frac{\varepsilon_t}{k_B}\sqrt{1 - \frac{2}{3+z}}, \tag{3.6}$$

where we introduced the dimensionless parameter

$$z \equiv \frac{1}{\varepsilon_d}\left(\frac{U}{N_c} - \mu\right). \tag{3.7}$$

These expressions show that the temperature is a complicated function of U, N_c, and μ and, therefore, the temperature behavior is not determined solely by the carrier density behavior.

For comparison we consider the Boltzmann ensemble of carriers where

$$U = \frac{3}{2}N_c k_B T, \tag{3.8}$$

and an increase in carrier density is accompanied by a proportional increase in energy density so that the temperature remains the same.

The situation is quite different for the Fermi ensemble. From Eq. (3.7) it follows that increasing N_c leads to decreasing z, hence, increasing the value of the fraction under the square root in Eq. (3.6) and ultimately to temperature decrease. Simultaneous changes (increase for both parameters) in U and μ ensures a slow linear decrease of carrier temperature while the laser is pumped and no substantial number of photons are generated in the medium. This, however, does not mean that carrier injection is a cooling factor. The temperature of the carriers remains higher than the lattice temperature at all times. When the laser threshold is reached the number of photons generated becomes large enough so that the absorption and emission processes along with FCA and TPA lead to a carrier temperature increase.

It is of interest to investigate the separate influence of FCA, TPA, and spontaneous (radiative) recombination. The influence of FCA in the steady state regime is demonstrated in Fig. 3.5 (p. 58) and as we can see it is a major heating factor. In contrast, as we pointed out earlier, TPA has little influence. Indeed, corresponding terms in Eqs. (2.1) have similar weights when $N_p \sim N_c$, i.e. for very high pumping rates. However, it is more appropriate to examine the effect of FCA and TPA in a passive medium with an external signal for the following reasons: Both FCA and TPA are proportional to the photon density and one needs a large number of photons to enhance their influence on carrier temperature for investigation. It is advantageous to use the photons of the external signal since the photon generation itself in the medium is an effective heating factor because mainly cold carriers participate in laser action. Carrier heating due to photon generation is demonstrated in Fig. 3.5 (p. 58) where one of the curves is obtained without FCA. There is noticeable heating even without FCA. We

consider the relative influence of FCA and TPA in detail in Chapter 6.

Calculations for the cw laser show that the influence of spontaneous radiative recombination on the carrier temperature and the steady-state laser operation is negligible. When FCA and TPA are present the spontaneous emission can always be neglected. There is a very small decrease in carrier temperature when the spontaneous term in Eq. (2.1a) is excluded. However, it is of interest to study how spontaneous recombination affects the carrier temperature. This problem is discussed in the next chapter in detail.

3.4. Laser Response to External Pulses

In order to examine the response of the laser to photon density perturbations by an external signal, we apply resonant optical pulses. In Fig. 3.7 (p. 66) we demonstrate the laser response to Gaussian pulses with (a) 10, (b) 25 and (c) 50 ps duration (FWHM). The external signals are normalized in such a way that all pulses carry the same energy, $\mathcal{E}_x$ =0.1 pJ (see Chapter 2 for description of the external pulses). The laser is pumped at a rate twice the threshold value. The photon densities are plotted as a function of time, along with the results of the model assuming equal lattice and carrier temperatures (i.e. assuming instantaneous temperature relaxation). The corresponding temperature behavior is presented in Fig. 3.8. (p. 67)

When the 50 ps pulse is applied, the laser response is virtually the same for the model inclusive of temperature dynamics as for the one without it; however, the response to the shorter pulses is different. The oscillations damp faster when the carrier temperature dynamics is taken into account, and this difference becomes more noticeable for shorter signal duration. Thus, the carrier temperature dynamics plays a significant

4. TEMPERATURE DYNAMICS OF A RECOMBINING FREE-CARRIER ENSEMBLE

In this section we consider the dynamical behavior of the temperature of an ensemble of particles during a radiative recombination process. The more general physical system that is relevant here can be described as a system of particles and antiparticles that can annihilate each other. In particular, we are interested in semiconductor media where electron-hole pairs recombine to produce photons. This process of annihilation will change the statistical characteristics of the carrier ensemble and, therefore, influence other associated processes such as interband transition probabilities. Thus, it is important to know how the carrier density (the chemical potential) and carrier energy density (carrier temperature) are changing due to radiative recombination in degenerate (Fermi ensemble) and non-degenerate (Boltzmann ensemble) semiconductors.

The radiative recombination process is accompanied by other processes that may change the statistical properties of the system under consideration. For instance, the photons produced during the recombination can be re-absorbed by the free-carrier absorption process. In addition, the electrons and holes can be trapped by impurities thus decreasing the density of carriers. This and other processes further complicate an already complicated analysis. For example, the recombination rate can be a function of several factors. In the analysis below we shall include one such factor, namely we shall consider radiative recombination taking into account the possibility that the radiation

recombination rate is a function of the carrier energy. All other processes that affect the statistical properties of the carriers simultaneously with the radiative recombination are not considered. Therefore, all the results of this analysis are exclusively due to the radiative recombination process.

4.1. Temperature Relaxation Rate

The temperature of the ensemble influences the behavior of both the particle density (N_i) and energy density (U_i), therefore the temperature dynamics can be deduced from the behavior of N_i and U_i. The sub-index i is a common index that refers to the electrons ($i = e$) and holes ($i = h$). Because the reasoning below is similar for electrons and holes we shall drop the sub-index for simplicity. The equations that describe the evolution of particle density can be written in the following way:

$$\frac{dN}{dt} = -\int_0^\infty w(\varepsilon)\rho(\varepsilon) f(\varepsilon,\mu,T)d\varepsilon \,, \tag{4.1}$$

where $w(\varepsilon)$ is the probability of recombination of particles with energy ε, $f(\varepsilon,\mu,T)$ is the distribution function for particles, T is the temperature, μ is the chemical potential, and $\rho(\varepsilon)$ is the density of states. Using temperature in the expression above means that we assume that a thermal equilibrium of the ensemble is established very fast so that the recombination process does not create a non-equilibrium ensemble. The spontaneous recombination time τ_s usually is on the order of few nanoseconds. The carrier ensemble reaches the quasi-equilibrium condition in less than 100 femtoseconds. Thus, our assumption is fairly reasonable.

The energy density equation has the following form:

$$\frac{dU}{dt} = -\int_0^\infty w(\varepsilon)(\varepsilon_g + \varepsilon)\rho(\varepsilon) f(\varepsilon) d\varepsilon \, . \tag{4.2}$$

The left-hand side of this expression can also be written in terms of its partial derivatives:

$$\frac{dU}{dt} = \frac{\partial U}{\partial N}\frac{dN}{dt} + \frac{\partial U}{\partial T}\frac{dT}{dt} \, . \tag{4.3}$$

This expression allows us to write an equation for the temperature evolution during the recombination process

$$\frac{dT}{dt} = \left(\frac{\partial U}{\partial T}\right)^{-1} \int_0^\infty w(\varepsilon)\left(\frac{\partial U}{\partial N} - \varepsilon_g - \varepsilon\right)\rho(\varepsilon) f(\varepsilon, \mu, T) d\varepsilon \, . \tag{4.4}$$

Further analysis of this expression requires more details of the system under consideration. We need explicit expressions for the density of states and the distribution function. Also we must specify the structure of the function $w(\varepsilon)$ and obtain expressions for N and U.

4.2. Energy Dependent Recombination Rate

For the probability of recombination $w(\varepsilon)$ we assume the following structural form

$$w(\varepsilon) = \frac{1}{\tau_s}\left(\frac{\varepsilon_g + \varepsilon}{\varepsilon_g}\right)^q , \tag{4.5}$$

where τ_s is an energy independent constant, ε_g is the bandgap energy, ε is the carrier energy measured from the band edge, and q is the parameter specified below. Equation (4.5) suggests that τ_s is the recombination rate from the band edge: $\tau_s^{-1} = w(0)$. The specific form of the function (4.5) is chosen based on the fact that the probability for

spontaneous recombination in free space is proportional to the squared matrix element of the dipole moment and cubed frequency of emitted photon. The parameter $\boldsymbol{q}$ accounts for any differences that may exist between spontaneous recombination processes in semiconductors and free space. If the matrix element of the dipole moment is independent of frequency then $\boldsymbol{q} = 3$. In general, however the parameter $\boldsymbol{q} \neq 3$. For example, calculation of the dipole moment in a quantum-well structure gives the frequency dependence ω^{-2} [98] (implying $\boldsymbol{q} = 1$). We do not exclude the possibility of other functional dependencies in different cases; therefore, for the sake of generality, throughout this chapter we shall keep $\boldsymbol{q}$ as a parameter.

Using the binomial series we can write a useful simple expression for recombination rate

$$w(\varepsilon) = \frac{1}{\tau_s}\left(1 + \frac{\varepsilon}{\varepsilon_g}\right)^q \approx \frac{1}{\tau_s}\left[1 + q\frac{\varepsilon}{\varepsilon_g}\right] \tag{4.6}$$

Here we used the fact that the thermal energy of carriers is much smaller than the band gap energy $\varepsilon \ll \varepsilon_g$.

4.3. Boltzmann Ensemble (Nondegenerate Semiconductor)

In nondegenerate semiconductors the carrier ensemble has characteristics of the Boltzmann ensemble. The corresponding distribution function is given by

$$f(\varepsilon) = \exp\left(\frac{\mu - \varepsilon}{k_B T}\right) \tag{4.7}$$

and the relationship between the carrier density and carrier energy density is

$$U = \frac{3}{2} N k_B T . \tag{4.8}$$

From this expression it follows that

$$\frac{\partial U}{\partial N} = \frac{3}{2} k_B T , \tag{4.9}$$

and

$$\frac{\partial U}{\partial T} = \frac{3}{2} N k_B . \tag{4.10}$$

Using these expressions and (4.6) in the integral (4.4) we obtain

$$\frac{dT}{dt} = \frac{2}{3Nk_B} \frac{1}{\tau_s} \int_0^\infty \left(1 + q \frac{\varepsilon}{\varepsilon_g} \right) \left(\frac{3}{2} k_B T - \varepsilon \right) \rho_0 \sqrt{\varepsilon} f(\varepsilon) d\varepsilon . \tag{4.11}$$

This integral can be simplified as:

$$\frac{dT}{dt} = \frac{2}{3Nk_B} \frac{1}{\tau_s} \left\{ \frac{3}{2} N k_B T - U + \frac{q}{\varepsilon_g} \frac{3}{2} U k_B T - \frac{q}{\varepsilon_g} \int_0^\infty \varepsilon^2 \rho_0 \sqrt{\varepsilon} f(\varepsilon) d\varepsilon \right\} =$$

$$= \frac{2}{3Nk_B} \frac{1}{\tau_s} \frac{q}{\varepsilon_g} \left\{ \frac{3}{2} U k_B T - \frac{5}{2} U k_B T \right\} = - \frac{2}{3N} \frac{1}{\tau_s} \frac{q}{\varepsilon_g} U T = -q \frac{1}{\tau_s} \frac{k_B T^2}{\varepsilon_g}$$

or

$$\frac{d(k_B T)}{dt} = - \frac{1}{\tau_s} \frac{q}{\varepsilon_g} (k_B T)^2 . \tag{4.12}$$

As we see the change in temperature due to spontaneous recombination depends on the sign of q. The temperature decreases if $q>0$, increases if $q<0$, and remains the same if $q=0$. This behavior has a simple interpretation. For positive q the hotter particles recombine faster than the colder ones, therefore the ensemble is cooled. For negative q the situation is reversed. At $q=0$ the recombination rate is the same for all particles and the temperature of the ensemble remains unchanged.

4.4. Fermi Ensemble (Degenerate Semiconductor)

We shall consider pure and heavily doped materials separately because they have different relationships between carrier density and carrier energy density.

Case (a): Parabolic band approximation

For degenerate semiconductors in the parabolic band approximation we have (see Appendix E for derivation, p. 166)

$$\boldsymbol{N} \approx \frac{2}{3}\rho_0\tilde{\mu}^{3/2}\left(1+\frac{1}{2}\boldsymbol{x}^2\right), \tag{4.13}$$

$$\boldsymbol{U} \approx \boldsymbol{N}\varepsilon_g + \frac{2}{5}\rho_0\tilde{\mu}^{5/2}\left(1+\frac{5}{2}\boldsymbol{x}^2\right), \tag{4.14}$$

where $\boldsymbol{x} \equiv \left(\frac{\pi}{2}\frac{\boldsymbol{k_B T}}{\mu}\right)$ and $\tilde{\mu} \equiv \mu - \varepsilon_g$. From these expressions we have

$$\boldsymbol{U} \approx \boldsymbol{N}\left[\varepsilon_g + \frac{3}{5}\tilde{\mu}\left(1+2\boldsymbol{x}^2\right)\right] = \boldsymbol{N}\left[\varepsilon_g + \frac{3}{5}\left(\tilde{\mu}+2\frac{\theta^2}{\tilde{\mu}}\right)\right]. \tag{4.15}$$

Now, we have

$$\frac{\partial \boldsymbol{U}}{\partial \boldsymbol{N}} = \frac{\boldsymbol{U}}{\boldsymbol{N}} + \frac{\partial \boldsymbol{U}}{\partial \tilde{\mu}}\frac{\partial \tilde{\mu}}{\partial \boldsymbol{N}}$$

where

$$\frac{\boldsymbol{U}}{\boldsymbol{N}} = \varepsilon_g + \frac{3}{5}\tilde{\mu}\left[1+2\boldsymbol{x}^2\right]$$

and

$$\frac{\partial \boldsymbol{U}}{\partial \tilde{\mu}}\frac{\partial \tilde{\mu}}{\partial \boldsymbol{N}} = \frac{3}{5}\boldsymbol{N}\left(1-2\boldsymbol{x}^2\right)\left[\frac{2}{3}\frac{\tilde{\mu}}{\boldsymbol{N}}\frac{1+\boldsymbol{x}^2/2}{1-\boldsymbol{x}^2/6}\right] \approx \frac{6}{5}\tilde{\mu}\left(\frac{2-3\boldsymbol{x}^2}{6-\boldsymbol{x}^2}\right).$$

Therefore,

$$\frac{\partial U}{\partial N} = \varepsilon_g + \frac{3}{5}\tilde{\mu}\left[\left(1+2x^2\right) + \frac{2\left(2-3x^2\right)}{\left(6-x^2\right)}\right] \approx \varepsilon_g + 3\tilde{\mu}\frac{2+x^2}{6-x^2}, \tag{4.16}$$

and

$$\frac{\partial U}{\partial T} = \frac{12}{5}\tilde{\mu}x^2\frac{N}{T}. \tag{4.17}$$

Using expressions (4.16), (4.17), and (4.6) in the integral (4.4) we obtain:

$$\frac{dT}{dt} = \frac{5T}{12N\tilde{\mu}x^2}\frac{1}{\tau_s}\int_0^\infty\left(1+q\frac{\varepsilon}{\varepsilon_g}\right)\left(3\tilde{\mu}\left(\frac{2+x^2}{6-x^2}\right)-\varepsilon\right)\rho_0\sqrt{\varepsilon}f(\varepsilon)d\varepsilon$$

or

$$\frac{dT}{dt} = \frac{5T}{12x^2}\frac{1}{\tau_s}\left\{3\left(\frac{2+x^2}{6-x^2}\right)\left[1+\frac{q}{\varepsilon_g}\frac{U-N\varepsilon_g}{N}\right]-\left[\frac{U-N\varepsilon_g}{N\tilde{\mu}}+\frac{q}{\varepsilon_g N\tilde{\mu}}\int_0^\infty\varepsilon^2\rho_0\sqrt{\varepsilon}f(\varepsilon)d\varepsilon\right]\right\}. \tag{4.18}$$

The integral in this expression can be calculated using the results of Appendix D (p. 162) (Eq.(D.17) with $\rho(\varepsilon) = \varepsilon^2\rho_0\sqrt{\varepsilon}$):

$$\int_0^\infty\frac{\rho_0\varepsilon^2\sqrt{\varepsilon}d\varepsilon}{1+\exp\left(\frac{\varepsilon-\tilde{\mu}}{k_BT}\right)} \approx \frac{2}{7}\rho_0\tilde{\mu}^{7/2}\left(1+\frac{35}{6}x^2\right) = \frac{1}{7}N\tilde{\mu}^2\left(\frac{6+35x^2}{2+x^2}\right). \tag{4.19}$$

Substituting this result into (4.18) we obtain

$$\frac{dT}{dt} = \frac{5T}{12x^2}\frac{1}{\tau_s}\left\{3\left(\frac{2+x^2}{6-x^2}\right)\left[1+q\frac{3}{5}\frac{\tilde{\mu}}{\varepsilon_g}\left(1+2x^2\right)\right]-\left[\frac{3}{5}\left(1+2x^2\right)+q\frac{\tilde{\mu}}{\varepsilon_g}\frac{1}{7}\left(\frac{6+35x^2}{2+x^2}\right)\right]\right\},$$

which simplifies to

$$\frac{dT}{dt} = \frac{5T}{12x^2}\frac{1}{\tau_s}\left\{\frac{6}{5}\left(\frac{2-3x^2}{6-x^2}\right)+q\frac{\tilde{\mu}}{\varepsilon_g}\frac{2}{35}\left(\frac{9-8x^2}{3+x^2}\right)\right\}$$

or

$$\frac{dT}{dt} = \frac{T\tilde{\mu}^2}{2\theta^2}\frac{1}{\tau_s}\left\{\left(\frac{2-3x^2}{6-x^2}\right) + q\frac{\tilde{\mu}}{\varepsilon_g}\frac{1}{21}\left(\frac{9-8x^2}{3+x^2}\right)\right\}. \tag{4.20}$$

Thus,

$$\frac{d\theta^2}{dt} = \frac{1}{\tau_s}\tilde{\mu}^2\left\{\left(\frac{2-3x^2}{6-x^2}\right) + q\frac{\tilde{\mu}}{\varepsilon_g}\frac{1}{21}\left(\frac{9-8x^2}{3+x^2}\right)\right\}. \tag{4.21}$$

For extremely low temperatures ($x \ll 1$) this expression become

$$\frac{d\theta^2}{dt} = \frac{1}{\tau_s}\frac{1}{3}\tilde{\mu}^2\left\{1 + q\frac{\tilde{\mu}}{\varepsilon_g}\frac{3}{7}\right\} \tag{4.22}$$

Case (b): Exponential Tail Approximation

In this case we have (see Appendix E, Eq.(E.6), p.166)

$$N \approx \rho_t \varepsilon_t \exp(\mu/\varepsilon_t)\left[1 + 2x^2/3\right], \tag{4.23}$$

and (Eq. (E.8))

$$U \approx N\left[\mu - \varepsilon_t + 4\varepsilon_t x^2/3\right], \tag{4.24}$$

where $x \equiv \left(\frac{\pi}{2}\frac{k_B T}{\varepsilon_t}\right)$. The energy density partial differentials are

$$\frac{\partial U}{\partial N} = \frac{U}{N} + \frac{\partial U}{\partial \tilde{\mu}}\frac{\partial \tilde{\mu}}{\partial N} = \mu - \varepsilon_t + \frac{4}{3}\varepsilon_t x^2 + N\frac{\varepsilon_t}{N} = \mu + \frac{4}{3}\varepsilon_t x^2, \tag{4.25}$$

$$\frac{\partial U}{\partial T} = \frac{8}{3}\varepsilon_t x^2 \frac{N}{T} \tag{4.26}$$

Using these expressions and (4.6) in the integral (4.4) we obtain:

$$\frac{dT}{dt} = \frac{3T}{8N\varepsilon_t x^2}\frac{1}{\tau_s}\int_0^\infty \left(1 + q\frac{\varepsilon}{\varepsilon_g}\right)\left(\mu + \varepsilon_t\frac{4x^2}{3} - \varepsilon\right)\rho_t \exp\left(\frac{\varepsilon}{\varepsilon_t}\right) f(\varepsilon)\, d\varepsilon \tag{4.27}$$

which simplifies to

$$\frac{dT}{dt}=\frac{3T}{8N\varepsilon_t x^2\tau_s}\left\{\left[\mu+\varepsilon_t\frac{4x^2}{3}\right]N-U+\frac{q}{\varepsilon_g}\left[\left(\mu+\varepsilon_t\frac{4x^2}{3}\right)U-\int_0^\infty\varepsilon^2\rho_t\exp\left(\frac{\varepsilon}{\varepsilon_t}\right)f(\varepsilon)d\varepsilon\right]\right\},$$

and

$$\frac{dT}{dt}=\frac{3T}{8x^2}\frac{1}{\tau_s}R, \tag{4.28}$$

where

$$R\equiv\left\{1+\frac{q}{\varepsilon_g\varepsilon_t}\left[\left(\frac{U}{N}+\varepsilon_t\right)\frac{U}{N}-\frac{1}{N}\int_0^\infty\varepsilon^2\rho_t\exp\left(\frac{\varepsilon}{\varepsilon_t}\right)f(\varepsilon)d\varepsilon\right]\right\}. \tag{4.29}$$

The integral in this expression can be calculated using the results of Appendix D (p. 162), Eq. (D.17) with $\rho(\varepsilon)=\varepsilon^2\rho_t\exp[\varepsilon/\varepsilon_t]$):

$$\int_0^\infty\varepsilon^2\rho_t\exp\left(\frac{\varepsilon}{\varepsilon_t}\right)f(\varepsilon)d\varepsilon\approx\rho_t\varepsilon_t\exp\left(\frac{\mu}{\varepsilon_t}\right)\left[\mu^2-2\mu\varepsilon_t+2\varepsilon_t^2+\frac{2}{3}x^2\left(\mu^2+2\mu\varepsilon_t\right)\right],$$

and using (4.23) we obtain

$$\int_0^\infty\varepsilon^2\rho_t\exp\left(\frac{\varepsilon}{\varepsilon_t}\right)f(\varepsilon)d\varepsilon\approx N\left[\mu^2-2\mu\varepsilon_t\frac{1-2x^2/3}{1+2x^2/3}+\frac{2\varepsilon_t^2}{1+2x^2/3}\right]. \tag{4.30}$$

For low temperatures we can use an approximate expression $\left(1+2x^2/3\right)^{-1}\approx1-2x^2/3$ in (4.30) and keep only the terms on the order of x^2. As a result the expression for R is simplified to the following expression

$$R=\left\{1+\frac{q}{\varepsilon_g\varepsilon_t}\left[\left(\mu-\varepsilon_t+\frac{4}{3}\varepsilon_t x^2\right)\left(\mu+\frac{4}{3}\varepsilon_t x^2\right)-\left(\mu^2-2\mu\varepsilon_t+2\varepsilon_t^2-\frac{4}{3}x^2\left(2\mu\varepsilon_t-\varepsilon_t^2\right)\right)\right]\right.,$$

or

$$R = \left\{1 + \frac{q}{\varepsilon_g}\left[\mu\left(1 + \frac{16}{3}x^2\right) - 2\varepsilon_t\left(1 + \frac{2}{3}x^2\right)\right]\right\}. \tag{4.31}$$

Thus,

$$\frac{d\theta^2}{dt} \approx \frac{1}{\tau_s}\frac{3}{4}\varepsilon_t^2\left\{1 + \frac{q}{\varepsilon_g}\left[\mu\left(1 + \frac{16}{3}x^2\right) - 2\varepsilon_t\left(1 + \frac{2}{3}x^2\right)\right]\right\}. \tag{4.32}$$

For extremely low temperatures ($x \ll 1$) this expression becomes

$$\frac{d\theta^2}{dt} \approx \frac{1}{\tau_s}\frac{3}{4}\varepsilon_t^2\left[1 + \frac{q}{\varepsilon_g}(\mu - 2\varepsilon_t)\right]. \tag{4.33}$$

The results for both pure and doped materials are similar and indicate that the behavior of the degenerate semiconductor is completely different from that of the nondegenerate semiconductor, in which the sign of parameter q determines the carrier temperature dynamical behavior due to spontaneous recombination. Here the differential of the carrier temperature at low temperatures is a strongly positive value for positive q and for $q = 0$, which indicates that spontaneous radiative recombination leads to heating of the carrier ensemble. For negative values of parameter q we still have a recombination heating except when $|q| > 7\varepsilon_g / 3(\mu - \varepsilon_g)$ for case (**a**), and $|q| > \varepsilon_g / (\mu - 2\varepsilon_t)$ for case (**b**). In the case (**a**) recombination cooling for negative q is highly unlikely because an extremely large value of q is required: $\mu - \varepsilon_g \ll \varepsilon_g$. For semiconductors with tail states (case (**b**)) the recombination cooling is possible if $q < -1.042$ (an estimate using $\mu = \varepsilon_g = 1$ eV and a band tail parameter $\varepsilon_t = 20$ meV).

The effect of recombination heating (or cooling), however, is not significant when a short (much shorter than a nanosecond) external pulse travels through the material.

This is a result of the longer time scale of the spontaneous recombination process. In general, for short-scale processes the recombination heating can be neglected as well as the spontaneous recombination process itself. For longer time scales, the actual change in temperature due to recombination heating is small compared to the temperature variations due to stimulated processes (see Chapter 3). If no stimulated processes are present, spontaneous recombination keeps the temperature of the carriers different from the lattice temperature.

5. CARRIER HEATING INFLUENCE ON GAIN

In this chapter we focus on the response of the gain and carrier temperature to an external pulse. In our analysis we are interested in dynamics related to carrier heating effects, namely local carrier temperature deviation from the lattice temperature and corresponding variation of the gain coefficient. Spatial behavior of the carrier temperature is irrelevant here since the external pulse front always confronts a carrier ensemble unperturbed by the pulse itself. In addition, the carrier ensemble is not influenced by carriers from adjacent regions already heated by the pulse because the pulse travels much faster than the heat transfers. Thus, unless a pump-probe experiment is numerically simulated or pulse reshaping is considered, the short samples (short enough to exclude propagation effects such as pulse reshaping) are convenient for investigation of carrier temperature and gain coefficient dynamics because spatial effects do not complicate the analysis.

Therefore we choose for our investigation a 1-μm thin sample that is assumed to be antireflection-coated so that the medium is a single-pass system. For such a short sample one can use the photon density equation (2.1a) with $\tau_p = L/v_{gr}$; for longer samples the photon density equation should be replaced by a traveling-wave equation (see, for example, Ref. [95]).

5.1. Medium Parameters

We use material parameters relevant to GaAs [99]. The parameter values used in calculations are presented in Table 5.1.

Table 5.1. Parameter Values for GaAs Medium

Parameter	Symbol	Value
Sample length	$\boldsymbol{L}$	1 μm
Active region width	$\boldsymbol{L}_{\mathrm{w}}$	2 μm
Active layer thickness	$\boldsymbol{L}_{\mathrm{t}}$	0.2 μm
Confinement factor	Γ	0.3
Spontaneous emission factor	β_{sp}	10^{-5}
Refractive index	$\boldsymbol{n}$	3.62
Group velocity index	$\boldsymbol{n}_{gr}$	4.5
Band gap energy	$\varepsilon_g\,(0)$	1.5077 eV
Band tailing parameter	ε_t	20 meV
Dopant concentration	ξ	10^{18} cm^{-3}
Energy density relaxation time	τ_l	5×10^{-13} sec
Spontaneous recombination time	τ_s	1×10^{-9} sec
Free carrier absorption cross-section	s_{FCA}	5×10^{-18} cm^2
Photon energy	$\hbar\omega$	1.5 eV
Lattice temperature	$\boldsymbol{T}_l$	70 K

The calculations are performed for 70 K lattice temperature. The choice of low lattice temperature allows us to use the analytical expressions for relationships between dynamic variables which simplify the problem to ordinary differential equations. For high lattice temperatures, as was mentioned in Chapter 2, the equations are integro-differential and a simple analysis is no longer possible.

We choose the lattice temperature as the initial condition for the carrier temperature in each numerical experiment. The steady-state values of all dynamic variables before the arrival of the external pulse are determined by the carrier injection rate. By the proper choice of the injection current one can make the sample absorbing, transparent, or amplifying. It is convenient to use, as a reference, the injection rate $\boldsymbol{J}_0$ that makes the sample transparent without any external signal. From Eq. (2.1b) we find the relationship between $\boldsymbol{J}_0$ and the carrier density at transparency to be $\boldsymbol{J}_0 = \boldsymbol{N}_{c0}/\tau_e$, and because in our model $\boldsymbol{N}_{c0}$ is a dynamic variable (see Eq. (5.6) below) the value of $\boldsymbol{J}_0$ depends on system parameters and is determined numerically. In particular, for the parameter values given in Table 5.1 (p. 80) we have $\boldsymbol{N}_{c0} \cong 1.67\times10^{18}$ cm^{-3} and the corresponding injection current is 0.106 mA.

The transparency condition here is identified formally with the condition of zero gain ($\boldsymbol{g} = 0$). However, because the FCA and TPA are not included in the gain function, the sample appears to be transparent to the external optical signal only when there is a small amplification in the medium, which compensates for the FCA, TPA and other minor losses. In other words, the sample must be slightly amplifying in order to exhibit zero net absorption, i.e., for the sample to return to its pre-pulse state immediately after the departure of the external pulse. In addition, because the transparency is achieved by

compensation of FCA and TPA (as well as interband absorption), which are dependent on the photon density, whether the sample will appear transparent or not depends on the external pulse energy and duration (see Section 5.5).

The external pulse also can change the carrier density dramatically. As a result the bandgap dependence on the carrier density must be taken into account. The bandgap narrowing due to many-body effects is accounted for by considering the bandgap energy as a function of carrier density according to the expression [100]:

$$\varepsilon_g(N_c) = \varepsilon_g(0) - 1.6\times10^{-8} N_c^{1/3}. \qquad (5.1)$$

The external pulse is coupled to the system via the coupling coefficient $\boldsymbol{k}$ given by (2.5); because our sample is antireflection coated, $\boldsymbol{k} = 1/\tau_p$. The FCA cross section is chosen to be s_{FCA} = 5×10^{-18} cm^2, this value leads to FCA losses equal to 10 cm^{-1} for N_c=2×10^{18} cm^{-3} which is consistent with the values given in the literature [73].

The TPA absorption coefficient is calculated according to Eq.(2.24). For given parameter values and ε_g calculated according to Eq. (5.1) we obtain α_{TPA}~6.28 cm/GW. This is a considerable underestimation compared with experimental results [83, 101]. In order to have more realistic values for our calculations we use Eq. (2.24) with $\boldsymbol{K}$=9700 which gives α_{TPA}~31.4 cm/GW. These values are given for orientation only because α_{TPA} is not a constant due to dependence on ε_g, which is a dynamic variable. Nevertheless, we note that the value of α_{TPA} does not change significantly when the change in carrier density is within a couple of orders of magnitude.

5.2. Gain Dynamics

The behavior of the amplifying medium is extensively studied both experimentally and theoretically using diode laser amplifiers (see Chapter 1 for overview). In this section we focus on carrier temperature and gain dynamics in a forward-biased GaAs *p-n* junction for different carrier injection rates. The calculations described in this section are performed using 0.5 ps (FWHM) Gaussian pulses with $\mathcal{E}_x = 0.1$ pJ energy, unless specified otherwise. The external pulse amplitude is peaked at $\boldsymbol{t} = 0$. The dynamics is observed for a fixed carrier injection rate, then we choose another value for the carrier injection rate and repeat the calculations.

The injection rates $\boldsymbol{J} = 0.99\boldsymbol{J}_0$ and $\boldsymbol{J} = 1.01\boldsymbol{J}_0$ are applied in order to obtain initially absorbing ($\boldsymbol{g} < 0$) and amplifying ($\boldsymbol{g} > 0$) media respectively. As we discussed in the previous section, a $\boldsymbol{J} = 1.0\boldsymbol{J}_0$ injection rate corresponds to an initially zero gain function ($\boldsymbol{g} = 0$); however the sample appears absorbing because of FCA and TPA. For the parameter values given in Table 5.1 (p. 80) the sample becomes really transparent for $\boldsymbol{J} \cong 1.00245\boldsymbol{J}_0$. In this case the carrier density immediately before and after the pulse is the same, i.e. the pulse does not experience net absorption or gain. Corresponding changes in the carrier density from before to after the pulse are $\Delta\boldsymbol{N}_c \cong 3.38\times10^{15}$ cm^{-3} for $\boldsymbol{J} = 0.99\boldsymbol{J}_0$, $\Delta\boldsymbol{N}_c \cong -2.07\times10^{15}$ cm^{-3} for $\boldsymbol{J} = 1.01\boldsymbol{J}_0$, and $\Delta\boldsymbol{N}_c = 0$ for $\boldsymbol{J} \cong 1.00245\boldsymbol{J}_0$.

Figure 5.1 (p. 84) demonstrates the gain dynamics (time evolution of the normalized gain function $\boldsymbol{gL}$) due to the external signal, namely, saturation and recovery in the cases of amplification, transparency, and absorption. In all cases there is noticeable carrier heating.

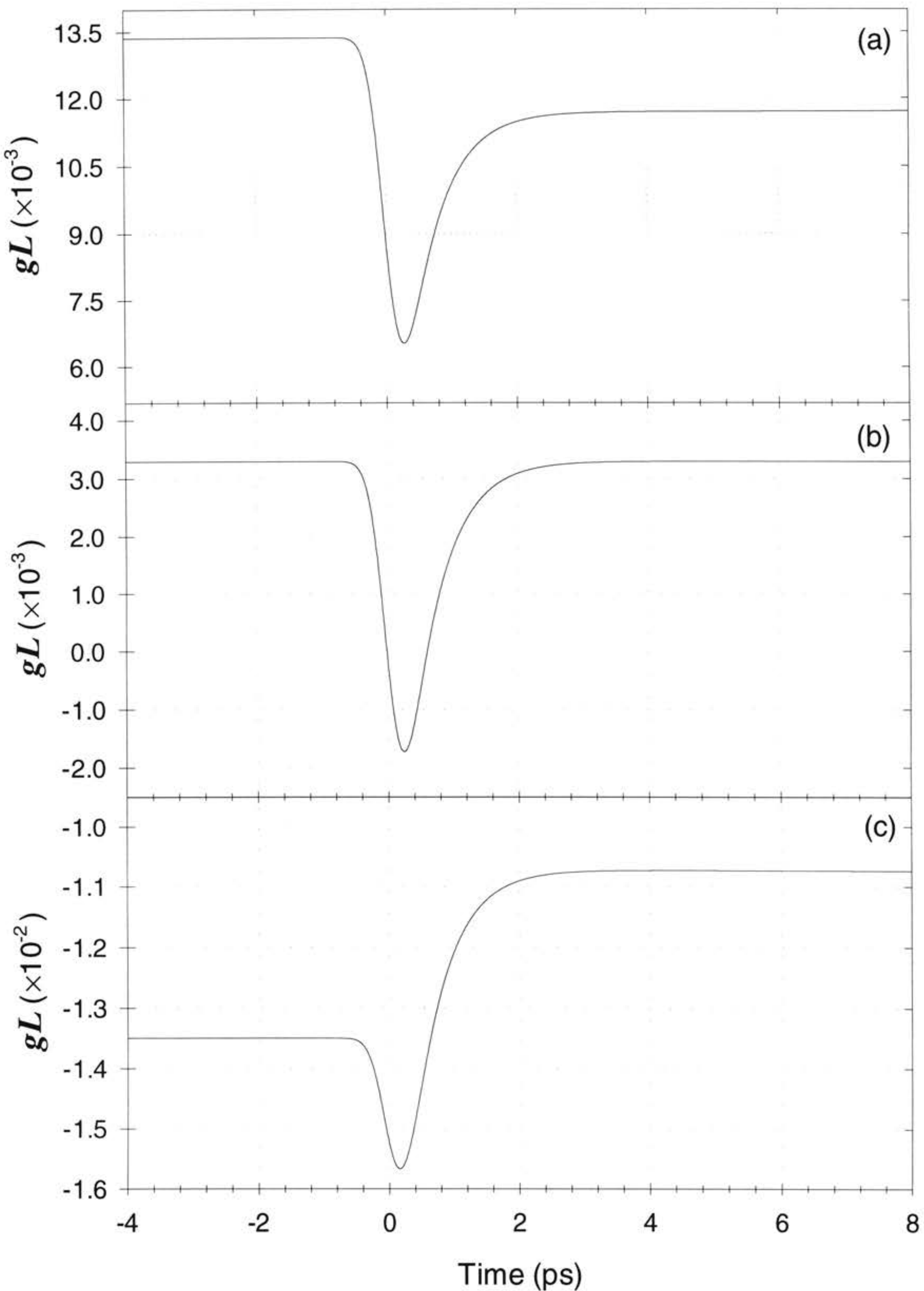

Figure 5.1. Subpicosecond gain dynamics; gain suppression due to carrier heating and recovery in the case of: (a) amplification; (b) transparency; (c) absorption.

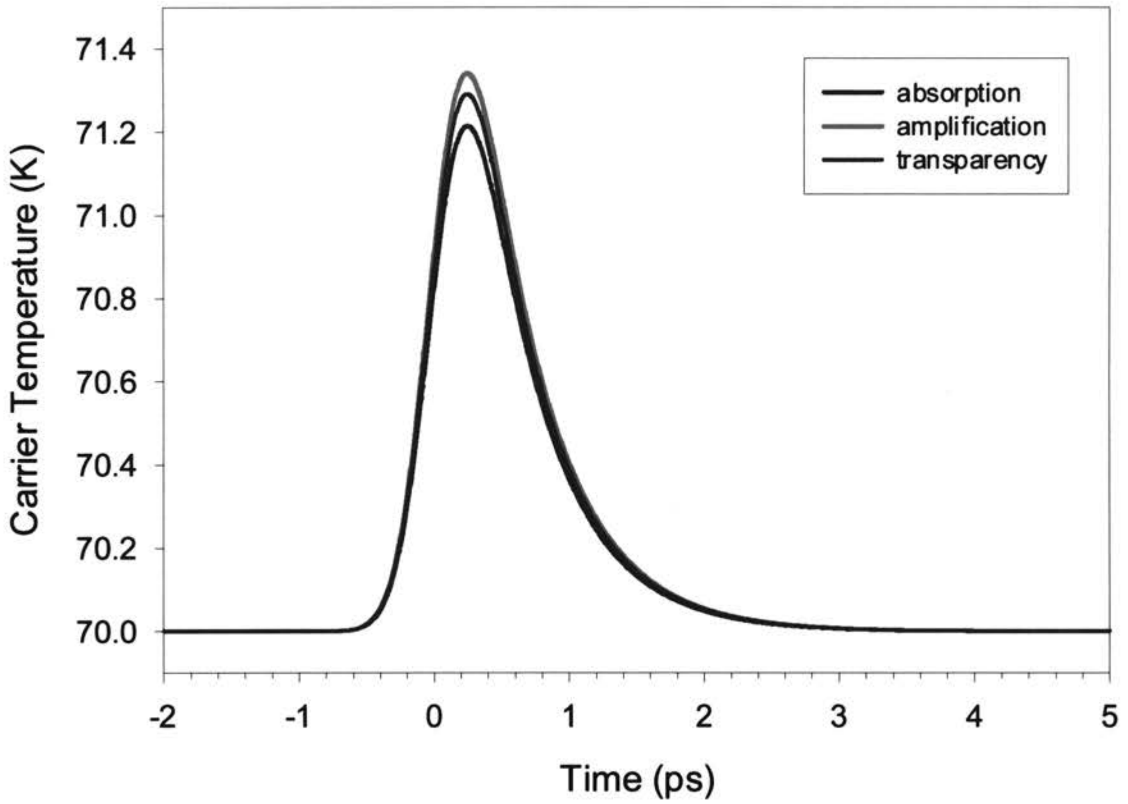

Figure 5.2. Carrier temperature behavior in the case of amplification (red), transparency (green), and absorption (blue).

Corresponding behavior of the carrier temperature is demonstrated in Fig. 5.2. There are slight differences in maximum carrier temperatures. The temperature is higher for a higher injection rate, which is natural because a high pumping rate leads to higher carrier density and therefore higher FCA that heats the system. These results show qualitative agreement between the model developed in this paper and the experimental results of Ref. [13] (see the next section for analysis).

Interestingly, when the sample has initially zero gain the carrier ensemble is heated more effectively. Figure 5.3 (p. 87) demonstrates the gain and carrier temperature behavior for the $\boldsymbol{g} = 0$ case. The gain behavior is similar to that of the absorbing medium but the temperature is much higher (compare Fig. 5.3b (p. 87) with Fig. 5.2).

In this case the process that has the major influence on the carrier system is FCA. Because of zero gain there are no interband transitions. For 0.1 pJ pulse energy TPA has a much smaller effect than FCA (see the next chapter for a more detailed comparison of these two processes). Thus initially the pulse transfers energy to the medium via FCA with very small initial changes in carrier density. This leads to significant carrier heating because FCA increases the energy per particle in the carrier ensemble.

Eventually interband transitions (net absorption) occur because FCA makes lower energy states available for electrons. As a result the medium with initially zero gain coefficient behaves as an absorbing medium which is demonstrated in Fig. 5.3a (p. 87).

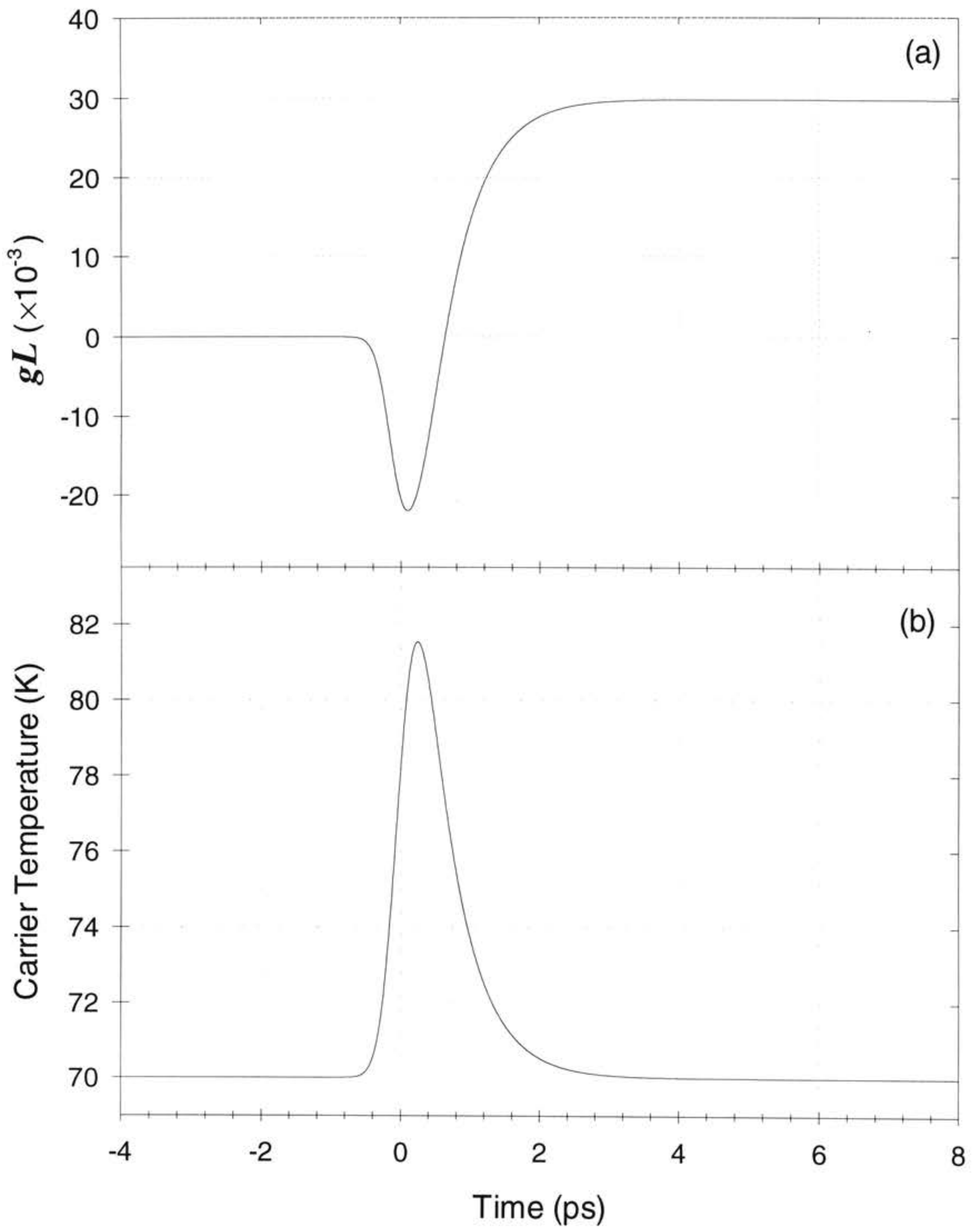

Figure 5.3. Gain (a) and carrier temperature (b) behavior in the case of a medium with initially zero gain.

5.3. Analysis of Carrier Heating Influence on Gain

The results presented above can be analyzed using analytical approximations obtained in the frame of the model described in Chapter 2. Near the transparency region, μ is close to the energy of the emitted photons and therefore

$$\frac{\mu - \hbar\omega}{2\varepsilon_d \theta} << 1. \tag{5.2}$$

The hyperbolic tangent function of small argument can be replaced by its argument and the gain function (2.36) can be approximated as

$$g \approx G(\omega)\frac{\mu - \hbar\omega}{2k_B T_e}. \tag{5.3}$$

Using the same approximation we can rewrite Eq.(2.49) in the form:

$$N_c = \frac{\rho_t \varepsilon_t}{1-\theta^2}\exp\left(\frac{\mu}{\varepsilon_t}\right) = \frac{\rho_t \varepsilon_t}{1-\theta^2}\exp\left(\frac{\hbar\omega}{\varepsilon_t}\right)\exp\left(\frac{\mu - \hbar\omega}{\varepsilon_t}\right) \approx N_{c0}\left(1 + \frac{\mu - \hbar\omega}{\varepsilon_t}\right), \tag{5.4}$$

where the transparency density is defined by

$$N_{c0} \equiv \frac{\rho_t \varepsilon_t}{1-\theta^2}\exp\left(\frac{\hbar\omega}{\varepsilon_t}\right). \tag{5.5}$$

Using expressions (5.3) and (5.4) one can write the gain function as:

$$g(N_c, \theta) = \frac{1}{2}\frac{G}{\theta}\frac{N_c - N_{c0}}{N_{c0}} = \gamma\left(N_c - N_{c0}\right), \tag{5.6}$$

where the parameter $\gamma = G/2N_{c0}\theta$ is the differential gain coefficient.

Equation (5.6) shows that heating of the carriers leads to gain suppression. For small variations of θ from θ_l and taking into account the temperature dependence of both γ and N_{c0}, we can expand g to first order in $\Delta\theta/\theta_l \equiv \left(\theta - \theta_l\right)/\theta_l$, and obtain

$$g(N_c,\theta) = \gamma_l\left[(N_c - N_{c0l})(1 - \Delta\theta/\theta_l) - bN_{c0l}\,\Delta\theta/\theta_l\right], \tag{5.7}$$

with $\gamma_l \equiv \gamma(\theta_l)$, $N_{c0l} \equiv N_{c0}(\theta_l)$, and $b \equiv 2\theta_l^2/(1+\theta_l^2)$.

One can see that the gain function (5.7) is different from that of the linear model given by Eq.(1.5). If we try to rewrite the gain function (5.7) in the form of Eq. (1.5), we find that β=b+1, γ=γ_l, and there exists a second temperature-dependent term, $\gamma_l N_{c0l}\,\Delta\theta/\theta_l$.

It is also relevant to compare Eq.(5.7) with Eq.(1.4), which is common in the literature [60– 62]. We can make this comparison by rewriting Eq. (5.7) in the following way:

$$g = \gamma_l(N_c - N_{c0l})(1-(b+1)\,\Delta\theta/\theta_l) - \gamma_l N_{c0l} b\,\Delta\theta/\theta_l\,, \tag{5.8}$$

and applying a Taylor expansion for the fractional temperature difference $\Delta\theta/\theta_l$ in terms of N_p to obtain $\Delta\theta/\theta_l = a_0 + a_1 N_p + \cdots$. In this expression a_0 and a_1 are parameters that can be calculated from carrier temperature equation (see Eq. (2.47)). The parameter a_0 is the fractional carrier temperature deviation when $N_p = 0$ and it depends on the pumping characteristics (see below threshold behavior of carrier temperature in laser, Chapter 3). Now the gain function can be presented in the same way as in Eq. (1.4) by writing

$$\gamma = \gamma_l\left[1-(b+1)a_0\right] \tag{5.9}$$

and

$$s = \frac{(b+1)a_1}{1-(b+1)a_0}. \tag{5.10}$$

Note however, that Eq.(5.8) includes an additional term, ($-\gamma_l N_{c0l} b\,\Delta\theta/\theta_l$), that also gives a contribution to gain suppression due to carrier heating, but which is independent of $N_c - N_{c0l}$. This term causes a decrease in g with an increase in carrier

temperature whether there is gain, transparency, or absorption. In the numerical calculations in the previous section we considered the behavior of the gain function when there is carrier heating in the following three different cases:

a) $N_c > N_{c0l}$ (amplifying medium); the carrier heating leads to a drop in the gain since both temperature-dependent terms in the gain function tend to suppress the gain.

b) $N_c = N_{c0l}$ (transparent medium); the only nonzero term in Eq.(5.9) is negative due to carrier heating, making the transparent medium absorptive.

c) $N_c < N_{c0l}$ (absorbing medium); in this case the two temperature-dependent terms play against each other. One term (proportional to $N_c - N_{c0l}$) tends to increase ***g***, while the other term tends to decrease it. When N_c is close to N_{c0l}, then the second term dominates, i.e., $bN_{c0l} >> (b+1)|N - N_{c0l}|$ and the gain decreases (absorption increases). When $N_c << N_{c0l}$, then $bN_{c0l} << (b+1)|N - N_{c0l}|$ and the gain increases (absorption decreases) (this case is considered in Chapter 6 in more detail). Moreover, these gain changes due to carrier heating relax much faster than the spontaneous recombination time and can only be observed on the subpicosecond time scale.

Thus, in the cases of gain, transparency, and absorption (for $N_c \sim N_{c0l}$), the gain function has a minimum when the carrier temperature is maximum. This is precisely the behavior that was observed by Kesler and Ippen in their experiment with laser amplifiers [13]. Figure 5.1 (p. 84) demonstrates qualitative behavior of the gain function similar to that observed in the Kesler-Ippen experiment and corresponds to the situation when $bN_{c0l} >> (b+1)|N - N_{c0l}|$. Because of this we see the dip in the gain function in all three cases.

It should be noted that in experiments the gain behavior is not measured directly. In ultrafast measurements based on pump-probe technique usually a transmission change is measured. For a single-pass system (antireflection coated sample) the transmission coefficient is given by

$$\boldsymbol{Tr} \equiv \frac{\boldsymbol{I}_{out}}{\boldsymbol{I}_{in}} = \exp(\boldsymbol{gL}). \tag{5.11}$$

Correspondingly the fractional transmission change related to the change in gain coefficient as follows:

$$\frac{\Delta \boldsymbol{Tr}}{\boldsymbol{Tr}} = \exp(\Delta \boldsymbol{gL}) - 1 \tag{5.12}$$

In our numerical analysis we use the value of $\boldsymbol{gL}$ to follow the gain dynamics.

5.4. Gain Behavior Far From Transparency Region

The results presented in Section 5.2 are obtained for a sample that is close to transparency. The analysis of gain behavior in the previous section suggests that in the case of an absorbing sample far from the transparency region, where $\boldsymbol{N}_c$ is much less than $\boldsymbol{N}_{c0t}$, the gain function will have a peak at the point of maximum carrier heating. To verify this result we carry out calculations using a sample with a low injection rate, $\boldsymbol{J} = 0.5\boldsymbol{J}_0$. The result is presented below in Fig. 5.4 (p. 92). As expected, there is a peak in the gain behavior that indicates absorption suppression due to carrier heating.

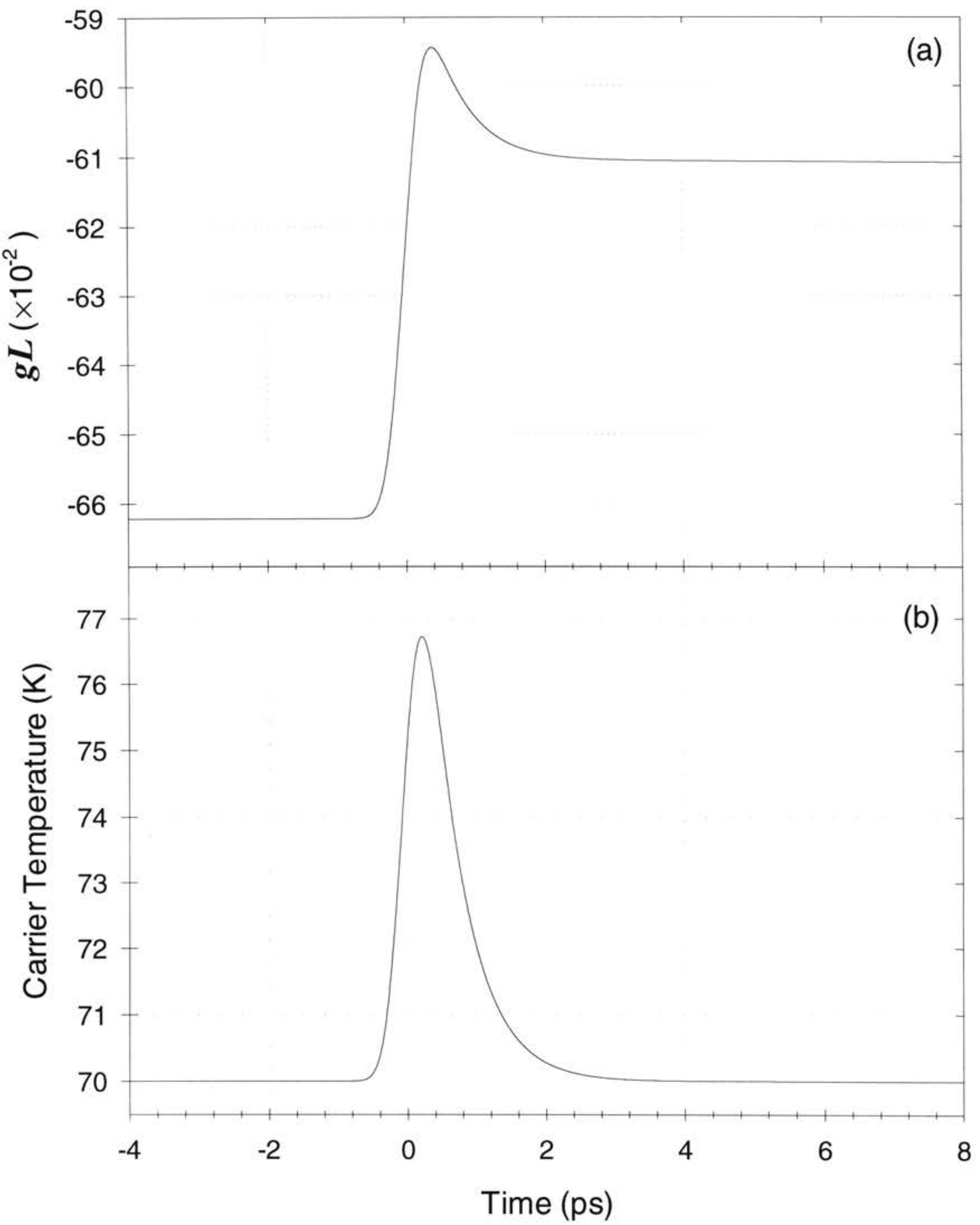

Figure 5.4. Gain (a) and carrier temperature (b) behavior in the case of an absorbing medium far from transparency ($\boldsymbol{J} = 0.5\,\boldsymbol{J}_0$).

For the injection rate $\boldsymbol{J} = 0.75\boldsymbol{J}_0$ there is no noticeable gain or absorption suppression, although there is carrier heating (see Fig. 5.5, p. 94). This indicates that carrier heating does not always lead to gain or absorption suppression. Also note that the carrier temperature is higher for the sample with larger absorption (the sample with $\boldsymbol{J} = 0.5\boldsymbol{J}_0$), although FCA initially is larger for the less-absorbing sample (because of larger carrier density). This is a result of heating due to carrier absorption; increasing carrier density in the conduction band means more energy in the carrier ensemble and also leads to larger FCA and therefore more heating. The carrier density changes from before to after the pulse are $\Delta N_c \cong 8.79\times10^{16}$ cm^{-3} for $\boldsymbol{J} = 0.5\boldsymbol{J}_0$ and $\Delta N_c \cong 5.72\times10^{16}$ cm^{-3} for $\boldsymbol{J} = 0.75\boldsymbol{J}_0$.

The results for an amplifying sample ($\boldsymbol{J} = 1.5\boldsymbol{J}_0$ and $\boldsymbol{J} = 1.25\boldsymbol{J}_0$) are qualitatively the same (see Fig.5.6, p. 95), as they should be according to the analysis in Section 5.3. Corresponding changes of the carrier density before and after the pulse are: $\Delta N_c \cong -1.57\times10^{17}$ cm^{-3} for $\boldsymbol{J} = 1.5\boldsymbol{J}_0$ and $\Delta N_c \cong -8.49\times10^{16}$ cm^{-3} for $\boldsymbol{J} = 1.25\boldsymbol{J}_0$.

The gain and carrier temperature behavior under the influence of short pulses with different energies is considered for a strongly absorbing or amplifying medium in the next chapter.

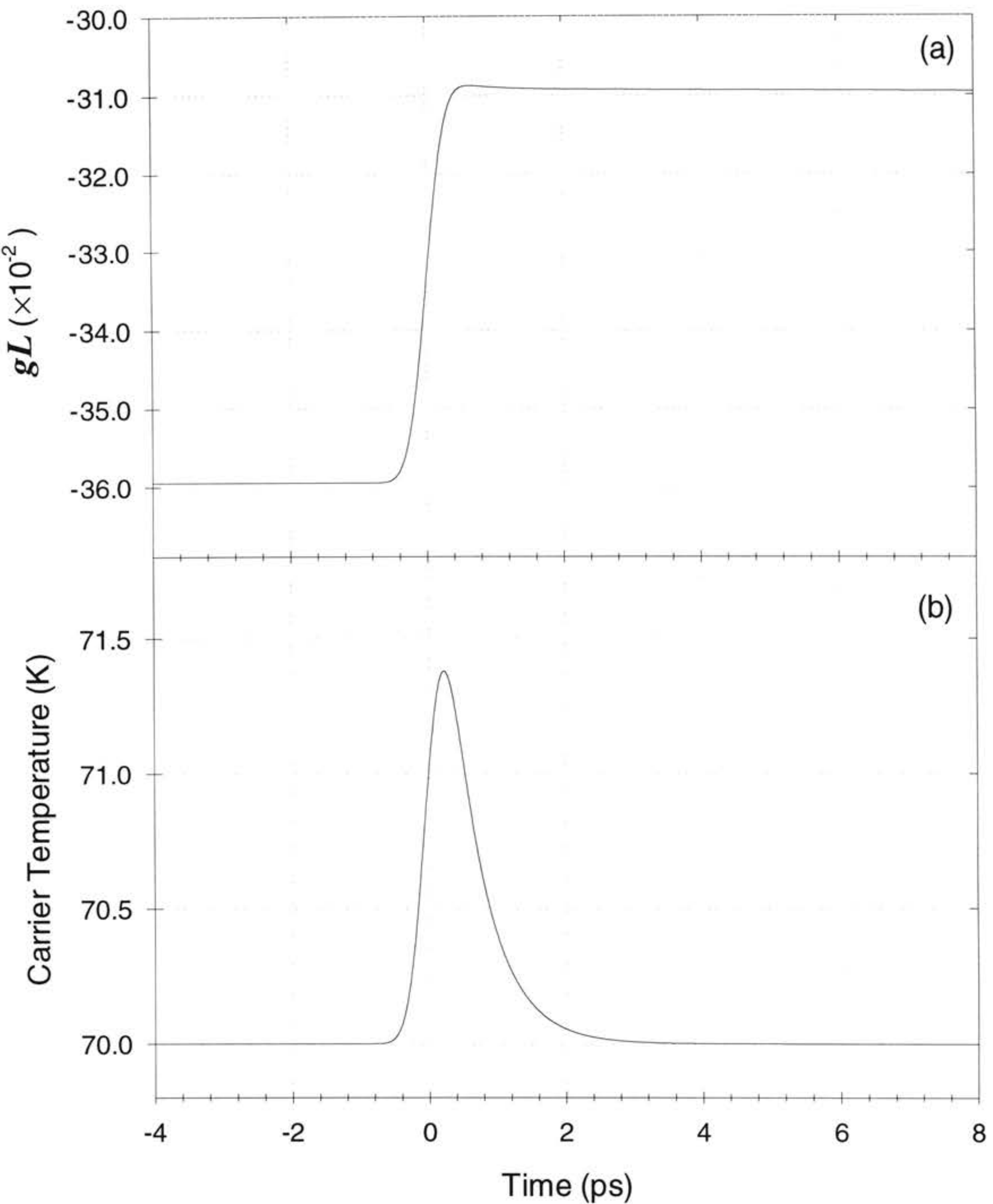

Figure 5.5. Gain (a) and carrier temperature (b) behavior in the case of an absorbing medium far from transparency ($\boldsymbol{J} = 0.75\,\boldsymbol{J}_0$).

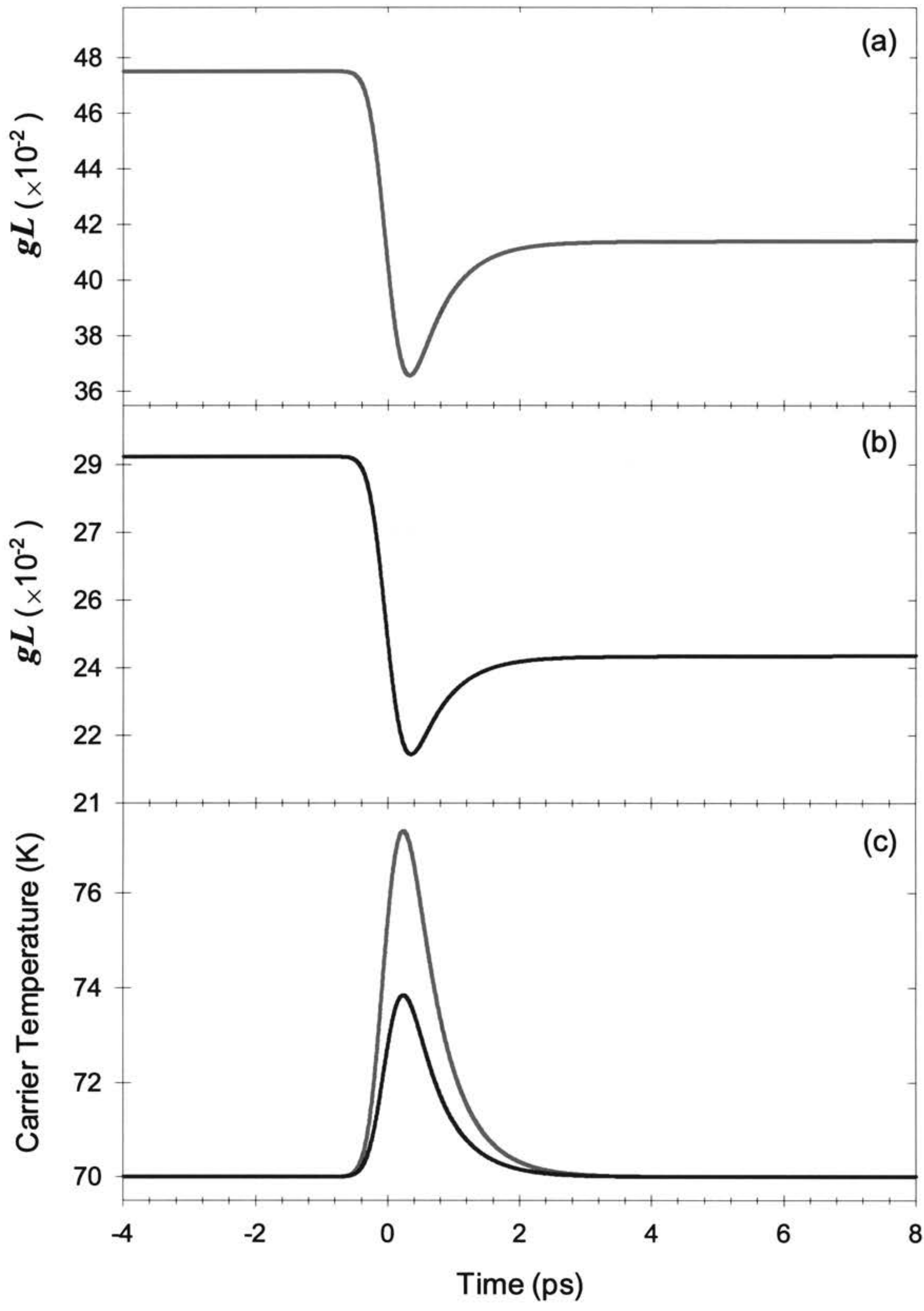

Figure 5.6. Gain (a, b) and carrier temperature (c) behavior in the case of an amplifying medium far from transparency ($J = 1.5\,J_0$ (red) and $J = 1.25\,J_0$ (blue)).

5.5. Gain Behavior in a Transparent Medium

As we mentioned earlier (Section 5.2) the sample is really transparent for injection rates higher than $\boldsymbol{J}_0$, which gives a zero gain coefficient. In this section we investigate the influence of external pulse parameters on the behavior of the sample. For this purpose we fix the carrier injection rate at $\boldsymbol{J} \cong 1.00245\boldsymbol{J}_0$, which makes the sample transparent for a pulse with 0.1 pJ energy and 0.5 ps duration (FWHM). We follow the gain behavior for a 0.5-ps pulse with energy 0.2 pJ and 0.05 pJ. Another set of calculations is carried out with 0.25-ps and 1.0-ps pulses with 0.1pJ energy. The results are presented in Figs. 5.7 and 5.8 (pp. 97-98). For comparison, in both figures we include the results of calculations for a 0.5 ps pulse with 0.1 pJ energy. As we see, whether the medium is transparent depends not only on the carrier injection rate and other medium parameters, but also on parameters of the external pulse. For example, if the medium is transparent for a 1-ps pulse with 0.1 pJ energy, then it is amplifying for a pulse with the same duration but lower energy and for a pulse with the same energy but longer duration. For a pulse with the same duration but higher energy and for a pulse with the same energy but shorter duration the medium will appear absorbing. The graphs for carrier density in Figs. 5.7b-5.8b clearly show the increase (decrease) of the carrier density in the case of absorption (amplification). In the case of transparency the gain coefficient and the carrier density are the same before and immediately after the pulse passes through the medium.

These results show that the external pulse influences the state of the medium; the transparent medium may appear as absorbing, amplifying or transparent depending on the energy and duration of the pulse. The Influence of an external pulse on the state of an absorbing or amplifying medium is considered in the next chapter.

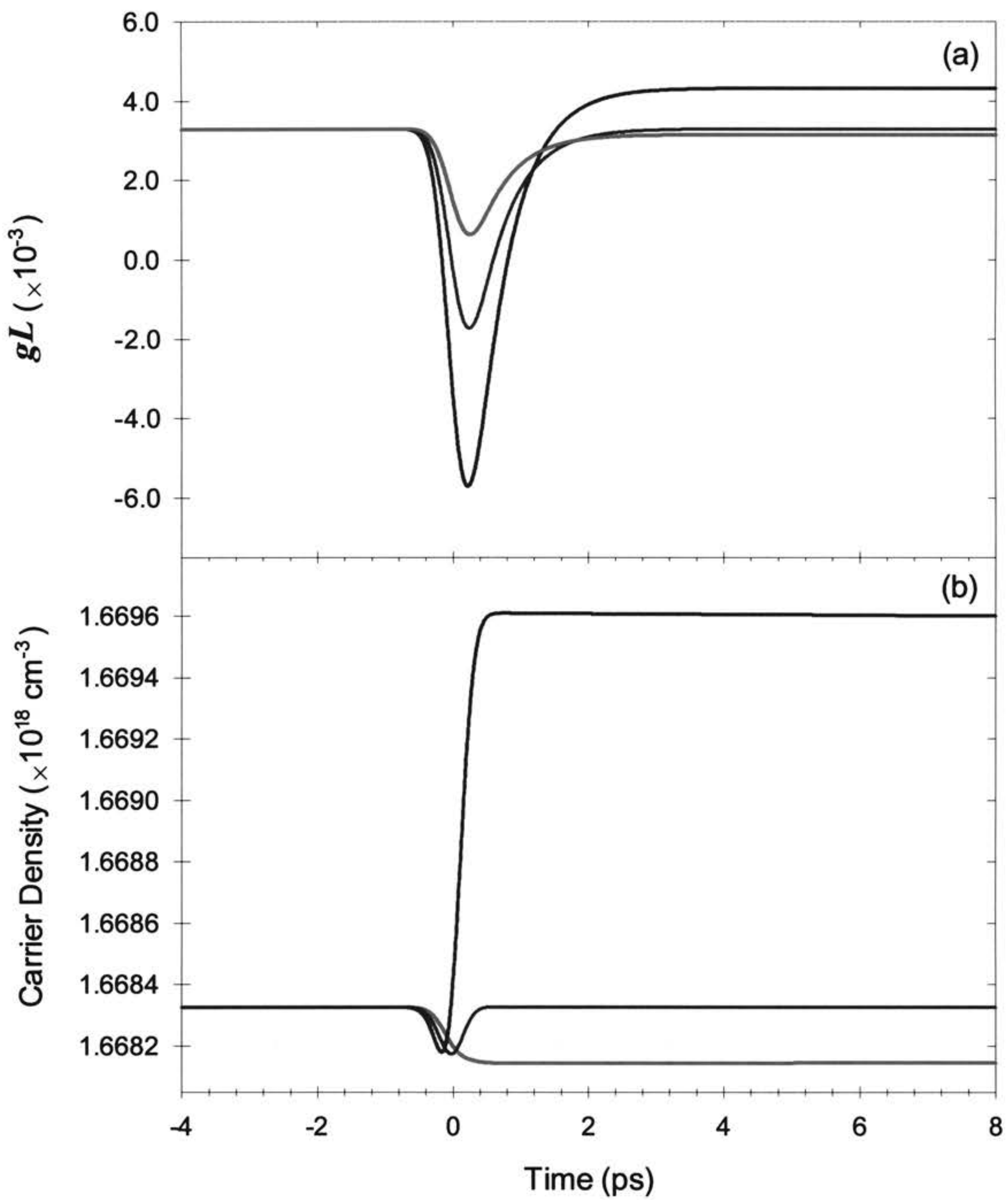

Figure 5.7. Gain (a) and carrier density (b) behavior in a medium that is transparent for the 1.0-ps pulse with 0.1 pJ energy (green curves). Blue curves correspond to a 1.0-ps pulse with 0.2 pJ energy and red curves correspond to a 1.0-ps pulse with 0.05 pJ energy.

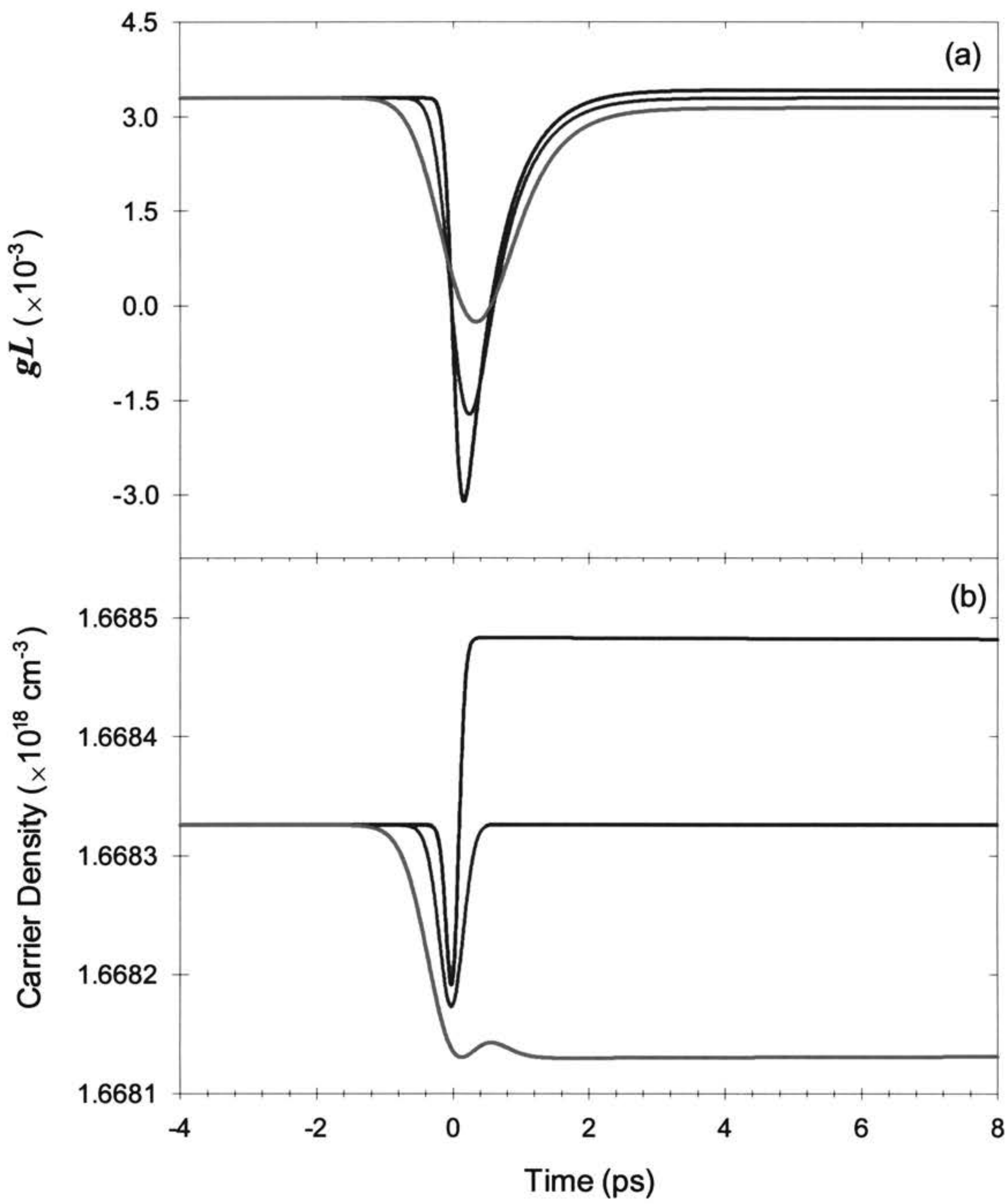

Figure 5.8. Gain (a) and carrier density (b) behavior in a medium that is transparent for the 1.0-ps pulse with 0.1 pJ energy (green curves). Blue curves correspond to a 0.25-ps and red curves correspond to a 1.0-ps pulse, both with 0.1 pJ energy.

6. GAIN AND CARRIER TEMPERATURE DYNAMICS

In the previous chapter we considered mainly the behavior of the medium that is close to transparency (weakly absorbing or amplifying, and transparent). Typical behavior of the gain and carrier temperature in a medium far from transparency was also demonstrated. In this chapter, we consider a medium far from transparency region (strongly absorbing or amplifying) in more detail. In particular, we change the external pulse energy and monitor the state of the medium before and after the pulse as well as the gain and carrier temperature dynamics during the interaction. The numerical procedure and medium parameters are the same as in Chapter 5 (see Section 5.1, Table 5.1, p. 80).

From a practical point of view the medium far from transparency is important because in most applications amplifiers operate in the high gain regime, far from the transparency region. Carrier dynamics in an absorbing medium is also of interest and relevant devices are saturable absorbers (reverse-biased *p-i-n* structures). (See Refs. [102–104] for carrier heating effects in these devices). Here, we focus on carrier temperature and gain dynamics in a forward-biased *p-n* structure in the case of strong absorption or amplification.

The analysis in the previous chapter (Section 5.3) shows that, generally, depending on carrier injection rate and pulse energy, we observe the following short-time behavior of the gain: i) gain suppression in an amplifying medium; ii) absorption enhancement both in a transparent (zero gain) medium and in an absorbing medium close

to transparency; and iii) absorption suppression in an absorbing medium far from transparency. The calculations show that in all these cases the suppression or enhancement is caused by substantial carrier heating and relaxes on the time scale of τ_l (see figures in Chapter 5).

6.1. Dynamic Behavior in an Amplifying Medium

The results described in this section are obtained using pulse energies ranging from $\mathcal{E}_x = 0.1$ pJ to 25.0 pJ with the injection rate $\boldsymbol{J_e} = 1.75\boldsymbol{J}_0$ (strongly amplifying medium). In figures 6.1 and 6.2 (pp. 101 - 102) we demonstrate the behavior of the dimensionless gain coefficient (***gL***) and carrier temperature.

The results for low energy pulses are qualitatively similar; an initially amplifying medium shows gain suppression accompanied by carrier heating. The gain function always stays in the amplifying region. For pulses with higher energy we see the usual gain suppression too, but in the case of the 5.0-pJ and 25-pJ pulses the gain function becomes negative for a short time. As a result some part of these pulses are actually absorbed. However, while the 5.0-pJ pulse is amplified, the 25-pJ pulse actually experiences absorption (as evident from the change in the carrier density before and after the pulse, see Fig. 6.3, p. 103). This is explained by the fact that the 25-pJ pulse saturates the gain faster than the 5.0-pJ pulse and a substantial part of the 25-pJ pulse sees an absorbing medium rather than an amplifying medium. The temperature curves (Figs. 6.1b and 6.2b) are qualitatively the same for all pulse energies. We note, however, that the maximum carrier temperature is not directly proportional to the pulse energy but shows some nonlinear dependence (see Section 6.4 for details).

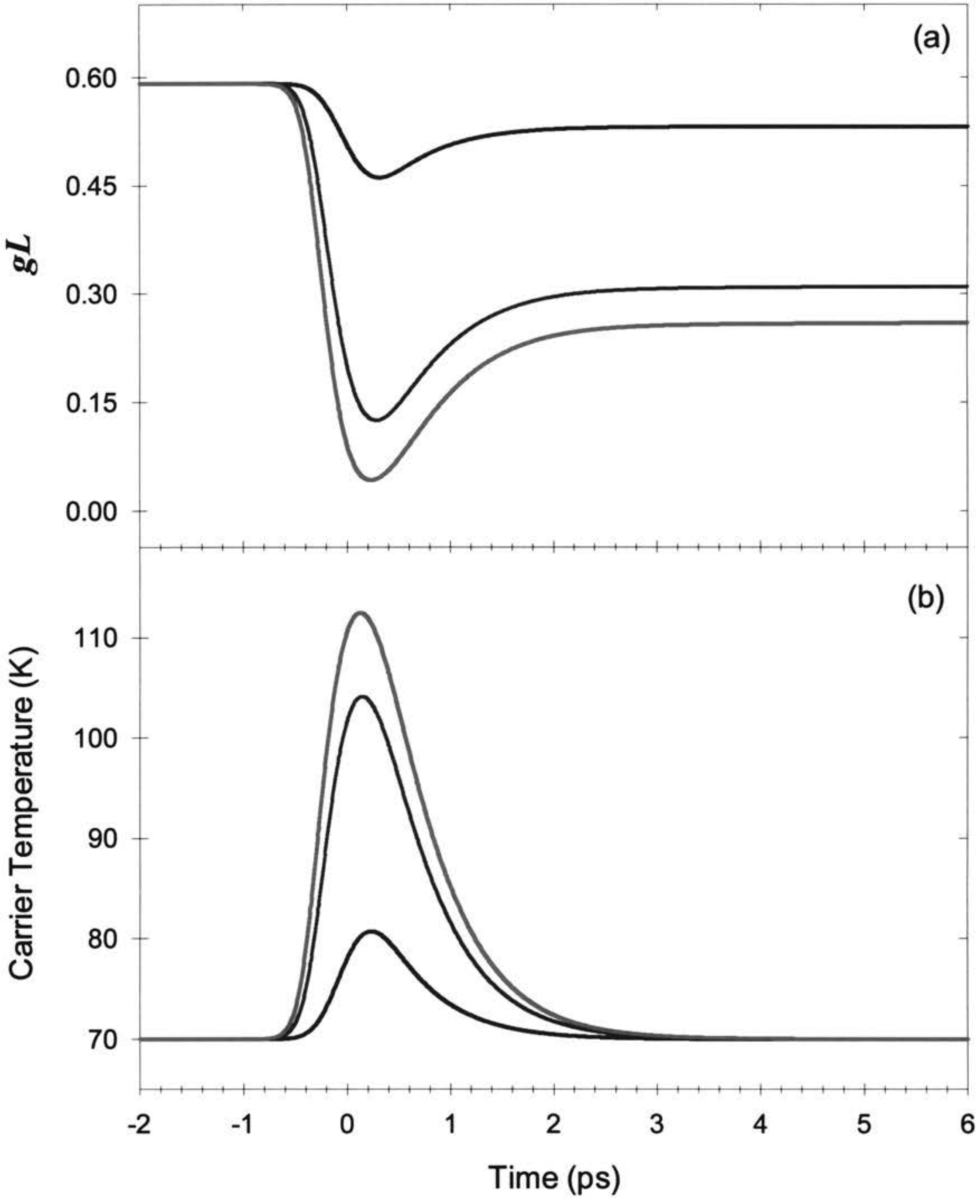

Figure 6.1. Gain (a) and carrier temperature (b) behavior in a strongly amplifying medium pumped at a rate of $1.75\boldsymbol{J}_0$. The external pulse has 1.0 ps (FWHM) duration with energy: 0.1 pJ (blue curves), 1.0 pJ (green curves), and 2.0 pJ (red curves).

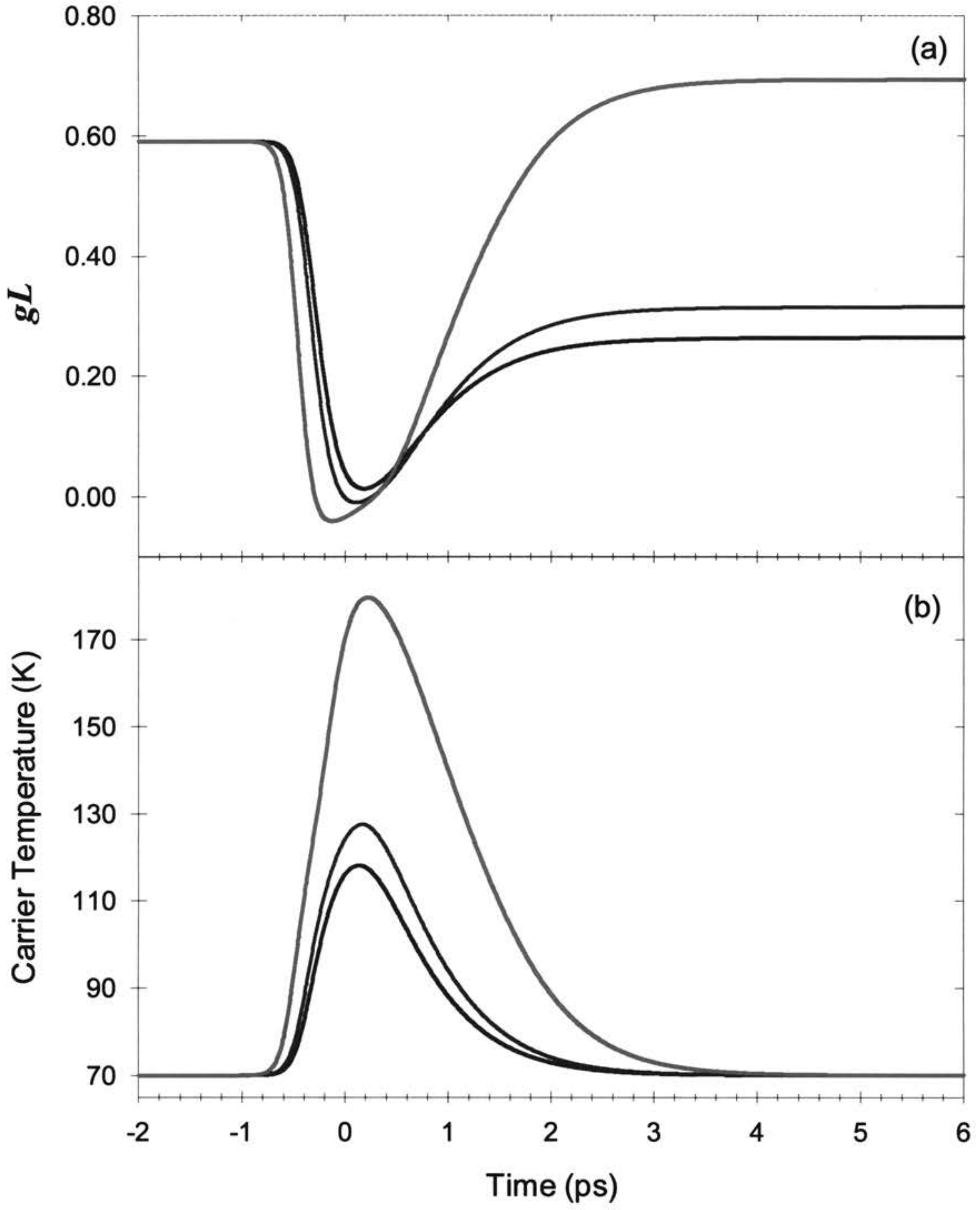

Figure 6.2. Gain (a) and carrier temperature (b) behavior in a medium pumped at a rate of $1.75\boldsymbol{J}_0$. The external pulse has 1.0 ps (FWHM) duration with energy: 3.0 pJ (blue curves), 5.0 pJ (green curves), and 25.0 pJ (red curves).

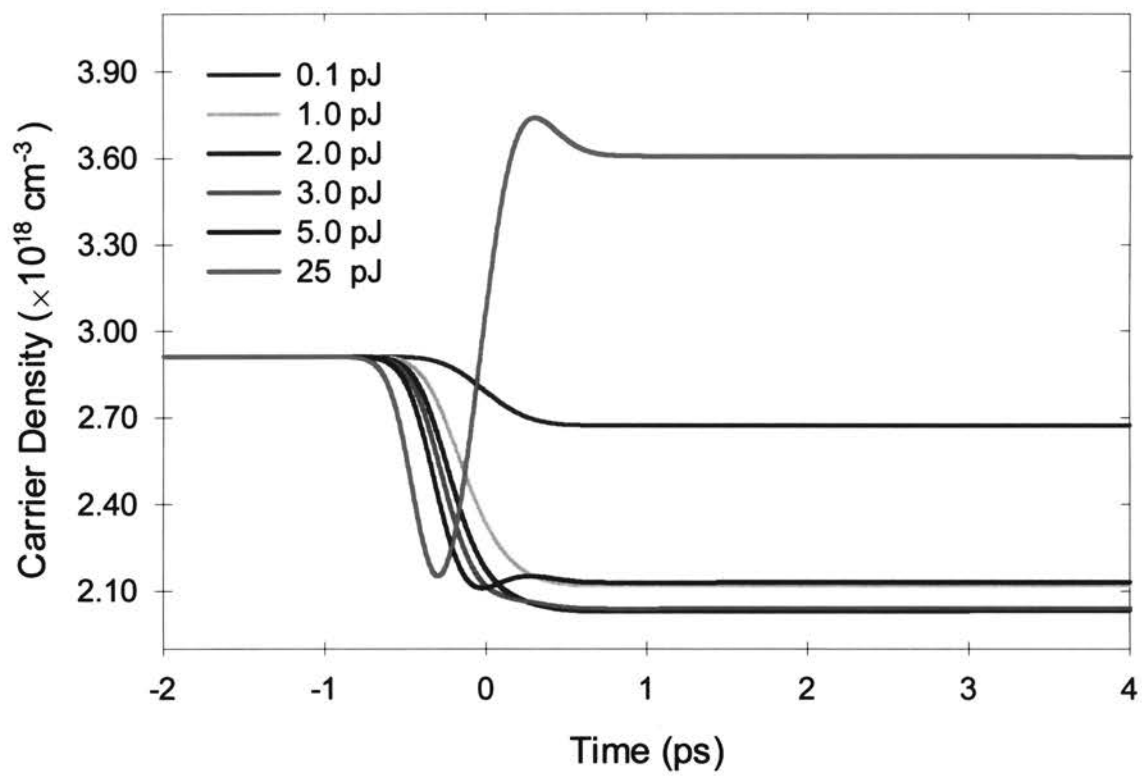

Figure 6.3. Carrier density behavior for various pulse energies.

6.2. Dynamic Behavior in An Absorbing Medium

The case of an initially absorbing medium is shown in Figs. 6.4 and 6.5 (pp. 105-106). Absorption suppression (the gain coefficient peak) caused by carrier heating is noticeable for the 0.1-pJ pulse (the blue curve in Fig. 6.4, p. 105). For the 1.0-pJ pulse (the green curve) the absorption suppression is hardly visible, and for the 2.0-pJ pulse there is no gain coefficient peak at all, although in all cases there is substantial carrier heating, as seen in Fig. 6.4b (p. 105). The carrier temperature behavior is quite similar for all three pulses; it is interesting that the 1.0-pJ pulse heats the carriers almost as effectively as the 2.0-pJ pulse (green and red curves in fig. 6.4b, p. 105). Also, comparison of the results for the 0.1-pJ and 1.0-pJ pulses show that there is

approximately 1.4 times difference in peak carrier temperature changes for pulses with energies that differ by a factor of ten.

To understand the behavior demonstrated in Figs. 6.4 and 6.5 (pp. 105 - 106) we compare the carrier densities before (t = -2 ps) and after (t = +6 ps) the external pulse. The carrier density changes from ~0.4×10^{18} cm^{-3} to ~0.5×10^{18} cm^{-3} for the 0.1-pJ pulse, to ~ 1.2×10^{18} cm^{-3} for the 1.0-pJ pulse, and to ~ 1.6×10^{18} cm^{-3} for the 2.0-pJ pulse. The higher energy pulses pump more energy into the medium, but they also produce a greater increase in the carrier density, hence less energy per particle. The increase in carrier density tends to lower the carrier temperature because absorption involves cold carriers (absorbed carriers occupy the bottom of the conduction band). The graph with carrier density plots for pulse energies ranging from 0.1 pJ to 25 pJ is presented in Fig. 6.6 (p. 107).

Next we apply pulses with energies $\mathcal{E}_x = 3.0$ pJ, 5.0 pJ and 25.0 pJ; the results are included in Fig. 6.5 (p. 106). We see both quantitative and qualitative changes in the dynamic behavior of the gain and carrier temperature from that presented in Fig. 6.4 (p. 105). Here the pulse energies are high enough to make the initially absorbing medium amplifying. Note that in the amplifying medium the energy of the 3-pJ pulse is not enough to bleach the medium (Fig. 6.2a), while here in the absorbing medium a pulse with the same energy bleaches the medium and makes it amplifying. The initially negative gain function reaches a slightly inclined plateau near the transparency region (g ~ 0) before becoming positive. The plateau is wider for higher energy pulses. Further increase of the gain coefficient is a consequence of carrier cooling, which is evident from the carrier temperature graph (Fig. 6.5b, p. 106).

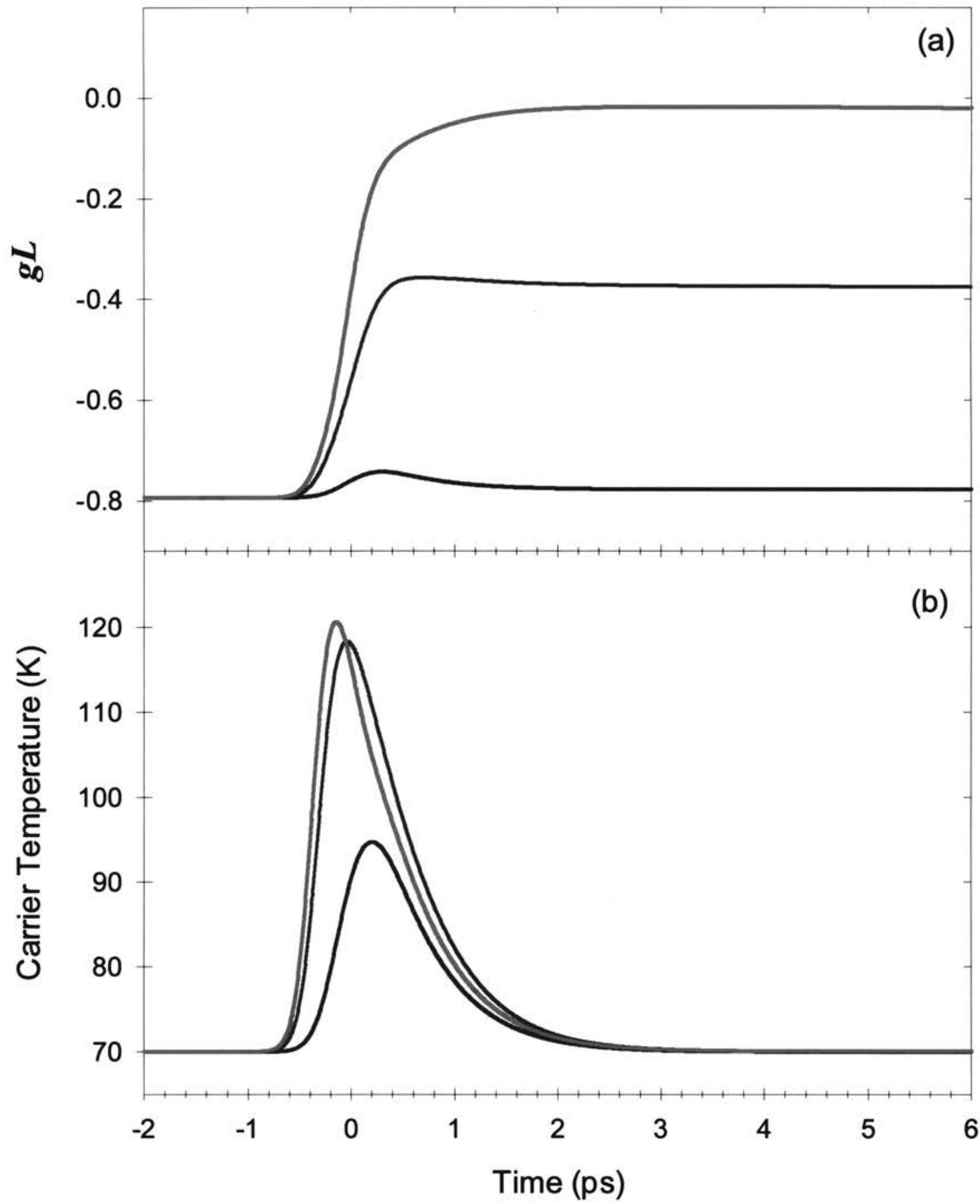

Figure 6.4. Gain (a) and carrier temperature (b) behavior in a strongly absorbing medium pumped at a rate of $0.25\boldsymbol{J}_0$. The external pulse has 1.0 ps (FWHM) duration with energy: 0.1 pJ (blue curves), 1.0 pJ (green curves), and 2.0 pJ (red curves).

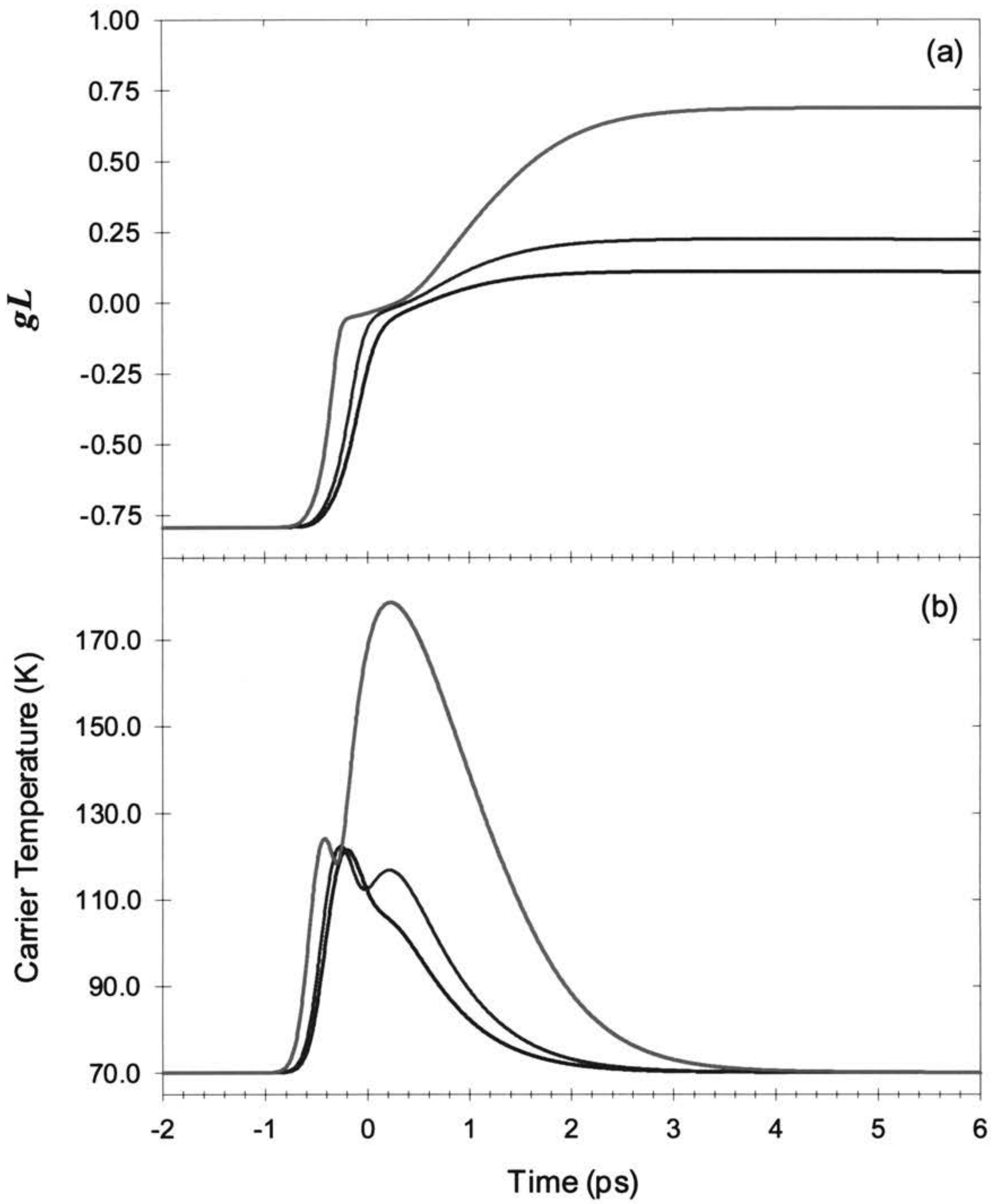

Figure 6.5. Gain (a) and carrier temperature (b) behavior in a strongly absorbing medium pumped at a rate of $0.25\boldsymbol{J}_0$. The external pulse has 1.0 ps (FWHM) duration with energy: 3.0 pJ (blue curves), 5.0 pJ (green curves), and 25.0 pJ (red curves).

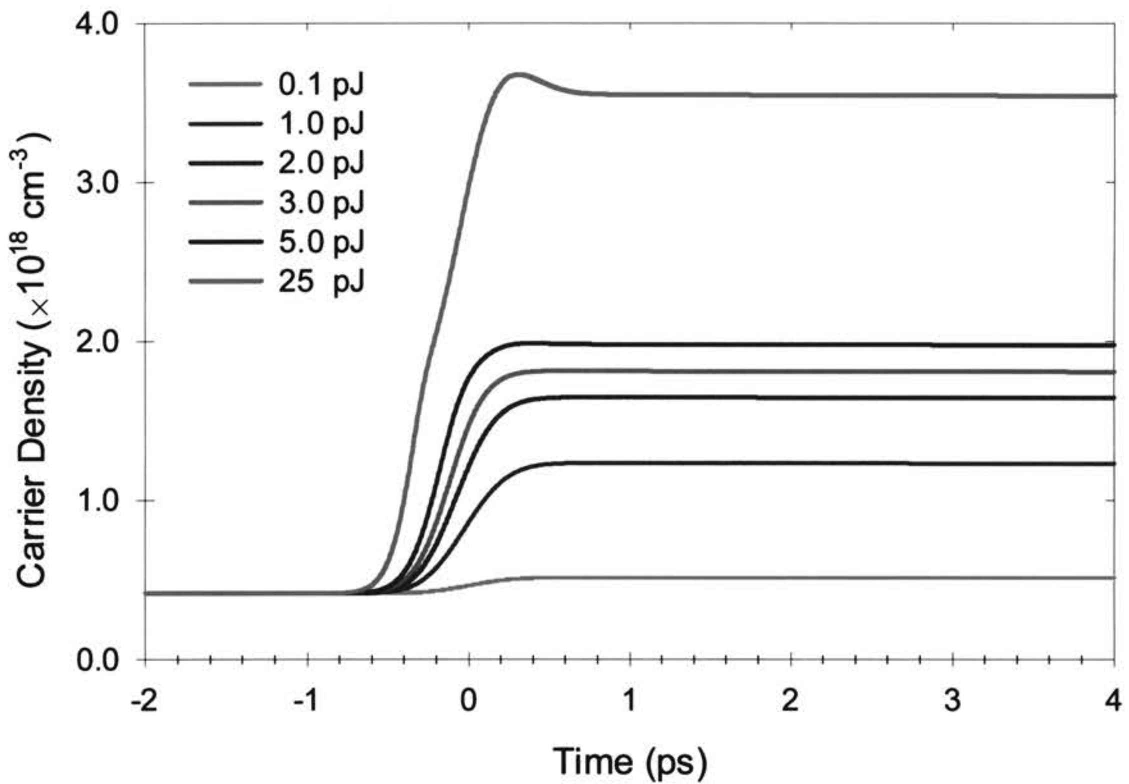

Figure 6.6. Carrier density behavior for various pulse energies.

The most unexpected behavior observed for higher pulse energies is the double-peak behavior of the carrier temperature. This indicates that the carrier temperature dynamics is significantly different from the single peak temperature behavior observed when an external pulse with smaller energy is applied (Fig. 6.4b, p. 105), i.e. the temperature behavior changes qualitatively when the applied pulse has energy enough to bleach the sample. A second temperature-peak appears and its amplitude increases with increasing pulse energy almost the same way as in the case of the amplifying medium. This type of behavior of carrier temperature is observed only in a strongly absorbing medium. For comparison we carry out calculations similar to those that led to the results presented in Figs. 6.4 and 6.5 (pp. 105-106) but with injection rates equal to $0.75\boldsymbol{J}_0$ and $0.5\boldsymbol{J}_0$. The results are presented in Figs. 6.7 and 6.8 (pp. 109-110).

The carrier temperature has only one peak when the pumping rate is $0.75\boldsymbol{J}_0$ (Fig. 6.7b, p. 109) and $0.5\boldsymbol{J}_0$ (Fig. 6.8b, p. 110); however in the latter case the maximum carrier temperature is preceded by a bump, which becomes a local maximum (the first peak) for lower pumping rates (Fig. 6.5b, p. 106) when high-energy pulses are applied. Thus, the pumping rate affects the carrier temperature dynamics.

In contrast, the gain behavior is remarkably similar for different pumping rates. The initial rapid raise of the gain coefficient leads to the increase in carrier density. As a result the carrier temperature significantly increases because of FCA and TPA (since they both are proportional to carrier density). In turn the high carrier temperature has a negative impact on the further increase of the gain coefficient, which is slowed down while temperature reaches its (second) peak. Finally, when the external pulse leaves the medium, the carriers cool down and the gain coefficient increases again. Further changes in the gain coefficient are due to carrier recombination, which leads to a gain decrease on the nanosecond time scale to its initial (pre-pulse) value determined by the pumping rate.

The above results suggest that the carrier temperature behavior needs more detailed investigation. We discuss the carrier temperature dynamics in more detail in the next section.

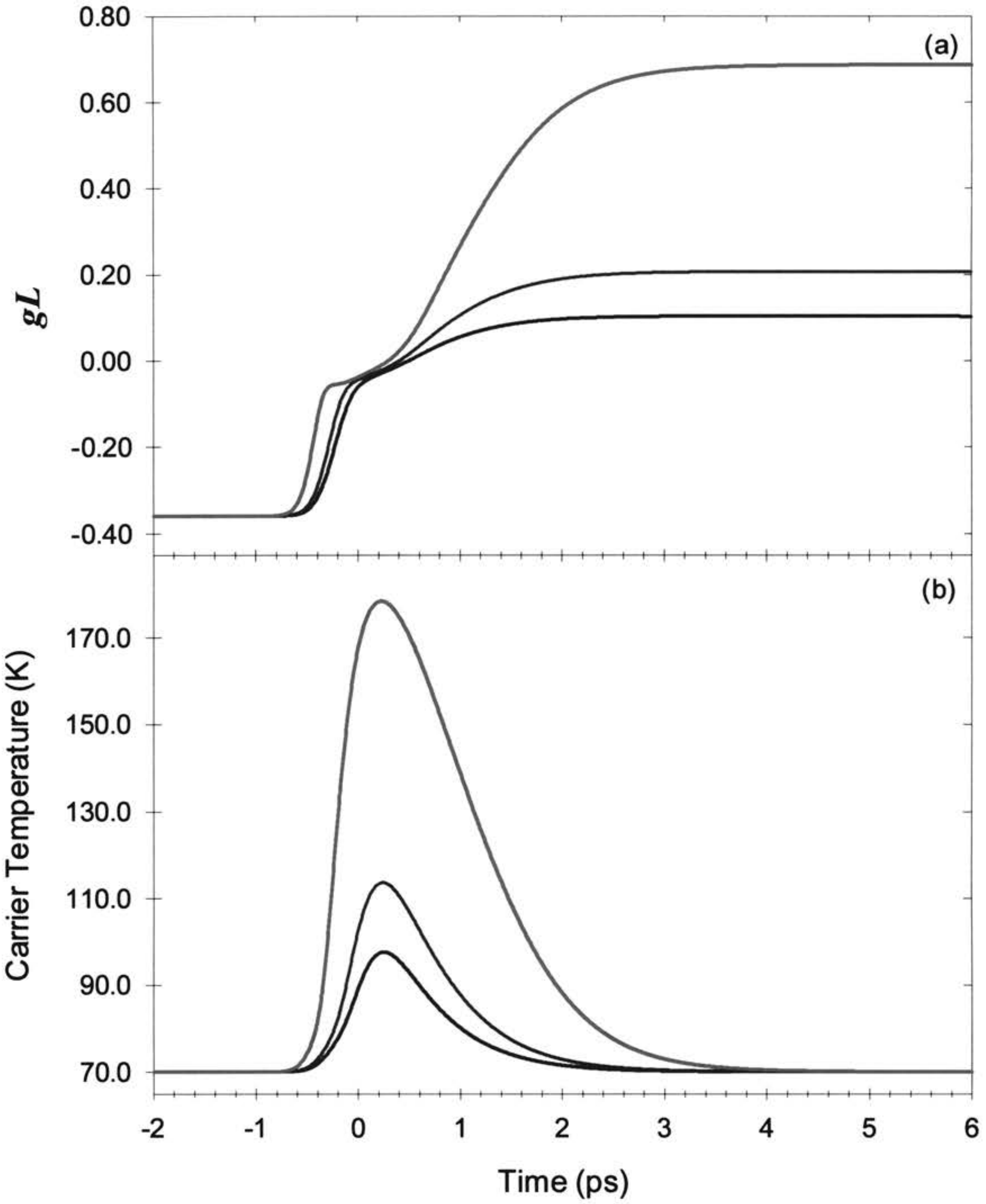

Figure 6.7. Gain (a) and carrier temperature (b) behavior in an absorbing medium pumped at a rate of $0.75\boldsymbol{J}_0$. The external pulse has 1.0 ps (FWHM) duration with energy: 3.0 pJ (blue curves), 5.0 pJ (green curves), and 25.0 pJ (red curves).

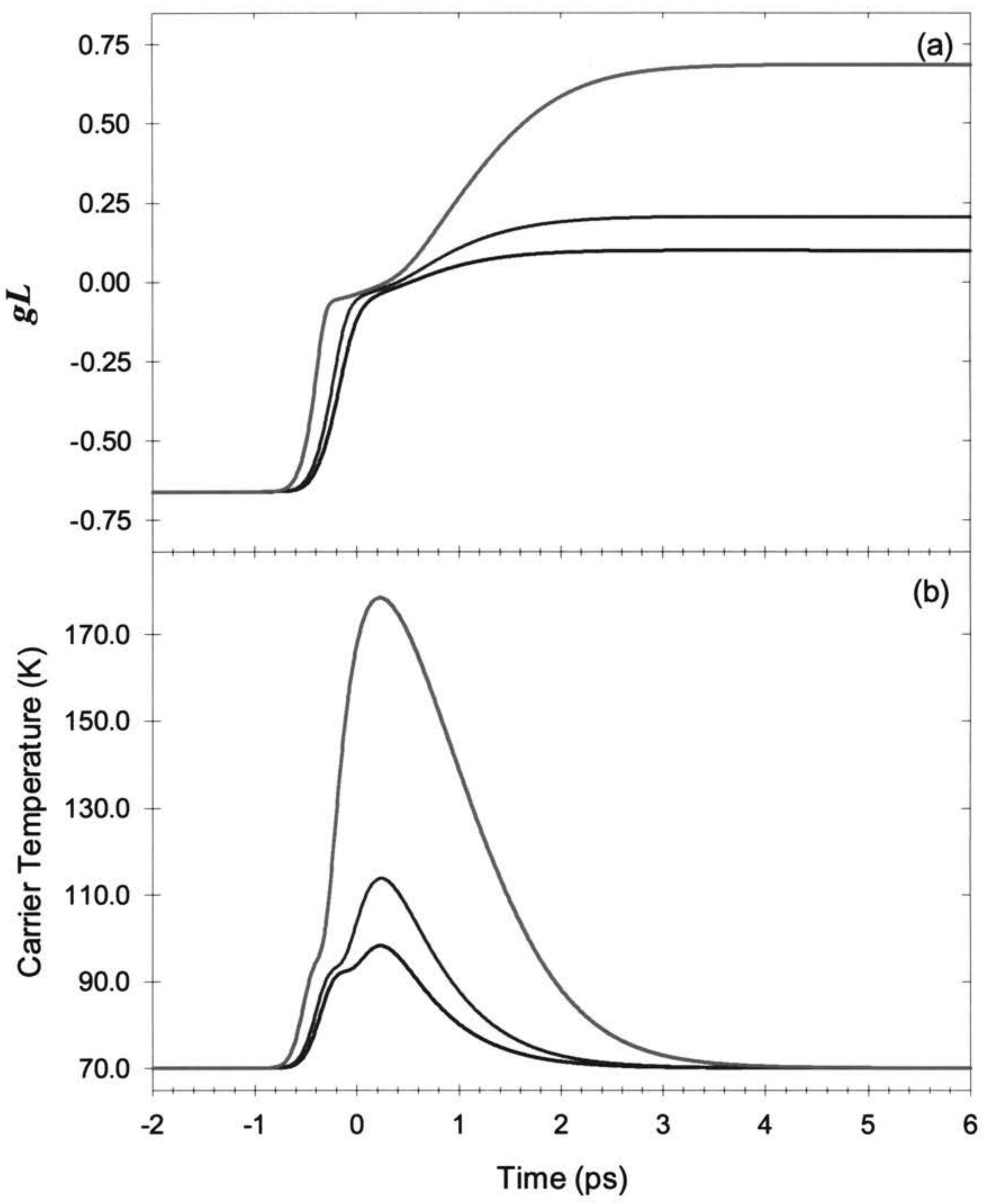

Figure 6.8. Gain (a) and carrier temperature (b) behavior in an absorbing medium pumped at a rate of $0.5\boldsymbol{J}_0$. The external pulse has 1.0 ps (FWHM) duration with energy: 3.0 pJ (blue curves), 5.0 pJ (green curves), and 25.0 pJ (red curves).

6.3. Carrier Temperature Behavior

In previous sections the carrier temperature behavior is described along with the gain behavior. In this section we focus on carrier temperature as a parameter that represents carrier heating efficiency. As a quantitative measure for heating efficiency we use the maximum temperature deviation from the lattice temperature ($\Delta \boldsymbol{T}_{\max}$). Generally, $\Delta \boldsymbol{T}_{\max}$ increases with increasing photon density in the medium. The photon density in the passive (non-lasing) medium, which is the case under consideration in this chapter, is directly proportional to the external pulse energy. However, as we shall see below, $\Delta \boldsymbol{T}_{\max}$ is not a linear function of the external pulse energy ($\mathcal{E}_x$). To clarify the functional dependence between them we present the graph of $\Delta \boldsymbol{T}_{\max}$ vs. $\mathcal{E}_x$ in the 0.1 pJ-50 pJ range. Figure 6.9 (p. 112) demonstrates the results calculated for amplifying (pumped at a rate of $\boldsymbol{J} = 1.75\boldsymbol{J}_0$), transparent ($\boldsymbol{J} = 1.0\boldsymbol{J}_0$) and absorbing ($\boldsymbol{J} = 0.25\boldsymbol{J}_0$) samples. The external pulse has 0.5 ps (FWHM) duration and the other parameters are the same as in Table 5.1 (p. 80).

In the case of amplifying and transparent samples we have a single temperature peak. In the case of absorbing sample there is a single peak for low energy pulses and two peaks for higher energy pulses (see the temperature graphs in this and previous chapters).

The first temperature peak observed in calculations for an absorbing sample increases rapidly for small energies and exhibits asymptotic behavior for high pulse energies (the horizontal asymptote is at the level of $\Delta \boldsymbol{T} \sim 55$ K). The higher the pulse energy the sooner the carrier temperature reaches the first peak. For the low energy

pulses this is the only maximum (see Figs. 6.4b and 6.5b, pp. 105 - 106). For 0.1-pJ pulse the temperature peak is reached after the pulse peak passes the medium ($t > 0$); for pulse energies higher than 1.0-pJ the temperature peak is reached before the pulse peak arrival ($t < 0$). This first peak increases with higher pulse energies and stops to increase when the external pulse bleaches the sample and the gain coefficient is close to zero. At this point the cooling effect due to the increased number of carriers overcomes the heating effect due to the energy influx and we see a decrease in temperature followed by further increase to the second maximum (see Fig. 6.5b, p. 106).

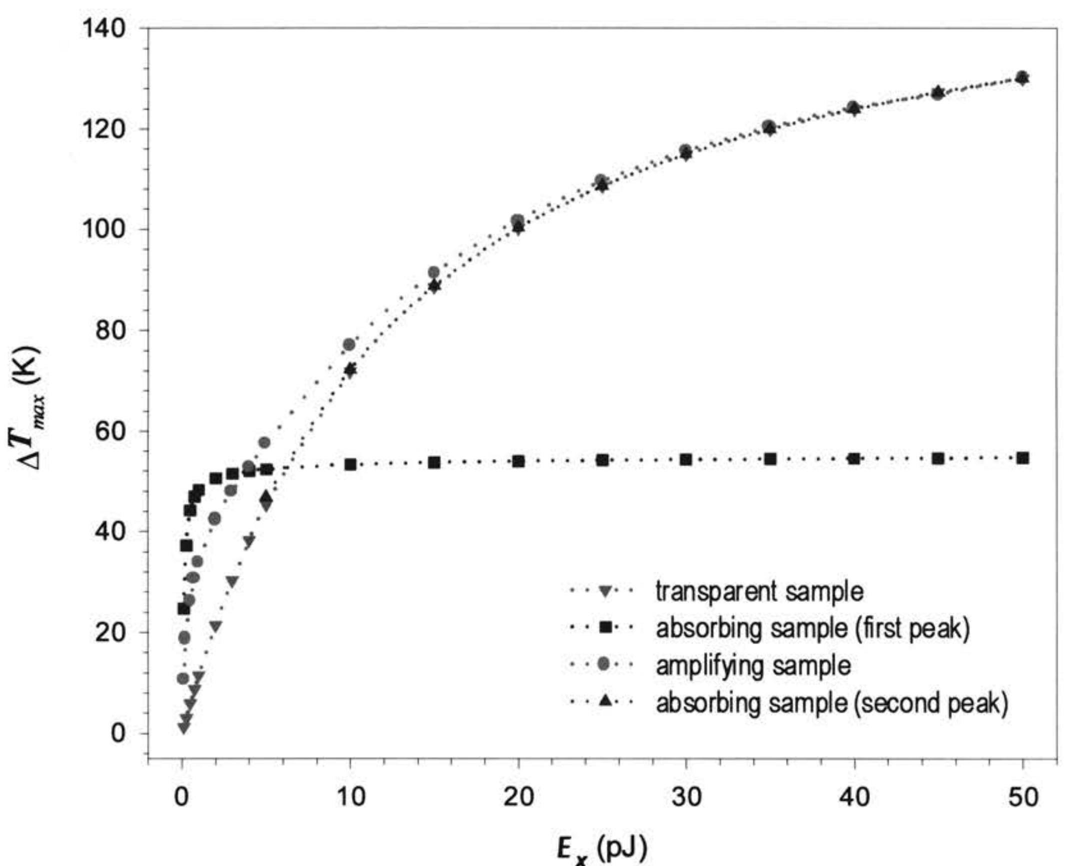

Figure 6.9. The maximum carrier-lattice temperature difference as a function of external pulse energy in a strongly amplifying (pumped at a rate of $\boldsymbol{J} = 1.75\boldsymbol{J}_0$), transparent ($\boldsymbol{J} = \boldsymbol{J}_0$) and strongly absorbing ($\boldsymbol{J} = 0.25\boldsymbol{J}_0$) medium.

The changes in the gain coefficient are less rapid close to transparency because of a less effective interaction between the medium and the external pulse; however the carrier temperature and, less rapidly, the gain coefficient, continue to increase while the pulse is still in the medium. The second temperature peak is reached after most of the pulse has passed the medium. Furthermore, the hot carriers relax, leading to an increase in the gain coefficient, which becomes positive as a result of carrier cooling.

The second temperature peak, which becomes as high as the first peak for about 6 -pJ pulses, increases with higher pulse energies, although it depends on the pulse energy nonlinearly (see below). For pulse energies larger than 20 pJ the second peak is almost the same as the only temperature peak observed in the calculations for an amplifying sample, where the peak is always reached after most of the pulse has passed the medium.

For low energy pulses the absorbing medium is heated more effectively than the amplifying medium. This suggests that carrier heating due to energy pumping into the carrier ensemble, which is the case in the absorbing sample, is more effective than carrier heating due to recombination of cold carriers in the amplifying sample. FCA and TPA have little impact for small energy pulses (see the next section for more details). For higher energy pulses, however, these processes play a greater role and, in fact, become major heating factors. As a result, we see almost equal temperature peaks for absorbing, transparent and amplifying media.

The data points in Fig. 6.9 (p. 112) are well fit by certain curves that are obtained using nonlinear regression. The data points for a transparent and absorbing sample (second peak) almost coincide. All four sets of data points can be fitted to the following curves, which are represented by a nonlinear function:

$$\Delta T = a + b \ln \mathcal{E}_x + c(\ln \mathcal{E}_x)^2 + d(\ln \mathcal{E}_x)^3 . \qquad (6.1)$$

The values for fitting parameters $\boldsymbol{a}$, $\boldsymbol{b}$, $\boldsymbol{c}$, and $\boldsymbol{d}$ are presented in Table 6.1.

Table 6.1. Curve Fitting Parameters

	a	*b*	*c*	*D*
Absorbing (1st peak, the blue curve)	48.1808	4.9347	-1.72951	0.233912
Absorbing (2nd peak, the green curve)	11.2415	15.6713	4.94831	-0.233562
Transparent (the pink curve)	11.2415	15.6713	4.94831	-0.233562
Amplifying (the red curve)	31.2872	14.1251	2.96306	0.0

It should be noted that the data points fit very well to the curve with corresponding parameters from Table 6.1 for low energies ($\mathcal{E}_x < 10$ pJ). For higher energies all data points (except for the first peak of temperature for the absorbing sample) fit to the curve that corresponds to the amplifying sample. This indicates that for high external pulse energies the carrier temperature behavior is mainly due to high photon density in the medium brought by the external signal. In particular, as we mentioned above, FCA and TPA become main heating factors. For low energy pulses the interband transitions have a more significant effect.

The complexity of functional relationship between of ΔT and $\mathcal{E}_x$ is a result of nonlinear relationships among dynamic variables and in general, due to the nonlinearity of the model equations. Thus, the carrier temperature behavior needs additional investigation. In particular, the role of each heating mechanism must be clarified. We devote the next section to this task.

6.4. Influence of Two-Photon and Free-Carrier Absorption

To clarify the carrier heating dependence on the external pulse energy we need to investigate how the main heating processes (FCA, TPA, and interband transitions) are affected when the pulse energy is increased. For this purpose we repeat all previous calculations with certain terms that represent FCA and TPA removed from the model separately and together. Comparison of these calculations with the results that include all heating mechanisms reveals the partial influence of particular heating processes.

The gain and temperature dynamics described above is a result of several processes. The carrier temperature increases due to the energy influx via interband absorption, FCA, and TPA, which in turn affects the gain coefficient. Also the carrier temperature can be affected by changing the carrier density. More carriers also mean less energy per particle, and the temperature, as a measure of average energy, may decrease. While interband absorption brings energy to the system it also increases the carrier density. This may decrease the temperature even though the total carrier energy is increased. FCA does not change the carrier density but it increases the total energy of the system, thus it is always a heating factor. TPA changes the carrier density but it creates mostly hot carriers. Although radiation takes energy away from the carrier ensemble it also takes away cold carriers, thus leading to higher temperatures.

To understand the source of the second peak in the temperature response shown in Fig. 6.5b (p. 106), we should identify which processes are significantly different in this case as compared with cases that show a single temperature-peak. The second peak appears only in the case of an absorbing medium far from transparency when the pulse energy is high enough to bleach the medium, so that we are dealing with substantial

changes in both carrier and photon densities. FCA is proportional to both carrier and photon densities and, therefore, in this case the efficiency of FCA is much higher than in the other cases. TPA also experiences significant growth in efficiency since it is proportional to the square of the photon density. So we expect both FCA and TPA to be responsible for the double-peak behavior. This conjecture is supported by the results obtained when FCA and TPA are eliminated (together and separately) from the numerical experiment by setting s_{FCA} and/or s_{TPA} equal to zero. The calculations are done for the same pulse energies as in previous sections. The results are presented below for amplifying and absorbing samples.

Amplifying Sample

The results for an amplifying sample are presented in Figs. 6.10-6.15 (pp. 118- 123). For low pulse energies the main heating factors appearing are the interband transitions and in a lesser degree FCA. The heating effect of TPA is negligible for the 0.1-pJ pulse but is more visible for higher energies. The influence of FCA and TPA is more noticeable for high-energy pulses because their terms in Eqs. (2.1) involve the photon density; however, most of the carrier heating is due to interband transitions for pulse energies less than 5 pJ. Interband transitions cause carrier heating because the carriers participating in these transitions are predominantly cold carriers. Thus, the temperature of the carriers increases even though the total energy of the electronic ensemble decreases. For the 5-pJ pulse FCA and TPA together are heating the system as much as interband transitions. For the 25-pJ pulse (Fig. 6.15, p. 123) TPA is a greater

heating factor than FCA, which is consistent with the TPA being a quadratic function of the photon density while FCA is a linear function of the photon density.

The figures below show that for high pulse energies FCA and TPA together are heating the carrier system more effectively than interband transitions. Note that when FCA and TPA are eliminated the 5-pJ and 25-pJ pulses do not change the sign of the gain function. Without FCA and TPA the 5-pJ pulse does not bleach the sample, and in the case of the 25-pJ pulse the gain coefficient reaches the zero level (at this point temperature reaches its maximum) but does not become negative. This is a natural result because in the system with zero gain there are no single-photon band-to-band transitions, hence there are no changes in carrier density and the chemical potential. Therefore, according to Eq. (2.37) the gain function must only increase, because the carrier temperature is decreasing.

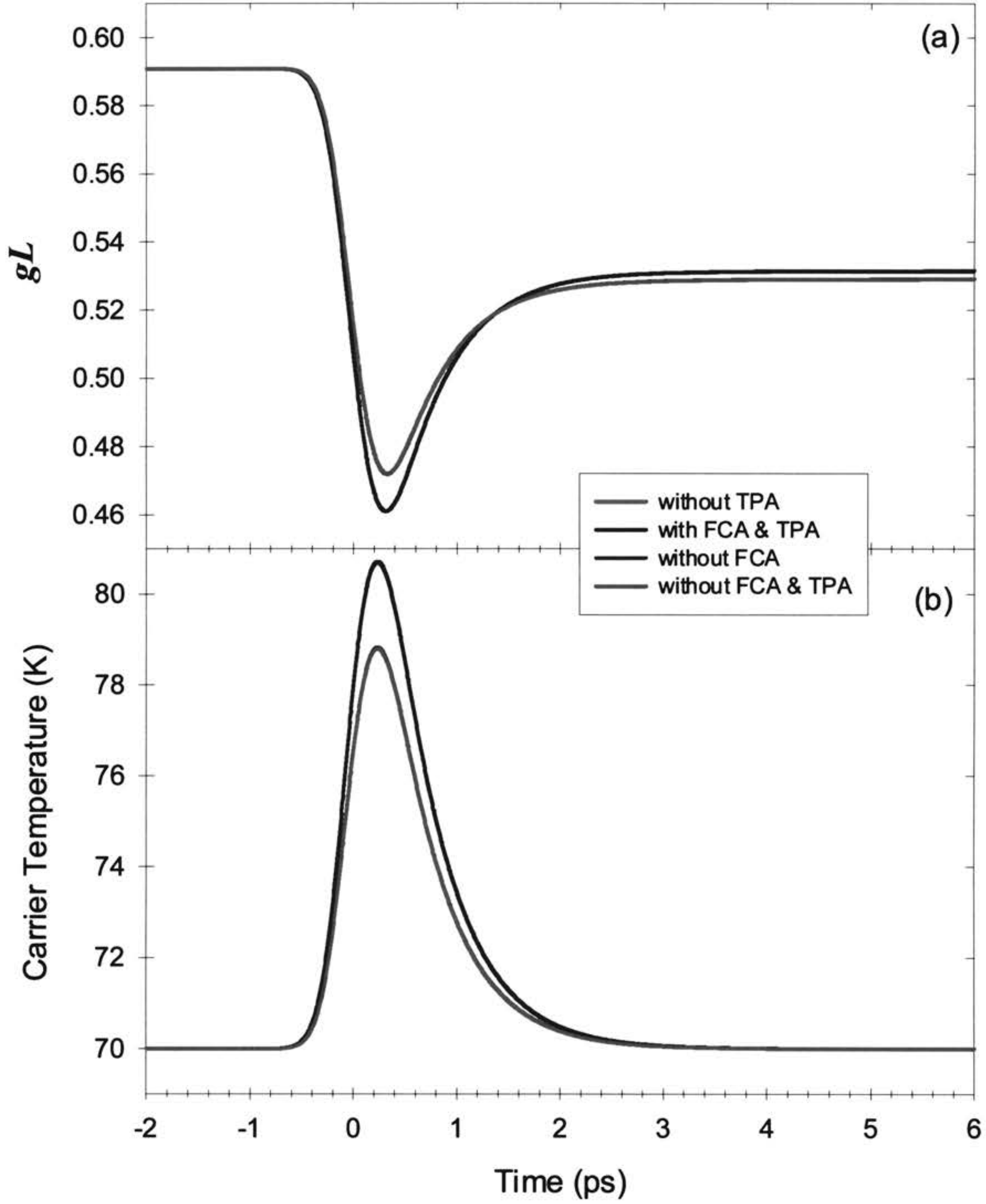

Figure 6.10. Gain (a) and carrier temperature (b) behavior in a strongly amplifying medium pumped at a rate of $1.75\boldsymbol{J}_0$. The external pulse has 1.0 ps (FWHM) duration and 0.1 pJ energy. The curves correspond to calculations with FCA and TPA (blue), without FCA (green), without TPA (red), and without FCA and TPA (pink). The blue curve is overlapped with the red, and the green curve overlapped with the pink curve.

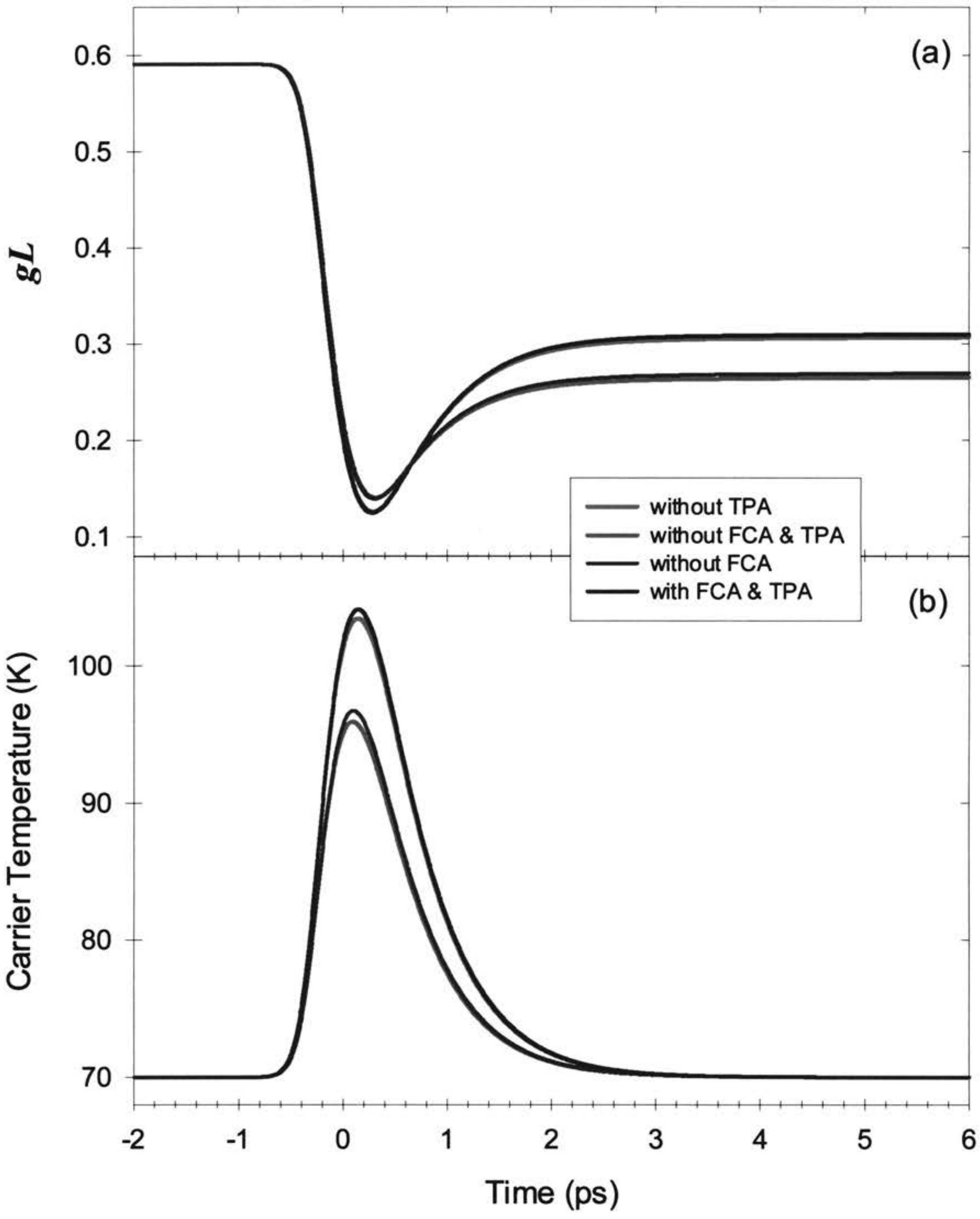

Figure 6.11. Gain (a) and carrier temperature (b) behavior in a strongly amplifying medium pumped at a rate of $1.75\boldsymbol{J}_0$. The external pulse has 1.0 ps (FWHM) duration and 1.0 pJ energy. The curves correspond to calculations with FCA and TPA (blue), without FCA (green), without TPA (red), and without FCA and TPA (pink). The blue curve is almost overlapped with the red, and the green curve overlapped with the pink curve.

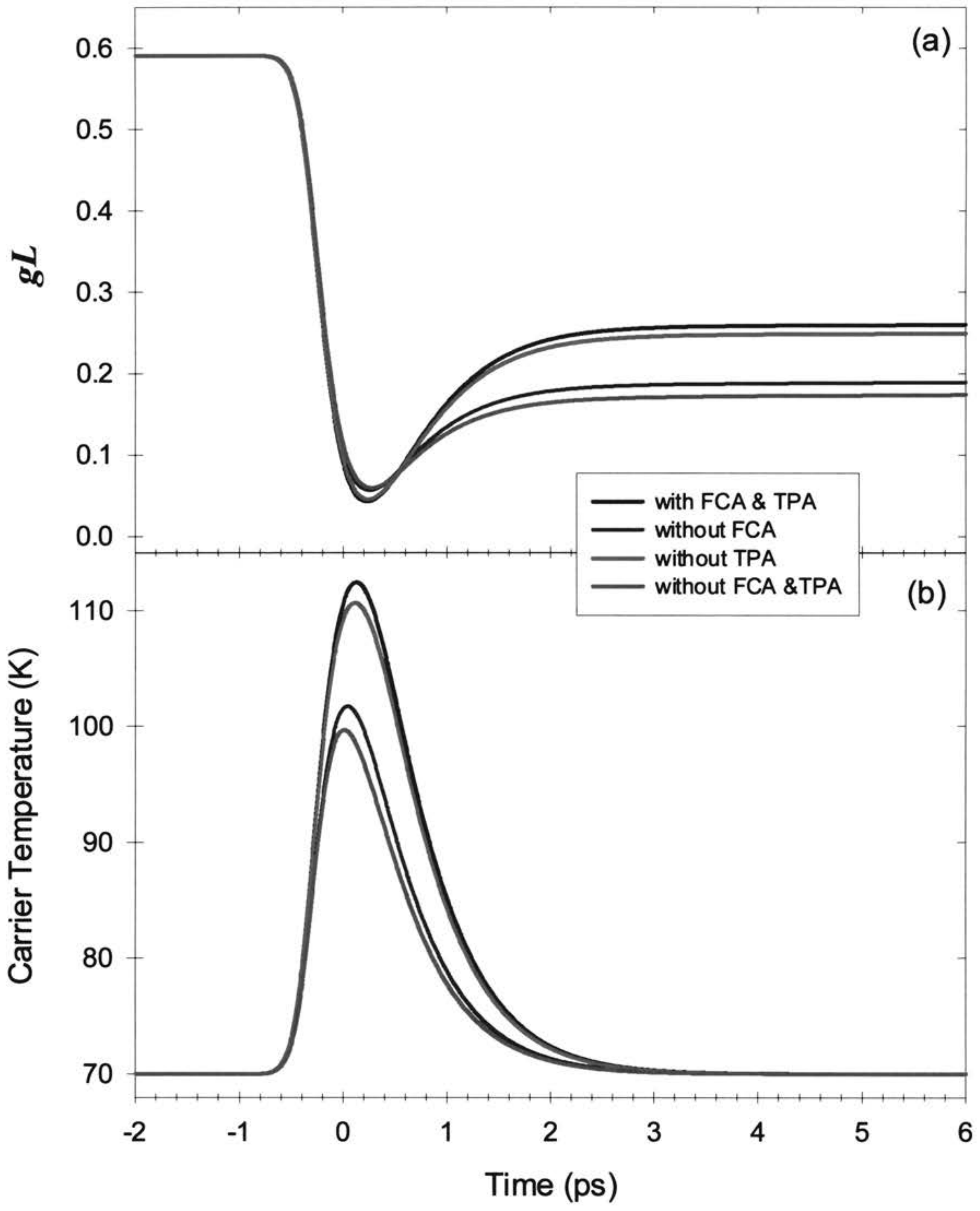

Figure 6.12. Gain (a) and carrier temperature (b) behavior in a strongly amplifying medium pumped at a rate of $1.75\boldsymbol{J}_0$. The external pulse has 1.0 ps (FWHM) duration and 2.0 pJ energy. The curves correspond to calculations with FCA and TPA (blue), without FCA (green), without TPA (red), and without FCA and TPA (pink).

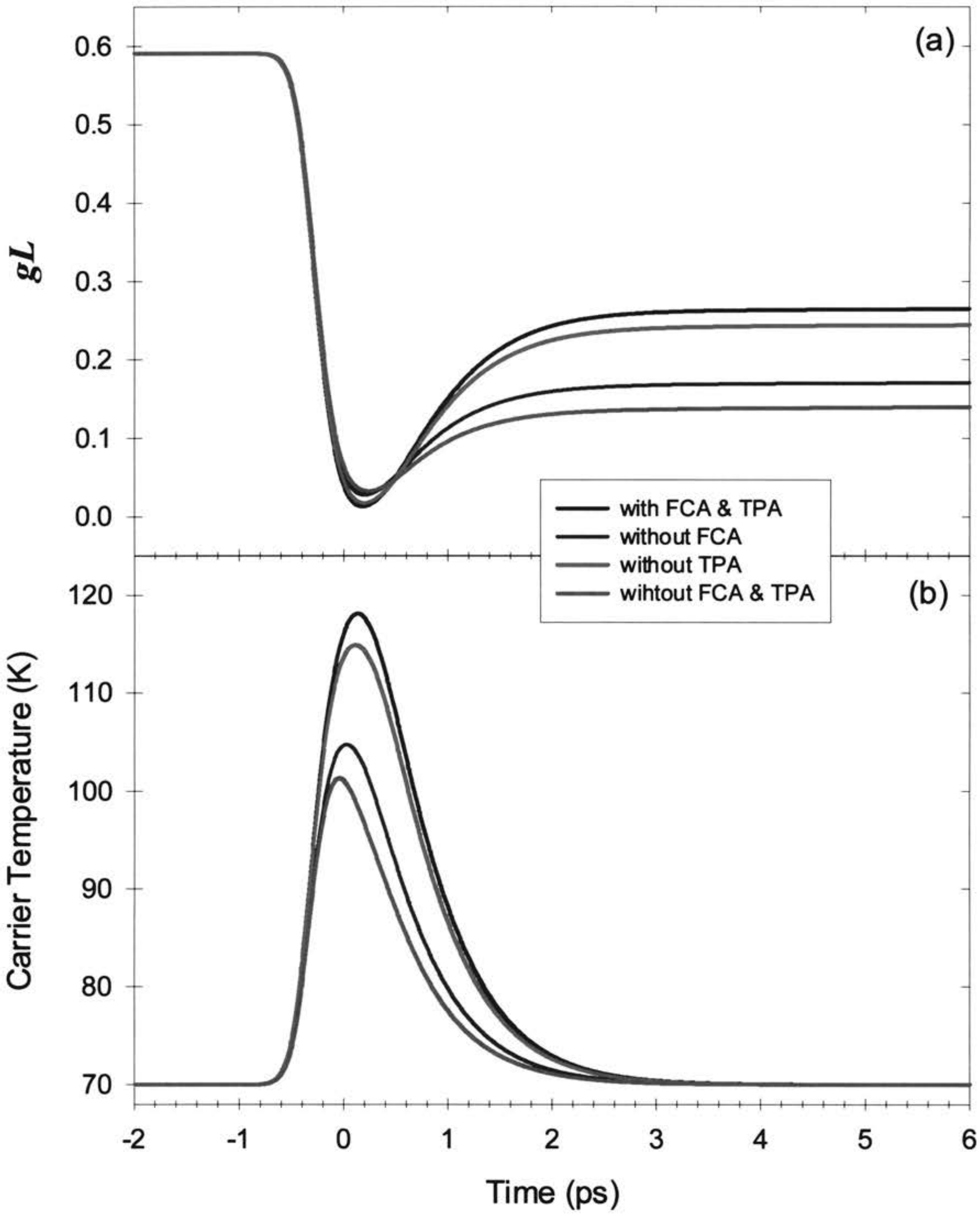

Figure 6.13. Gain (a) and carrier temperature (b) behavior in a strongly amplifying medium pumped at a rate of $1.75\boldsymbol{J}_0$. The external pulse has 1.0 ps (FWHM) duration and 3.0 pJ energy. The curves correspond to calculations with FCA and TPA (blue), without FCA (green), without TPA (red), and without FCA and TPA (pink).

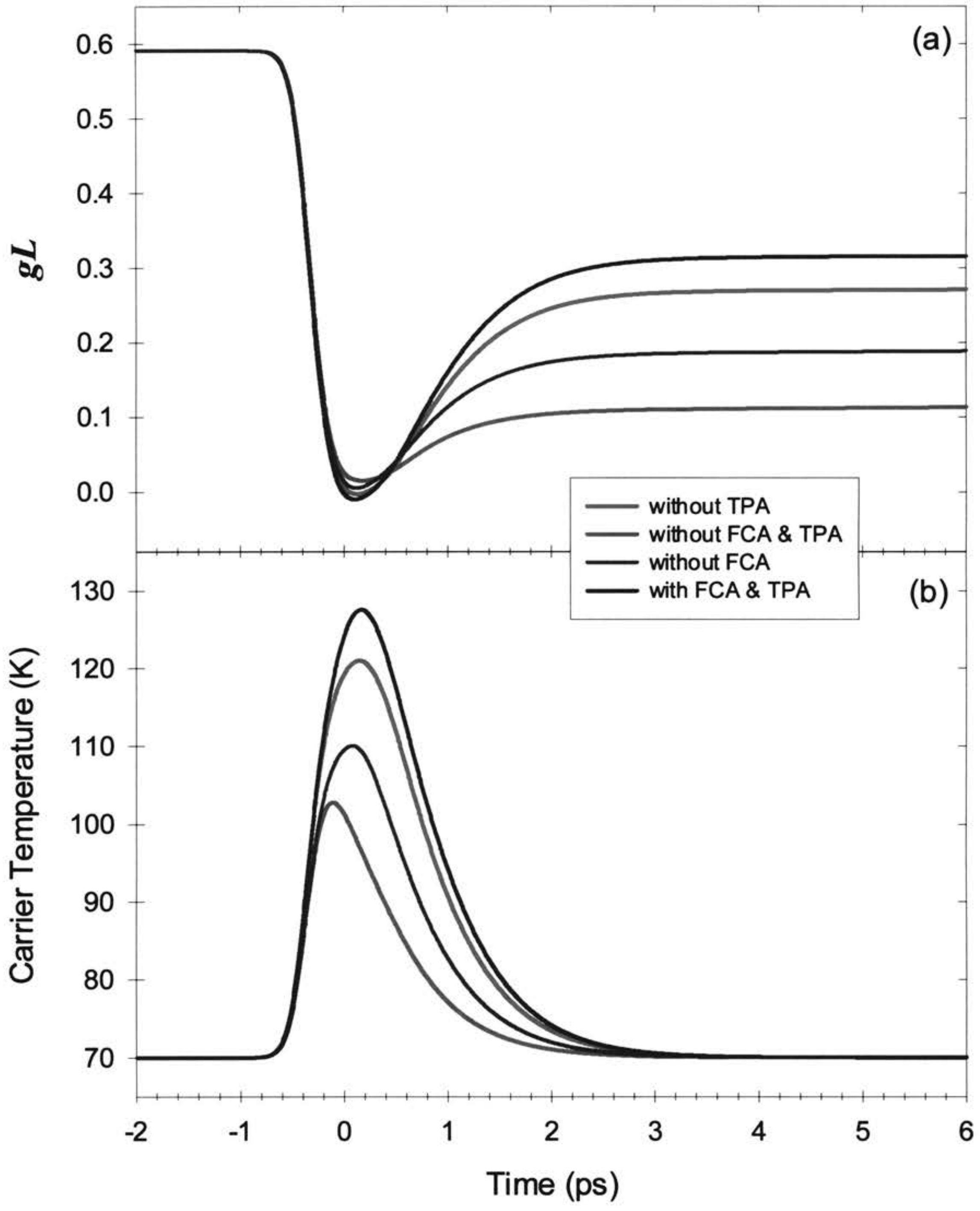

Figure 6.14. Gain (a) and carrier temperature (b) behavior in a strongly amplifying medium pumped at a rate of $1.75\boldsymbol{J}_0$. The external pulse has 1.0 ps (FWHM) duration and 5.0 pJ energy. The curves correspond to calculations with FCA and TPA (blue), without FCA (green), without TPA (red), and without FCA and TPA (pink).

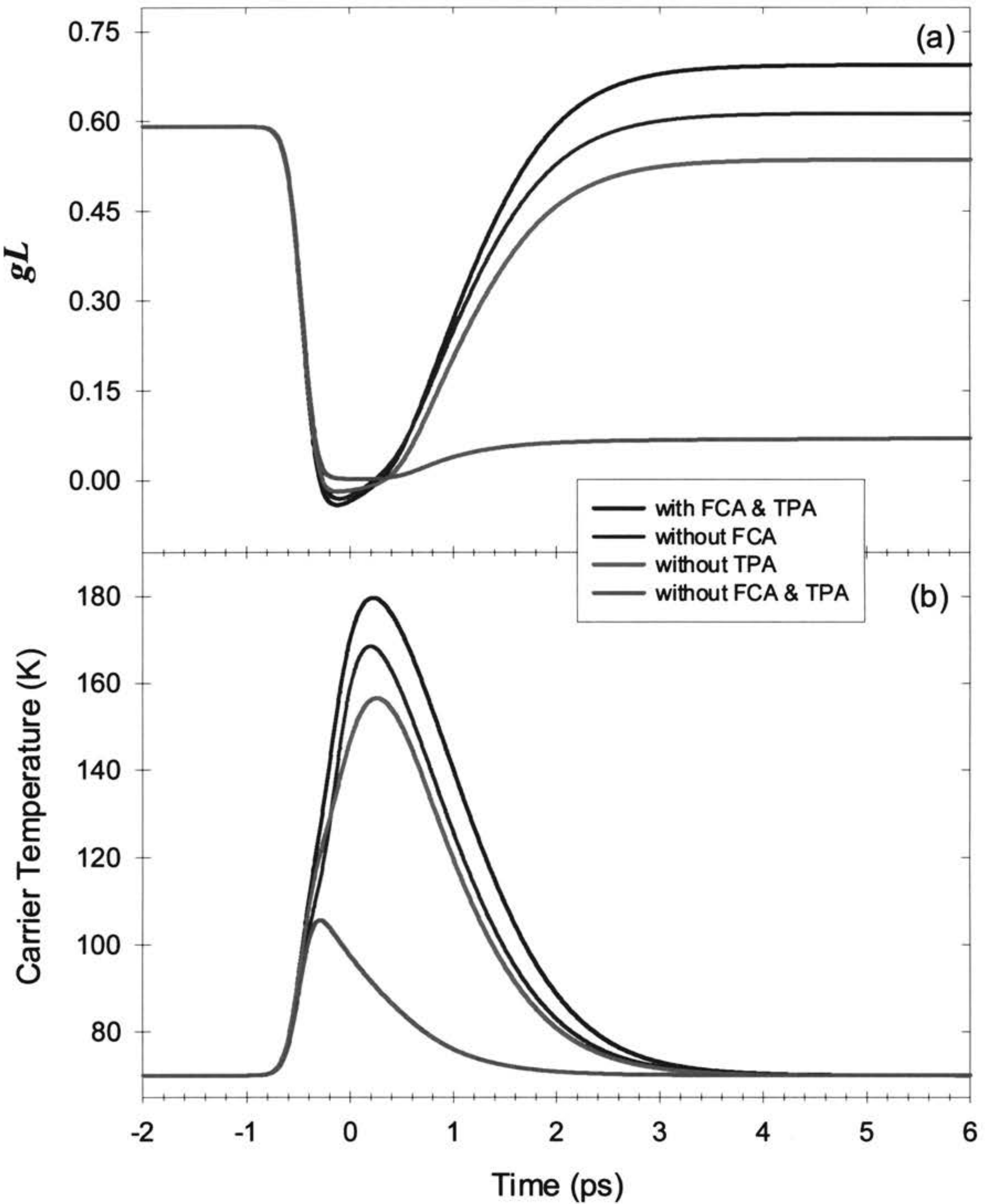

Figure 6.15. Gain (a) and carrier temperature (b) behavior in a strongly amplifying medium pumped at a rate of $1.75\boldsymbol{J}_0$. The external pulse has 1.0 ps (FWHM) duration and 25.0 pJ energy. The curves correspond to calculations with FCA and TPA (blue), without FCA (green), without TPA (red), and without FCA and TPA (pink).

Absorbing Sample

In the absorbing medium interband transitions dominate the dynamics for low energy pulses (Figs. 6.16-6.18, pp. 126 - 128), however, in contrast to the dynamics in an amplifying sample, the influence of FCA is much smaller, which is explained by a small carrier density. For higher energy pulses interband transitions dominate the early dynamics but become less important after the gain reaches the plateau near the transparency region (see Figs. 6.19-6.21, pp. 129 - 131). When the medium becomes transparent the interband absorption stops and the carrier temperature relaxes due to interaction with the lattice (phonon emission). Finally, the medium becomes amplifying when the carriers cool down.

Note that without FCA and TPA the gain function remains close to the transparency region, although carrier cooling leads to a slight increase in the gain function afterwards. However, when FCA or TPA is present, the second peak appears in the temperature graphs.

The emergence of the second temperature peak is already visible in 3-pJ pulse (Fig. 6.19, p. 129), but a clear peak is observed only for higher energy pulses (Figs. 6.20 and 6.21, pp. 130 - 131). Furthermore, the first peak appears in the absorption region when the pulse is partially absorbed and the dominant heating factor is the (single-photon) absorption (note the small difference at the first peak between the curves with and without FCA and TPA). The second peak appears when the pulse is completely absorbed and the medium is in the transparency region where the FCA and TPA are the dominant heating mechanisms. As in the case of the amplifying sample, for the 5-pJ pulse (Fig. 6.20, p. 130) FCA is dominant; for the 25-pJ pulse (Fig. 6.21, p. 131) TPA

has more influence.

With FCA and TPA the medium absorbs more, increasing the carrier density. The FCA does not change the carrier density by itself, but it assists the single-photon absorption by making electronic states available at the bottom of the energy band.

Another observation that we would like to point out is the non-cumulative influence of FCA and TPA. The maximum change in carrier temperature due to the total heating effect of FCA and TPA is less than the sum of the changes obtained when only FCA or TPA is included. They are independent heating factors, but they heat the carrier ensemble more efficiently when they act separately. This is especially evident for high-energy pulses when FCA and TPA have quantitatively similar effects (Figs. 6.20 and 6.21, pp. 130 - 131). Both FCA and TPA create carriers in the same region of the energy levels in the conduction band - approximately $\hbar\omega$ above the band edge. Having more carriers in this region leads to lower probabilities of transitions from the band edge (FCA) and from the valence band (TPA). Thus in this context FCA and TPA are self- and mutually saturating processes.

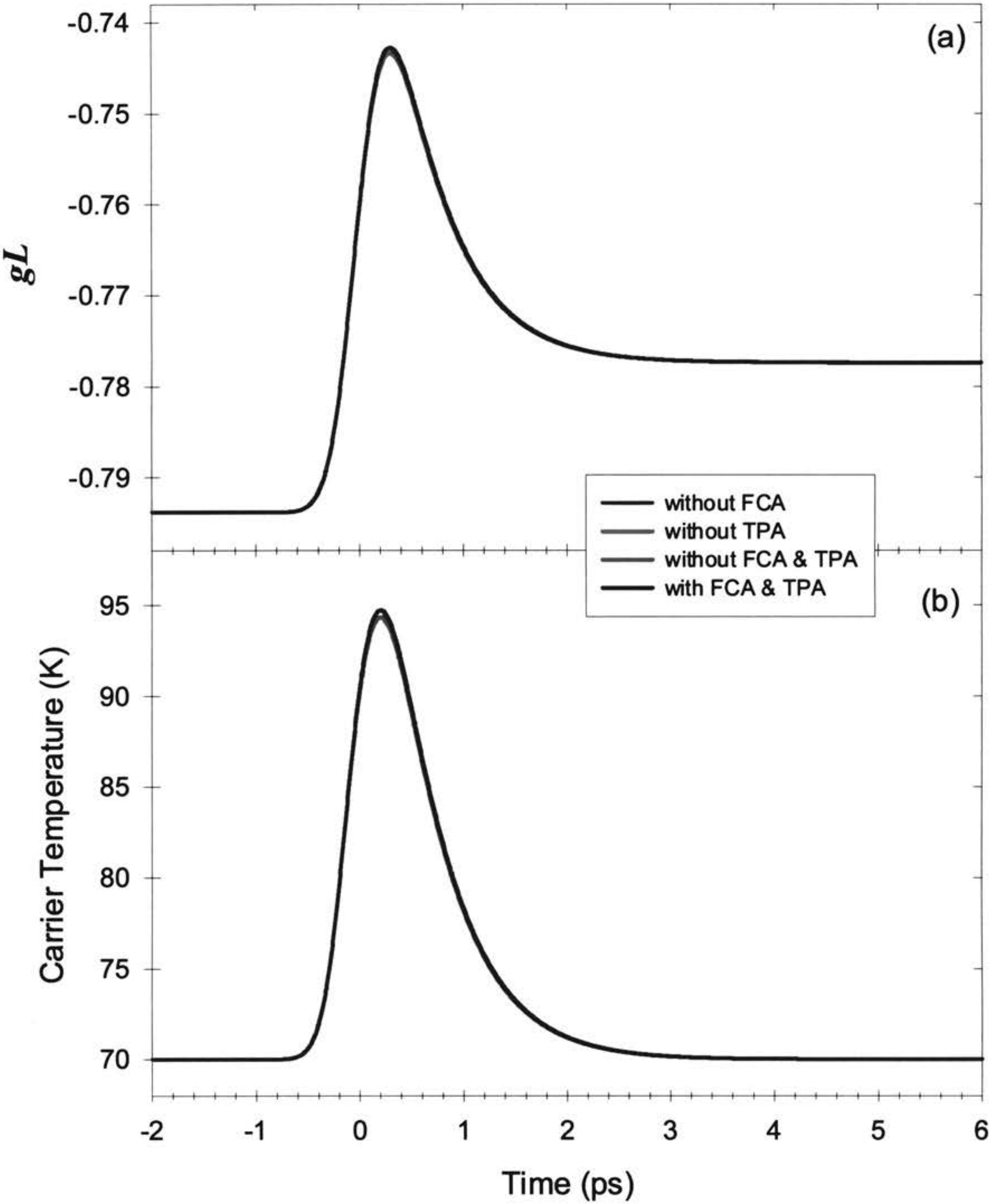

Figure 6.16. Gain (a) and carrier temperature (b) behavior in a strongly absorbing medium pumped at a rate of $0.25\boldsymbol{J}_0$. The external pulse has 1.0 ps (FWHM) duration and 0.1 pJ energy. The curves correspond to calculations with FCA and TPA (blue), without FCA (green), without TPA (red), and without FCA and TPA (pink). All curves are overlapped.

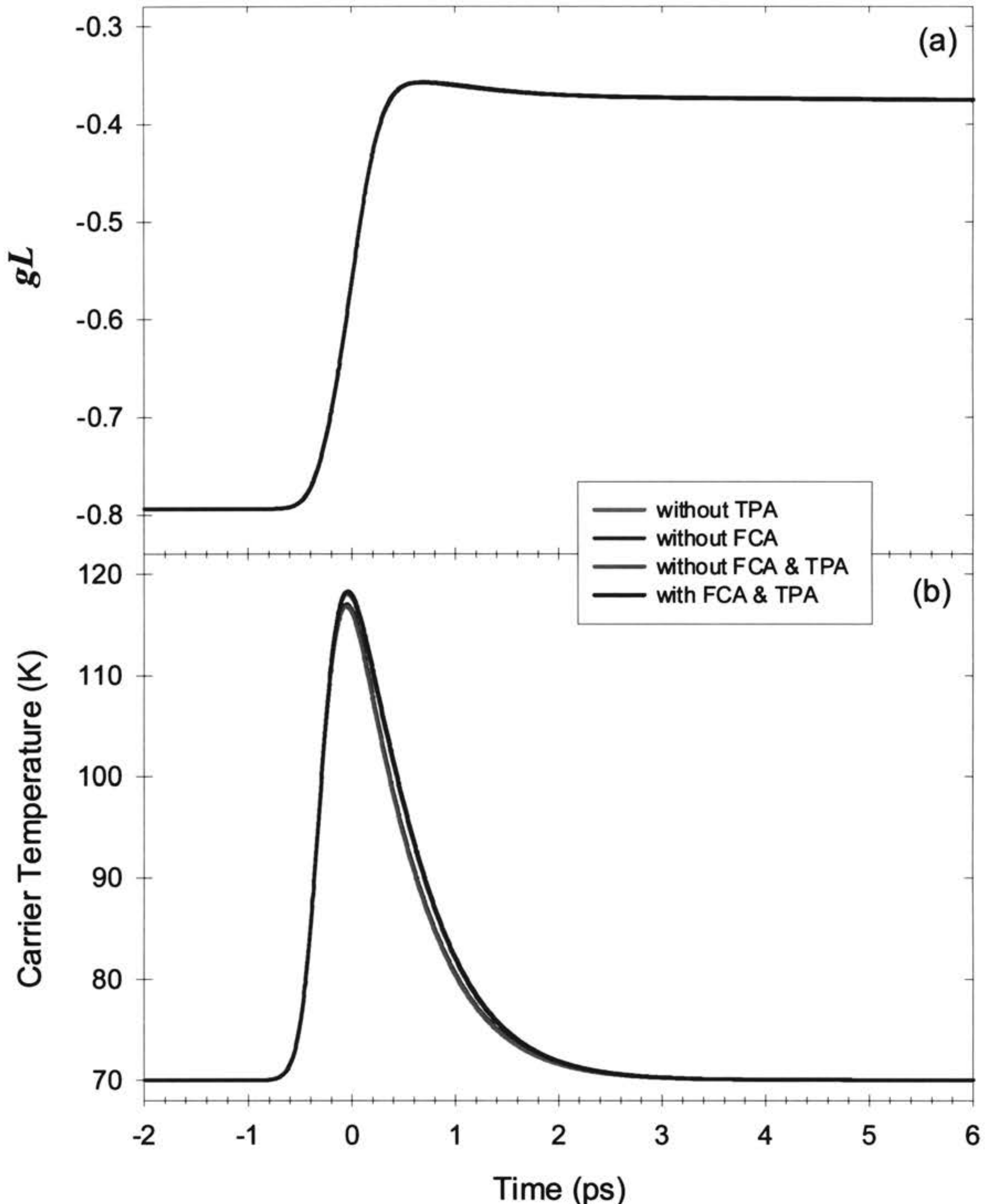

Figure 6.17. Gain (a) and carrier temperature (b) behavior in a strongly absorbing medium pumped at a rate of $0.25\boldsymbol{J}_0$. The external pulse has 1.0 ps (FWHM) duration and 1.0 pJ energy. The curves correspond to calculations with FCA and TPA (blue), without FCA (green), without TPA (red), and without FCA and TPA (pink). The gain curves are overlapped. In temperature graph the blue curve is almost overlapped with red, and the green curve overlapped with pink curve.

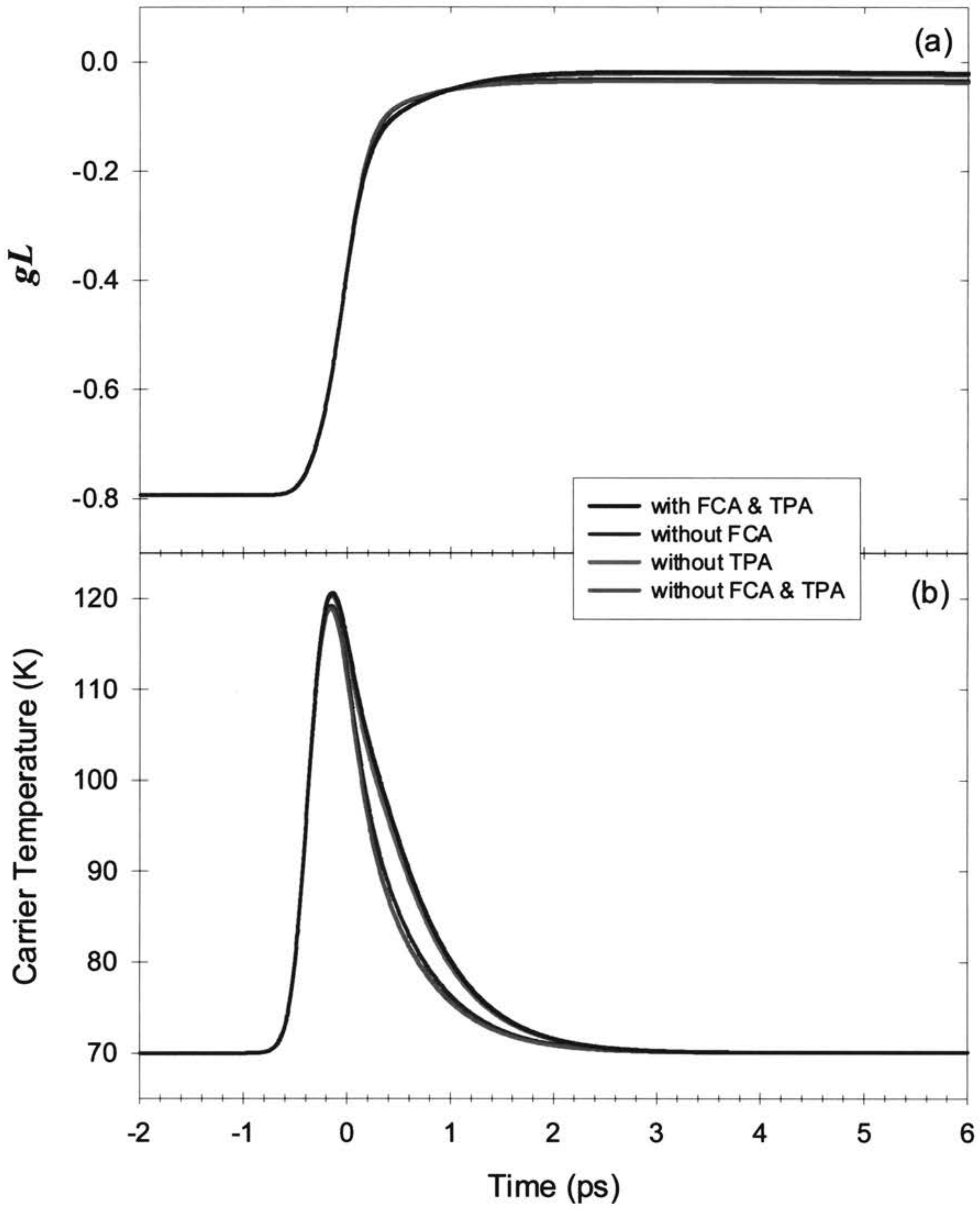

Figure 6.18. Gain (a) and carrier temperature (b) behavior in a strongly absorbing medium pumped at a rate of $0.25\boldsymbol{J}_0$. The external pulse has 1.0 ps (FWHM) duration and 2.0 pJ energy. The curves correspond to calculations with FCA and TPA (blue), without FCA (green), without TPA (red), and without FCA and TPA (pink). The blue curves are almost overlapped with the red, and the green curves are overlapped with pink curve.

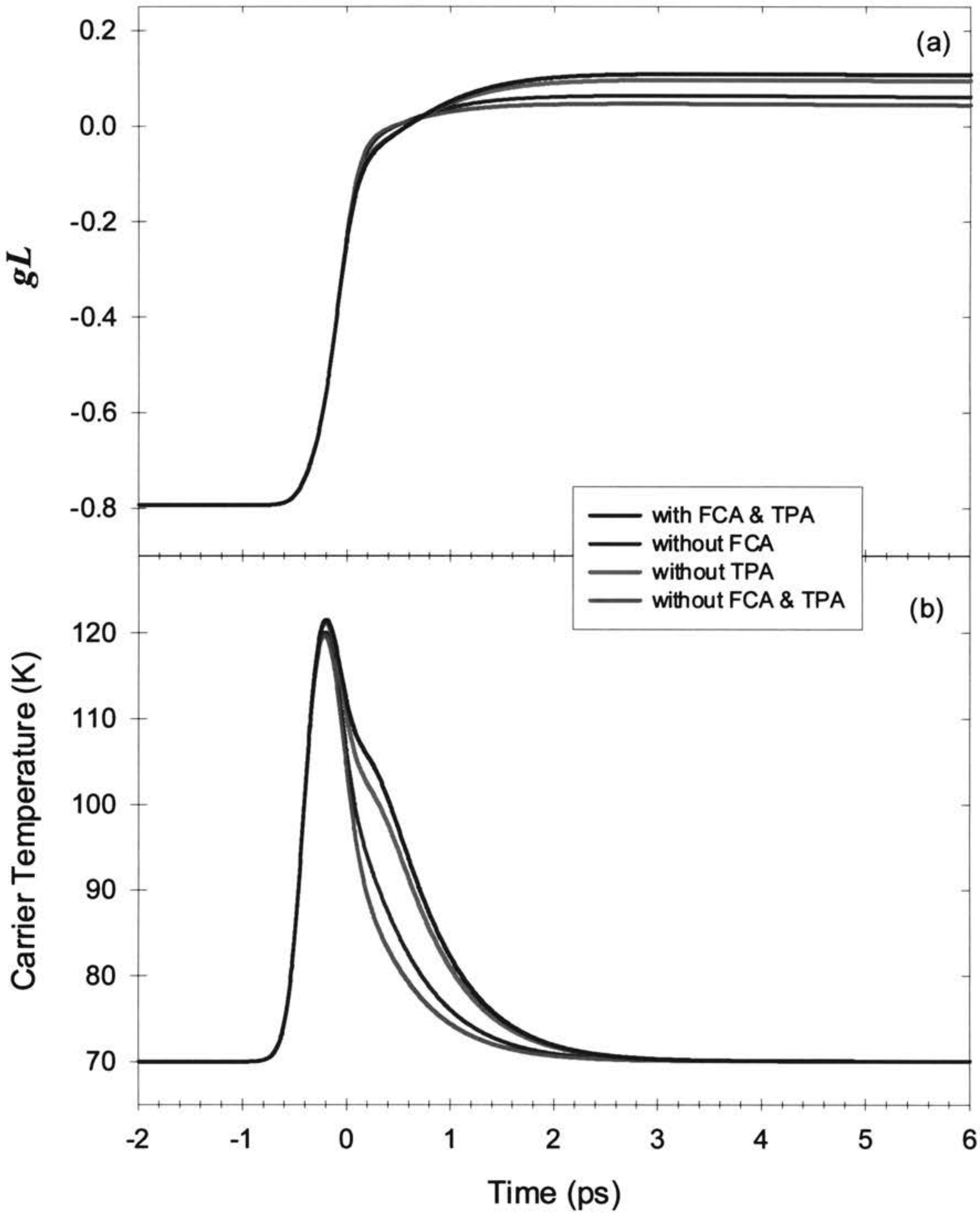

Figure 6.19. Gain (a) and carrier temperature (b) behavior in a strongly absorbing medium pumped at a rate of $0.25J_0$. The external pulse has 1.0 ps (FWHM) duration and 3.0 pJ energy. The curves correspond to calculations with FCA and TPA (blue), without FCA (green), without TPA (red), and without FCA and TPA (pink).

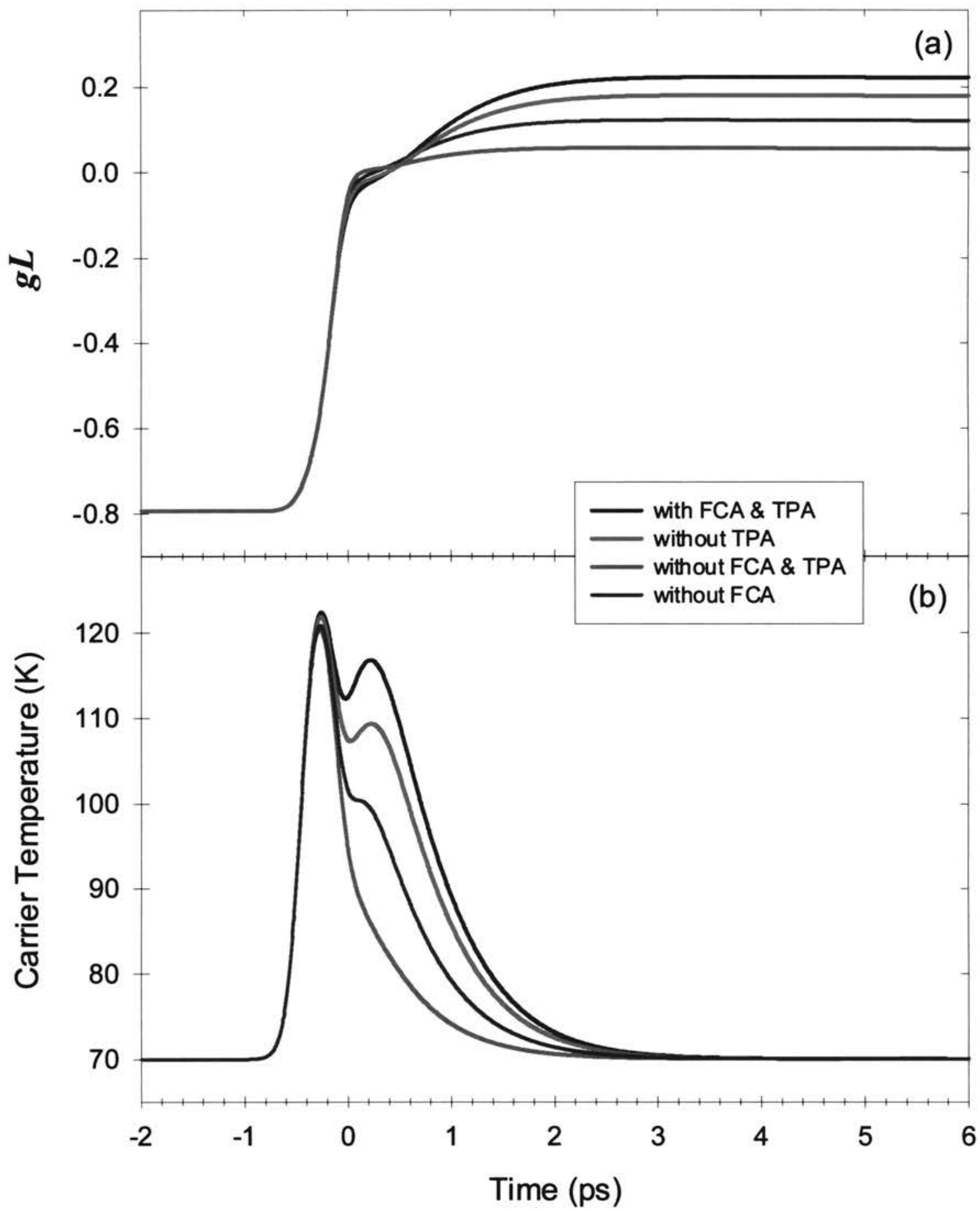

Figure 6.20. Gain (a) and carrier temperature (b) behavior in a strongly absorbing medium pumped at a rate of $0.25J_0$. The external pulse has 1.0 ps (FWHM) duration and 5.0 pJ energy. The curves correspond to calculations with FCA and TPA (blue), without FCA (green), without TPA (red), and without FCA and TPA (pink).

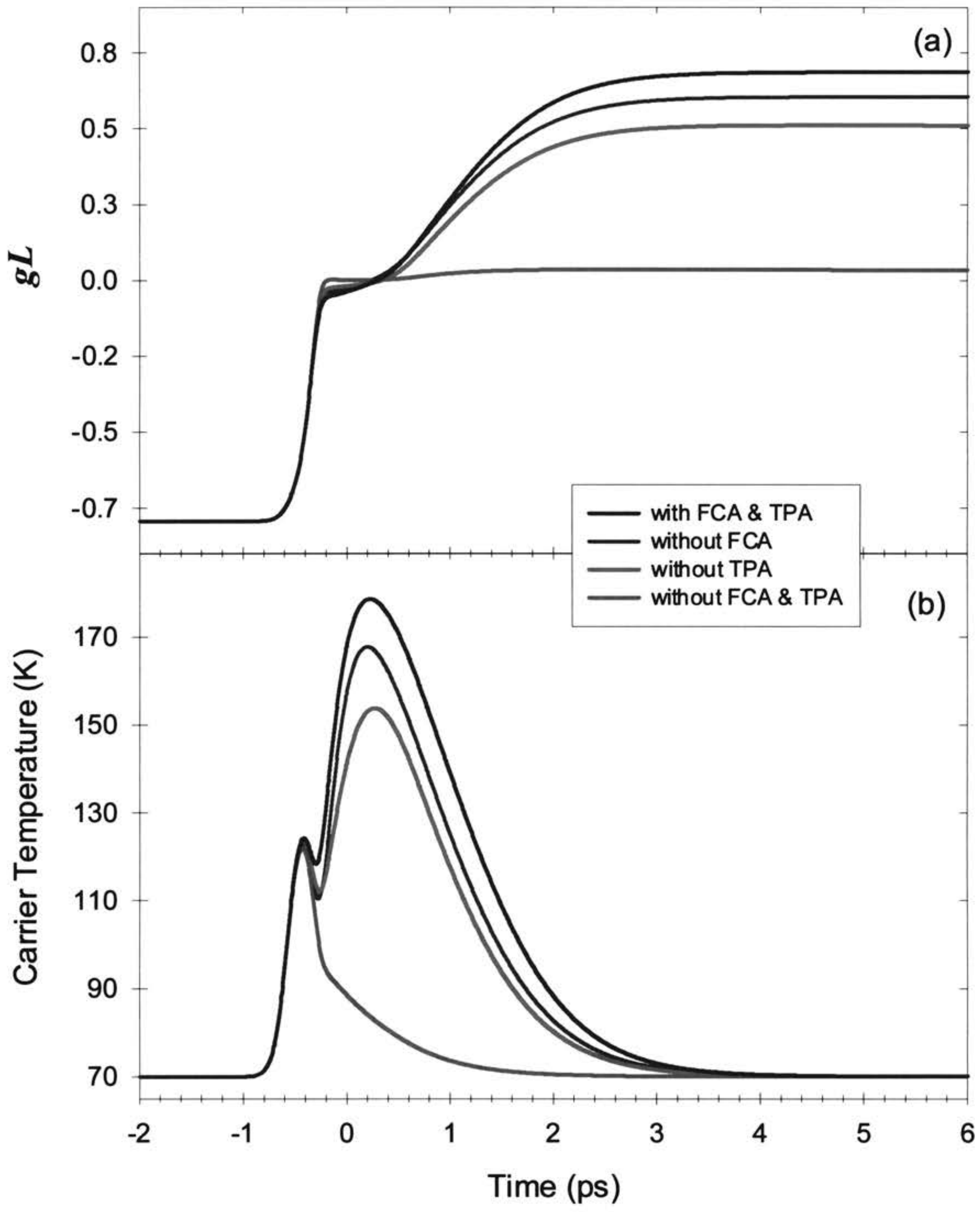

Figure 6.21. Gain (a) and carrier temperature (b) behavior in a strongly absorbing medium pumped at a rate of $0.25\boldsymbol{J}_0$. The external pulse has 1.0 ps (FWHM) duration and 25.0 pJ energy. The curves correspond to calculations with FCA and TPA (blue), without FCA (green), without TPA (red), and without FCA and TPA (pink).

Summary of Temperature Behavior With and Without FCA and TPA

Finally, to summarize the carrier temperature behavior with and without FCA and TPA we present graphs for the maximum temperature deviation from the lattice temperature as a function of external pulse energy. Figures 6.22 and 6.23 (pp. 133 - 134) demonstrate the results obtained for amplifying (pumped at a rate of $\boldsymbol{J}=1.75\boldsymbol{J}_0$), transparent ($\boldsymbol{J}=1.0\boldsymbol{J}_0$), and absorbing ($\boldsymbol{J}=0.25\boldsymbol{J}_0$) samples. The results for the absorbing sample are presented below in separate graphs: Figs. 6.23a for the first peak and 6.23b the second peak, respectively (p. 134).

These graphs are obtained using data points taken from the earlier calculations for gain and carrier temperature dynamics shown in Figs. 6.10 - 6.21 (pp. 118- 123, 126 - 131). Additional calculations are carried out for pulse energies higher than 25 pJ (and certain low energies), with and without FCA and TPA.

The result for an amplifying sample obtained without FCA and TPA (Fig. 6.22a, blue curve, p. 133) is remarkably similar to the result for the first peak of an absorbing sample (Fig. 6.23a, p. 134). The corresponding curve for an initially transparent sample shows no difference between the lattice and carrier temperatures (Fig. 6.22b, blue curve, p. 133). This indicates that initial carrier heating in non-transparent samples is mainly due to the interband transitions.

Furthermore, from Figs. 6.22a and 6.23 it is evident that in an initially absorbing sample interband transitions lead to more effective heating than in an initially amplifying sample. In an initially transparent sample without FCA and TPA there is no net interband transition, consequently no carrier heating at all.

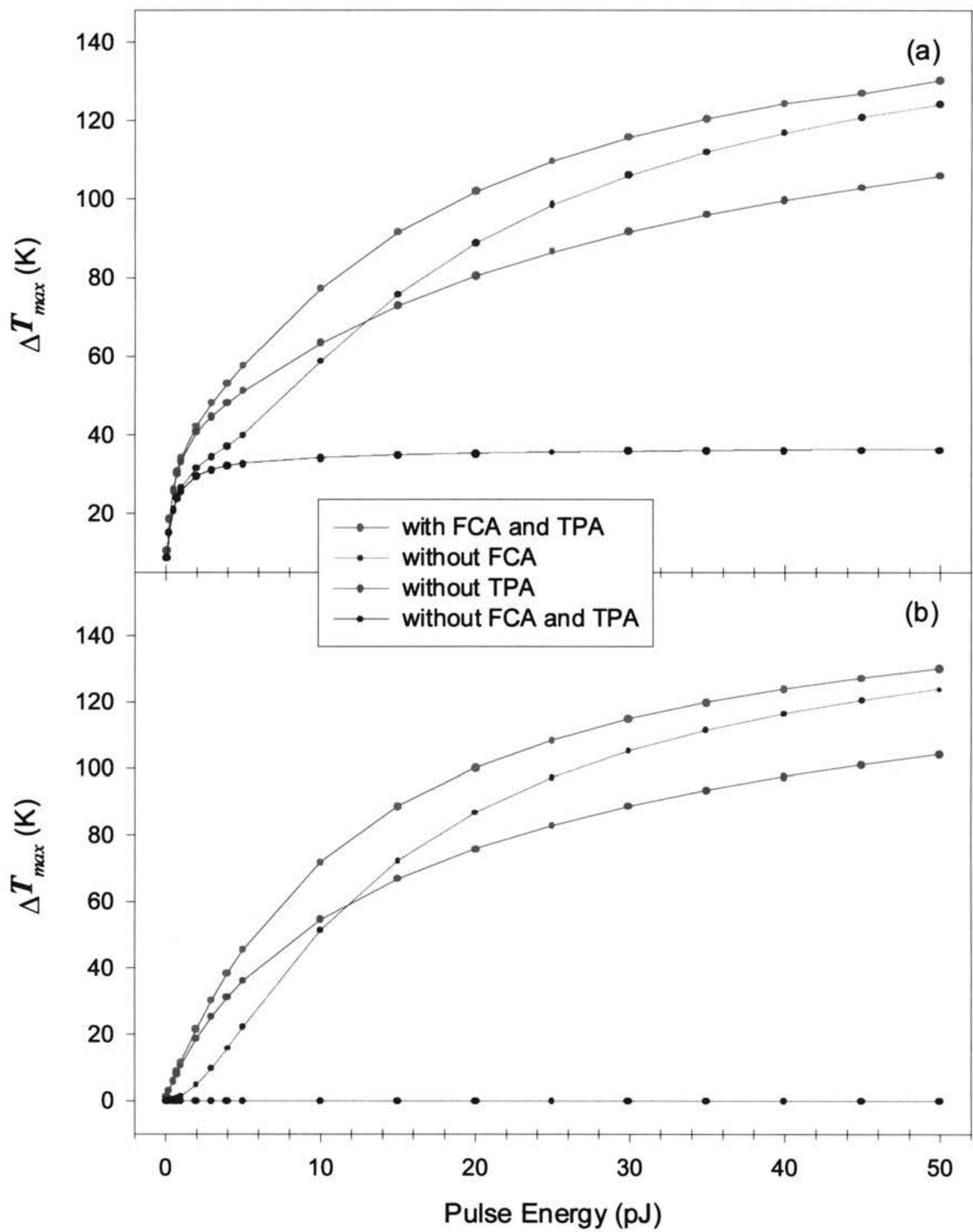

Figure 6.22. The maximum carrier- lattice temperature difference as a function of external pulse energy in (a) a strongly amplifying (pumped at a rate of $\boldsymbol{J} = 1.75\boldsymbol{J}_0$) medium and (b) a transparent ($\boldsymbol{J} = \boldsymbol{J}_0$) medium.

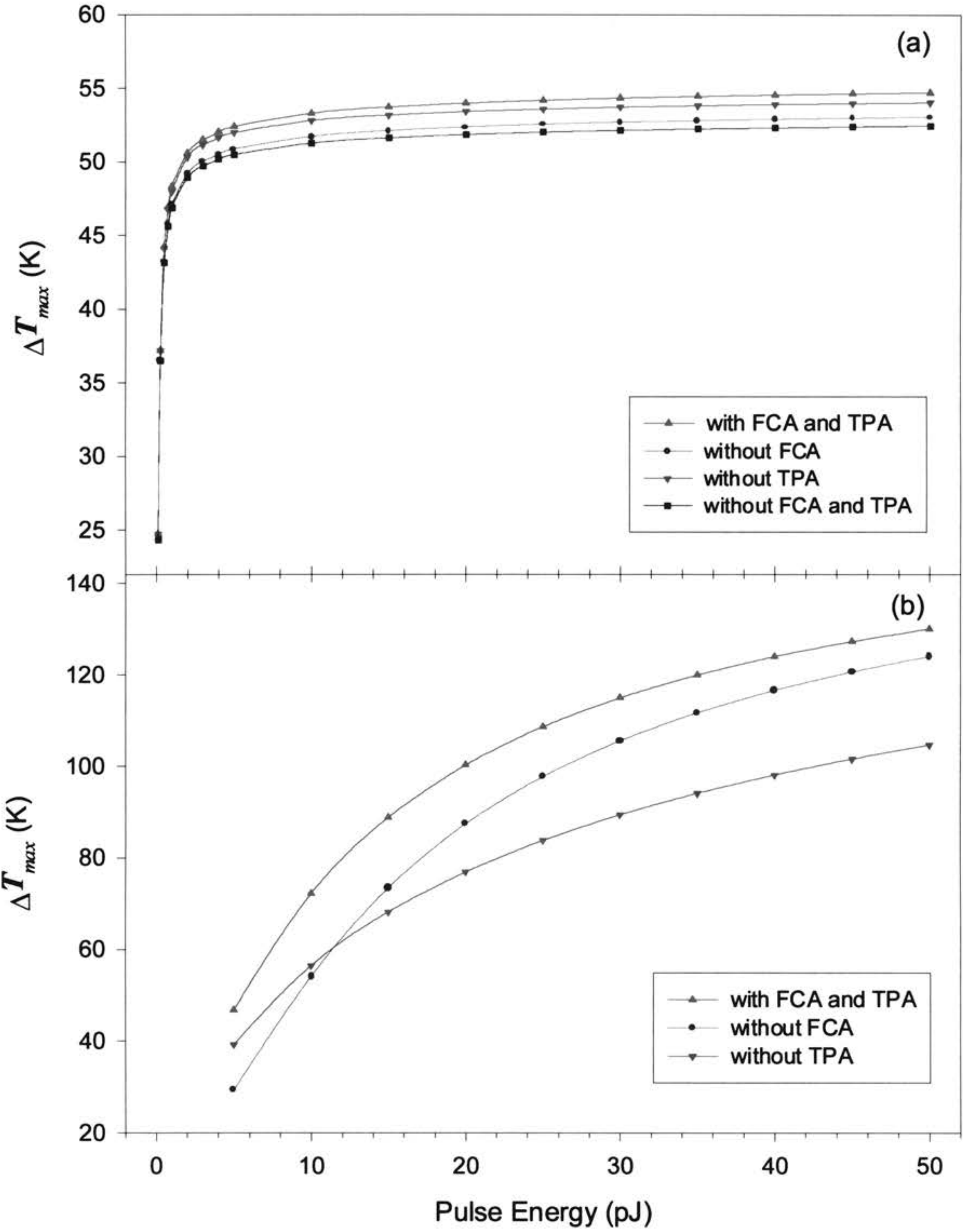

Figure 6.23. The first (a) and second (b) peaks of the carrier- lattice temperature difference as a function of external pulse energy in a strongly absorbing ($J = 0.25J_0$) medium.

For higher pulse energies, due to saturation the maximum temperature curve reaches a horizontal asymptote, which indicates an upper limit of carrier heating due to interband transitions. Nevertheless, for low-energy pulses interband transitions are the dominant heating factor. Even when high-energy pulses are applied and FCA along with TPA are taken into account the initial carrier heating is due to interband transitions. This is evident from the double-peak behavior of the carrier temperature. To understand this behavior we consider the evolution of the three main processes (interband transitions, FCA and TPA) that affect carrier temperature in an initially absorbing sample.

Because initial carrier density in the conduction band is small the process that has highest probability to absorb the photons is the interband transition. Both FCA and TPA have much less probability at the beginning. Interband transitions lead to higher free-carrier density, hence more FCA. Increasing photon density leads to higher probability of FCA, TPA and saturation of interband transitions. Thus, all three processes reach their maximum efficiency at different times. As a result the temperature peak does not coincide with the photon density peak. For example, when a 0.1 - pJ external pulse is applied the temperature peak appears only after most of the external pulse is absorbed (see Fig. 6.16b, p. 126). In the case of a 1-pJ pulse the temperature peak appears before the external pulse peak reaches the medium (Fig. 6.17b, p. 127). In these examples the single-photon interband transition is the dominant heating factor. In the case of a 2-pJ pulse FCA has noticeable influence after most of the pulse is absorbed, while the single-photon interband transition is the dominant heating factor at the beginning, before the external pulse peak reaches the medium (Fig. 6.18b, p. 128).

With increasing pulse energy the carrier temperature peak appears at earlier times, because high-energy pulses saturate the medium earlier. In contrast, FCA and TPA reach the maximum efficiency almost simultaneously and only after most of the external pulse is absorbed. The efficiency of FCA and TPA increases with pulse energy. As a result a second temperature peak appears (Fig. 6.20, p. 130), which become larger than the first peak for high-energy pulses (Fig. 6.21, p. 131). Thus, in an initially absorbing sample there are two peaks in the carrier temperature curve because of the time delay between processes that affect the carrier temperature.

The double-peak temperature behavior is observed only in strongly absorbing samples because in amplifying, transparent and weakly absorbing samples there is a significant carrier heating due to FCA and TPA from the beginning. As a result when the initially dominant heating process (the single-photon interband transition) reaches the saturation level, FCA and TPA are strong enough to ensure further temperature increase. Thus we see only one temperature peak, although there is a time delay between processes that affect the carrier temperature, which is more visible when high-energy pulses are applied (see Figs. 6.14 – 6.15, pp. 122-123).

Another piece of information that we obtain from Figs. 6.22 and 6.23 is the energy of the external pulse that causes equal heating due to FCA and TPA, $\mathcal{E}_{eq}$. For all samples and chosen parameter values we obtain $\mathcal{E}_{eq} \approx 12$ pJ. In the case of the amplifying sample the value is slightly larger. When $\mathcal{E}_x > \mathcal{E}_{eq}$, TPA has a larger influence than FCA, which is more effective when $\mathcal{E}_x < \mathcal{E}_{eq}$ (see also discussion in Section. 6.4).

Mathematically $\mathcal{E}_{eq}$ can be estimated by equating TPA and FCA terms in Eq. (2.1) (p. 18): $s_{TPA} N_p = s_{FCA} N_c$, and using Eq.(2.10) (p. 21). However, calculation of integral (2.10) requires knowledge of N_p and, therefore, N_c at all times. In addition both FCA and TPA cross-sections are not constants, which complicates the calculation of $\mathcal{E}_{eq}$. Thus, carrier temperature graphs (Figs. 6.22 and 6.23) present useful information about the relative efficiencies of FCA and TPA.

7. SUMMARY AND CONCLUSIONS

A system of modified rate equations that includes the carrier temperature as a dynamical variable is used to describe the interaction of electromagnetic radiation with semiconductors. We develop a model that takes into account the nonlinear functional dependence of the gain coefficient on carrier density and temperature. The model gives a simple description of the gain and carrier temperature dynamics and allows for a clear interpretation of results. The rate equations for photon and carrier densities are modified to include a third rate equation for the energy density, and by using an analytical approximation for the complex dependence of the gain on the chemical potential and temperature of the carriers. The model relies on the assumption of a quasi-equilibrium Fermi-Dirac carrier distribution and, therefore, all dynamic behavior results from the interactions of the quasi-equilibrium carrier ensemble with the external pulse and the lattice. We are effectively treating the carrier temperature as a dynamic variable. Non-equilibrium processes such as spectral hole burning are not present in this model – and probably they have no significant impact on the picosecond time scale.

One of the purposes of our approach to the problem of carrier heating in semiconductor laser media was to develop a simple model. We have derived approximate analytical relations between dynamic variables that significantly simplify both the numerical analysis and the physical interpretation. If we use the general expressions for relationships between dynamical variables, then the validity of our model

is limited only by the duration of the generated or external pulses, which cannot be shorter than the times for the polarization relaxation and the establishment of quasi-equilibrium. However, in this case the numerical analysis becomes more complex and the physical interpretation less transparent.

We investigate the evolution of the dynamical variables during a typical laser turn-on transition to cw behavior. We find that in the cw lasing regime the carrier temperature is always greater than the lattice temperature, but that this temperature difference has little impact on the output power. This result is valid for conditions both near and also well above threshold.

Investigation of the laser operating in cw regime subject to external pulses show that when long pulses (several tens of picoseconds) are applied the laser response is virtually the same for the model inclusive of temperature dynamics as for the one without it; however, the response to the shorter pulses is different. The oscillations damp faster when the carrier temperature dynamics is taken into account, and this difference becomes more noticeable for shorter signal duration. Thus, the carrier temperature dynamics plays a significant role in the dynamical response of the laser on time scales up to several tens of picoseconds.

Calculations with pulses of higher and lower energy show qualitatively similar results. Except for faster oscillation damping, the character of the photon density oscillations in the cw laser caused by the external pulse is similar to that of those calculated without carrier temperature dynamics regardless of the pulse energy or duration.

The temperature dynamics, which is central to our model, is reflected in the behavior of the gain function. We study this behavior through the response of a laser or laser medium to an applied optical pulse. Gain dynamics is indirectly observed in the response of a laser to a sufficiently short picosecond pulse, where we show that there is a noticeable change compared to models without the temperature dynamics. However, application of a subpicosecond pulse to a laser medium allows direct observation of gain dynamics.

We have considered the dynamic behavior of the gain and carrier temperature in a short semiconductor laser medium, subject to external optical pulses, on a picosecond time scale. We investigate the response of weakly amplifying, transparent, and weakly absorbing media. By applying pulses of different energies to strongly absorbing media, we see variation in the evolution of the gain that demonstrates the role played by carrier density in addition to that of carrier heating.

We study the cases for media whose pre-pulse states are strongly absorbing, transparent, and strongly amplifying at the frequency of the pulse. The results show that the various physical processes that influence the gain and the carrier temperature contribute differently depending on the initial state of the medium and the pulse energy. In particular, we note the competing effects associated with the pulse changing the energy density and the carrier density simultaneously. We also point out how FCA and TPA can dominate when the gain is near the transparency region. This leads to initial gain suppression followed by gain enhancement due to interband absorption made possible by FCA and TPA. It can also lead to a double peak in the carrier temperature response and a plateau followed by an increase in the gain as shown. Although FCA and TPA are both

heating factors, however their influence is non-cumulative.

Finally, we note that although the bandgap energy is a function of carrier density due to many-body effects, which leads to bandgap shrinkage, this functional dependence (see Eq. (5.1), p. 82) does not noticeably affect the dynamic behavior of the gain and the carrier temperature for pulse energies considered in this work. Higher pulse energies and, hence, more dramatic changes in the carrier density, are expected to have a more visible influence.

The results presented in this thesis can be verified with existing experimental techniques. Additional controllable signals can be used to provide more accurate information about the gain and carrier temperature dynamics. For example, a low frequency ($\omega << \varepsilon_g/\hbar$) external signal can be used to heat the electron ensemble without changing the carrier density. This will significantly increase the role of FCA without direct influence on interband transitions and TPA, thus highlighting the influence of FCA.

8. BIBLIOGRAPHY

1. N. G. Basov, O. N. Krokhin, Yu. M. Popov, Production of Negative-Temperature States in p-n Junctions of Degenertate Semiconductors, Sov. Phys. JETP, **13**, 1320 (1961).

2. M. G. A. Bernard, G. Duraffourg, Laser Conditions in Semiconductors, Phys. Status Solidi **1**, 699 (1961).

3. W. P. Dumke, Interband Transitions and Maser Action, Phys. Rev. **127**, 1559 (1962).

4. R. N. Hall, G. E. Fenner, J. D. Kingsley, T. J. Soltys, R. O. Carlson, Coherent light emission from GaAs junctions, Phys. Rev. Lett. **9**, 366 (1962).

5. M. I. Nathan, W. P. Dumke, G. Burns, F. H. Dill, Jr., G. Lasher, Stimulated emission of radiation from GaAs p-n junctions, Appl. Phys. Lett. **1**, 62 (1962).

6. N. Holonyak, Jr., S. F. Bevacqua, Coherent (visible) light emission from $Ga(Al_{1-x}P_x)$ junctions, Appl. Phys. Lett. **1**, 82 (1962).

7. T. M. Quist, R. H. Rediker, R. J. Keyes, W. E. Krag, B. Lax, A. L. McWhorter, H. J. Zeiger, Semiconductor maser of GaAs, Appl. Phys. Lett. **1**, 82 (1962).

8. V. S. Bagaev, N. G. Basov, B. M. Vul, B. D. Kopylovskii, O. N. Krokhin, E. P. Markin, Yu. M. Popov, A. N. Khvoscev, A. P. Shotov, Doklady Akad. Nauk. SSSR **150**, 275 (1963).

9. E. P. Ippen, C. V. Shank, Techniques for Measurement, in *Ultrashort Light Pulses*, S.L. Shapiro (ed.), (Springer–Verlag, Berlin, 1977).

10. J. Shah, Ultrafast spectroscopy of semiconductors and semiconductor nanostructures, Berlin ; New York : Springer, 1996.

11. M. S. Stix, M. P. Kesler, E. P. Ippen, Observations of subpicosecond dynamics in GaAlAs laser diodes, Appl. Phys. Lett. **48**, 1722 (1986).

12. W. Z. Lin, L. G. Fujimoto, E. P. Ippen, R. A. Logan, Femtosecond carrier dynamics in GaAs, Appl. Phys. Lett. **50**, 124 (1987).

13. M. P. Kesler, E. P. Ippen, Subpicosecond gain dynamics in GaAlAs laser diodes, Appl. Phys. Lett. **51**, 1765 (1987).

14. *Hot Carriers in Semiconductors*, Proceeding of the Fifth International Conference, Eds. J. Shah and G. J. Iafrate, Boston, MA, July 20–24, 1987, (Pergamon, Great Britain, 1988).

15. K. L. Hall, J. Mark, E. P. Ippen, and G. Eisenstein, Femtosecond gain dynamics in InGaAsP optical amplifiers, Appl. Phys. Lett. **56**, 1740 (1990).

16. J. Mark and J. Mørk, Subpicosecond gain dynamics in InGaAsP optical amplifiers: Experiment and theory, Appl. Phys. Lett. **61**, 2281 (1992).

17. G. H. B. Thompson, *Physics of Semiconductor Laser Devices*, (Wiley, New York, 1980).

18. G. P. Agrawal, N. K. Dutta, *Semiconductor Lasers*, (Van Nostrand Reinhold, New York, 1993).

19. W. W.Chow, S. W. Koch, M. Sargent III, *Semiconductor-Laser Physics*, (Springer-Verlag, Berlin, 1994).

20. L. A. Coldren, S. W. Corzine, *Diode Lasers and Photonic Integrated Circuits*, (Wiley, New York, 1995).

21. S. L. Chuang, *Physics of Optoelectronic Devices*, (Wiley , New York, 1995), p. 358.

22. A. N. Oraevsky, Multitemperatue model and laser dynamics, Sov. J. Quant. Elecron. **20**, 1371 (1990).

23. A. N. Oraevsky, M. M. Clark, D. K. Bandy, "Many–temperature model of laser with dynamics", Opt. Commun. **85**, 360 (1991).

24. A. Yariv, Quantum Electronics, (Wiley, New York, 1989).

25. L. D. Landau, E. M. Lifshitz, Statistical physics (Nauka, Moscow, 1995).

26. A. S. Kompaneyets, Theoretical Physics (Dover Publications, New York, 1962).

27. B. K. Ridley, Quantum Processes in Semiconductors, (Clarendon Press, Oxford, UK, 1993).

28. W.–Z. Lin, R. W. Schoenlein, J. G. Fujimoto, E. P. Ippen, Femtosecond Absorption Saturation Studies of Hot Carriers in GaAs and AlGaAs, IEEE J. Quantum Electron. **24**, 267 (1988).

29. R. E. Peierls, Quantum theory of solids.(Clarendon Press, Oxford, UK, 1955).

30. C. Kittel, *Quantum theory of solids,* (Wiley, New York, 1963).

31. N. W. Ashcroft, N. D. Mermin, *Solid State Physics* (Saunders College, Philadelphia, 1976).

32. K. Böer, *Survey of Semiconductor Physics*, (Van Nostrand Reinhold, New York, 1992).

33. H. Haug, S. Schmitt–Rink, Electron theory of the optical properties of laser-excited semiconductors, Prog. Quant. Electr. **9**, pp.3-100, 1984.

34. H. Haug, S. W. Koch, Quantum theory of the optical and electronic properties of semiconductors, (World Scientific, Singapore 1994).

35. H. Haug, A.–P. Jauho, Quantum kinetics in transport and optics of semiconductors, (Springer, Berlin, 1996).

36. M. Asada, Y. Suematsu, Density–Matrix Theory of Semiconductor Lasers with Relaxation Broadening Model – Gain and Gain-Suppression in Semiconductor Lasers, IEEE Journal of Quant. Electr., QE-**21**, 434 (1985).

37. V. M. Galitskii, V. F. Elesin, Electron kinetics and stationary generation in semiconductor lasers, Sov.Phys.–JETP, **37**, 351 (1973).

38. V. M. Galitskii, V. F. Elesin, Kinetic theory of generation of a strong field in semiconductor lasers, Sov.Phys. – JETP, **41**, 104 (1975).

39. V. M. Galitskii, V. F. Elesin, *Resonant Interaction of Electromagnetic fields with Semiconductors*, (Energoatomizdat, Moscow, 1986) (in russian).

40. L. Allen, J. H. Eberly, *Optical resonance and two-level atoms* (Wiley, New York, 1975).

41. M. Lindberg, S. W. Koch, Effective Bloch Equations for Semiconductors, Phys. Rev. B **38**, 3342 (1988).

42. C. M. Bowden, G. P. Agrawal, Generalized Bloch–Maxwell formulation for semiconductor lasers, Opt. Commun. **100**, 147 (1993).

43. C. M. Bowden, G. P. Agrawal, Maxwell–Bloch formulation for semiconductors: Effects of coherent Coulomb exchange, Phys.Rev. A **51**, 4132 (1995).

44. J. Yao, G. P. Agrawal, P. Gallion, C. M. Bowden, Semiconductor laser dynamics beyond the rate-equation limit, Opt. Commun. **119**, 246 (1995).

45. O. Hess, T. Kuhn, Maxwell–Bloch equations for spatiallly inhomogeneous semiconductor lasers. I. Theretical formulation, Phys. Rev. A, **54**, 3347 (1996).

46. O. Hess, T. Kuhn, Maxwell–Bloch equations for spatiallly inhomogeneous semiconductor lasers. II. Spatiotemporal dynamics, Phys. Rev. A, **54**, 3360 (1996).

47. L. A. Rivlin, A. T. Semenov, and S. D. Yakubovich, *Dynamics and spectra of semiconductor lasers*, (Radio i Svyaz, Moscow, 1983), (in Russian).

48. L. A. Rivlin, Dynamics and emission Spectra of Semiconductor Lasers, J. of Sov. Las. Res. **7**,11(1986).

49. H. Haug, Quantum–Mechanical Rate Equations for Semiconductor Lasers, Phys. Rev. **184**, 338 (1969).

50. R. Lang, K. Kobayashi, External optical feedback effects on semiconductor injection laser properties, IEEE J. Quantum Electron. QE-**16**, 347 (1980).

51. R.–Q. Hui, S.–P. Tao, Improved Rate Equations for External Cavity Semiconductor Lasers, IEEE J. Quantum Electron. QE-**25**, 1580 (1989).

52. G. Björk, Y. Yamamoto, analysis of Semiconductor Microcavity Lasers Using Rate Equations, IEEE J. Quantum Electron. QE-**27**, 2386 (1991).

53. K. D. LaViolette, P.–L. Liu, Noise–Driven Rate Equation Analysis of Quantum-Well, Microcavity Lasers, IEEE Photon. Tech. Lett. **3**, 782 (1991).

54. B. J. Thedrez, C. H. Lee, A Reassessment of Standard Rate Equations for Low Facet Reflectivity Semiconductor Lasers Using Traveling Wave Rate Equations, IEEE J. Quantum Electron. QE-**28**, 2706 (1992).

55. G. Morthier, An Accurate Rate-Equation Description for DFB Lasers and Some Interesting Results, IEEE J. Quantum Electron. **33**, 231 (1997).

56. J.–P. Zhang, The Dynamic Properties and Stability Analysis for Vertical-Cavity Surface-Emitting Lasers, IEEE J. Quantum Electron. **31**, 2127 (1995).

57. J. Shah, R. F. Leheny, R. E.Nahory, Hot–carrier effects in 1.3-μ $In_{1-x}Ga_xAs_yP_{1-y}$ light emitting diodes, Appl. Phys. Lett. **39**, 618 (1981).

58. T. L. Koch, L. C. Chiu, C. Harder, A. Yariv, Picosecond carrier dynamics and laser action in optically pumped buried heterostructure lasers, Appl. Phys. Lett. **41**, 6 (1982).

59. L. A. Rivlin, Febrile reaction of electrons in semiconductor laser to an ultrashort light pulse, Sov. J. Quantum Electron. **15**, 453 (1985).

60. B. N. Gomatam, A. P. DeFonzo, Theory of hot carrier effects on non-linear gain in GaAs-GaAlAs lasers and amplifiers, IEEE J. Quantum Electron. QE-**26**, 1689 (1990).

61. M. Willatzen, A. Uskov, J. Mørk, H. Olesen, B. Tromborg, A.–P. Jauho, Nonlinear gain suppression in semiconductor lasers due to carrier heating, IEEE Photon. Tech. Lett. **3**, 606 (1991).

62. M. Willatzen, T. Takahashi, Y. Arakawa, Nonlinear gain effects due to carrier heating and spectral hole burning in strained-quantum well lasers, IEEE Photon. Tech. Lett. **4**, 682, (1992).

63. A. V. Uskov, J. Mørk, J. Mark, Theory of short-pulse gain saturation in semiconductor laser amplifiers, IEEE Photon. Technol. Lett., **4**, 443 (1992).

64. V. I. Tolstikhin, M. Willander, Carrier heating effects in dynamic-single-frequency GaInAsP-InP laser diodes, IEEE J. Quantum Electron. **31**, 814 (1995).

65. C. Z. Ning, R. A. Indik, J. V. Moloney, Self-consistent approach to thermal effects in vertical-cavity surface-emitting lasers, J. Opt. Soc. Am. B **12**, 1993 (1995).

66. C.-Y. Tsai, C.-Y. Tsai, R. M. Spencer, Y.-H. Lo, L. F. Eastman, Nonlinear gain coefficients in semiconductor lasers: Effects of carrier heating, IEEE J. Quantum Electron. QE-**32**, 201 (1996).

67. A. N. Oraevsky, T. Sarkisyan, D. K. Bandy, Dynamics of the temperature of a recombining ensemble of fermions, JETP Lett. **62**, 674 (1995).

68. A. N. Oraevsky, T. V. Sarkisyan, D. K. Bandy, "Nonlinear Gain and the Bistable Regime of Free-Running Oscillation in a Semiconductor Laser", Laser Physics, **7**, 920 (1997).

69. T. V. Sarkisyan, A. N. Oraevsky, A. T. Rosenberger, R. L. Rolleigh, D. K. Bandy, Nonlinear gain and carrier temperature dynamics in semiconductor laser media, J. Opt. Soc. Am. B, **15**, 1107 (1998).

70. T. V. Sarkisyan, A. T. Rosenberger, A. N. Oraevsky, D. K. Bandy, Gain and Carrier Temperature Response of Semiconductor Laser Media to Short Optical Pulses, J. Opt. Soc. Am. B, (2000) (in press).

71. D. K. Bandy, T. V. Sarkisyan, A. T. Rosenberger, A. N. Oraevsky, Gain dynamics in semiconductor active and passive media with external signal, Paper WI5, OSA Annual Meeting, October 12-17, Long Beach, CA, 1997.

72. T. V. Sarkisyan, D. K. Bandy, A. T. Rosenberger, A. N. Oraevsky, Gain response to short perturbation of the carrier ensemble parameters in semiconductor laser media, Paper MH3, OSA Annual Meeting, October 4-9, Baltimore, MD, 1998.

73. H. C. Casey, Jr., M. B. Panish, *Heterostructure Lasers*, Part B: Materials and Operating Characteristics, (Academic Press, New York, 1978), p. 181.

74. P. T. Landsberg, *Recombination in Semiconductors*, (Cambridge University Press, 1991).

75. G. E. Pikus, *Fundamentals of the Theory of Semiconductor* Devices, (Nauka, Moscow, 1965).

76. A.Anselm, *Introduction to Semiconductor Theory*, (Nauka, Moscow, 1978).

77. P. Y. Yu, M. Cardona, *Fundamentals of Semiconductors*, (Springer, Berlin, 1996).

78. C. M. Wolfe, N. Holonyak, Jr., G. E. Stillman, *Physical Properties of Semiconductors*, (Prentice Hall, Englewood Cliffs, 1989).

79. P. K. Basu, *Theory of Optical Processes in Semiconductors*, ((Clarendon Press, Oxford, 1997).

80. H. Y. Fan, Effects of free Carriers on the Optical Properties, in *Semiconductors and Semimetals*, **3**, (Eds. R.K. Wilardson, A.C. Beer) p. 405 (Academic Press, New York, 1967).

81. N. G. Basov, A. Z. Grasyuk, I. G. Zubarev, V. A. Katulin, O. N. Krokhin, Semiconductor quantum generator with two-photon optical excitation, Sov. Phys. JETP, **23**, 366 (1966).

82. B. S. Wherrett, Scaling rules for multiphoton interband absorption in semiconductors, J. Opt. Soc. Amer. B, **1**, 67 (1984).

83. M. Sheik-Bahae, D. C. Hutchings, D. J. Hagan, E. W. Van Stryland, Dispersion of Bound Electronic Nonlinear Refraction in Solids, IEEE J. Quantum Electron. **27**, 1296 (1991).

84. K. Leo, J. H. Collet, Influence of electron-hole scattering on the plasma thermalization in doped GaAs, Phys. Rev. B, **44**, 5535 (1991).

85. V. Sa-yakanit, "Electron density of states in a Gaussian random potential: Path-integral approach", Phys. Rev. B **19**, 2266 (1979).

86. W. Sritrakool, V. Sa-yakanit, H. R. Glyde, "Band tails in disordered systems", Phys. Rev. B **33**, 1199 (1986).

87. C. J. Hwang, Properties of spontaneous and Stimulated Emission in GaAs Junction Lasers. I. Densities of States in the Active Regions, Phys. Rev. B, **2**, 4117 (1970).

88. F. Urbach, The Long-Wavelength Edge of Photographic Sensitivity and of the Electronic Absorption of Solids, Phys. Rev. **92**, 1324 (1953).

89. M. V. Kurik, Urbach Rule, Phys. Stat. Sol. (a) **8**, 9 (1971).

90. C. Ell, Urbach Tail, Optical Stark Effect, and their Connection to Quantum Kinetic Equations, in *Microscopic Theory of Semiconductors*, S.W. Koch (Ed.) (World Scientific, Singapore, 1995).

91. A. Uskov, J. Mørk, J. Mark, Wave Mixing in Semiconductor Laser Amplifiers Due to Carrier Heating and Spectral-Hole Burning, IEEE J. Quantum Electron. **30**, 1769 (1994).

92. J. Wang, H. C. Schweizer, A Quantitative Comparison of the Classical Rate-Equation Model with the Carrier Heating Model on Dynamics of the Quantum-Well Laser: The Role of Carrier Energy Relaxation, Electron-Hole Interaction, and Augier Effect, IEEE J. Quantum Electron. **33**, 1350 (1997).

93. W. H. Press, B. P. Flannery, S. A. Teukolsky, W. T. Vetterling, *Numerical Recipes*, (Cambridge University Pres, 1986).

94. V. I. Tolstikhin, M. Wilander, Competition between carrier concentration and temperature influences on gain as means for improving modulation response of semiconductor laser. J. Appl. Phys., **77**, 488 (1995).

95. J. Mørk, A. Mecozzi, Theory of the ultrafast optical response of active semiconductor waveguides, J. Opt. Soc. Am. B, **13**, 1803 (1996).

96. A. Mecozzi, J. Mørk, Theory of heterodyne pump-probe experiments with femtosecond pulses, J. Opt. Soc. Am. B, **13**, 2437 (1996).

97. A. Mecozzi, J. Mørk, Theory of heterodyne pump-probe experiments with femtosecond pulses, J. Opt. Soc. Am. B, **14**, 761 (1997).

98. M. Asada, A. Kameyama, Y. Suematsu, "Gain and intervalence band absorption in quantum-well lasers", IEEE J. Quant. Electron. **QE-20**, 745 (1984).

99. *Semiconductors: Group IV elements and III-V Compounds*, Ed. O.Madelung, (Springer-Verlag, Berlin 1991) pp.101-113.

100. H. C. Casey, Jr., F. Stern, Concentration-dependent absorption and spontaneous emission in heavily doped GaAs, J. Appl. Phys. **47**, 631 (1976).

101. A. Villeneuve, M. Sundheimer, N. Finalayson, G. I. Stegeman, S. Morasca, C. Rigo, R. Calvani, C. DeBernardi, Two-photon absorption in $In_{1-x-y}Ga_xAl_yAs$/InP waveguides at communications wavelengts, Appl. Phys. Lett. **56**, 1865 (1990).

102. J. R. Karin, A. V. Uskov, R. Nagarajan, J. E. Bowers, J. Mørk, "Carrier heating dynamics in semiconductor waveguide saturable absorbers", Appl. Phys. Lett., **65**, 2708 (1994).

103. A.V. Uskov, J.R. Karin, R. Nagarajan, J.E. Bowers, "Dynamics of carrier heating and sweepout in waveguide saturable absorbers", IEEE J. of Selected Topics in Quantum Electron. **1**, 552 (1995).

104. A. V. Uskov, J. R. Karin, J. E. Bowers, J.G. McInerney, J. Le Bihan, "Effects of carrier cooling and carrier heating in saturation dynamics and pulse propagation through bulk semiconductor absorbers", IEEE J. of Quantum Electron. **34**, 2162 (1998).

APPENDICES

APPENDIX A. RELATIONSHIP BETWEEN ELECTROMAGNETIC FIELD AND PHOTON DENSITY

Thermodynamic expression of the internal energy density in a medium with electromagnetic field is given by [1]

$$\boldsymbol{dU} = \boldsymbol{Td}\mathbf{S} + \zeta \boldsymbol{d}\rho + \frac{1}{4\pi}\vec{\boldsymbol{E}} \cdot \boldsymbol{d}\vec{\boldsymbol{D}} + \frac{1}{4\pi}\vec{\boldsymbol{H}} \cdot \boldsymbol{d}\vec{\boldsymbol{B}}, \qquad \text{(A. 1).}$$

where $\boldsymbol{T}$ is the temperature of the medium, **S** is the entropy, ζ is the chemical potential per unit mass ($\zeta = \mu / \boldsymbol{m}$, μ is the chemical potential per particle, $\boldsymbol{m}$ is the mass of the molecule), ρ is the density of the medium, $\boldsymbol{E}$ is the electric field, $\boldsymbol{D}$ the electric displacement, $\boldsymbol{H}$ is the magnetic field, and $\boldsymbol{B}$ is the magnetic induction. For constant density and entropy the time derivative of energy density gives the expression for the divergence of the Poynting vector:

$$\vec{\nabla} \cdot \vec{\boldsymbol{S}} = -\frac{\partial \boldsymbol{U}}{\partial \boldsymbol{t}}. \qquad \text{(A. 2)}$$

This expression can also be obtained using definition of the Poynting vector and Maxwell's equations as follows

$$\vec{\nabla} \cdot \vec{\boldsymbol{S}} = \frac{\boldsymbol{c}}{4\pi}\vec{\nabla} \cdot \left[\vec{\boldsymbol{E}} \times \vec{\boldsymbol{H}}\right] = \frac{\boldsymbol{c}}{4\pi}\left[\vec{\boldsymbol{H}} \cdot \left(\vec{\nabla} \times \vec{\boldsymbol{E}}\right) - \vec{\boldsymbol{E}} \cdot \left(\vec{\nabla} \times \vec{\boldsymbol{H}}\right)\right] = -\frac{1}{4\pi}\left(\vec{\boldsymbol{E}} \cdot \frac{\partial \vec{\boldsymbol{D}}}{\partial \boldsymbol{t}} + \vec{\boldsymbol{H}} \cdot \frac{\partial \vec{\boldsymbol{B}}}{\partial \boldsymbol{t}}\right). \qquad \text{(A. 3)}$$

Thus, at constant entropy and density Eq. (A.1) for non-dispersive medium gives

---

[1] L.D. Landau, E.M. Lifshits, Electrodynamics of continuous media, (Nauka, Moscow, 1992).

$$U = \frac{1}{8\pi}\left(\varepsilon E^2 + \mu H^2\right), \tag{A. 4}$$

where ε is the dielectric function, and μ is the magnetic susceptibility (not to be confused with the chemical potential).

In a dispersive medium the corresponding expression for the energy density calculated for complex fields is given by [1]:

$$U = \frac{1}{16\pi}\left[\frac{d(\varepsilon\omega)}{d\omega} EE^* + \frac{d(\mu\omega)}{d\omega} HH^*\right] \tag{A. 5}$$

The real and complex fields are related as follows:

$$E_{\text{Re}} = \frac{1}{2}\left(E + E^*\right) \Rightarrow E_{\text{Re}}^2 = \frac{1}{4}\left(E^2 + 2EE^* + E^{*2}\right). \tag{A. 6}$$

Time averaging will eliminate second harmonic terms, E^2 and E^{*2}, and, therefore, we obtain $\overline{E_{\text{Re}}^2} = EE^*/2$.

Thus, in terms of real fields (A.5) become

$$U = \frac{1}{8\pi}\left[\frac{d(\varepsilon\omega)}{d\omega}\overline{|E|^2} + \frac{d(\mu\omega)}{d\omega}\overline{|H|^2}\right], \tag{A. 7}$$

so that Eq.(A.7) and Eq.(A.4) are consistent with each other when dispersion is neglected. This result is obtained for fields of form $f = f(t)\exp(-i\omega t)$ with slowly varying amplitude.

For a monochromatic plane wave this expression can be simplified using the relationship between magnetic and electric fields obtained from Maxwell's equations:

$$\vec{H} = \frac{c}{\omega\mu}\left[\vec{k} \times \vec{E}\right], \tag{A. 8}$$

where $k = \sqrt{\varepsilon\mu}\,\omega/c$. From (A.8) follows that $\varepsilon EE^* = \mu HH^*$ and using (A.5) we obtain

$$U = \frac{1}{16\pi\mu\omega}\left[\mu\omega\frac{d(\varepsilon\omega)}{d\omega} + \varepsilon\omega\frac{d(\mu\omega)}{d\omega}\right]EE^* = \frac{1}{16\pi\mu\omega}\frac{d(\mu\varepsilon\omega^2)}{d\omega}EE^* \quad \text{(A. 9)}$$

The differential in this expression can be simplified as follows

$$\frac{d(\mu\varepsilon\omega^2)}{d\omega} = c^2\frac{dk^2}{d\omega} = 2c^2k\frac{dk}{d\omega} = 2c\sqrt{\mu\varepsilon}\,\omega\frac{dk}{d\omega}. \quad \text{(A. 10)}$$

As a result we obtain

$$U = \frac{c}{8\pi}\sqrt{\frac{\varepsilon}{\mu}}\frac{dk}{d\omega}EE^* \quad \text{(A. 11)}$$

Using definitions of the refractive index $n \equiv \sqrt{\varepsilon\mu}$ and the group velocity $v_{gr} = d\omega/dk$ we obtain

$$U = \frac{1}{2\mu}nn_{gr}\frac{EE^*}{4\pi}, \quad \text{(A. 12)}$$

where $n_{gr} \equiv c/v_{gr}$ and is known as group velocity index. Dividing (A.12) by photon energy and taking into account the fact that for most semiconductors $\mu \cong 1$, we obtain the relationship between photon density and electric field:

$$N_p = nn_{gr}\frac{EE^*}{8\pi\hbar\omega} \quad \text{(A. 13)}$$

Using the relationship between intensity and field

$$I \equiv c\frac{n}{2}\frac{|E|^2}{4\pi}, \quad \text{(A. 14)}$$

we obtain

$$N_p = \frac{I}{v_{gr}\cdot\hbar\omega} \quad \text{(A. 15)}$$

Derivation of (A.13) is done using expressions obtained for a transparent dielectric medium. Nevertheless, we can consider a laser diode as a transparent medium

and absorption or gain can be considered as specific factors that change the intensity of field. Thus using (A.13) in semiconductor media is justified.

Using obtained expressions and Eq. (1.1) one can connect the gain (absorption) coefficient with the photon density

$$\frac{dN_p}{dz} = \left(\frac{\partial}{\partial z} + \frac{1}{v_{gr}} \frac{\partial}{\partial t} \right) N_p = g N_p , \tag{A. 16}$$

and for time rate of change of the photon density of a pulse traveling in the medium at given position we have

$$\frac{dN_p}{dt} = v_{gr} g N_p . \tag{A. 17}$$

APPENDIX B. DERIVATION OF PHOTON DENSITY EQUATION FROM THE FIELD EQUATION

We begin with the equation describing the time dependence of the slowly varying amplitude of the electromagnetic field ***E***:

$$\frac{dE}{dt} = -\frac{1}{2\tau_c}(1+i\Delta)E + \frac{1}{2}(1+i\alpha)gE + \kappa F \ , \qquad \text{(B. 1)}$$

where $\Delta \equiv 2(\omega_c - \omega)\tau_c$, ω_c is the cavity eigenfrequency, α is the linewidth enhancement factor, and ***F*** is the external field amplitude. Here we have neglected spontaneous emission, free carrier absorption, two-photon absorption and other minor effects. Equation (B.1) is similar to Lang-Kobayashi equations (see Ref. [50] in the main text) without delayed optical feedback.

The field coupling coefficient is given by [2]

$$\kappa = \frac{1-R}{\tau_{rt}\sqrt{R}}, \qquad \text{(B. 2)}$$

where ***R*** is the power reflection coefficient of the laser facet through which the external signal is entering the laser medium and τ_{rt} is the laser cavity roundtrip time.

Consider the external signal as a multimode field with a random modal phase distribution:

$$F(t) = \sum_{\Omega} F_{\Omega}(t) e^{-i(\Delta\Omega t + \phi_{\Omega})}, \qquad \text{(B. 3)}$$

---

[2] N. Schunk, K. Petermann, Noise Analysis of Injection-Locked Semiconductor Injection Lasers, IEEE Journal of Quant. Electron. QE-22, 642 (1986).

where $\Delta\Omega = \Omega - \omega$, and φ_Ω is randomly distributed in the interval $(0,2\pi)$. This form of the external signal is justified because mainly we deal with short pulses, which contain many modes.

To derive the equation for photon density we write a formal solution of Eq.(B.1) in the form:

$$\boldsymbol{E} = \kappa \exp\left[-\frac{1}{2}\boldsymbol{D}(\boldsymbol{t})\right]\int_0^t \exp\left[\frac{1}{2}\boldsymbol{D}(\boldsymbol{t}')\right]\boldsymbol{F}(\boldsymbol{t}')\boldsymbol{dt}' \tag{B. 4}$$

where

$$\boldsymbol{D}(\boldsymbol{t}) = \int_0^t \left(\frac{1}{\tau_c} - \boldsymbol{g} + \boldsymbol{i}(\Delta - \alpha \boldsymbol{g})\right)\boldsymbol{dt}'. \tag{B. 5}$$

The solution (B.4) satisfies the initial condition $\boldsymbol{E}=0$ at $\boldsymbol{t}=0$. This initial condition is chosen for convenience since the final result does not depend on initial conditions. In principle we can satisfy any initial condition if we add to expression (B.4) the general solution of Eq.(B.1) for $\boldsymbol{F}=0$. We calculate the value $\boldsymbol{EE}^*$ which is proportional to the photon density in a cavity (see Appendix A, p. 151):

$$\boldsymbol{EE}^* = \kappa^2 \exp[-\operatorname{Re}\boldsymbol{D}(\boldsymbol{t})]\int_0^t \boldsymbol{dt}'\int_0^t \boldsymbol{dt}'' \exp\left[\frac{1}{2}\boldsymbol{D}(\boldsymbol{t}') + \frac{1}{2}\boldsymbol{D}^*(\boldsymbol{t}'')\right]\boldsymbol{F}(\boldsymbol{t}')\boldsymbol{F}^*(\boldsymbol{t}''). \tag{B. 6}$$

Now we must calculate

$$\boldsymbol{F}(\boldsymbol{t}')\boldsymbol{F}^*(\boldsymbol{t}'') = \sum_{\Omega,\Omega'} \boldsymbol{F}_\Omega(\boldsymbol{t}')\boldsymbol{F}^*_{\Omega'}(\boldsymbol{t}'')\boldsymbol{e}^{-i(\Delta\Omega t' - \Delta\Omega' t'' + \phi_\Omega - \phi_{\Omega'})}. \tag{B. 7}$$

Assume that the external signal has a broad band spectrum so that $\boldsymbol{F}_\Omega(\boldsymbol{t})$ is a slowly varying function of Ω. Now split the sum (B.7) into two parts:

$$\sum_{\Omega,\Omega'} \boldsymbol{F}_\Omega(\boldsymbol{t}')\boldsymbol{F}^*_{\Omega'}(\boldsymbol{t}'')\boldsymbol{e}^{-i(\Delta\Omega t' - \Delta\Omega' t'' + \phi_\Omega - \phi_{\Omega'})} = \sum_{\Omega} \boldsymbol{F}_\Omega(\boldsymbol{t}')\boldsymbol{F}^*_{\Omega}(\boldsymbol{t}'')\boldsymbol{e}^{-i\Delta\Omega(t' - t'')} +$$

$$+ \sum_{\Omega\neq\Omega'} \boldsymbol{F}_\Omega(\boldsymbol{t}')\boldsymbol{F}^*_{\Omega'}(\boldsymbol{t}'')\boldsymbol{e}^{-i(\Delta\Omega t' - \Delta\Omega' t'' + \phi_\Omega - \phi_{\Omega'})}. \tag{B. 8}$$

Since $F_\Omega(t)$ is a slowly varying function of Ω we can use the following approximation:

$$\sum_\Omega F_\Omega(t')F_\Omega^*(t'')e^{-i\Delta\Omega(t'-t'')} \approx F_\omega(t')F_\omega^*(t'')\sum_\Omega e^{-i\Delta\Omega(t'-t'')} \tag{B. 9}$$

and

$$\sum_{\Omega\neq\Omega'} F_\Omega(t')F_{\Omega'}^*(t'')e^{-i(\Delta\Omega' t'-\Delta\Omega t''+\phi_\Omega-\phi_{\Omega'})} \approx F_\omega(t')F_\omega^*(t'')\sum_{\Omega\neq\Omega'} e^{-i(\Delta\Omega' t'-\Delta\Omega t''+\phi_\Omega-\phi_{\Omega'})} = 0, \tag{B. 10}$$

where ω is the central frequency of the external pulse. The last sum is equal to zero since the phases in the exponent are randomly distributed in the interval (0, 2π). Now we replace the sum on the right side of Eq. (B.9) by the integral

$$F_\omega(t')F_\omega^*(t'')\sum_\Omega e^{-i\Delta\Omega(t'-t'')} \approx \frac{F_\omega(t)F_\omega^*(t'')}{\Delta\Omega_0}\int e^{-i\Delta\Omega(t'-t'')}d(\Delta\Omega) \approx$$

$$\approx 2\pi\frac{F_\omega(t')F_\omega^*(t'')}{\Delta\Omega_0}\delta(t'-t''), \tag{B. 11}$$

where $\Delta\Omega_0$ is the frequency interval between adjacent modes. After substitution of the relation (B.11) into (B.6) and integration over t'' we obtain

$$EE^* = 2\pi\frac{\kappa^2}{\Delta\Omega_0}\exp[-\operatorname{Re}D(t)]\int_0^t \exp[\operatorname{Re}D(t')]\left|F_\omega(t')\right|^2 dt'. \tag{B. 12}$$

Converting Eq.(B.12) back to a differential equation and multiplying by $nn_{gr}/(8\pi\cdot\hbar\omega)$ we obtain

$$\frac{dN_p}{dt}+\frac{1}{\tau_c}N_p - g(n)N_p = kN_{px}, \tag{B. 13}$$

where $N_{px}(t) \equiv \frac{nn_{gr}}{\Delta\Omega_0\tau_c 8\pi\hbar\omega}\left|F_\omega(t)\right|^2$ is the density of external signal photons and $k \equiv 2\pi\kappa^2\tau_c$,. The terms describing spontaneous emission, the free carrier absorption, and two-photon absorption (which are small compared to interband absorption) are introduced phenomenologically.

APPENDIX C. SPONTANEOUS RECOMBINATION RATE

The functional dependence of the spontaneous radiative recombination rate on the density of carriers depends on the degree of statistical degeneracy of the carriers. We discuss this problem below.

The spontaneous radiative recombination rate can be presented in general form as a function of carrier density and temperature:

$$\boldsymbol{R}_{sp}(\boldsymbol{N}_c,\boldsymbol{T}_c)=\frac{4}{(2\pi\hbar)^6}\iint \boldsymbol{w}_{cv}(\boldsymbol{p},\boldsymbol{p}')\boldsymbol{f}_e^c(\boldsymbol{p})\boldsymbol{f}_h^v(\boldsymbol{p}')\boldsymbol{dpdp}', \quad \text{(C. 1)}$$

where $w_{cv}(p,p')$ is the probability of interband recombination of carriers with momenta p and p', and f_e^c and f_h^v are distribution functions of carriers in the valence and conduction bands correspondingly. The factor 4 appears due to spin degeneracy of electrons and holes.

The integral (C.1) can be simplified by taking into account the following circumstances: i) in an isotropic material distribution functions depend only on energy, ii) in direct gap semiconductors optical transitions preserve the momentum of carriers.

This means that $w_{cv}(p,p')\cong w(\varepsilon)\delta(p-p')$ and (C.1) can be rewritten in the following form:

$$\boldsymbol{R}_{sp}(\boldsymbol{N}_c,\boldsymbol{T}_c)=\frac{4\boldsymbol{C}}{(2\pi\hbar)^3}\int \boldsymbol{w}(\varepsilon)\boldsymbol{f}_c\left(\frac{\boldsymbol{m}}{\boldsymbol{m}_e}\varepsilon\right)\boldsymbol{f}_v\left(\frac{\boldsymbol{m}}{\boldsymbol{m}_h}\varepsilon\right)\sqrt{\varepsilon}\boldsymbol{d}\varepsilon, \quad \text{(C. 2)}$$

where $m_{e,h}$ is electron (hole) effective mass in the conduction (valence) band,

$$\varepsilon = \frac{p^2}{2m}, \tag{C. 3}$$

$$\frac{1}{m} = \frac{1}{m_e} + \frac{1}{m_h}, \tag{C. 4}$$

$$C = \frac{4\pi\sqrt{2}m^{3/2}}{(2\pi\hbar)^3}, \tag{C. 5}$$

and

$$f_{c,v}(\varepsilon) = \left[\exp\left(\frac{\varepsilon - \mu_{e,h}}{k_B T_{e,h}}\right) + 1\right]^{-1} \tag{C. 6}$$

Here we use the parabolic band approximation.

The probability of transition $w(\varepsilon)$ depends on the carrier energy $\varepsilon_g + \varepsilon$. As far as ε is determined by the carrier temperature, one can take $\varepsilon_g >> \varepsilon$ and neglect the energy dependence of the probability of recombination. Therefore one can replace $w(\varepsilon)$ by the constant w_0.

The density of the carriers is defined by

$$N_{e,h} = 2C\left(\frac{m_{e,h}}{m}\right)^{3/2} \int_0^\infty \left[\exp\left(\frac{\varepsilon - \mu_{e,h}}{k_B T_{e,h}}\right) + 1\right]^{-1} \sqrt{\varepsilon} d\varepsilon. \tag{C. 7}$$

If the ensemble of carriers is far from degeneracy,

$$\exp\left(\frac{\varepsilon - \mu_{e,h}}{k_B T_{e,h}}\right) >> 1$$

and in this case we obtain

$$N_{e,h} = C\sqrt{\pi}\left(\frac{m_{e,h}}{m}k_B T_{e,h}\right)^{3/2} \exp\left(\frac{\mu_{e,h}}{k_B T_{e,h}}\right). \tag{C. 8}$$

Assuming common temperature for electrons and holes $T_e = T_h \equiv T_c$ we obtain

$$R_{sp}(N_c, T_c) = N_e N_h \int R_{sp}(\varepsilon, T_c) d\varepsilon = N_e N_h R_{sp}(T_c), \tag{C. 9}$$

where

$$R_{sp}(T_c) = \frac{2}{\sqrt{\pi}} \frac{1}{(2\pi\hbar)^3} \frac{1}{C}\left(\frac{m^2}{m_e m_h}\right)^{3/2} \frac{w_0}{(k_B T_c)^{3/2}}. \tag{C. 10}$$

Under the condition of electro-neutrality, $N_e = N_h \equiv N_c$, the expression (C.9) leads to a quadratic dependence of the spontaneous recombination rate on carrier density.

Consider the case of degeneracy when the distribution function is equal to 1 for $\varepsilon \leq \mu_{e,h}$ and zero for $\varepsilon \geq \mu_{e,h}$. Calculation of the integrals (C.2) and (C.7) gives

$$N_{e,h} = \frac{4}{3}\left(\frac{m_{e,h}}{m}\mu_{e,h}\right)^{3/2} C, \tag{C. 11}$$

$$R_{sp}(N_c, T_c) = 2\frac{w_0}{(2\pi\hbar)^3} \frac{4}{3}\left(\frac{m_{e,h}}{m}\mu_{e,h}\right)^{3/2} C = 2\frac{w_0}{(2\pi\hbar)^3} N_c \tag{C. 12}$$

Thus in this case the spontaneous recombination rate is proportional to the density of carriers; therefore one can introduce the spontaneous recombination time

$$\frac{1}{\tau_s} = 2\frac{w_0}{(2\pi\hbar)^3}. \tag{C. 13}$$

Apparently, the spontaneous recombination rate cannot be described by a simple analytic formula in any range of densities and temperatures. Therefore we propose an approximation of the integral (C.9) in the form

$$\boldsymbol{R}_{sp}(\boldsymbol{N}_c, \boldsymbol{T}_c) = \boldsymbol{R}_{sp}(\boldsymbol{T}_c)\frac{\boldsymbol{N}_c^2}{1+\boldsymbol{N}_c/\boldsymbol{N}_{c0}}. \tag{C. 14}$$

The ratio N_c/N_{c0} is known as *the degeneracy parameter* [3]. At $N_c << N_{c0}$ the formula (C.14) is identical to the case of the Boltzmann statistics of the carriers. Now we require that (C.14) must be identical to (C.12) in the other limiting case when $N_c >> N_{c0}$. From this condition we obtain

$$N_{c0} = 2\left[\left(m_e + m_h\right)\frac{k_B T}{2\pi\hbar^2}\right]^{3/2}. \tag{C. 15}$$

This is an expression for the *degeneracy concentration* of the Fermi ensemble of particles with mass $M = m_e + m_h$ [4]. The most typical situation in semiconductors is $m_e << m_h$, and N_{c0} is practically equal to the degeneracy concentration of holes and significantly higher than that of the electrons in the conduction band. In a semiconductor laser we deal with a statistically degenerate ensemble of carriers and, therefore, assumption of linear dependence on carrier density for spontaneous radiative recombination is justified.

[3] B.R. Nag, *Theory of Electrical Transport in Semiconductors*, (Pergamon Press, 1972).
[4] R. Kubo, *Statistical Mechanics*, (North-Holland, Amsterdam, 1971).

APPENDIX D. CALCULATION OF INTEGRALS WITH THE EXACT FERMI FUNCTION

We need to calculate an integral of the following form

$$\boldsymbol{I} = \int_{0}^{\infty} \rho(\varepsilon) \boldsymbol{f}(\varepsilon) d\varepsilon \,, \tag{D. 1}$$

where $\rho(\varepsilon)$ is some differentiable function and

$$\boldsymbol{f}(\varepsilon, \mu, \boldsymbol{T}) = \left[1 + \exp\left(\frac{\varepsilon - \mu}{\boldsymbol{k}_B \boldsymbol{T}} \right) \right]^{-1} \tag{D. 2}$$

Introducing new notations $\vartheta \equiv \boldsymbol{k}_B \boldsymbol{T}$ and $\vartheta \boldsymbol{x} \equiv \varepsilon - \mu$ we obtain

$$\boldsymbol{I} = \int_{-\mu/\vartheta}^{\infty} \frac{\rho(\mu + \vartheta \boldsymbol{x}) \vartheta \boldsymbol{dx}}{1 + \boldsymbol{e}^{\boldsymbol{x}}} = \vartheta \int_{0}^{\mu/\vartheta} \frac{\rho(\mu - \vartheta \boldsymbol{x}) \boldsymbol{dx}}{1 + \boldsymbol{e}^{-\boldsymbol{x}}} + \vartheta \int_{0}^{\infty} \frac{\rho(\mu + \vartheta \boldsymbol{x}) \boldsymbol{dx}}{1 + \boldsymbol{e}^{\boldsymbol{x}}} =$$

$$= \vartheta \int_{0}^{\mu/\vartheta} \rho(\mu - \vartheta \boldsymbol{x}) \boldsymbol{dx} - \vartheta \int_{0}^{\mu/\vartheta} \frac{\rho(\mu - \vartheta \boldsymbol{x}) \boldsymbol{dx}}{1 + \boldsymbol{e}^{\boldsymbol{x}}} + \vartheta \int_{0}^{\infty} \frac{\rho(\mu + \vartheta \boldsymbol{x}) \boldsymbol{dx}}{1 + \boldsymbol{e}^{\boldsymbol{x}}} \,, \tag{D. 3}$$

where we replaced $\left(1 + \boldsymbol{e}^{-\boldsymbol{x}}\right)^{-1}$ by $1 - \left(1 + \boldsymbol{e}^{\boldsymbol{x}}\right)^{-1}$. Now introducing $\boldsymbol{y} \equiv \mu - \vartheta \boldsymbol{x}$ we obtain

$$\boldsymbol{I} = -\int_{\mu}^{0} \rho(\boldsymbol{y}) \boldsymbol{dy} + \vartheta \int_{\mu/\vartheta}^{\infty} \frac{\rho(\mu - \vartheta \boldsymbol{x}) \boldsymbol{dx}}{1 + \boldsymbol{e}^{\boldsymbol{x}}} + \vartheta \int_{0}^{\infty} \frac{\rho(\mu + \vartheta \boldsymbol{x}) - \rho(\mu - \vartheta \boldsymbol{x}) \boldsymbol{dx}}{1 + \boldsymbol{e}^{\boldsymbol{x}}} \,, \tag{D. 4}$$

or taking into account that $\boldsymbol{dy} = \boldsymbol{d}\varepsilon$ we write

$$\boldsymbol{I} = \int_{0}^{\mu} \rho(\varepsilon) \boldsymbol{d}\varepsilon + \vartheta \int_{\mu/\vartheta}^{\infty} \frac{\rho(\mu - \vartheta \boldsymbol{x}) \boldsymbol{dx}}{1 + \boldsymbol{e}^{\boldsymbol{x}}} + \vartheta \int_{0}^{\infty} \frac{\rho(\mu + \vartheta \boldsymbol{x}) - \rho(\mu - \vartheta \boldsymbol{x}) \boldsymbol{dx}}{1 + \boldsymbol{e}^{\boldsymbol{x}}} \,. \tag{D. 5}$$

In the next step we neglect the second term in above expression because its lower limit has very large value $\mu/\vartheta >> 1$ (for moderate temperatures) and the under-integral expression is an exponentially decreasing function.

Using Taylor expansion

$$\rho(\mu + \vartheta x) = \sum_{n=0}^{\infty} \frac{\rho^{(n)}(\mu)}{n!}(\vartheta x)^n .$$

we simplify the numerator of the last term

$$\rho(\mu + \vartheta x) - \rho(\mu - \vartheta x) = \left[\rho(\mu) + \rho'(\mu)\vartheta x + \rho''(\mu)\frac{(\vartheta x)^2}{2!} + \rho'''(\mu)\frac{(\vartheta x)^3}{3!} + \cdots \right] -$$

$$- \left[\rho(\mu) + \rho'(\mu)(-\vartheta x) + \rho''(\mu)\frac{(-\vartheta x)^2}{2!} + \rho'''(\mu)\frac{(-\vartheta x)^3}{3!} + \cdots \right] =$$

$$= 2\rho'(\mu)\vartheta x + 2\rho'''(\mu)\frac{(\vartheta x)^3}{3!} + \cdots .$$

Thus, we obtain

$$\left[\rho(\mu + \vartheta x) - \rho(\mu - \vartheta x)\right] = 2\sum_{n=1}^{\infty} \frac{\rho^{(2n-1)}(\mu)}{(2n-1)!}(\vartheta x)^{2n-1} , \tag{D. 6}$$

and the integral (D.5) becomes

$$I = \int_0^{\mu} \rho(\varepsilon) d\varepsilon + 2\vartheta \sum_{n=1}^{\infty} \frac{\rho^{(2n-1)}(\mu)}{(2n-1)!} \int_0^{\infty} \frac{(\vartheta x)^{2n-1} dx}{1+e^x} =$$

$$= \int_0^{\mu} \rho(\varepsilon) d\varepsilon + 2\sum_{n=1}^{\infty} \frac{\rho^{(2n-1)}(\mu)}{(2n-1)!}(\vartheta)^{2n} J_{2n} , \tag{D. 7}$$

where

$$J_{2n} \equiv \int_0^{\infty} \frac{x^{2n-1} dx}{1+e^x} . \tag{D. 8}$$

For simplicity of formulas we replace $2n$ by α and evaluate this integral in the following way. Using the following relationship (formula 1.112 #1 in Ref.[5])

$$\frac{1}{1+e^{x}} = \frac{e^{-x}}{1+e^{-x}} = e^{-x}\sum_{j=0}^{\infty}(-1)^{j}e^{jx}\ , \qquad \text{(D. 9)}$$

we can write

$$J_{\alpha} = \int_{0}^{\infty} x^{\alpha-1}e^{-x}\sum_{j=0}^{\infty}(-1)^{j}e^{jx}dx = \sum_{j=0}^{\infty}(-1)^{j}\int_{0}^{\infty}x^{\alpha-1}e^{-x(j+1)}dx =$$

$$= \sum_{j=0}^{\infty}(-1)^{j}\int_{0}^{\infty}\frac{\left[x(j+1)\right]^{\alpha-1}e^{-x(j+1)}}{(j+1)^{\alpha-1}}dx = \sum_{j=0}^{\infty}\frac{(-1)^{j}}{(j+1)^{\alpha}}\int_{0}^{\infty}\left\{\left[x(j+1)\right]^{\alpha-1}e^{-x(j+1)}\right\}d\left[x(j+1)\right],$$

and since the last integral by definition is Euler's Gamma function we obtain

$$J_{\alpha} = \sum_{j=0}^{\infty}\frac{(-1)^{j}}{(j+1)^{\alpha}}\Gamma(\alpha) \qquad \text{(D. 10)}$$

This expression can be simplified further using the following relation (0.233 #4 in Ref.[5]

$$\sum_{j=1}^{\infty}\frac{(-1)^{j+1}}{j^{\alpha}} = \left(1-2^{1-\alpha}\right)\zeta(\alpha) \qquad \text{(D. 11)}$$

where $\zeta(\alpha)$ is Riemann's zeta function.

Thus,

$$J_{\alpha} = \left(1-2^{1-\alpha}\right)\Gamma(\alpha)\zeta(\alpha) \qquad \text{(D. 12)}$$

In particular case of an even integer number: $\alpha = 2n$ (n = 1,2,3,…)

$$J_{2n} = \left(1-2^{1-2n}\right)\Gamma(2n)\zeta(2n) = \frac{2^{2n-1}-1}{2^{2n-1}}\Gamma(2n)\zeta(2n) \qquad \text{(D. 13)}$$

Next we use expressions (Ref.[5] formula 8.339 #1)

---

[5] I.S. Gradshtetyn, I.M. Ryzhik, Table of integrals, series, and products, (Academic Press, Orlando, 1980).

$$\Gamma(2n) = (2n-1)! \tag{D. 14}$$

and (Ref.[5] formula 9.542 #1)

$$\zeta(2n) = \frac{2^{2n-1}}{(2n)!}\pi^{2n}\left|B_{2n}\right| \tag{D. 15}$$

where B_{2n} are Bernoulli numbers. Below we list low-index Bernoulli numbers (Ref.[5] formula 9.71).

$$B_0 = 1, \quad B_1 = -\frac{1}{2}, \quad B_2 = \frac{1}{6}, \quad B_4 = -\frac{1}{30}, \quad B_6 = \frac{1}{42}, \quad B_8 = -\frac{1}{30}.$$

Finally we obtain

$$J_{2n} = \frac{2^{2n-1}-1}{2n}\pi^{2n}\left|B_{2n}\right|. \tag{D. 16}$$

In particular

$$J_2 = \frac{\pi^2}{12}, \qquad J_4 = \frac{7\pi^4}{120}, \qquad J_6 = \frac{31\pi^6}{252}.$$

Using these results we obtain

$$I = \int_0^{\mu}\rho(\varepsilon)d\varepsilon + \frac{\pi^2}{6}\vartheta^2\rho'(\mu) + \frac{7\pi^4}{360}\vartheta^4\rho'''(\mu) + \cdots. \tag{D. 17}$$

APPENDIX E. EXPRESSIONS FOR CARRIER DENSITY AND CARRIER ENERGY DENSITY

Expressions for parabolic band edge model

The density of state has a form

$$\rho(\varepsilon) = \frac{1}{2\pi}\left(\frac{2m}{\hbar}\right)^{3/2}\sqrt{\varepsilon} \equiv \rho_0\sqrt{\varepsilon}\,. \qquad \text{(E. 1)}$$

We use Eq. (D.17) with the chemical potential measured from the band edge because in undoped material there are no available states in the gap.

$$\int_0^{\mu}\rho(\varepsilon)d\varepsilon = \rho_0\frac{2}{3}\mu^{3/2}, \quad \rho'(\mu) = \rho_0\frac{1}{2\mu^{1/2}}, \qquad \rho'''(\mu) = \rho_0\frac{3}{8\mu^{5/2}}\,.$$

Using the above expressions we obtain

$$N_c(\mu,\vartheta) = \frac{2}{3}\rho_0\mu^{3/2}\left[1+\frac{1}{2}\left(\frac{\pi}{2}\frac{\vartheta}{\mu}\right)^2+\frac{7}{40}\left(\frac{\pi}{2}\frac{\vartheta}{\mu}\right)^4+\cdots\right]. \qquad \text{(E. 2)}$$

Here we use the notations introduced in Appendix D (p. 162). The expression for carrier energy density is obtained similarly using $\rho_0\varepsilon\sqrt{\varepsilon}$ instead of $\rho_0\sqrt{\varepsilon}$. The result is

$$U(\mu,\vartheta) = \frac{2}{5}\rho_0\mu^{5/2}\left[1+\frac{5}{2}\left(\frac{\pi}{2}\frac{\vartheta}{\mu}\right)^2-\frac{7}{24}\left(\frac{\pi}{2}\frac{\vartheta}{\mu}\right)^4+\cdots\right]. \qquad \text{(E. 3)}$$

In the calculations above we imply that the bottom of the band corresponds to the zero level of energy. If, say, the top of the valence band is chosen as a zero level then μ must be replaced by $\mu - \varepsilon_g$ and in the expression for energy density an additional term

$N_c\varepsilon_g$ that is not associated with the energy of thermal motion (corresponds to self-energy) should be added.

In low temperature limit an approximate expression that links U and N_c is:

$$U \approx \frac{3}{5}N_c\mu\left[1+2\left(\frac{\pi}{2}\frac{\vartheta}{\mu}\right)^2-\frac{5}{4}\left(\frac{\pi}{2}\frac{\vartheta}{\mu}\right)^4\right]. \tag{E. 4}$$

Expressions for exponential band tail model

The density of states has a form

$$\rho(\varepsilon)=\rho_t\exp(\varepsilon/\varepsilon_t). \tag{E. 5}$$

In this case it is convenient to measure the chemical potential from the middle of the band gap because of tail states in the gap.

$$\int_0^\mu \rho(\varepsilon)d\varepsilon=\rho_t\varepsilon_t\exp(\mu/\varepsilon_t),\quad \rho'(\mu)=\rho_t\frac{1}{\varepsilon_t}\exp(\mu/\varepsilon_t),\qquad \rho'''(\mu)=\rho_t\frac{1}{\varepsilon_t^3}\exp(\mu/\varepsilon_t).$$

Using above expressions we obtain

$$N(\mu,\vartheta)=\rho_t\varepsilon_t\exp(\mu/\varepsilon_t)\left[1+\frac{2}{3}\left(\frac{\pi}{2}\frac{\vartheta}{\varepsilon_t}\right)^2+\frac{14}{45}\left(\frac{\pi}{2}\frac{\vartheta}{\varepsilon_t}\right)^4+...\right]. \tag{E. 6}$$

The expression for carrier energy density is obtained similarly using the expression $\varepsilon\rho_t\exp(\varepsilon/\varepsilon_t)$ instead of $\rho_t\exp(\varepsilon/\varepsilon_t)$.

$$\int_0^\mu \varepsilon\rho_t\exp(\varepsilon/\varepsilon_t)d\varepsilon=\rho_t\varepsilon_t^2\int_0^{\mu/\varepsilon_t}x\exp(x)dx=\rho_t\varepsilon_t\exp(\mu/\varepsilon_t)\left[(\mu-\varepsilon_t)+\varepsilon_t\exp(-\mu/\varepsilon_t)\right].$$

The last term can be neglected because $\varepsilon_t \ll \mu$.

$$\rho'(\mu)=\rho_t\frac{\mu}{\varepsilon_t}\exp(\mu/\varepsilon_t)+\rho_t\exp(\mu/\varepsilon_t)=\rho_t\varepsilon_t\exp(\mu/\varepsilon_t)\left(\frac{\mu+\varepsilon_t}{\varepsilon_t^2}\right),$$

$$\rho'''(\mu) = \rho_t \frac{\mu}{\varepsilon_t^3} \exp(\mu/\varepsilon_t) + 3\rho_t \frac{1}{\varepsilon_t^2} \exp(\mu/\varepsilon_t) = \rho_t \varepsilon_t \exp(\mu/\varepsilon_t) \left(\frac{\mu + 3\varepsilon_t}{\varepsilon_t^4} \right).$$

The result is

$$\boldsymbol{U}(\mu,\vartheta) = \rho_t \varepsilon_t \exp(\mu/\varepsilon_t) \left[\mu \left(1 + \frac{2}{3}\left(\frac{\pi}{2}\frac{\vartheta}{\varepsilon_t}\right)^2 + \frac{14}{45}\left(\frac{\pi}{2}\frac{\vartheta}{\varepsilon_t}\right)^4 + \cdots \right) + \right.$$

$$\left. + \varepsilon_t \left(1 + \frac{2}{3}\left(\frac{\pi}{2}\frac{\vartheta}{\varepsilon_t}\right)^2 + \frac{14}{45}\left(\frac{\pi}{2}\frac{\vartheta}{\varepsilon_t}\right)^4 + \ldots \right) - 2\varepsilon_t + 2\varepsilon_t \frac{14}{45}\left(\frac{\pi}{2}\frac{\vartheta}{\varepsilon_t}\right)^4 + \cdots \right]$$

or

$$\boldsymbol{U}(\mu,\vartheta) = \boldsymbol{N}(\mu,\vartheta) \left[\mu + \varepsilon_t - 2\varepsilon_t \frac{1 - \frac{14}{45}\left(\frac{\pi}{2}\frac{\vartheta}{\varepsilon_t}\right)^4 - \cdots}{\left(1 + \frac{2}{3}\left(\frac{\pi}{2}\frac{\vartheta}{\varepsilon_t}\right)^2 + \frac{14}{45}\left(\frac{\pi}{2}\frac{\vartheta}{\varepsilon_t}\right)^4 + \cdots \right)} \right]. \tag{E. 7}$$

For low temperatures this expression becomes

$$\boldsymbol{U}(\mu,\vartheta) \approx \boldsymbol{N}(\mu,\vartheta) \left[\mu - \varepsilon_t + \frac{4}{3}\varepsilon_t \left(\frac{\pi}{2}\frac{\vartheta}{\varepsilon_t}\right)^2 \right] \tag{E. 8}$$

APPENDIX F. CALCULATION OF INTEGRALS WITH AN APPROXIMATE FERMI FUNCTION

We need to calculate an integral of form similar to (D.1) but using an approximate Fermi distribution function given by Eq.(2.49) (p. 40). We carry out calculations for parabolic band-edge and exponential band-tail approximations separately.

Expressions for parabolic band-edge model

For undoped material we have

$$\rho(\varepsilon) = \frac{1}{2\pi}\left(\frac{2m}{\hbar}\right)^{3/2}\sqrt{\varepsilon} \equiv \rho_0\sqrt{\varepsilon}\,. \tag{F. 1}$$

With the chemical potential measured from the band edge we have

$$N_c = \int_0^{\mu}\rho_0\sqrt{\varepsilon}\left[1-\frac{1}{2}\exp\left[\frac{\varepsilon-\mu}{\vartheta}\right]\right]d\varepsilon + \int_{\mu}^{\infty}\rho_0\sqrt{\varepsilon}\cdot\frac{1}{2}\exp\left[\frac{\mu-\varepsilon}{\vartheta}\right]d\varepsilon =$$

$$= \rho_0\left\{\int_0^{\mu}\sqrt{\varepsilon}d\varepsilon - \frac{1}{2}\int_0^{\mu}\sqrt{\varepsilon}\exp\left[\frac{\varepsilon-\mu}{\vartheta}\right]d\varepsilon + \frac{1}{2}\int_{\mu}^{\infty}\sqrt{\varepsilon}\cdot\exp\left[\frac{\mu-\varepsilon}{\vartheta}\right]d\varepsilon\right\}. \tag{F. 2}$$

The first integral is straightforward:

$$\int_0^{\mu}\sqrt{\varepsilon}d\varepsilon = \frac{2}{3}\mu^{3/2}. \tag{F. 3}$$

The second integral and third integrals are expressed through the incomplete gamma functions (Ref.[5] formula 8.35):

$$\int_0^{\mu}\sqrt{\varepsilon}\exp\left(\frac{\varepsilon-\mu}{\vartheta}\right)d\varepsilon=\int_0^{\mu}\sqrt{\mu-x}\exp\left(-\frac{x}{\vartheta}\right)dx=\vartheta^{3/2}\exp\left(-\frac{\mu}{\vartheta}\right)\int_0^{\mu/\vartheta}\sqrt{t}\exp(-t)dt=$$

$$=\vartheta^{3/2}\exp\left(-\frac{\mu}{\vartheta}\right)\gamma\left(\frac{3}{2},\frac{\mu}{\vartheta}\right)=\vartheta^{3/2}\exp\left(-\frac{\mu}{\vartheta}\right)\left[\Gamma\left(\frac{3}{2}\right)-\Gamma\left(\frac{3}{2},\frac{\mu}{\vartheta}\right)\right], \qquad \text{(F. 4)}$$

where we used intermediate notations $x\equiv\mu-\varepsilon,\quad t\equiv x/\theta$.

$$\int_{\mu}^{\infty}\sqrt{\varepsilon}\cdot\exp\left[-\frac{\varepsilon}{\vartheta}\right]d\varepsilon=\vartheta^{3/2}\Gamma\left(\frac{3}{2},\frac{\mu}{\vartheta}\right). \qquad \text{(F. 5)}$$

Using these calculations we can write

$$N_c=\rho_0\left\{\frac{2}{3}\mu^{3/2}-\frac{1}{2}\vartheta^{3/2}\exp\left(-\frac{\mu}{\vartheta}\right)\left[\Gamma\left(\frac{3}{2}\right)-\Gamma\left(\frac{3}{2},\frac{\mu}{\vartheta}\right)\right]+\frac{1}{2}\vartheta^{3/2}\exp\left(\frac{\mu}{\vartheta}\right)\Gamma\left(\frac{3}{2},\frac{\mu}{\vartheta}\right)\right\}=$$

$$=\frac{2}{3}\rho_0\mu^{3/2}\left\{1+\frac{3}{2}\left(\frac{1}{z}\right)^{3/2}\left[\Gamma\left(\frac{3}{2},z\right)\cosh(z)-\frac{\sqrt{\pi}}{2}\exp(-z)\right]\right\}. \qquad \text{(F. 6)}$$

The incomplete gamma function $\Gamma(\alpha, x)$ has an asymptotic representation for large values of x (Ref.[5] formula 8.357):

$$\Gamma(\alpha,x)=x^{\alpha-1}\exp(-x)\left[\sum_{m=0}^{M-1}\frac{(-1)^m\Gamma(1-\alpha+m)}{x^m\Gamma(1-\alpha)}+O\left(|x|^{-M}\right)\right]. \qquad \text{(F. 7)}$$

In particular

$$\Gamma\left(3/2,z\right)=z^{1/2}\exp(-z)\left[1+\frac{1}{2z}-\frac{1}{4z^2}+\frac{3}{4z^3}+O\left(|z|^{-4}\right)\right]. \qquad \text{(F. 8)}$$

For large z we can replace cosh(z) by exp(z)/2 and, keeping only the lower order terms in above approximation, obtain

$$N_c=\frac{2}{3}\rho_0\mu^{3/2}\left\{1+\frac{3}{4}\left(\frac{1}{z}+\frac{1}{2z^2}-\frac{1}{4z^3}+\frac{3}{4z^4}\right)\right\}. \qquad \text{(F. 9)}$$

Calculations for the energy density are similar:

$$U = \int_0^{\mu} \rho_0 \varepsilon\sqrt{\varepsilon}\left[1 - \frac{1}{2}\exp\left[\frac{\varepsilon - \mu}{\vartheta}\right]\right]d\varepsilon + \int_{\mu}^{\infty} \rho_0 \varepsilon\sqrt{\varepsilon} \cdot \frac{1}{2}\exp\left[\frac{\mu - \varepsilon}{\vartheta}\right]d\varepsilon =$$

$$= \rho_0 \left\{\int_0^{\mu} \varepsilon\sqrt{\varepsilon}d\varepsilon - \frac{1}{2}\int_0^{\mu} \varepsilon\sqrt{\varepsilon}\exp\left[\frac{\varepsilon - \mu}{\vartheta}\right]d\varepsilon + \frac{1}{2}\int_{\mu}^{\infty} \varepsilon\sqrt{\varepsilon} \cdot \exp\left[\frac{\mu - \varepsilon}{\vartheta}\right]d\varepsilon\right\}. \tag{F. 10}$$

The first integral is straightforward:

$$\int_0^{\mu} \varepsilon\sqrt{\varepsilon}d\varepsilon = \frac{2}{5}\mu^{5/2}. \tag{F. 11}$$

$$\int_0^{\mu} \varepsilon\sqrt{\varepsilon}\exp\left(\frac{\varepsilon - \mu}{\vartheta}\right)d\varepsilon = \int_0^{\mu} (\mu - x)^{3/2}\exp\left(-\frac{x}{\vartheta}\right)dx = \vartheta^{5/2}\exp\left(-\frac{\mu}{\vartheta}\right)\int_0^{\mu/\vartheta} t^{3/2}\exp(-t)dt =$$

$$= \vartheta^{5/2}\exp\left(-\frac{\mu}{\vartheta}\right)\gamma\left(\frac{5}{2}, \frac{\mu}{\vartheta}\right) = \vartheta^{5/2}\exp\left(-\frac{\mu}{\vartheta}\right)\left[\Gamma\left(\frac{5}{2}\right) - \Gamma\left(\frac{5}{2}, \frac{\mu}{\vartheta}\right)\right], \tag{F. 12}$$

and

$$\int_{\mu}^{\infty} \varepsilon\sqrt{\varepsilon} \cdot \exp\left[-\frac{\varepsilon}{\vartheta}\right]d\varepsilon = \vartheta^{5/2}\Gamma\left(\frac{5}{2}, \frac{\mu}{\vartheta}\right). \tag{F. 13}$$

Thus

$$U = \rho_0 \left\{\frac{2}{5}\mu^{5/2} - \frac{1}{2}\vartheta^{5/2}\exp\left(-\frac{\mu}{\vartheta}\right)\left[\Gamma\left(\frac{5}{2}\right) - \Gamma\left(\frac{5}{2}, \frac{\mu}{\vartheta}\right)\right] + \frac{1}{2}\vartheta^{3/2}\exp\left(\frac{\mu}{\vartheta}\right)\Gamma\left(\frac{5}{2}, \frac{\mu}{\vartheta}\right)\right\} =$$

$$= \frac{2}{5}\rho_0\mu^{5/2}\left\{1 + \frac{5}{2}\left(\frac{1}{z}\right)^{5/2}\left[\Gamma\left(\frac{5}{2}, z\right)\cosh(z) - \frac{3\sqrt{\pi}}{4}\exp(-z)\right]\right\}. \tag{F. 14}$$

Using the following approximation,

$$\Gamma\left(5/2, z\right) = z^{3/2}\exp(-z)\left[1 - \frac{3}{z} + \frac{3}{2z^2} - \frac{3}{4z^3} + O\left(|z|^{-4}\right)\right], \tag{F. 15}$$

and for large z replacing $\cosh(z)$ by $\exp(z)/2$ we obtain

$$U = \frac{2}{5}\rho_0\mu^{5/2}\left\{1+\frac{5}{4}\left(\frac{1}{z}-\frac{3}{z^2}+\frac{3}{2z^3}+\frac{3}{4z^4}\right)\right\}. \tag{F. 16}$$

For low temperature we have an approximate expression,

$$U \approx \frac{3}{5}N\mu\left\{1+\frac{1}{2}\frac{\vartheta}{\mu}-\frac{67}{16}\left(\frac{\vartheta}{\mu}\right)^2\right\}. \tag{F. 17}$$

Expressions for exponential band tail model

Several expressions are used to clarify the sequence of the steps. These expressions appear between the lines during the evaluation of the integrals and show either the new notations that were introduced or approximations based on which some terms were neglected.

The density of states has a form

$$\rho(\varepsilon) = \rho_t \exp(\varepsilon/\varepsilon_t). \tag{F. 18}$$

Using (2.49) and (F.18) in (2.14) we obtain

$$N_c = \int_0^{\mu}\rho_t \exp\left(\frac{\varepsilon}{\varepsilon_t}\right)\left[1-\frac{1}{2}\exp\left[\frac{\varepsilon-\mu}{\vartheta}\right]\right]d\varepsilon + \int_{\mu}^{\infty}\rho_t \exp\left(\frac{\varepsilon}{\varepsilon_t}\right)\cdot\frac{1}{2}\exp\left[\frac{\mu-\varepsilon}{\vartheta}\right]d\varepsilon =$$

$$= \rho_t\left\{\int_0^{\mu}\exp\left(\frac{\varepsilon}{\varepsilon_t}\right)d\varepsilon - \frac{1}{2}\int_0^{\mu}\exp\left(\frac{\varepsilon}{\varepsilon_t}+\frac{\varepsilon}{\vartheta}-\frac{\mu}{\vartheta}\right)d\varepsilon + \frac{1}{2}\int_{\mu}^{\infty}\exp\left(\frac{\varepsilon}{\varepsilon_t}-\frac{\varepsilon}{\vartheta}+\frac{\mu}{\vartheta}\right)d\varepsilon\right\} =$$

$$= \rho_t\left\{\varepsilon_t\left[\exp\left(\frac{\mu}{\varepsilon_t}\right)-1\right] - \frac{1}{2}\exp\left(-\frac{\mu}{\vartheta}\right)\int_0^{\mu}\exp(\alpha_+\varepsilon)d\varepsilon + \frac{1}{2}\exp\left(+\frac{\mu}{\vartheta}\right)\int_{\mu}^{\infty}\exp(\alpha_-\varepsilon)d\varepsilon\right\} =$$

$$\alpha_{\pm} \equiv \frac{1}{\varepsilon_t} \pm \frac{1}{\vartheta};\quad \begin{matrix}\alpha_+ > 0\\ \alpha_- < 0\end{matrix}$$

$$=\rho_t\left\{\varepsilon_t\left[\exp\left(\frac{\mu}{\varepsilon_t}\right)-1\right]-\exp\left(-\frac{\mu}{\vartheta}\right)\frac{\left[\exp(\alpha_+\mu)-1\right]}{2\alpha_+}+\exp\left(\frac{\mu}{\vartheta}\right)\frac{\left[\exp(\alpha_-\infty)-\exp(\alpha_-\mu)\right]}{2\alpha_-}\right\}=$$

$$\alpha_-<0\Rightarrow\exp(\alpha_-\infty)\to 0$$

$$=\rho_t\left\{\varepsilon_t\left[\exp\left(\frac{\mu}{\varepsilon_t}\right)-1\right]-\frac{\varepsilon_t\vartheta}{2(\varepsilon_t+\vartheta)}\left[\exp\left(\frac{\mu}{\varepsilon_t}\right)-\exp\left(-\frac{\mu}{\vartheta}\right)\right]-\frac{\varepsilon_t\vartheta}{2(\varepsilon_t-\vartheta)}\exp\left(\frac{\mu}{\varepsilon_t}\right)\right\}\approx$$

$$\mu>>\vartheta\Rightarrow\exp\left(-\frac{\mu}{\vartheta}\right)\to 0$$

$$\approx\rho_t\varepsilon_t\exp\left(\frac{\mu}{\varepsilon_t}\right)\left\{1-\exp\left(-\frac{\mu}{\varepsilon_t}\right)-\frac{\vartheta^2}{\vartheta^2-\varepsilon_t^2}\right\}\approx$$

$$\mu>>\varepsilon_t\Rightarrow\exp\left(-\frac{\mu}{\varepsilon_t}\right)\to 0$$

$$\approx\rho_t\varepsilon_t\exp\left(\frac{\mu}{\varepsilon_t}\right)\left\{1-\frac{\vartheta^2}{\vartheta^2-\varepsilon_t^2}\right\}=\rho_t\varepsilon_t\exp\left(\frac{\mu}{\varepsilon_t}\right)\left\{\frac{\varepsilon_t^2}{\varepsilon_t^2-\vartheta^2}\right\}. \tag{F. 19}$$

The final result for carrier density is

$$\boldsymbol{N}_c=\frac{\rho_t\varepsilon_t}{1-\theta^2}\exp\left(\frac{\mu}{\varepsilon_t}\right). \tag{F. 20}$$

where $\theta\equiv\vartheta/\varepsilon_t$.

For carrier energy density we have

$$\boldsymbol{U}=\int_0^\mu\rho_t\varepsilon\exp\left(\frac{\varepsilon}{\varepsilon_t}\right)\left[1-\frac{1}{2}\exp\left[\frac{\varepsilon-\mu}{\vartheta}\right]\right]\boldsymbol{d}\varepsilon+\int_\mu^\infty\rho_0\varepsilon\exp\left(\frac{\varepsilon}{\varepsilon_t}\right)\cdot\frac{1}{2}\exp\left[\frac{\mu-\varepsilon}{\vartheta}\right]\boldsymbol{d}\varepsilon=$$

$$=\rho_t\left\{\int_0^\mu\varepsilon\exp\left(\frac{\varepsilon}{\varepsilon_t}\right)\boldsymbol{d}\varepsilon-\frac{1}{2}\int_0^\mu\varepsilon\exp\left(\frac{\varepsilon}{\varepsilon_t}+\frac{\varepsilon}{\vartheta}-\frac{\mu}{\vartheta}\right)\boldsymbol{d}\varepsilon+\frac{1}{2}\int_\mu^\infty\varepsilon\exp\left(\frac{\varepsilon}{\varepsilon_t}-\frac{\varepsilon}{\vartheta}+\frac{\mu}{\vartheta}\right)\boldsymbol{d}\varepsilon\right\}=$$

$$=\rho_t\left\{\int_0^\mu\varepsilon\exp\left(\frac{\varepsilon}{\varepsilon_t}\right)\boldsymbol{d}\varepsilon-\frac{1}{2}\exp\left(-\frac{\mu}{\vartheta}\right)\int_0^\mu\varepsilon\exp(\alpha_+\varepsilon)\boldsymbol{d}\varepsilon+\frac{1}{2}\exp\left(\frac{\mu}{\vartheta}\right)\int_\mu^\infty\varepsilon\exp(\alpha_-\varepsilon)\boldsymbol{d}\varepsilon\right\}=$$

$$=\rho_t\left\{\varepsilon_t^2\left(\exp\left(\frac{\varepsilon}{\varepsilon_t}\right)\left(\frac{\varepsilon}{\varepsilon_t}-1\right)\Big|_0^{\mu}\right)-\frac{1}{2\alpha_+^2}\exp\left(-\frac{\mu}{\vartheta}\right)\left(\exp(\alpha_+\varepsilon)(\alpha_+\varepsilon-1)\Big|_0^{\mu}\right)+\right.$$

$$\left.+\frac{1}{2\alpha_-^2}\exp\left(\frac{\mu}{\vartheta}\right)\left(\exp(\alpha_-\varepsilon)(\alpha_-\varepsilon-1)\Big|_{\mu}^{\infty}\right)\right\}=$$

$$=\rho_t\left\{\varepsilon_t^2\left[\exp\left(\frac{\mu}{\varepsilon_t}\right)\left(\frac{\mu}{\varepsilon_t}-1\right)+1\right]-\frac{1}{2\alpha_+^2}\exp\left(-\frac{\mu}{\vartheta}\right)\left[\exp(\alpha_+\mu)(\alpha_+\mu-1)+1\right]+\right.$$

$$\left.+\frac{1}{2\alpha_-^2}\exp\left(\frac{\mu}{\vartheta}\right)\left[\lim_{\varepsilon\to\infty}\left[\exp(\alpha_-\infty)(\alpha_-\infty-1)\right]-\exp(\alpha_-\mu)(\alpha_-\mu-1)\right]\right\}=$$

$$\alpha_-<0\Rightarrow\lim_{\varepsilon\to\infty}\exp(\alpha_-\varepsilon)(\alpha_-\varepsilon-1)=0$$

$$=\rho_t\varepsilon_t\exp\left(\frac{\mu}{\varepsilon_t}\right)\left\{\mu-\varepsilon_t+\varepsilon_t\exp\left(-\frac{\mu}{\varepsilon_t}\right)-\frac{1}{2\varepsilon_t\alpha_+^2}\left[(\alpha_+\mu-1)+\frac{\exp(-\mu/\vartheta)}{\exp(\mu/\varepsilon_t)}\right]+\right.$$

$$\left.+\frac{1}{2\varepsilon_t\alpha_-^2}(1-\alpha_-\mu)\right\}=$$

$$\mu>>\varepsilon_t\Rightarrow\exp\left(-\frac{\mu}{\varepsilon_t}\right)\to 0,\quad \mu>>\vartheta\Rightarrow\exp\left(-\frac{\mu}{\vartheta}\right)\to 0$$

$$=\rho_t\varepsilon_t\exp\left(\frac{\mu}{\varepsilon_t}\right)\left\{\mu-\varepsilon_t-\frac{(\alpha_+\mu-1)}{2\varepsilon_t\alpha_+^2}+\frac{(1-\alpha_-\mu)}{2\varepsilon_t\alpha_-^2}\right\}=$$

$$=\rho_t\varepsilon_t\exp\left(\frac{\mu}{\varepsilon_t}\right)\left\{\mu-\varepsilon_t-\frac{1}{2\varepsilon_t}\left[-\frac{\mu}{\alpha_+}-\frac{\mu}{\alpha_-}+\frac{1}{\alpha_+^2}+\frac{1}{\alpha_-^2}\right]\right\}=$$

$$=\rho_t\varepsilon_t\exp\left(\frac{\mu}{\varepsilon_t}\right)\left\{\mu-\varepsilon_t-\frac{1}{2\varepsilon_t}\left[-\mu\left(\frac{\alpha_++\alpha_-}{\alpha_+\alpha_-}\right)+\frac{\alpha_+^2+\alpha_-^2}{\alpha_+^2\alpha_-^2}\right]\right\}=$$

$$=\rho_t\varepsilon_t\exp\left(\frac{\mu}{\varepsilon_t}\right)\left\{\mu-\varepsilon_t-\frac{1}{2\varepsilon_t}\left[-2\frac{\mu}{\varepsilon_t}\frac{\varepsilon_t^2\vartheta^2}{\vartheta^2-\varepsilon_t^2}+\frac{\varepsilon_t^4\vartheta^4}{\left[\vartheta^2-\varepsilon_t^2\right]^2}\frac{2\left[\vartheta^2+\varepsilon_t^2\right]}{\varepsilon_t^2\vartheta^2}\right]\right\}=$$

$$= \rho_t \varepsilon_t \exp\left(\frac{\mu}{\varepsilon_t}\right)\left\{\mu - \varepsilon_t + \frac{\mu\theta^2}{1-\theta^2} + \frac{1+\theta^2}{\left[1-\theta^2\right]^2}\varepsilon_t\theta^2\right\} =$$

$$= \frac{\rho_t \varepsilon_t}{1-\theta^2} \exp\left(\frac{\mu}{\varepsilon_t}\right)\left\{(\mu - \varepsilon_t)(1-\theta^2) + \mu\theta^2 + \frac{1+\theta^2}{1-\theta^2}\varepsilon_t\theta^2\right\} =$$

$$= N_c \left\{\mu - \varepsilon_t\left[1-\theta^2 - \frac{1+\theta^2}{1-\theta^2}\theta^2\right]\right\}. \qquad \text{(F. 21)}$$

$$U = N_c \left\{\mu - \varepsilon_t \frac{1-3\theta^2}{1-\theta^2}\right\}. \qquad \text{(F. 22)}$$

For $\theta \ll 1$ one can expand Eqs. (F.20) and (F.22) in terms of θ and keep only the lowest order terms:

$$N_c(\mu,\theta) = \rho_t \varepsilon_t (1+\theta^2)\exp\left(\mu / \varepsilon_t\right); \qquad \text{(F. 23)}$$

$$U(\mu,\theta) = N_c\left[\mu - \varepsilon_t + 2\varepsilon_t\theta^2\right]. \qquad \text{(F. 24)}$$

APPENDIX G. CALCULATION OF INTEGRALS FOR PUMPING TERMS WITH A BARRIER

We need to calculate an integral of form (D.1) but with some finite upper limit ε_b. Initially we will assume $\varepsilon_b > \mu$; the other case, $\varepsilon_b < \mu$, is considered afterwards.

Using the method of calculation presented in Appendix D (p. 162) does not lead to analytical results. If we proceed in the same way and use the same notations then case Eq. (D.5) become

$$\boldsymbol{I} = \int_0^{\mu} \rho(\varepsilon) d\varepsilon + \vartheta \int_{\mu/\vartheta}^{\frac{\varepsilon_b-\mu}{\vartheta}} \frac{\rho(\mu - \vartheta x) dx}{1+e^x} + \vartheta \int_0^{\frac{\varepsilon_b-\mu}{\vartheta}} \frac{\rho(\mu+\vartheta x) - \rho(\mu - \vartheta x) dx}{1+e^x}. \qquad \text{(G. 1)}$$

In Appendix E (p. 166) we neglected the second integral because its lower limit has very large value $\mu/\vartheta >> 1$ (for moderate temperatures), the upper limit was infinity and the integrand is an exponentially decreasing function. Here we cannot do that because the second integral is not negligibly small:

$$\vartheta \int_{\mu/\vartheta}^{\frac{\varepsilon_b-\mu}{\vartheta}} \frac{\rho(\mu - \vartheta x) dx}{1+e^x} = -\int_0^{2\mu-\varepsilon_b} \frac{\rho(\varepsilon) d\varepsilon}{1+\exp\left(\frac{\mu-\varepsilon}{\vartheta}\right)} =$$

$$= \int_0^{2\mu-\varepsilon_b} \frac{\rho(\varepsilon) d\varepsilon}{1+\exp\left(\frac{\varepsilon-\mu}{\vartheta}\right)} - \int_0^{2\mu-\varepsilon_b} \rho(\varepsilon) d\varepsilon = \boldsymbol{I}(2\mu - \varepsilon_b) - \int_0^{2\mu-\varepsilon_b} \rho(\varepsilon) d\varepsilon \equiv \tilde{\boldsymbol{I}}(2\mu - \boldsymbol{b}) \qquad \text{(G. 2)}$$

where we used $\left(1+e^{-x}\right)^{-1} = 1 - \left(1+e^{x}\right)^{-1}$. Plugging (G.2) into Eq. (G.1) we obtain

$$\tilde{I}(b) - \tilde{I}(2\mu - b) = \vartheta \int_0^{\frac{b-\mu}{\vartheta}} \frac{\rho(\mu + \vartheta x) - \rho(\mu - \vartheta x) dx}{1 + e^x} \tag{G. 3}$$

which is just an identity. Thus, this method does not work for finite upper limits.

Below we calculate the desired analytical expressions using the method presented in Appendix F (p. 169).

Expressions for parabolic band edge model

For undoped material we have

$$\rho(\varepsilon) = \frac{1}{2\pi}\left(\frac{2m}{\hbar}\right)^{3/2} \sqrt{\varepsilon} \equiv \rho_0 \sqrt{\varepsilon} \; . \tag{G. 4}$$

With the chemical potential measured from the band edge we have

$$I_J = \int_0^{\mu} \rho_0 \sqrt{\varepsilon}\left[1 - \frac{1}{2}\exp\left[\frac{\varepsilon - \mu}{\vartheta}\right]\right] d\varepsilon + \int_{\mu}^{\varepsilon_b} \rho_0 \sqrt{\varepsilon} \cdot \frac{1}{2}\exp\left[\frac{\mu - \varepsilon}{\vartheta}\right] d\varepsilon =$$

$$= \rho_0 \left\{ \int_0^{\mu} \sqrt{\varepsilon} d\varepsilon - \frac{1}{2}\int_0^{\mu} \sqrt{\varepsilon} \exp\left[\frac{\varepsilon - \mu}{\vartheta}\right] d\varepsilon + \frac{1}{2}\int_{\mu}^{\varepsilon_b} \sqrt{\varepsilon} \cdot \exp\left[\frac{\mu - \varepsilon}{\vartheta}\right] d\varepsilon \right\}. \tag{G. 5}$$

The first integral is straightforward

$$\int_0^{\mu} \sqrt{\varepsilon} d\varepsilon = \frac{2}{3}\mu^{3/2}. \tag{G. 6}$$

The remaining integrals can be expressed through the incomplete gamma functions (Ref.[5] Section 8.35). We have already calculated the second integral in Appendix F (Eq. (F.4), p. 170):

$$\frac{1}{2}\int_0^{\mu} \sqrt{\varepsilon} \exp\left(\frac{\varepsilon - \mu}{\vartheta}\right) d\varepsilon = \frac{1}{2}\vartheta^{3/2} \exp\left(-\frac{\mu}{\vartheta}\right)\left[\Gamma\left(\frac{3}{2}\right) - \Gamma\left(\frac{3}{2}, \frac{\mu}{\vartheta}\right)\right], \tag{G. 7}$$

The third integral has a similar structure

$$\frac{1}{2}\int_{\mu}^{\varepsilon_b}\sqrt{\varepsilon}\exp\left(\frac{\mu-\varepsilon}{\vartheta}\right)d\varepsilon = \frac{1}{2}\left[\int_{0}^{\varepsilon_b}\sqrt{\varepsilon}\exp\left(\frac{\mu-\varepsilon}{\vartheta}\right)d\varepsilon - \int_{0}^{\mu}\sqrt{\varepsilon}\exp\left(\frac{\mu-\varepsilon}{\vartheta}\right)d\varepsilon\right] =$$

$$= \frac{1}{2}\vartheta^{3/2}\exp\left(\frac{\mu}{\vartheta}\right)\left[\int_{0}^{\varepsilon_b/\vartheta}\sqrt{t}\exp(-t)dt - \int_{0}^{\mu/\vartheta}\sqrt{t}\exp(-t)dt\right] =$$

$$= \frac{\vartheta^{3/2}}{2}\exp\left(\frac{\mu}{\vartheta}\right)\left[\gamma\left(\frac{3}{2},\frac{\varepsilon_b}{\vartheta}\right) - \gamma\left(\frac{3}{2},\frac{\mu}{\vartheta}\right)\right] =$$

$$= \frac{\vartheta^{3/2}}{2}\exp\left(\frac{\mu}{\vartheta}\right)\left[\Gamma\left(\frac{3}{2},\frac{\mu}{\vartheta}\right) - \Gamma\left(\frac{3}{2},\frac{\varepsilon_b}{\vartheta}\right)\right] \tag{G. 8}$$

where we used relationship between incomplete gamma functions (Ref.[5] formula 8.356 #3). Using these results we can obtain

$$I_J = \rho_0\left\{\frac{2}{3}\mu^{3/2} + \frac{1}{2}\vartheta^{3/2}\left[2\Gamma\left(\frac{3}{2},\frac{\mu}{\vartheta}\right)\cosh\left(\frac{\mu}{\vartheta}\right) - \Gamma\left(\frac{3}{2}\right)\exp\left(-\frac{\mu}{\vartheta}\right)\right] - \right.$$

$$\left. - \frac{1}{2}\vartheta^{3/2}\exp\left(\frac{\mu}{\vartheta}\right)\Gamma\left(\frac{3}{2},\frac{\varepsilon_b}{\vartheta}\right)\right\} =$$

$$= \frac{2}{3}\rho_0\mu^{3/2}\left\{1 + \frac{3}{2}\left(\frac{1}{z}\right)^{3/2}\left[\Gamma\left(\frac{3}{2},z\right)\cosh(z) - \frac{\sqrt{\pi}}{4}e^{-z} - \frac{1}{2}\Gamma\left(\frac{3}{2},\frac{z\varepsilon_b}{\mu}\right)e^{z}\right]\right\}. \tag{G. 9}$$

Comparing this expression with Eq. (F.6) we obtain

$$I_J = N_c - \frac{1}{2}\rho_0\mu^{3/2}\left(\frac{1}{z}\right)^{3/2}\Gamma\left(\frac{3}{2},\frac{z\varepsilon_b}{\mu}\right)e^{z} \tag{G. 10}$$

We can simplify this expression using an asymptotic representation of the incomplete gamma function for large values of z (Eq. (G.7)).

$$\Gamma\left(\frac{3}{2},\frac{z\varepsilon_b}{\mu}\right)=\left(\frac{z\varepsilon_b}{\mu}\right)^{1/2}e^{\left(-\frac{z\varepsilon_b}{\mu}\right)}\left[1+\frac{\mu}{2\varepsilon_b z}-\frac{\mu^2}{4(\varepsilon_b z)^2}+\frac{3\mu^3}{4(\varepsilon_b z)^3}+\boldsymbol{O}\left(\left|z\frac{\varepsilon_b}{\mu}\right|^{-4}\right)\right]. \qquad \text{(G. 11)}$$

Keeping only the lower order terms in above approximation we obtain

$$\boldsymbol{I}_J\approx \boldsymbol{N}_c-\frac{1}{2}\rho_0\mu^{3/2}\left(\frac{\varepsilon_b}{\mu}\right)^{3/2}\exp\left[-z\left(\frac{\varepsilon_b}{\mu}-1\right)\right]\left(\frac{1}{z}\frac{\mu}{\varepsilon_b}+\frac{1}{2z^2}\left(\frac{\mu}{\varepsilon_b}\right)^2-\frac{1}{4z^3}\left(\frac{\mu}{\varepsilon_b}\right)^3\right) \qquad \text{(G. 12)}$$

or using Eq.(F.9)

$$\boldsymbol{I}_J\approx \boldsymbol{N}_c\left\{1-\frac{3}{4}\left(\frac{\varepsilon_b}{\mu}\right)^{3/2}\exp\left[-z\left(\frac{\varepsilon_b}{\mu}-1\right)\right]\frac{\left(\frac{1}{z}\frac{\mu}{\varepsilon_b}+\frac{1}{2z^2}\left(\frac{\mu}{\varepsilon_b}\right)^2-\frac{1}{4z^3}\left(\frac{\mu}{\varepsilon_b}\right)^3\right)}{1+\frac{3}{4}\left(\frac{1}{z}+\frac{1}{2z^2}-\frac{1}{4z^3}\right)}\right\}. \qquad \text{(G. 13)}$$

As expected, in the high barrier limit

$$\lim_{\varepsilon_b\to\infty}\boldsymbol{I}_J(\varepsilon_b)=\boldsymbol{N}_c.$$

For $\varepsilon_b<\mu$ the integral (G.6) become

$$\boldsymbol{I}_J=\int_0^{\varepsilon_b}\rho_0\sqrt{\varepsilon}\left[1-\frac{1}{2}\exp\left[\frac{\varepsilon-\mu}{\vartheta}\right]\right]\boldsymbol{d}\varepsilon=\frac{2}{3}\rho_0\varepsilon_b^{3/2}-\frac{1}{2}\vartheta^{3/2}\exp\left(-\frac{\mu}{\vartheta}\right)\left[\Gamma\left(\frac{3}{2}\right)-\Gamma\left(\frac{3}{2},\frac{\varepsilon_b}{\vartheta}\right)\right]=$$

$$=\frac{2}{3}\rho_0\mu^{3/2}\left\{\left(\frac{\varepsilon_b}{\mu}\right)^{3/2}-\frac{3}{4}\left(\frac{1}{z}\right)^{3/2}e^{-z}\left[\Gamma\left(\frac{3}{2},\frac{z\varepsilon_b}{\mu}\right)-\frac{\sqrt{\pi}}{2}\right]\right\}, \qquad \text{(G. 14)}$$

where we used Eq.(G.7). Using approximation for gamma function (see Eq.(G.11) above) we obtain:

$$\boldsymbol{I}_J=\frac{2}{3}\rho_0\varepsilon_b^{3/2}\left\{1-\frac{3}{4}\exp\left[-z\left(\frac{\varepsilon_b}{\mu}+1\right)\right]\left(\frac{1}{z}\frac{\mu}{\varepsilon_b}+\frac{1}{2z^2}\left(\frac{\mu}{\varepsilon_b}\right)^2-\frac{1}{4z^3}\left(\frac{\mu}{\varepsilon_b}\right)^3\right)\right\} \qquad \text{(G. 15)}$$

or

$$I_J \approx N_c \left(\frac{\varepsilon_b}{\mu}\right)^{3/2} \frac{\left\{1 - \frac{3}{4}\exp\left[-z\left(\frac{\varepsilon_b}{\mu}+1\right)\right]\left(\frac{1}{z}\frac{\mu}{\varepsilon_b} + \frac{1}{2z^2}\left(\frac{\mu}{\varepsilon_b}\right)^2 - \frac{1}{4z^3}\left(\frac{\mu}{\varepsilon_b}\right)^3\right)\right\}}{\left\{1 + \frac{3}{4}\left(\frac{1}{z} + \frac{1}{2z^2} - \frac{1}{4z^3}\right)\right\}}. \qquad \text{(G. 16)}$$

When the barrier is negligible we obtain

$$\lim_{\varepsilon_b \to 0} I(\varepsilon_b) = 0.$$

Because the approximations that we have used during the derivations are the using the low-temperature limit, Eqs.(G.13) and (G.16) converge in the limit of $\varepsilon_b = \mu$ only at zero temperature.

Next we calculate the integral

$$I_Q = \int_0^{\varepsilon_b} \varepsilon \rho(\varepsilon) f(\varepsilon, \mu, T) d\varepsilon . \qquad \text{(G. 17)}$$

The logic of calculations is the same as for (G.5). We start from the case when the barrier is higher than Fermi energy of carriers, $\varepsilon_b > \mu$. The resulting expression is:

$$I_Q = \rho_0 \left\{ \frac{2}{5}\mu^{5/2} + \frac{1}{2}\vartheta^{5/2}\left[2\Gamma\left(\frac{5}{2},\frac{\mu}{\vartheta}\right)\cosh\left(\frac{\mu}{\vartheta}\right) - \Gamma\left(\frac{5}{2}\right)\exp\left(-\frac{\mu}{\vartheta}\right)\right] - \right.$$

$$\left. - \frac{1}{2}\vartheta^{5/2}\exp\left(\frac{\mu}{\vartheta}\right)\Gamma\left(\frac{5}{2},\frac{\varepsilon_b}{\vartheta}\right)\right\} =$$

$$= \frac{2}{5}\rho_0\mu^{5/2}\left\{1 + \frac{5}{2}\left(\frac{1}{z}\right)^{5/2}\left[\Gamma\left(\frac{5}{2},z\right)\cosh(z) - \frac{3\sqrt{\pi}}{4}e^{-z} - \frac{1}{2}\Gamma\left(\frac{5}{2},\frac{z\varepsilon_b}{\mu}\right)e^{z}\right]\right\}. \qquad \text{(G. 18)}$$

Comparing this expression with Eq. (F.11) we obtain

$$I_Q = U - \frac{1}{2}\rho_0\mu^{5/2}\left(\frac{1}{z}\right)^{5/2}\Gamma\left(\frac{5}{2},\frac{z\varepsilon_b}{\mu}\right)e^{z}. \qquad \text{(G. 19)}$$

Using approximation (F.15) for the incomplete gamma function we obtain

$$\boldsymbol{I}_Q \approx \boldsymbol{U} - \frac{1}{2}\rho_0\mu^{5/2}\left(\frac{\varepsilon_b}{\mu}\right)^{5/2}\exp\left[-z\left(\frac{\varepsilon_b}{\mu}-1\right)\right]\left(\frac{1}{z}\frac{\mu}{\varepsilon_b}-\frac{3}{z^2}\left(\frac{\mu}{\varepsilon_b}\right)^2+\frac{3}{2z^3}\left(\frac{\mu}{\varepsilon_b}\right)^3\right), \quad \text{(G. 20)}$$

or, using Eq.(F.16),

$$\boldsymbol{I}_Q \approx \boldsymbol{U}\left\{1-\frac{\frac{5}{4}\left(\frac{\varepsilon_b}{\mu}\right)^{5/2}\exp\left[-z\left(\frac{\varepsilon_b}{\mu}-1\right)\right]\left(\frac{1}{z}\frac{\mu}{\varepsilon_b}-\frac{3}{z^2}\left(\frac{\mu}{\varepsilon_b}\right)^2+\frac{3}{2z^3}\left(\frac{\mu}{\varepsilon_b}\right)^3\right)}{1+\frac{5}{4}\left(\frac{1}{z}-\frac{3}{z^2}+\frac{3}{2z^3}+\frac{3}{4z^4}\right)}\right\}. \quad \text{(G. 21)}$$

As it should be,

$$\lim_{\varepsilon_b\to\infty}\boldsymbol{I}_Q(\varepsilon_b)=\boldsymbol{U}.$$

For $\varepsilon_b < \mu$ the integral (G.17) become

$$\boldsymbol{I}_Q = \int_0^{\varepsilon_b}\rho_0\varepsilon\sqrt{\varepsilon}\left[1-\frac{1}{2}\exp\left[\frac{\varepsilon-\mu}{\vartheta}\right]\right]d\varepsilon = \frac{2}{5}\rho_0\varepsilon_b^{5/2}-\frac{1}{2}\vartheta^{5/2}\exp\left(-\frac{\mu}{\vartheta}\right)\left[\Gamma\left(\frac{5}{2}\right)-\Gamma\left(\frac{5}{2},\frac{\varepsilon_b}{\vartheta}\right)\right]=$$

$$=\frac{2}{5}\rho_0\mu^{5/2}\left\{\left(\frac{\varepsilon_b}{\mu}\right)^{5/2}-\frac{5}{4}\left(\frac{1}{z}\right)^{5/2}e^{-z}\left[\Gamma\left(\frac{5}{2},\frac{z\varepsilon_b}{\mu}\right)-\frac{3\sqrt{\pi}}{2}\right]\right\}. \quad \text{(G. 22)}$$

Using approximation (F.15) for the incomplete gamma function we obtain

$$\boldsymbol{I}_Q \approx \frac{2}{5}\rho_0\mu^{5/2}\left(\frac{\varepsilon_b}{\mu}\right)^{5/2}\left\{1-\frac{5}{4}\exp\left[-z\left(\frac{\varepsilon_b}{\mu}+1\right)\right]\left(\frac{1}{z}\frac{\mu}{\varepsilon_b}-\frac{3}{z^2}\left(\frac{\mu}{\varepsilon_b}\right)^2+\frac{3}{2z^3}\left(\frac{\mu}{\varepsilon_b}\right)^3\right)\right\} \quad \text{(G. 23)}$$

or

$$\boldsymbol{I}_Q \approx \boldsymbol{U}\left(\frac{\varepsilon_b}{\mu}\right)^{5/2}\left\{\frac{1-\frac{5}{4}\exp\left[-z\left(\frac{\varepsilon_b}{\mu}+1\right)\right]\left(\frac{1}{z}\frac{\mu}{\varepsilon_b}-\frac{3}{z^2}\left(\frac{\mu}{\varepsilon_b}\right)^2+\frac{3}{2z^3}\left(\frac{\mu}{\varepsilon_b}\right)^3\right)}{1+\frac{5}{4}\left(\frac{1}{z}-\frac{3}{z^2}+\frac{3}{2z^3}+\frac{3}{4z^4}\right)}\right\}. \quad \text{(G. 24)}$$

As in the case of $\boldsymbol{I}_J$, Eqs.(G.24) and (G.21) for $\boldsymbol{I}_Q$ converge in the limit of $\varepsilon_b = \mu$ only at zero temperature.

Expressions for exponential band tail model

We use the same technique of derivation as in Appendix F (p. 169). The density of states has a form given by Eq. (F.18) (see p. 172). First we consider the case $\varepsilon_b > \mu$. Using (2.49) and (F.18) in (2.14) we obtain

$$\boldsymbol{I}_J = \int_0^{\mu} \rho_t \exp\left(\frac{\varepsilon}{\varepsilon_t}\right)\left[1 - \frac{1}{2}\exp\left[\frac{\varepsilon-\mu}{\vartheta}\right]\right]\boldsymbol{d}\varepsilon + \int_{\mu}^{\varepsilon_b} \rho_t \exp\left(\frac{\varepsilon}{\varepsilon_t}\right)\cdot\frac{1}{2}\exp\left[\frac{\mu-\varepsilon}{\vartheta}\right]\boldsymbol{d}\varepsilon =$$

$$= \rho_t\left\{\int_0^{\mu}\exp\left(\frac{\varepsilon}{\varepsilon_t}\right)\boldsymbol{d}\varepsilon - \frac{1}{2}\int_0^{\mu}\exp\left(\frac{\varepsilon}{\varepsilon_t} + \frac{\varepsilon}{\vartheta} - \frac{\mu}{\vartheta}\right)\boldsymbol{d}\varepsilon + \frac{1}{2}\int_{\mu}^{\varepsilon_b}\exp\left(\frac{\varepsilon}{\varepsilon_t} - \frac{\varepsilon}{\vartheta} + \frac{\mu}{\vartheta}\right)\boldsymbol{d}\varepsilon\right\} =$$

$$= \rho_t\left\{\varepsilon_t\left[\exp\left(\frac{\mu}{\varepsilon_t}\right) - 1\right] - \frac{1}{2}\exp\left(-\frac{\mu}{\vartheta}\right)\int_0^{\mu}\exp(\alpha_+\varepsilon)\boldsymbol{d}\varepsilon + \frac{1}{2}\exp\left(+\frac{\mu}{\vartheta}\right)\int_{\mu}^{\varepsilon_b}\exp(\alpha_-\varepsilon)\boldsymbol{d}\varepsilon\right\} =$$

$$\alpha_{\pm} \equiv \frac{1}{\varepsilon_t} \pm \frac{1}{\vartheta}; \quad \begin{matrix}\alpha_+ > 0\\ \alpha_- < 0\end{matrix}$$

$$= \rho_t\left\{\varepsilon_t\left[\exp\left(\frac{\mu}{\varepsilon_t}\right) - 1\right] - \exp\left(-\frac{\mu}{\vartheta}\right)\frac{\left[\exp(\alpha_+\mu) - 1\right]}{2\alpha_+} + \exp\left(\frac{\mu}{\vartheta}\right)\frac{\left[\exp(\alpha_-\varepsilon_b) - \exp(\alpha_-\mu)\right]}{2\alpha_-}\right\} =$$

$$= \rho_t\left\{\varepsilon_t\left[\exp\left(\frac{\mu}{\varepsilon_t}\right) - 1\right] - \frac{\varepsilon_t\vartheta}{2(\varepsilon_t + \vartheta)}\left[\exp\left(\frac{\mu}{\varepsilon_t}\right) - \exp\left(-\frac{\mu}{\vartheta}\right)\right] - \right.$$

$$\left. + \frac{\varepsilon_t\vartheta}{2(\varepsilon_t - \vartheta)}\left[\exp\left(\frac{\mu}{\varepsilon_t}\right) - \exp\left(\frac{\varepsilon_b}{\varepsilon_t} - \frac{\varepsilon_b - \mu}{\vartheta}\right)\right]\right\} \approx$$

$$\mu >> \vartheta \Rightarrow \exp\left(-\frac{\mu}{\vartheta}\right) \to 0$$

$$\approx \rho_t \varepsilon_t \exp\left(\frac{\mu}{\varepsilon_t}\right)\left\{1-\exp\left(-\frac{\mu}{\varepsilon_t}\right)-\frac{\vartheta^2}{\vartheta^2-\varepsilon_t^2}-\frac{\vartheta}{2(\varepsilon_t-\vartheta)}\exp\left(\frac{\varepsilon_b-\mu}{\varepsilon_t}-\frac{\varepsilon_b-\mu}{\vartheta}\right)\right\} \approx$$

$$\mu >> \varepsilon_t \Rightarrow \exp\left(-\frac{\mu}{\varepsilon_t}\right) \to 0$$

$$\approx \rho_t \varepsilon_t \exp\left(\frac{\mu}{\varepsilon_t}\right)\left\{1-\frac{\vartheta^2}{\vartheta^2-\varepsilon_t^2}-\frac{\vartheta}{2(\varepsilon_t-\vartheta)}\exp\left[-\frac{(\varepsilon_b-\mu)}{\varepsilon_t}\left(\frac{\varepsilon_t}{\vartheta}-1\right)\right]\right\} \approx$$

$$\approx \boldsymbol{N}_c - \rho_t \varepsilon_t \exp\left(\frac{\mu}{\varepsilon_t}\right)\frac{\vartheta}{2(\varepsilon_t-\vartheta)}\exp\left[-\frac{(\varepsilon_b-\mu)}{\varepsilon_t}\left(\frac{\varepsilon_t}{\vartheta}-1\right)\right] \approx$$

$$\approx \boldsymbol{N}_c\left\{1-\frac{1}{2}\theta(1+\theta)\exp\left[-\frac{(\varepsilon_b-\mu)}{\varepsilon_t}\left(\frac{1-\theta}{\theta}\right)\right]\right\}, \qquad \text{(G. 25)}$$

where we have used notations from Appendix F and Eq.(F.19) (p. 173).

For very large barrier we have

$$\lim_{\varepsilon_b \to \infty} \boldsymbol{I}_J(\varepsilon_b) = \boldsymbol{N}_c .$$

For $\varepsilon_b < \mu$ we have

$$\boldsymbol{I}_J = \int_0^{\varepsilon_b} \rho_t \exp\left(\frac{\varepsilon}{\varepsilon_t}\right)\left[1-\frac{1}{2}\exp\left[\frac{\varepsilon-\mu}{\vartheta}\right]\right] d\varepsilon = \rho_t\left\{\int_0^{\varepsilon_b}\exp\left(\frac{\varepsilon}{\varepsilon_t}\right)d\varepsilon - \frac{1}{2}\int_0^{\varepsilon_b}\exp\left(\frac{\varepsilon}{\varepsilon_t}+\frac{\varepsilon}{\vartheta}-\frac{\mu}{\vartheta}\right)d\varepsilon\right\} =$$

$$= \rho_t\left\{\varepsilon_t\left[\exp\left(\frac{\varepsilon_b}{\varepsilon_t}\right)-1\right]-\frac{1}{2}\exp\left(-\frac{\mu}{\vartheta}\right)\int_0^{\varepsilon_b}\exp(\alpha_+\varepsilon)d\varepsilon\right\} =$$

$$= \rho_t\left\{\varepsilon_t\left[\exp\left(\frac{\varepsilon_b}{\varepsilon_t}\right)-1\right]-\exp\left(-\frac{\mu}{\vartheta}\right)\frac{\left[\exp(\alpha_+\varepsilon_b)-1\right]}{2\alpha_+}\right\} =$$

$$= \rho_t \varepsilon_t\left\{\left[\exp\left(\frac{\varepsilon_b}{\varepsilon_t}\right)-1\right]-\frac{\vartheta}{2(\varepsilon_t+\vartheta)}\left[\exp\left(\frac{\varepsilon_b}{\varepsilon_t}+\frac{\varepsilon_b-\mu}{\vartheta}\right)-\exp\left(-\frac{\mu}{\vartheta}\right)\right]\right\} \approx$$

$$\mu >> \vartheta \Rightarrow \exp\left(-\frac{\mu}{\vartheta}\right) \to 0$$

$$\approx \rho_t \varepsilon_t \exp\left(\frac{\mu}{\varepsilon_t}\right)\left\{\exp\left(\frac{\varepsilon_b-\mu}{\varepsilon_t}\right)-\exp\left(-\frac{\mu}{\varepsilon_t}\right)-\frac{\vartheta}{2(\varepsilon_t+\vartheta)}\exp\left(\frac{\varepsilon_b-\mu}{\varepsilon_t}+\frac{\varepsilon_b-\mu}{\vartheta}\right)\right\}\approx$$

$$\mu >> \varepsilon_t \Rightarrow \exp\left(-\frac{\mu}{\varepsilon_t}\right) \to 0$$

$$\approx \rho_t \varepsilon_t \exp\left(\frac{\mu}{\varepsilon_t}\right)\left\{\exp\left(\frac{\varepsilon_b-\mu}{\varepsilon_t}\right)-\frac{\vartheta}{2(\varepsilon_t+\vartheta)}\exp\left(\frac{\varepsilon_b-\mu}{\varepsilon_t}+\frac{\varepsilon_b-\mu}{\vartheta}\right)\right\}\approx$$

$$\approx \boldsymbol{N}_c\left(1-\theta^2\right)\left\{\exp\left(\frac{\varepsilon_b-\mu}{\varepsilon_t}\right)-\frac{\theta}{2(1+\theta)}\exp\left[\left(\frac{\varepsilon_b-\mu}{\varepsilon_t}\right)\left(\frac{1+\theta}{\theta}\right)\right]\right\}. \tag{G. 26}$$

For a negligible barrier this expression becomes zero:

$$\lim_{\varepsilon_b \to 0} \boldsymbol{I}_J(\varepsilon_b) = 0.$$

In the limit of $\varepsilon_b = \mu$ the expressions (G.25) and (G.26) coincide even for nonzero temperatures:

$$\boldsymbol{I}_J(\varepsilon_b = \mu) \approx \boldsymbol{N}_c\left(1-\frac{\theta}{2}-\frac{\theta^2}{2}\right). \tag{G. 27}$$

Next we calculate $\boldsymbol{I}_Q$ beginning with the case $\varepsilon_b > \mu$.

$$\boldsymbol{I}_Q = \int_0^{\mu} \rho_t \varepsilon \exp\left(\frac{\varepsilon}{\varepsilon_t}\right)\left[1-\frac{1}{2}\exp\left[\frac{\varepsilon-\mu}{\vartheta}\right]\right]d\varepsilon + \int_{\mu}^{\varepsilon_b} \rho_0 \varepsilon \exp\left(\frac{\varepsilon}{\varepsilon_t}\right)\cdot\frac{1}{2}\exp\left[\frac{\mu-\varepsilon}{\vartheta}\right]d\varepsilon =$$

$$= \rho_t \left\{\int_0^{\mu} \varepsilon \exp\left(\frac{\varepsilon}{\varepsilon_t}\right)d\varepsilon - \frac{1}{2}\exp\left(-\frac{\mu}{\vartheta}\right)\int_0^{\mu} \varepsilon \exp(\alpha_+ \varepsilon)d\varepsilon + \frac{1}{2}\exp\left(\frac{\mu}{\vartheta}\right)\int_{\mu}^{\varepsilon_b} \varepsilon \exp(\alpha_- \varepsilon)d\varepsilon\right\} =$$

$$= \rho_t \left\{\varepsilon_t^2\left(\exp\left(\frac{\varepsilon}{\varepsilon_t}\right)\left(\frac{\varepsilon}{\varepsilon_t}-1\right)\Bigg|_0^{\mu}\right) - \frac{1}{2\alpha_+^2}\exp\left(-\frac{\mu}{\vartheta}\right)\left(\exp(\alpha_+\varepsilon)(\alpha_+\varepsilon-1)\big|_0^{\mu}\right) + \right.$$

$$+\frac{1}{2\alpha_-^2}\exp\left(\frac{\mu}{\vartheta}\right)\left(\exp(\alpha_-\varepsilon)(\alpha_-\varepsilon-1)\Big|_{\mu}^{\varepsilon_b}\right)\Bigg\}=$$

$$=\rho_t\left\{\varepsilon_t^2\left[\exp\left(\frac{\mu}{\varepsilon_t}\right)\left(\frac{\mu}{\varepsilon_t}-1\right)+1\right]-\frac{1}{2\alpha_+^2}\exp\left(-\frac{\mu}{\vartheta}\right)\left[\exp(\alpha_+\mu)(\alpha_+\mu-1)+1\right]+\right.$$

$$\left.+\frac{1}{2\alpha_-^2}\exp\left(\frac{\mu}{\vartheta}\right)\left[\exp(\alpha_-\varepsilon_b)(\alpha_-\varepsilon_b-1)-\exp(\alpha_-\mu)(\alpha_-\mu-1)\right]\right\}=$$

$$=\rho_t\varepsilon_t\exp\left(\frac{\mu}{\varepsilon_t}\right)\left\{\mu-\varepsilon_t+\varepsilon_t\exp\left(-\frac{\mu}{\varepsilon_t}\right)-\frac{1}{2\varepsilon_t\alpha_+^2}\left[(\alpha_+\mu-1)+\frac{\exp(-\mu/\vartheta)}{\exp(\mu/\varepsilon_t)}\right]+\right.$$

$$\left.+\frac{1}{2\alpha_-^2}\left[\exp(\alpha_-(\varepsilon_b-\mu))(\alpha_-\varepsilon_b-1)-(\alpha_-\mu-1)\right]\right\}=$$

$$\mu>>\varepsilon_t\Rightarrow\exp\left(-\frac{\mu}{\varepsilon_t}\right)\to 0,\quad \mu>>\vartheta\Rightarrow\exp\left(-\frac{\mu}{\vartheta}\right)\to 0$$

$$=\rho_t\varepsilon_t\exp\left(\frac{\mu}{\varepsilon_t}\right)\left\{\mu-\varepsilon_t-\frac{(\alpha_+\mu-1)}{2\varepsilon_t\alpha_+^2}+\frac{(1-\alpha_-\mu)}{2\varepsilon_t\alpha_-^2}-\frac{(1-\alpha_-\varepsilon_b)}{2\varepsilon_t\alpha_-^2}\exp\left[\alpha_-(\varepsilon_b-\mu)\right]\right\}=$$

$$=\boldsymbol{U}-\rho_t\varepsilon_t\exp\left(\frac{\mu}{\varepsilon_t}\right)\frac{(1-\alpha_-\varepsilon_b)}{2\varepsilon_t\alpha_-^2}\exp\left[\alpha_-(\varepsilon_b-\mu)\right]=$$

$$=\boldsymbol{U}-\rho_t\varepsilon_t\exp\left(\frac{\mu}{\varepsilon_t}\right)\frac{1}{2}\left(1+\frac{\varepsilon_b}{\varepsilon_t}\frac{1-\theta}{\theta}\right)\frac{\varepsilon_t\theta^2}{(1-\theta)^2}\exp\left[-\left(\frac{\varepsilon_b-\mu}{\varepsilon_t}\right)\frac{1-\theta}{\theta}\right]=$$

$$=\boldsymbol{U}\left\{1-\frac{1}{2}\theta^2\frac{1+\theta}{1-\theta}\frac{\left(1+\frac{\varepsilon_b}{\varepsilon_t}\frac{1-\theta}{\theta}\right)}{\frac{\mu}{\varepsilon_t}-\frac{1-3\theta^2}{1-\theta^2}}\exp\left[-\left(\frac{\varepsilon_b-\mu}{\varepsilon_t}\right)\frac{1-\theta}{\theta}\right]\right\}. \qquad \text{(G. 28)}$$

For a very large barrier we have

$$\lim_{\varepsilon_b\to\infty}\boldsymbol{I}_Q(\varepsilon_b)=\boldsymbol{U}.$$

For $\varepsilon_b < \mu$ we have

$$I_Q = \int_0^{\varepsilon_b} \rho_t \varepsilon \exp\left(\frac{\varepsilon}{\varepsilon_t}\right)\left[1 - \frac{1}{2}\exp\left[\frac{\varepsilon - \mu}{\vartheta}\right]\right] d\varepsilon =$$

$$= \rho_t \left\{ \int_0^{\varepsilon_b} \varepsilon \exp\left(\frac{\varepsilon}{\varepsilon_t}\right) d\varepsilon - \frac{1}{2}\int_0^{\varepsilon_b} \varepsilon \exp\left(\frac{\varepsilon}{\varepsilon_t} + \frac{\varepsilon}{\vartheta} - \frac{\mu}{\vartheta}\right) d\varepsilon \right\} =$$

$$= \rho_t \left\{ \int_0^{\varepsilon_b} \varepsilon \exp\left(\frac{\varepsilon}{\varepsilon_t}\right) d\varepsilon - \frac{1}{2}\exp\left(-\frac{\mu}{\vartheta}\right)\int_0^{\varepsilon_b} \varepsilon \exp(\alpha_+ \varepsilon) d\varepsilon \right\} =$$

$$= \rho_t \left\{ \varepsilon_t^2 \left(\exp\left(\frac{\varepsilon}{\varepsilon_t}\right)\left(\frac{\varepsilon}{\varepsilon_t} - 1\right)\Bigg|_0^{\varepsilon_b} \right) - \frac{1}{2\alpha_+^2}\exp\left(-\frac{\mu}{\vartheta}\right)\left(\exp(\alpha_+ \varepsilon)(\alpha_+ \varepsilon - 1)\Big|_0^{\varepsilon_b}\right) \right\} =$$

$$= \rho_t \left\{ \varepsilon_t^2 \left[\exp\left(\frac{\varepsilon_b}{\varepsilon_t}\right)\left(\frac{\varepsilon_b}{\varepsilon_t} - 1\right) + 1 \right] - \frac{1}{2\alpha_+^2}\exp\left(-\frac{\mu}{\vartheta}\right)\left[\exp(\alpha_+ \varepsilon_b)(\alpha_+ \varepsilon_b - 1) + 1\right] \right\} =$$

$$= \rho_t \varepsilon_t^2 \exp\left(\frac{\varepsilon_b}{\varepsilon_t}\right) \left\{ \frac{\varepsilon_b}{\varepsilon_t} - 1 + \exp\left(-\frac{\varepsilon_b}{\varepsilon_t}\right) - \frac{1}{2\varepsilon_t^2 \alpha_+^2}\left[\exp\left(\frac{\varepsilon_b - \mu}{\vartheta}\right)(\alpha_+ \varepsilon_b - 1) + \frac{\exp\left(\frac{-\mu}{\vartheta}\right)}{\exp\left(\frac{\varepsilon_b}{\vartheta}\right)} \right] \right\} =$$

$$\mu >> \vartheta \Rightarrow \exp\left(-\frac{\mu}{\vartheta}\right) \to 0$$

$$= \rho_t \varepsilon_t^2 \exp\left(\frac{\varepsilon_b}{\varepsilon_t}\right) \left\{ \frac{\varepsilon_b}{\varepsilon_t} - 1 + \exp\left(-\frac{\varepsilon_b}{\varepsilon_t}\right) - \frac{1}{2\varepsilon_t^2 \alpha_+^2}\left[\exp\left(\frac{\varepsilon_b - \mu}{\vartheta}\right)(\alpha_+ \varepsilon_b - 1) \right] \right\} =$$

$$= U(1 - \theta^2) \frac{e^{(\varepsilon_b - \mu)/\varepsilon_t} \left\{ \frac{\varepsilon_b}{\varepsilon_t} - 1 + e^{-\varepsilon_b/\varepsilon_t} - \frac{1}{2}\frac{\theta^2}{(1+\theta)^2}\left[e^{(\varepsilon_b - \mu)/\theta}\left(\frac{\varepsilon_b}{\varepsilon_t}\frac{\theta + 1}{\theta} - 1\right) \right] \right\}}{\frac{\mu}{\varepsilon_t} - \frac{1 - 3\theta^2}{1 - \theta^2}}, \qquad \text{(G. 29)}$$

or

$$I_Q = N_c \varepsilon_t \left(1 - \theta^2\right) \exp\left(\frac{\varepsilon_b - \mu}{\varepsilon_t}\right) \tilde{R}, \tag{G. 30}$$

where $\tilde{R}$ denotes the expression in figure brackets in (G.29).

In the limit of $\varepsilon_b = \mu$ expressions (G.28) and (G.29) coincide even for nonzero temperatures:

$$I_Q(\varepsilon_b = \mu) \approx U\left(1 - \frac{\theta}{2} - \frac{\theta^2}{2}\right). \tag{G. 31}$$

APPENDIX H. DIMENSIONLESS MODEL EQUATIONS

Dimensionless model equations (Eqs. (2.1), p. 18) are obtained through the following procedure:

$$(2.1\text{a})\times\frac{\tau_s}{\tilde{N}},\ (2.1\text{b})\times\frac{\tau_s}{\tilde{N}},\ \text{and}\ (2.1\text{c})\times\frac{\tau_s}{\tilde{N}\hbar\tilde{\omega}},$$

where $\tilde{N}$ is some constant with dimensionality cm^{-3} and $\tilde{\omega}$ is some reference frequency. For stable numerical code, the parameter $\tilde{N}$ should be on the order of the carrier density ($\propto 10^{17}$-10^{18} cm^{-3}); we use $\tilde{N}=10^{18}$ cm^{-3}. The parameter $\tilde{\omega}$ is chosen in such a way that $\hbar\tilde{\omega}$ is equal to the bandgap energy (0.99 eV) of the laser medium (InGaAsP alloy) which was used in cw laser dynamics.

The dimensionless equations used in numerical analysis are

$$\frac{dX}{d\tau} = -\gamma_c X + \Gamma G X + \Gamma\beta_{sp} Y - \sigma_{FCA} XY - \sigma_{TPA} X^2 + \chi X_{px}, \tag{H. 1}$$

$$\frac{dY}{d\tau} = P - Y - GX + \sigma_{TPA} X^2, \tag{H. 2}$$

$$\frac{dZ}{d\tau} = Z_p - Z - \varphi G X - \gamma_l (Z - Z_l) + \varphi\sigma XY + 2\sigma_{TPA} X^2, \tag{H. 3}$$

where we used the following notations for dimensionless values

$$X \equiv \frac{N_p}{\tilde{N}};\ Y \equiv \frac{N_c}{\tilde{N}};\ Z \equiv \frac{U}{\tilde{N}\hbar\tilde{\omega}};\ X_{px} \equiv \frac{N_{px}}{\tilde{N}};\ \gamma_c \equiv \frac{\tau_s}{\tau_c};\ \gamma_l \equiv \frac{\tau_s}{\tau_l};\ G \equiv g\tau_s;\ \chi \equiv k\tau_s;$$

$$\varphi \equiv \frac{\omega}{\tilde{\omega}};\ P \equiv \frac{J\tau_s}{\tilde{N}};\ Z_p \equiv \frac{Q\tau_s}{\tilde{N}\hbar\tilde{\omega}};\ Z_l \equiv \frac{U_l}{\tilde{N}\hbar\tilde{\omega}};\ \sigma_{FCA} \equiv v_{gr} s_{FCA} \tau_s \tilde{N};\ \sigma_{TPA} \equiv v_{gr} s_{TPA} \tau_s \tilde{N}.$$

VITA

Tigran Sarkisyan

Candidate for the Degree of

Doctor of Philosophy

Thesis: CARRIER TEMPERATURE AND GAIN DYNAMICS IN SEMICONDUCTOR LASER MEDIA

Major field: Physics

Biographical:

Personal Data: Born in Kadjaran, Armenia, July 17, 1966.

Education: Undergraduate education in Physics Department of Yerevan State University, Armenia; transferred to Moscow Engineering Physics Institute in February 1988; received Master of Science degree in Physics (Diploma of Engineer-Physicist) from Moscow Engineering Physics Institute, Russia, in March 1991. Completed the requirements for the Doctor of Philosophy degree in Physics at Oklahoma State University in May 2000.

Experience: Research Scientist in the P. N. Lebedev Physics Institute of Russian Academy of Sciences, May 1991 – February 1995; Research and Teaching Assistant, Department of Physics, Oklahoma State University, June 1995 to May 2000.

Professional Memberships: Optical Society of America, American Physical Society.